Catalytic C-C Bond Cleavage for the Production of Chemicals from Lignin

MIX
Paper from
responsible sources
FSC
www.fsc.org
FSC® C012854

Catalytic C-C Bond Cleavage for the Production of Chemicals from Lignin

Het katalytisch breken van C-C bindingen voor de productie van chemicaliën uit lignine

(met een samenvatting in het Nederlands)

Proefschrift

ter verkrijging van de graad van doctor aan de Universiteit Utrecht op gezag van de rector magnificus, prof.dr. G.J. van der Zwaan, ingevolge het besluit van het college voor promoties in het openbaar te verdedigen op woensdag 16 maart 2016 des ochtends te 10.30 uur

door

Robin Jastrzebski

geboren op 27 april 1987 te Utrecht

Promotor: Prof.dr.ir. B.M. Weckhuysen

Copromotor: Dr. P.C.A. Bruijnincx

I don't know where I'm going from here,
but I promise it won't be boring.
- David Bowie

Contents

Chapter 1

Introduction

1.1 Lignin as a Feedstock for the Chemical Industry

In recent years, there has been considerable interest in the replacement of fossil fuels and resources as feedstock for (transportation) energy and chemicals with more sustainable alternatives. One important driver is the future availability of the fossil materials, particularly crude oil. Proven reserves of crude oil amount to ca. 50 years at current usage levels, although, due to discovery of new reserves, this has remained so for the last 20 years.[1] Nevertheless, increasing demand has led to oil prices rising up to $110 per barrel as recently as 2014. Although oil prices have plummeted since then due to oversupply, this has immediately led to a large reduction of investments by oil companies. Current low market prices are also below production prices for a large number of wells and are therefore unlikely to last in the medium to long term.[2] A second, more pressing driver is the emission of carbon dioxide by combustion of fossil fuels (and eventually from chemicals as well, either through biodegradation or more importantly, waste incineration). The link between anthropogenic carbon dioxide emissions and global warming has been well established and efforts to reduce carbon dioxide emissions to prevent further global warming are urgently needed.[3] Finally, as a result of changes in the overall fossil feedstock composition, some components have become less available and alternatives need to found. For example, in the United States, large-scale extraction of shale gas has partially displaced crude oil as feedstock for the chemical industry; however, shale gas does not provide convenient access to aromatic molecules and an alternative renewable feedstock may be able to fill the gap.[4] Government policy and mandates play an important role in tackling these issues and ensuring the implementation of renewable feedstocks. Both in the United States and the European Union, ambitious goals have been set to this extent. For example, in the United States, the production of 20% of the transportation fuels and 25% of chemical commodities from biomass is envisaged by 2030.[5] The European Union has set a mandatory target of 20% of renewable energy by 2020, which includes a 10% biofuel fraction.[6]

In terms of technologies available or under development to address these challenges, there are a number of alternatives for energy: solar, wind, hydro and biomass may all contribute to a sustainable energy mix. On the other hand, for the production of chemicals, options are more limited: a source of carbon is required, which can either be carbon dioxide from the air or biomass. As the former approach appears elegant, this has led to considerable interest in the development of 'artificial leafs,' which reduce environmental carbon dioxide to simple (oxygenated) hydrocarbons using sunlight and water, analogous to photosynthesis.[7,8] While possible, there are still significant technological challenges in this field. More fundamentally, however, the intrinsically low concentration of atmospheric carbon dioxide (ca. 400 ppm) means that reactivity will be low and extremely large amounts of such leafs will be necessary to attain commercially interesting amounts of reduced carbon; such carbon dioxide to hydrocarbon schemes are

therefore only feasible if a highly concentrated stream of carbon dioxide is available, e.g. from burning fossil fuels.[9] On the other hand, when using biomass, the concentration of the dilute atmospheric carbon dioxide has already been taken care of by nature. In fact, while photosynthesis may appear to be an inefficient process in term of energy storage (ca. 2-4% of input solar energy can be converted to biomass for the most efficient photosynthesisers),[10] it is very efficient in concentrating the dilute carbon dioxide present in the atmosphere. A second advantage over the artificial leaf approach is that more complex functionalised molecules are directly available in the biomass. Particularly when targeting chemicals, this means that less effort is required to build the carbon skeleton and introduce the appropriate functionalities.

In order to limit competition for resources with agriculture for food supply, it is undesirable to use edible (or at least, the edible fractions of) plants, as is the case for most present-day first-generation biofuels. In addition, for the sake of efficiency it is desirable to use as much of the captured carbon as possible. This means that so-called second-generation processes that make use of 'lignocellulosic' biomass, are the feedstock of choice. Lignocellulose primarily constitutes the cell wall material of branches, stalks and stems of most plants and is therefore the bulk of the dry weight of the plant mass. This lignocellulosic biomass (which in this context is implied when simply referred to as the biomass) itself consists of three main fractions: cellulose (40-45 wt%, a linear polymer of glucose), hemicellulose (30 wt%, a polymer of mainly pentose sugars) and lignin (15-40 wt%, a polymer of aromatics units).[11] Analogous to crude oil processing, the biomass can be fractionated into its constituents, which can subsequently be further upgraded and converted to products with the desirable properties for the envisaged application; so-called 'biorefineries' have been proposed for this purpose.[12-14] As a traditional oil refinery, such a biorefinery would produce not a single product, but a rather a combination of fuels and chemicals, ideally making full and effective use of the whole biomass feedstock. Most research has focused on the use the carbohydrate fraction, though, either through fermentation or chemical conversion.

Lignin is generally considered to be the most difficult of the three fractions to valorise, due to the fact that it does not have a well-defined structure and has multiple (strong) bond motifs linking the different monomers. Within the cell wall, its primary function is cross-linking the carbohydrate components, conferring structural strength to the plant, as well as acting as a hydrophobic water barrier.[15] Generally, lignin can be thought of as the product of the radical polymerisation of the three monolignols *p*-courmaryl alcohol, coniferyl alcohol and sinapyl alcohol, which results primarily in the formation of aryl alkyl ethers, as well as a number of carbon-carbon bond motifs (Figure 1.1, see Chapter 2 for details).[16] Commercial application of lignin is presently limited: while large quantities are separated from the biomass in the paper and pulp industry, the majority is burned to provide power for operating the plants. The remaining energy is sold to
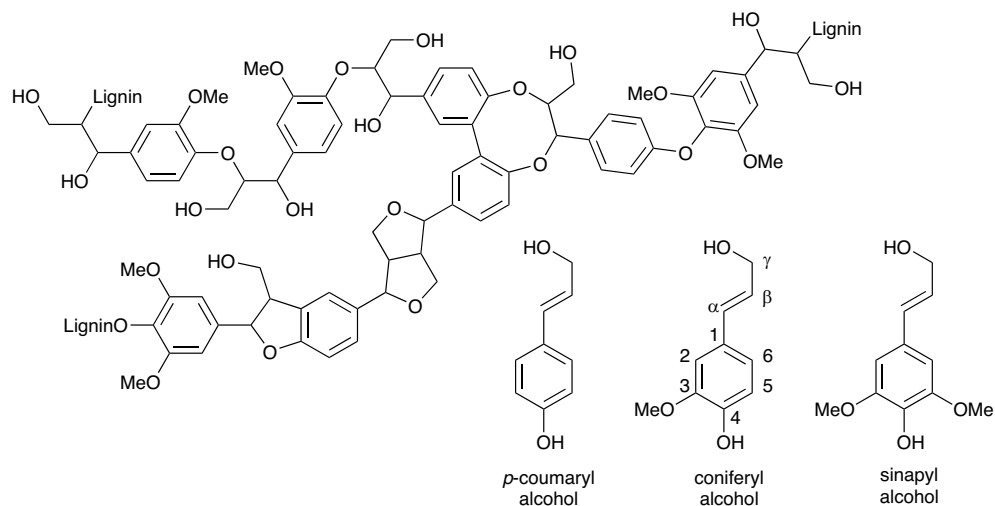
Figure 1.1: Representation of a lignin fragment including a number of common bond motifs (top), as well the monolignols from which lignin is mainly derived (bottom).

local electricity grids. In these applications, lignin is currently one of the most important biofuels.[17] The production of vanillin by Borregaard is currently the only example of a process that converts lignin to a value-added chemical. The scale this process is operated on is, however, very small in volume compared to the total amounts of lignin that are currently produced in the paper and pulp industry. In addition, even larger amounts of lignin will become available from the production of 2nd generation biofuels.

Lignin is nonetheless a very interesting material both as a feedstock for fuels as well as for chemicals. It has the highest energy content of all biomass constituents and the very fact that it constitutes such a considerable fraction of the biomass means that considering it as waste material is simply not viable for the efficient and economic operation of a biorefinery. Most importantly, however, lignin is the only biomass component of abundance with aromatic units in its structure. Aromatics are important building blocks for the chemical industry, acting as precursors for a large number of bulk and specialty chemicals, leading to diverse products such as fibres, paints, fragrances and pharmaceuticals. The ability to directly obtain aromatics from biomass would thus be very attractive.

The challenge is then to effectively separate the lignin from the other biomass constituents and convert it into valuable chemicals; catalysis will play an important role in this. Considering the breadth of the topic, an overview of lignin chemistry is presented separately in Chapter 2. The biosynthesis and the resulting structure, as well as opportunities for modifying lignin through genetic engineering are discussed. The most relevant methods for lignin isolation and its consequences for the properties of the isolated material are covered, as well as catalytic approaches for the depolymerisation of lignin.

1.2 Catalytic Carbon-Carbon Bond Cleavage

The transition from oil as the primary feedstock for the chemical industry to biomass will to some degree also require a fundamental change in the type of chemistry employed. Oil-derived precursors are typically completely defunctionalised, a considerable part of chemistry deals with the introduction of functional groups. By contrast, the typical platform molecules derived from biomass are highly functionalised and the removal of functional groups is instead required to arrive at desired target products. From the point of view of making chemicals, it is then desirable to make maximum use of the existing complexity and functionality and to only selectively remove those functions that are not required.[18] Reductive cleavage of carbon-oxygen bonds is the most frequently investigated method for removing these functionalities, but complimentary selective methods that allow alternative transformations are also required. Carbon-carbon bond cleavage methods may partially fulfil this need, for example by being able to adjust the carbon-chain length of starting materials or by transforming cyclic starting materials into a linear carbon chain.

Catalytic, selective carbon-carbon bond cleavage remains to this day extremely challenging. An important reason for this is a fundamental one: carbon-carbon bonds are comparatively strong with (homolytic) bond dissociation energies for a single bond ranging between 84-136 kcal/mol.[19] Successful cleavage therefore requires concomitant formation of even stronger bonds or a large energy input (in the form of heat). In addition, most carbon-carbon bonds are not strongly polarized, so that there is no convenient 'handle' for reagents or catalysts to heterolytically split such bonds.

Nevertheless, research into carbon-carbon bond cleavage with the ability to cleave specific bonds is an active area of research;[20-22] particularly complexes of the late transition metal complexes have been used as catalysts for this reaction. Targeting only a single specific bond in the carbon skeleton of a molecule requires making clever use of the specific chemical environment in which the carbon-carbon bond to be cleaved is located. For example, some functional groups (particularly cyanides and carbonyls) have a rather weak carbon-carbon bond and are therefore intrinsically more amenable to being cleaved; this principle underlies the catalytic decarbonylation reaction that is employed in the first part of this thesis. On the other hand, if the substrate can strongly coordinate to the metal centre, this means that only certain carbon-carbon bonds are in proximity of the reactive site, which can either be the transition metal itself, or a secondary reagent, such as oxygen. It is the very specific coordination and redox chemistry of 1,2-arenediols coupled with an iron(III) centre that makes possible the oxidative ring cleavage that is employed in the second part of this thesis. These two reactions are discussed in more detail in the next sections.

1.2.1 Decarbonylation

The mismatch between the structure of the carbon skeleton of lignin and potential aromatic products is an important motivation to employ carbon-carbon bond cleavage strategies in lignin valorisation. As is evidenced from Figure 1.1, the repeating carbon unit is (primarily) a nine-carbon propylbenzene, while many potentially interesting aromatic products, including benzene, toluene and phenol and catechol, do not feature this propyl substituent. At the same time, if lignin depolymerisation is carried out using acid-catalysed hydrolysis to break the aryl ether bonds, this leads to the formation of aldehyde monomers. As will be discussed in more detail in Chapters 2 & 3, these aldehyde monomers are susceptible to repolymerisation reactions, forming new carbon-carbon bonds. Effectively removing or 'trapping' these aldehydes is therefore an attractive strategy to improve on acid-catalysed lignin depolymerisation processes. Indeed, by combining acid-catalysed hydrolysis with *in-situ* decarbonylation of the generated aldehyde monomers, the effectiveness of the depolymerisation can not only be increased significantly, but also would provide access to products that no longer feature a propyl substituent. The successful application of such a tandem strategy to various lignins is described in Chapter 3.

The decarbonylation of aldehydes overcomes several of the principal challenges in carbon-carbon bond cleavage by using (a) a relatively active substrate (the carbon-carbonyl BDE is only 85 kcal/mol); (b) a thermodynamically highly stable end product (carbon monoxide) and (c) a stable intermediate in the form of a transition metal carbonyl species. One of the oldest reported selective decarbonylation reactions was reported in 1965 by Tsuji and made use of a stoichiometric amount of Wilkinson's catalyst $Rh(PPh_3)_3Cl$.[23] The resulting rhodium carbonyl complex is so stable, however, that attempts to employ this complex for catalytic decarbonylation proved more challenging: a temperature of 200 °C was required to perform the reaction catalytically. True *catalytic* decarbonylation was possible with the $[Rh(dppp)_2]Cl$ (dppp = 1,3-bis(diphenylphosphino)propane) complex, which was able to decarbonylate a number of aldehydes at 115 °C or 140 °C; the ability to perform the reaction catalytically was attributed to the much weaker binding of carbon monoxide to the cationic rhodium complex.[24] This system has been successfully applied in organic syntheses,[25-27] but due to the sensitivity of the $[Rh(dppp)_2]Cl$ complex[28] it was found to be more convenient to prepare the active catalyst *in-situ* from an appropriate rhodium precursor and an excess of the dppp ligand, which is a generally applicable and robust approach.[29-32] More recently an iridium-based system has also been described for decarbonylation under mild conditions.[33-35]

The mechanism of the rhodium-catalysed decarbonylation has been studied using a combined experimental and computational approach.[36] A positive Hammett effect (i.e. those with electron-withdrawing substituents reacted more quickly) was observed in a systematic variation of substrate structure, suggesting the rate-determining step to
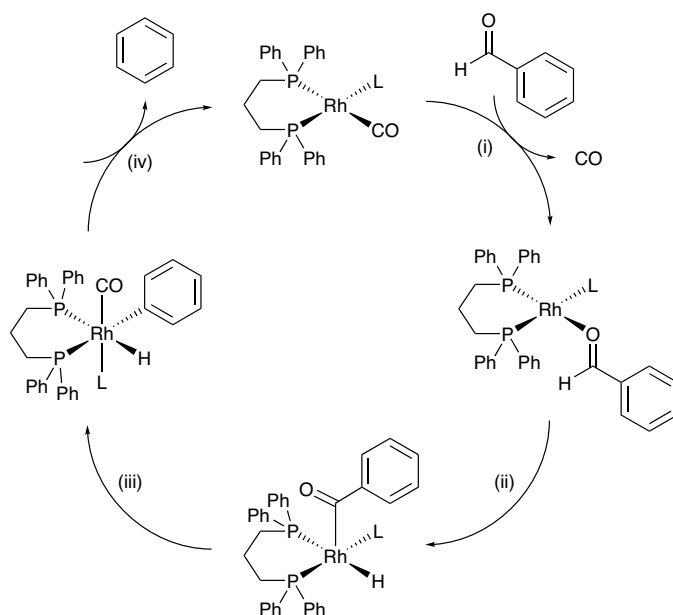
Figure 1.2: Proposed catalytic cycle for the decarbonylation of aldehydes by a [Rh(dppp)]$^+$ complex. The cycle proceeds through (i) dissociation of carbon monoxide with simultaneous association of the aldehyde; (ii) oxidative addition of the carbonyl C-H bond; (iii) migratory extrusion of the carbonyl and (iv) reductive elimination of the decarbonylated product. Adapted from Fristrup *et al.*[36]

involve an accumulation of negative charge on the substrate. The catalytically active species was proposed to be a square-planar four-coordinate complex with one phosphine ligand bound in a bidentate fashion. Based on this and computational studies, a catalytic cycle involving four steps (Figure 1.2) was proposed: (i) dissociation of carbon monoxide with concomitant coordination of the aldehyde; (ii) oxidative addition of the aldehyde to form a tetragonal pyramidal complex; (iii) migratory extrusion of the carbonyl to form an octahedral complex and (iv) carbon-hydrogen bond formation by reductive elimination, which restores the starting square-planar rhodium complex. Except for (iv), all steps were found to be endothermic; consequently, the square-planar carbonyl complex is also the resting state of the catalyst. The migratory extrusion was found to be rate-determining; this may proceed through a number of different isomers which are all close in energy as long as the hydride is not *trans* to the position where the carbonyl to be extruded goes. The experimentally observed and computationally determined kinetic isotope effects for the mechanism were in good agreement, lending credence to the proposed mechanism.

1.2.2 Catechol Dioxygenation

Carbon-carbon bond cleavage also plays an important role in biochemical metabolic pathways; ultimately the breakdown of more complex molecules into carbon dioxide is the process that powers life. Many of the biochemical carbon-carbon bond cleavage reactions employed are oxidative in nature: the formation of a stable carbon-oxygen bond is thermodynamically favoured (and the released energy allows powering other reactions). The triplet ground state of oxygen, however, means that reaction with singlet organic substrates is a spin-forbidden process and therefore proceeds very slowly (which conveniently prevents all organic matter from spontaneously combusting). To overcome the spin-forbidden nature of oxidation by molecular oxygen, nature has developed a toolbox of enzymes, often using first-row transition metals as co-factors. Because the reactions can then only take place in a confined active site in the enzyme, such reactions can also be carried out with great selectivity.

One particularly interesting class of enzymes that oxidatively catalyse carbon-carbon bond cleavage reactions are the catechol dioxygenases.[37-39] As their name implies, these enzymes insert both oxygen atoms of dioxygen into catechols (i.e. 1,2-benzenediols), leading to cleavage of an *aromatic* carbon-carbon bond, opening the ring and affording a dearomatised linear product. Given the stability of aromatic carbon-carbon bonds this is quite a remarkable feat; in fact these enzymes enable *the* key step in the aerobic microbial catabolic breakdown of aromatic compounds.[40] Based on regioselectivity, this enzyme family can be further sub-divided into *intradiol* and *extradiol* dioxygenases (Figure 1.3), affording either *cis,cis*-muconic acid derivatives or muconic semialdehydes, respectively. Although these two families perform similar reactions on the same substrates, they are not structurally related and mechanistically distinct.[41] Given their potential relevance for lignin valorisation, the focus here is on the intradiol dioxygenases.

The selective carbon-carbon bond cleavage shown by the catechol dioxygenases has triggered considerable interest in the mechanism of these reactions.[38,41,42] Early mechanistic work revealed that intradiol catechol dioxygenases require an iron(III) co-factor (whereas the extradiol catechol dioxygenases require iron(II));[43] in addition, isotopic labelling studies with molecular oxygen revealed both inserted oxygen atoms in the muconic acid to be derived from molecular oxygen reagent and not the solvent (water).[44] Determination of the crystal structures of protocatechuate 3,4-dioxygenase, which has
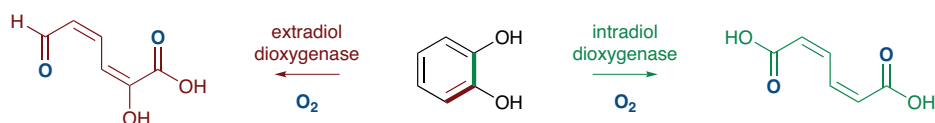

Figure 1.3: Catechol dioxygenases may cleave the catechol ring with molecular oxygen either adjacent to the diol functionality (extradiol, left, red) or in between (intradiol, right, green).

been investigated most as a prototypical intradiol catechol dioxygenase, provided an unparalleled insight into the structural features of the enzyme.[45,46] Unlike a large number of enzymes catalysing oxidation reactions with an iron co-factor, the iron centre is not bound in a heme group; rather the iron is coordinated directly to three coordinating protein amino acids (two histidines, one tyrosine) in a facial triad structural motif geometry, which is also found in a large number of other non-heme iron-containing enzymes.[37,47] In contrast with the heme coordination environment, where the two potential open coordination sites are located *trans* to each other, the facial triad potentially offers three open *fac* coordination sites. Indeed, determination of the crystal structure of a substrate-bound protocatechuate 3,4-dioxygenase revealed the catechol to bind as a dianionic catecholate to afford a square pyramidal coordination geometry around iron (Figure 1.4). In addition there is a fourth tyrosine ligand that stabilises the iron(III) centre when no substrate is bound, but dissociates upon catechol binding.

Further mechanistic investigations revealed the intradiol dioxygenation to proceed in a two-step process: the first oxygen is inserted directly into the ring of the catechol, to a afford a 7-membered cyclic muconic acid anhydride; the second oxygen (as an iron(III) oxo) is protonated to afford a water molecule that then rapidly hydrolyses the acid anhydride to afford the corresponding muconic acid.[49] Although other intermediates are extremely short-lived, use of mechanistic probe molecules and computational work has provided insight in the intermediate steps of the catalytic cycle, though (Figure 1.5).[50,51] The crucial intermediate appears to be a bridging peroxo species, of which a crystal structure has only very recently been determined.[52] This bridging peroxide can undergo a facile homolytic oxygen-oxygen bond cleavage; the resulting substrate-centred radical
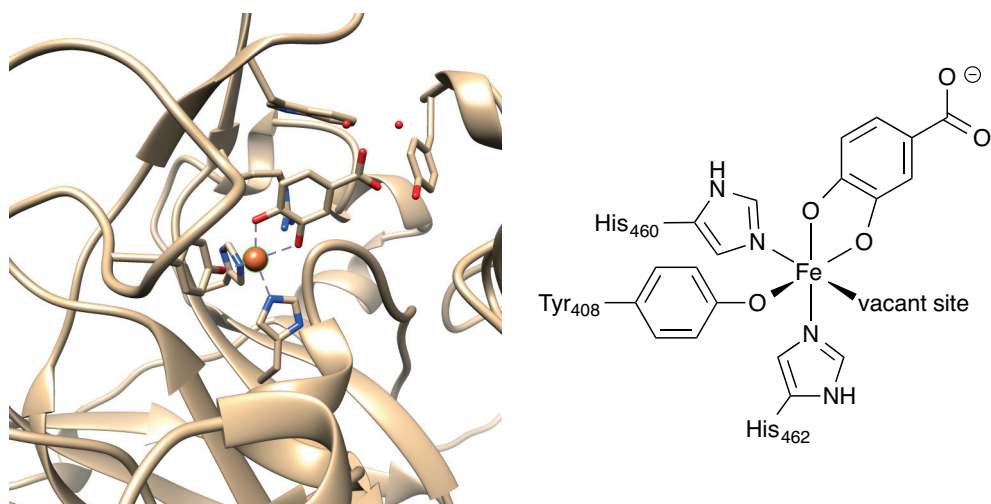

Figure 1.4: Cartoon representation of the active site of protocatechuate 3,4-dioxygenase with bound substrate based on crystal structure data (left)[46] and a schematic representation adapted from Yamahara *et al*.[48]
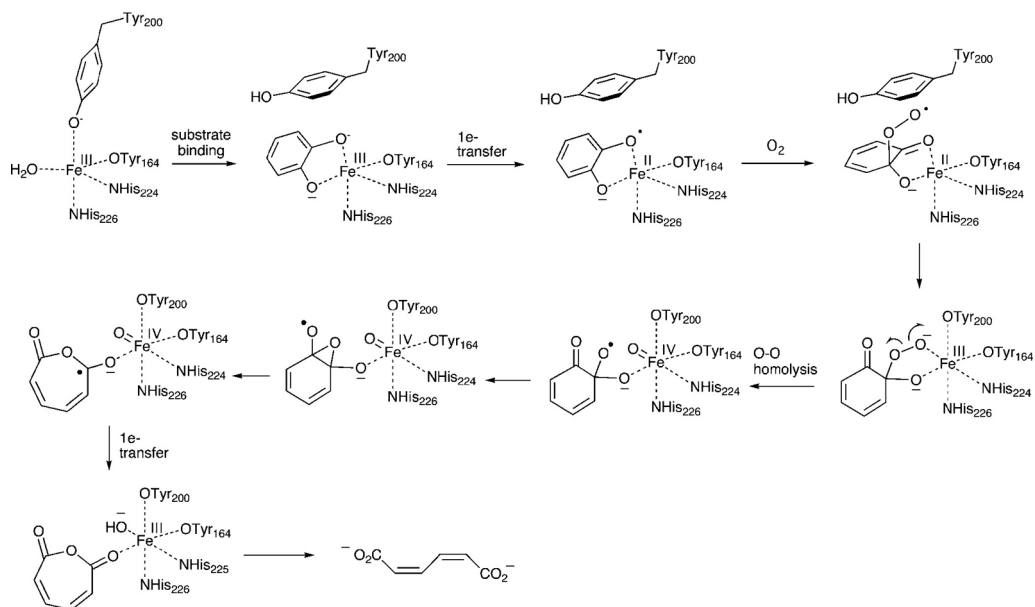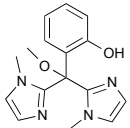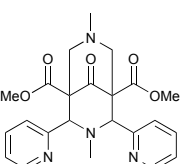
Figure 1.5: Mechanism of intradiol catechol dioxygenation by catechol 1,2-dioxygenase from *Acinetobacter sp.* as proposed by Xin and Bugg, involving a homolytic oxygen-oxygen cleavage. The first steps are drawn as a substrate activation mechanism. In addition, it is not certain whether axial tyrosine-200 remains detached from the iron(III) center in the later steps of the mechanism or becomes reattached (as drawn). Reproduced from Xin *et al.*[51]

can then readily rearrange to the product muconic anhydride. What remains subject of debate, however, is how the bridging peroxide species is formed in the first place and particularly, whether the molecular oxygen directly attacks the catecholate substrate (so-called substrate activation mechanism) or first coordinates to the iron-centre and only then attacks the catecholate substrate (so-called oxygen activation mechanism).

The combination of this remarkable reactivity and the desire to study it in systems which can be more easily characterised has also led to the investigation of synthetic iron(III) complexes as intradiol catechol dioxygenation catalysts. An early report in 1976 provided the first functional mimic of a catechol dioxygenation reaction by iron(III), although the reaction conditions (iron salts dissolved in neat acetic acid, with peracetic acid as the oxidant) can hardly be considered comparable to the enzymatic system.[53,54] Nevertheless, *cis,cis*-muconic acid could be isolated in 76% yield, thus showing at least the same chemo- and regioselectivity. The first well-defined iron(III) complex was reported in 1982: an iron(III) nitriloacetate complex was able to catalyse the intradiol dioxygenation of 3,5-di-*tert*-butylcatechol, a convenient model compound that reacts much faster than the native substrates.[55] Although the reaction proceeded very sluggishly and required up to 7 days to go to completion, up to 80 turnovers could be obtained, clearly showing the catalytic nature of the system.

Table 1.1: Overview of selected iron(III) complexes with 3,5-di-*tert*-butylcatechol and key spectral and reactivity data.

	Ligand	Solvent	λ_{max} (nm)	kO_2 (M^{-1} s^{-1})[a]	I/E[b]	Ref.
1		DMF	414, 620	$1.6 \cdot 10^{-2}$	-	[58]
2		DMF	440, 682	$4.2 \cdot 10^{-2}$	-	[58]
3		DMF	488, 762	$1.8 \cdot 10^{-1}$	-	[58]
4		CH$_3$CN	568, 883	$1.5 \cdot 10^{1}$	-	[57]
5		MeOH	865	4.3	-	[59]
6		MeOH	842	1.0	-	[59]
7		MeOH	569, 877	2.9	-	[60]
8		DMF	550, 925	$2.6 \cdot 10^{-2}$	-	[61]
9		DMF	557, 941	$1.6 \cdot 10^{-1}$	-	[61]
10		CH$_3$CN	488, 753	$4.8 \cdot 10^{1}$	~ 1	[62]
11		CH$_3$CN	553, 784	$3.8 \cdot 10^{-1}$	-	[63]
12		CH$_3$CN	444, 694	n.d.[c]	0	[64]

	Ligand	Solvent	λ_{max} (nm)	kO_2 (M^{-1} s^{-1})^a	I/E^b	Ref.
13		MeOH	544, 720(sh)	n.d.^{d}	~ 1	65
14		CH$_3$CN	610, 910	$3.8 \cdot 10^{-3}$	-	66

^{a} Pseudo first-order rate constant for the dioxygenation reaction. ^{b} Ratio of intradiol/extradiol products; if no value is given exclusively intradiol products were observed. ^{c} Reaction required ca. 6 h to go to completion. ^{d} Reaction required ca. 2 weeks to afford 60% conversion.
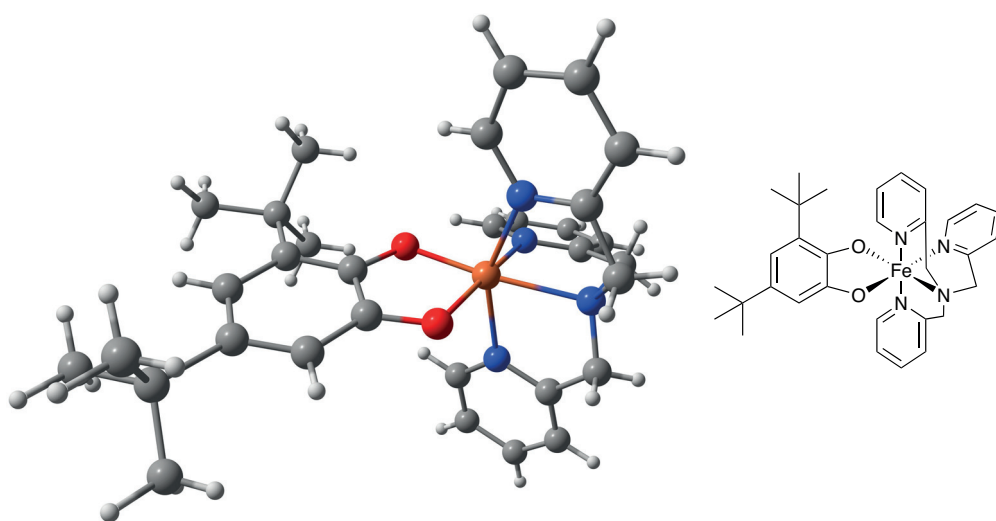
Figure 1.6: Three-dimensional representation and line structure of the [Fe(tpa)(dbc)]$^+$ complex based on crystal structure data.[57]

Since then, a large number of iron(III) complexes with tripodal tetradentate ligands have been reported that are active for catechol intradiol dioxygenation; an overview of selected complexes is presented in Table 1.1. Although there are significant structural differences, the complexes share a number of electronic features with the enzymes; as for the substrate-bound enzymes, two strong absorption bands are observed in the near infrared and visible spectrum (at ca. 500 nm and ca. 800 nm). These absorption bands are attributed to charge-transfer interactions between the bound catecholate substrate and iron(III) centre and were shown to be quite sensitive to the ligand field around the

Figure 1.7: Proposed redox equilibrium between iron(III) catecholato and iron(II) semiquinonato species and modes of oxygen attack. The iron(II) semiquinonato would have a carbon-centred radical that would be susceptible to attack by molecular oxygen.

metal ion: the absorption maximum of the near-infrared band was therefore found to be a good proxy for the Lewis acidity of the iron centre.[56] X-ray crystal structures of a considerable number of complexes have also been determined; a representative example is presented in Figure 1.6. As is the case in the enzymes, the catec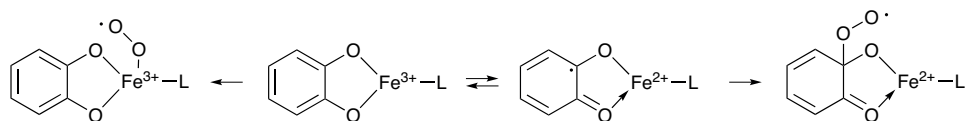hol substrate is bound as a dianion in a bidentate manner, affording a distorted octahedral coordination geometry. Magnetic measurements showed the complexes to be high-spin, in agreement with the enzymatic systems.

As the iron complexes can be more easily studied and appear to be good functional models, these also made a significant contribution to the mechanistic understanding of the enzyme-catalysed cleavage reaction. Specifically, pseudo first-order rate constants for the dioxygenation reaction can be conveniently determined by measuring the decay of the charge-transfer bands upon exposure to oxygen; consistent use of the same model substrate 3,5-di-*tert*-butylcatechol therefore allows dioxygenation activity to be reasonably compared even between different systems reported by different authors. Some trends could thus be identified: in general, iron complexes with weaker electron-donors and consequently more Lewis acidic iron centres (as indicated by the location of the charge-transfer bands) were found to be more active.[58] This, together with the fact that the intradiol-selective model complexes have an octahedral coordination sphere and are thus coordinatively saturated, lent credence to a substrate activation mechanism, whereby oxygen directly attacks the catecholate ring.[57] Activation of the catecholate was proposed to proceed through an iron(III)-catecholato/iron(II)-semiquinonato redox couple (Figure 1.7), with the carbon-centred radical in the semiquinonato allowing the spin-forbidden attack of oxygen on the catecholate to proceed. Experimental evidence for such a semiquinonato species (specifically, bond lengths determined by X-ray crystallography) at the same time was rather weak.[57,67] Furthermore, certainly not all complexes share in this relationship between Lewis acidity and activity; while for example #8, #11 and #14 in Table 1.1 all have a very similar coordination environments the reactivity differs by two orders of magnitude.[61,63,66] It should also be noted that even the most active complex, when applied to the native substrates, is still several orders of magnitude slower than the enzymatic systems.[68]

If instead an oxygen-activation mechanism is operative one might naïvely believe that a complex with a free-coordination site would be much more active. Work by Dei *et al.* revealed this to be not the case with the tridentate 1,4,9-triazacyclononane ligand;[64] quite remarkably, *extradiol* cleavage was seen instead of the expected *intradiol* products. This appeared to be a more general phenomenon for tridentate ligands; which is quite remarkable as extradiol enzymes contain an iron(II), rather than iron(III) centre.[69,70] Small changes in ligand structure, even for tetradentate ligands, may also shift the selectivity and reactivity, for example #11 in Table 1.1 affords exclusively intradiol products, whereas #12, differing by only two methyl substituents, reacts two orders of magnitude faster, but affords a mixture of intradiol and extradiol products.[62,63] A very close mimic of the first coordination sphere of 1,2-catechol dioxygenase was found to afford both intradiol and extradiol cleavage products and reacts several orders of magnitude slower (Table 1.1, #14).[65] It thus seems that selectivity for intradiol or extradiol cleavage is not just dependent on the oxidation state of iron, but that both processes *can* occur (possibly through a common intermediate) and that the outcome is ultimately determined by the precise geometry of the relevant intermediates and transition state. This then also demonstrates the limitations of simple coordination complexes as models for enzymes: additional, second-sphere residues clearly play an important role in adjusting the geometry during the various elementary steps such that both activity and selectivity can be controlled.

While studies of intradiol catechol dioxygenation have hitherto mostly focused on mechanistic understanding, true *catalysis* with these complexes on relevant substrates is to date a largely unexplored topic. Nevertheless, the abundant guaiacyl (2-methoxyphenol) moiety in lignin is *almost* a catechol; simple ether hydrolysis could readily afford catecholic substrates.[71-74] Furthermore, in recent years depolymerisation methods have become available that allow one to obtain catecholic products directly from lignin.[75,76] While it may seem counterintuitive to go through the trouble of obtaining aromatic compounds from the lignin in order to then ring-cleave them, currently many aromatics in the petrochemical industry also serve as feedstock for non-aromatic end products, with adipic acid production being the best-known.[77] Being able to obtain such products from lignin is therefore an attractive and interesting prospect.

1.3 Aim and Outline of the Thesis

The aim of this thesis is to develop and understand new catalytic routes for the production of chemicals from lignin, with an emphasis on catalysing carbon-carbon bond cleavage reactions. Given the necessity to both depolymerise the lignin macromolecule, as well as further process the thus obtained lignin-derived small molecules, new catalytic processes for both steps are presented.

Lignin valorisation is a complex topic and its full appreciation requires the combination of various fields; *Chapter 2* therefore presents a broad overview of its biology, chemistry and catalysis. The biological synthesis of lignin and the resulting molecular structure of the material are described, as well as attempts to alter the involved biological pathways to afford lignins that can be more easily processed. The chemistry of the most important pulping methods (Kraft and organosolv) to remove lignin from the lignocellulosic biomass and the consequences this has for the isolated lignin material are discussed as well. Finally, recent research in the catalytic depolymerisation of lignin is covered. This is subdivided in a section covering mild methods, which selectively target specific bonds within the lignin, and harsh methods, which uses a regime wherein both thermal and catalytic reactions can take place. While not meant to be exhaustive, this overview highlights recurring themes and challenges in catalytic lignin valorisation.

Part I of this thesis concerns itself with the depolymerisation of lignin. In *Chapter 3* a novel lignin depolymerisation procedure is presented that combines a hydrolytic alkyl-ether cleavage step catalysed by water-stable Lewis acids with a rhodium-catalysed decarbonylation in a one-pot reaction. In studies on model compounds it is demonstrated that this tandem approach allows reactive trapping of intermediates, which would otherwise condense back to larger fragments, leading to loss of efficiency. An alternative pathway, leading to the formation of styrenes or 4-(1-propenyl)phenols, is also shown to be accessible with the same catalytic system. The desired pathway can be selected by choosing the appropriate amount and strength of Lewis acid catalyst and affords the corresponding desired products from multiple lignin sources.

Part II deals with the catechol intradiol dioxygenation reaction as a method for the valorisation of lignin-derived small aromatics. *Chapter 4* presents the first example of *catalytic* intradiol cleavage of catechol by a non-heme iron(III) complex to obtain *cis,cis*-muconic acid esters, which are shown to be easily further converted into the nylon-6,6 monomer dimethyl adipate. *Chapter 5* further expands on this route and particularly investigates the intradiol dioxygenation at elevated temperatures and pressures, allowing high activity to be obtained. In *Chapter 6* a combined experimental and theoretical study on the mechanism of the catechol intradiol dioxygenation is presented. The study resolves the mechanistic controversy presented above and highlights the properties that are required for the development of more active, novel systems.

In *Part III*, the procedures developed for catechol intradiol dioxygenation are applied to an actual lignin stream. *Chapter 7* describes the intradiol catechol dioxygenation of catechols that are obtained by depolymerisation of candlenut lignin by a copper-doped porous metal oxide catalyst and highlights some the challenges associated with transitioning processes from pure compounds to actual lignin streams. *Chapter 8* summarises the key findings of this thesis and provides a number of concluding remarks as well as suggestions for future research.

1.4 References

1   U.S. Energy Information Administration, *International Energy Statistics*, *http://www.eia.gov/cfapps/ipdbproject/iedindex3.cfm* (accessed 11th of November, 2015)

2   International Energy Agency, *World Energy Outlook 2015*, International Energy Agency, Paris, France, 2015.

3   IPCC, 2013, *Climate Change 2013: The Physical Science Basis. Contribution of Working Group I to the Fifth Assessment Report of the Intergovernmental Panel on Climate Change*, Cambridge University Press, Cambridge, United Kingdom and New York, NY, USA, 2013.

4   P. C. A. Bruijnincx and B. M. Weckhuysen, *Angew. Chem. Int. Ed.*, 2013, **52**, 11980–11987.

5   R. D. Perlack, L. F. Wright, A. F. Turhollow, R. L. Graham, B. J. Stokes and D. C. Erback, *Biomass as Feedstock for a Bioenergy and Bioproducts Industry: the Technical Feasibility of a Billion-Ton Annual Supply*, US Department of Agriculte and US Department of Energy, 2005.

6   European Parliament and Council, *Directive 2009/28/EC: The promotion of the use of energy from renewable sources,* 23 April 2009

7   D. G. Nocera, *Acc. Chem. Res.*, 2012, **45**, 767–776.

8   E. M. Nichols, J. J. Gallagher, C. Liu, Y. Su, J. Resasco, Y. Yu, Y. Sun, P. Yang, M. C. Y. Chang and C. J. Chang, *Proc. Natl. Acad. Sci. U.S.A.*, 2015, **112**, 11461–11466.

9   J. Kim, C. A. Henao, T. A. Johnson, D. E. Dedrick, J. E. Miller, E. B. Stechel and C. T. Maravelias, *Energy Environ. Sci.*, 2011, **4**, 3122–3132.

10 X.-G. Zhu, S. P. Long and D. R. Ort, *Curr. Opin. Biotech.*, 2008, **19**, 153–159.

11 C. Xu, R. A. D. Arancon, J. Labidi and R. Luque, *Chem. Soc. Rev.*, 2014, **43**, 7485–7500.

12 S. Fernado, Adhikari, C. Chandrapal and N. Murali, *Energy Fuels*, 2006, **20**, 1727–1737.

13 Y. H. P. Zhang, *J. Ind. Microbiol. Biotechnol.*, 2008, **35**, 367–375.

14 A. J. Ragauskas, G. T. Beckham, M. J. Biddy, R. Chandra, F. Chen, M. F. Davis, B. H. Davison, R. A. Dixon, P. Gilna, M. Keller, P. Langan, A. K. Naskar, J. N. Saddler, T. J. Tschaplinski, G. A. Tuskan and C. E. Wyman, *Science*, 2014, **344**, 1246843–1246843.

15 J. Zakzeski, P. C. A. Bruijnincx, A. L. Jongerius and B. M. Weckhuysen, *Chem. Rev.*, 2010, **110**, 3552–3599.

16 F. S. Chakar and A. J. Ragauskas, *Ind. Crops Prod.*, 2004, **20**, 131–141.

17 R. J. A. Gosselink, E. de Jong, B. Guran and A. Abächerli, *Ind. Crops Prod.*, 2004, **20**, 121–129.

18 M. Dusselier, M. Mascal and B. F. Sels, *Top. Curr. Chem.*, 2014, **353**, 1–40.

19 Bond Dissociation Energies, in *CRC Handbook of Chemistry and Physics, 96th Edition*, eds. W. M. Haynes, T. J. Bruno and D. R. Lide, CRC Press/Taylor and Francis, Boca Raton, FL, 2015.

20 C.-H. Jun, *Chem. Soc. Rev.*, 2004, **33**, 610–618.

21 M. Murakami and T. Matsuda, *Chem. Commun.*, 2011, **47**, 1100–1105.

22 F. Chen, T. Wang and N. Jiao, *Chem. Rev.*, 2014, **114**, 8613–8661.

23 J. Tsuji and K. Ohno, *Tetrahedron Lett.*, 1965, **6**, 3969–3971.

24 D. H. Doughty and L. H. Pignolet, *J. Am. Chem. Soc.*, 1978, **100**, 7083–7085.

25 R. K. Boeckman Jr, J. Zhang and M. R. Reeder, *Org. Lett.*, 2002, **4**, 3891–3894.

26 T. Shibata, N. Toshida and K. Takagi, *J. Org. Chem.*, 2002, **67**, 7446–7450.

27 G. S. Weatherhead, G. A. Cortez, R. R. Schrock and A. H. Hoveyda, *Proc. Natl. Acad. Sci. U.S.A.*, 2004, **101**, 5805–5809.

28 T. Hansson and B. Wickberg, *J. Org. Chem.*, 1992, **57**, 5370–5376.

29 M. D. Meyer and L. I. Kruse, *J. Org. Chem.*, 1984, **49**, 3195–3199.

30 T. Morimoto, K. Fuji, K. Tsutsumi and K. Kakiuchi, *J. Am. Chem. Soc.*, 2002, **124**, 3806–3807.

31 M. Kreis, A. Palmelund, L. Bunch and R. Madsen, *Adv. Synth. Catal.*, 2006, **348**, 2148–2154.

32 R. N. Monrad and R. Madsen, *J. Org. Chem.*, 2007, **72**, 9782–9785.

33 T. Shibata, N. Toshida, M. Yamasaki, S. Maekawa and K. Takagi, *Tetrahedron*, 2005, **61**, 9974–9979.

34   T. Iwai, T. Fujihara and Y. Tsuji, *Chem. Commun.*, 2008, 6215–6217.

35   E. P. K. Olsen, T. Singh, P. Harris, P. G. Andersson and R. Madsen, *J. Am. Chem. Soc.*, 2015, **137**, 834–842.

36   P. Fristrup, M. Kreis, A. Palmelund, P.-O. Norrby and R. Madsen, *J. Am. Chem. Soc.*, 2008, **130**, 5206–5215.

37   M. Costas, M. P. Mehn, M. P. Jensen and L. Que Jr., *Chem. Rev.*, 2004, **104**, 939–986.

38   T. D. H. Bugg, *Tetrahedron*, 2003, **59**, 7075–7101.

39   F. H. Vaillancourt, J. T. Bolin and L. D. Eltis, *Crit. Rev. Biochem. Mol. Biol.*, 2006, **41**, 241–267.

40   S. Harayama, M. Kok and E. L. Neidle, *Annu. Rev. Microbiol.*, 1992, **46**, 565–601.

41   E. I. Solomon, T. C. Brunold, M. I. Davis, J. N. Kemsley, S.-K. Lee, N. Lehnert, F. Neese, A. J. Skulan, Y.-S. Yang and J. Zhou, *Chem. Rev.*, 2000, **100**, 235–350.

42   T. D. H. Bugg, in *Iron-Containing Enzymes*, eds. S. P. de Visser and D. Kumar, Royal Society of Chemistry, Cambridge, 2011, pp. 42–66.

43   M. Suda, K. Hashimoto, H. Matsuoka and T. Kamahora, *J. Biochem.*, 1951, **38**, 289–296.

44   O. Hayaishi, M. Katagiri and S. Rothberg, *J. Am. Chem. Soc.*, 1955, **77**, 5450–5451.

45   D. H. Ohlendorf, J. D. Lipscomb and P. C. Weber, *Nature*, 1988, **336**, 403–405.

46   A. M. Orville, J. D. Lipscomb and D. H. Ohlendorf, *Biochemistry*, 1997, **36**, 10052–10066.

47   P. C. A. Bruijnincx, G. van Koten and R. J. M. Klein Gebbink, *Chem. Soc. Rev.*, 2008, **37**, 2716.

48   R. Yamahara, S. Ogo, H. Masuda and Y. Watanabe, *J. Inorg. Biochem.*, 2002, **88**, 284–294.

49   R. J. Mayer and L. Que, *J. Biol. Chem.*, 1984, **259**, 13056–13060.

50   T. Borowski and P. E. M. Siegbahn, *J. Am. Chem. Soc.*, 2006, **128**, 12941–12953.

51   M. Xin and T. D. H. Bugg, *J. Am. Chem. Soc.*, 2008, **130**, 10422–10430.

52   C. J. Knoot, V. M. Purpero and J. D. Lipscomb, *Proc. Natl. Acad. Sci. U.S.A.*, 2015, **112**, 388–393.

53   A. J. Pandell, *J. Org. Chem.*, 1976, **41**, 3992–3996.

54   A. J. Pandell, *J. Org. Chem.*, 1983, **48**, 3908–3912.

55   M. G. Weller and U. Weser, *J. Am. Chem. Soc.*, 1982, **104**, 3752–3754.

56   D. D. Cox, S. J. Benkovic, L. M. Bloom, F. C. Bradley, M. J. Nelson, L. Que Jr. and D. E. Wallick, *J. Am. Chem. Soc.*, 1988, **110**, 2026–2032.

57   H. G. Jang, D. D. Cox and L. Que Jr., *J. Am. Chem. Soc.*, 1991, **113**, 9200–9204.

58   D. D. Cox and L. Que Jr., *J. Am. Chem. Soc.*, 1988, **110**, 8085–8092.

59   M. Pascaly, M. Duda, A. Rompel, B. H. Sift, W. Meyer-Klaucke and B. Krebs, *Inorg. Chim. Acta*, 1999, **291**, 289–299.

60   M. Pascaly, M. Duda, F. Schweppe, K. Zurlinden, F. K. Müller and B. Krebs, *J. Chem. Soc., Dalton Trans.*, 2001, 828–837.

61   P. Mialane, L. Tchertanov, F. Banse, J. Sainton and J.-J. Girerd, *Inorg. Chem.*, 2000, **39**, 2440–2444.

62   N. Raffard, R. Carina, A. J. Simaan, J. Sainton, E. Rivière, L. Tchertanov, S. Bourcier, G. Bouchoux, M. Delroisse, F. Banse and J. J. Girerd, *Eur. J. Inorg. Chem.*, 2001, **2001**, 2249–2254.

63   W. O. Koch and H.-J. Krüger, *Angew. Chem. Int. Ed.*, 1995, **34**, 2671–2674.

64   A. Dei, D. Gatteschi and L. Pardi, *Inorg. Chem.*, 1993, **32**, 1389–1395.

65   P. C. A. Bruijnincx, M. Lutz, A. L. Spek, W. R. Hagen, G. van Koten and R. J. M. Klein Gebbink, *Inorg. Chem.*, 2007, **46**, 8391–8402.

66   P. Comba, H. Wadepohl and S. Wunderlich, *Eur. J. Inorg. Chem.*, 2011, **2011**, 5242–5249.

67   A. J. Simaan, M.-L. Boillot, E. Rivière, A. Boussac and J.-J. Girerd, *Angew. Chem. Int. Ed.*, 2000, **39**, 196–198.

68   T. A. Walsh, D. P. Ballou, R. Mayer and L. Que Jr., *J. Biol. Chem.*, 1983, **258**, 14422–14427.

69   G. Lin, G. Reid and T. D. H. Bugg, *Chem. Commun.*, 2000, 1119–1120.

70   G. Lin, G. Reid and T. D. H. Bugg, *J. Am. Chem. Soc.*, 2001, **123**, 5030–5039.

71   A. Baeyer, *Chem. Ber.*, 1875, **8**, 153–155.

72   H. D. Dakin, H. T. Clarke and E. T. Taylor, *Org. Synth.*, 1923, **3**, 28.

73   W. H. Perkin, *J. Chem. Soc., Trans.*, 1890, **57**, 587–589.

74   S. B. Waghmode, G. Mahale, V. P. Patil, K. Renalson and D. Singh, *Synth. Commun.*, 2013, **43**, 3272–3280.

75   K. Barta, G. R. Warner, E. S. Beach and P. T. Anastas, *Green Chem.*, 2014, **16**, 191–196.

76   E. Feghali, G. Carrot, P. Thuéry, C. Genre and T. Cantat, *Energy Environ. Sci.*, 2015, **8**, 2734–2743.

77   A. Castellan, J. C. J. Bart and S. Cavallaro, *Catal. Today*, 1991, **9**, 237–254.

Chapter 2

Lignin: Biology, Chemistry and Catalysis

Abstract

Lignin is an abundant biopolymer with a high carbon content and high aromaticity. Despite its potential as a raw material for the fuel and chemical industries, lignin remains the most poorly utilised of the lignocellulosic biopolymers. Effective valorisation of lignin requires careful fine-tuning of multiple 'upstream' (i.e., lignin bioengineering, lignin isolation and 'early-stage catalytic conversion of lignin') and 'downstream' (i.e., lignin depolymerisation and upgrading) process stages, demanding input and understanding from a broad array of scientific disciplines. This chapter provides a "beginning-to-end" analysis of the recent advances reported in lignin valorisation. Particular emphasis is placed on the improved understanding of lignin's biosynthesis and structure, differences in structure and chemical bonding between native and technical lignins, emerging catalytic valorisation strategies, and the relationships between lignin structure and catalyst performance.

2.1 Introduction

Lignocellulosic biomass, an intricate and complex architecture of three classes of biopolymers – cellulose, hemicelluloses and lignin – is an abundant and renewable resource. The separation, isolation, and subsequent chemical transformation of the three constituent polymer groups can afford a broad and multifunctional array of bio-derived value-added fuels, chemicals and materials. If these products are obtained by an integrated system of (catalytic) reaction pathways, i.e., in a so-called biorefinery operation, the maximum potential of each component and thus the biomass feed as a whole can be achieved.

Lignin, a complex and water-insoluble aromatic polymer, is derived primarily from methoxylated hydroxycinnamyl alcohol building blocks, the prototypical monolignols. Unlike cellulose, with a well-defined sequence of monomeric units that are linked by regular β-1,4-glycosidic bonds, lignin is characterised by a variety of distinct and chemically different bonding motifs, each demanding different conditions for cleavage when selective depolymerisation is targeted. Although structurally more complex, the higher carbon-content and lower oxygen content of lignin, relative to the polysaccharide or holocellulose fraction, render it an attractive feedstock for the production of biofuels and chemicals. Notably, the highly-functionalised and aromatic nature of lignin presents the potential for the direct preparation of aromatic specialty and fine chemicals, circumventing the requirement for full defunctionalisation to 'BTX' (benzene, toluene and xylenes) and subsequent refunctionalisation to desired platform chemicals. Nonetheless, owing to challenges associated with effective separation of oxygenated aromatics *via* distillation or other means, full defunctionalisation to arenes and alkanes will also be of importance for the production of chemicals and fuel components from lignin and its products. Such opportunities for valorisation together with its abundance have, amongst other reasons, motivated significant research activity into the catalytic valorisation of lignin.

An understanding of (and control over) the coupled and interdependent processing steps, for conversion of the initial biomass feedstock to the intended lignin-derived product, requires a collaborative approach encompassing a variety of scientific disciplines (e.g., genetic engineering to increase the homogeneity of the polymer or the proportion of easily-cleavable linkages, the development of effective analytical techniques for lignin structural determination, reactor engineering and improved catalytic systems for the depolymerisation of lignin and downstream processing, and related processes for product separation), as outlined in several review articles (Table 2.1).

Various reviews of lignin research are available, but they typically cover limited or specific aspects, or focus only on one or few stages of the lignin valorisation pathway. Here we aim to offer a "start-to-finish" analysis of the progress achieved in lignin valorisation,

Table 2.1: Selected lignin review articles published since 2010, highlighting different focal topics, ordered from primarily concerned with upstream (e.g., lignin biosynthesis, structure) to downstream (e.g., catalytic transformations) process steps.

Focal Topic	Ref.
Lignin biosynthesis & structure	1-9
Bioengineering of lignins	8-13
Biotic/abiotic stress and effects on lignification	6,11
Lignin depolymerisation	14
Catalytic (deoxygenative) valorisation to fuel and chemicals	15-18
Pyrolysis, hydrodeoxygenation, catalytic upgrading	19-21
Oxidative valorisation of lignin	22-24
Lignin for polymers and composites	25-30
Lignin analytics	31-37
Biodegradation of lignin	38-40

with a particular focus on the past five years, considering all of the interconnected stages of catalytic lignin biorefinering. On this basis, biosynthesis/genetic engineering of the lignin phenylpropanoid pathway, early-stage catalytic conversion of lignin (ECCL) beginning with lignocellulosic biomass, and the catalytic valorisation of isolated technical lignins to products are each discussed in sequence, where possible drawing connections between separate stages of processing. Particular emphasis is placed on the characteristics of the interunit bonding in the lignins, and the profound impact of various 'upstream' biorefining processes on the abundance of different labile (e.g., C–O) and recalcitrant (e.g., C–C) linkages (and thus also on the downstream processing of technical lignins). This chapter also aims to demystify or update several of the general statements and some of the misapprehensions often encountered in the current literature, thereby fostering a better understanding of the relationships between lignin molecular properties and the performance of catalytic systems.

This chapter is broadly subdivided into 'upstream' and 'downstream' sections – defined as the processes leading up to the separation and isolation of lignin (from the polysaccharide fraction), and subsequent depolymerisation and chemical modification of the isolated lignins to yield valorised products, respectively. Whilst this arbitrary division is imperfect (e.g., ECCL can be regarded as a combination of upstream and downstream elements), it is useful from a conceptual point of view as it mirrors the activities of the petrochemical industry.

The upstream section introduces the biosynthetic 'phenylpropanoid pathway' with the genes and enzymes involved in the biosynthesis of lignins' monomeric units. Phenylpropanoid genetic engineering strategies to give altered lignins are compared and

contrasted. Subsequently, the chemical structure and bonding properties of native or protolignin (i.e., the lignins occurring in the plant cell wall) in addition to those of some technical isolated lignins (e.g., kraft and organosolv lignins) are reviewed, showing the relationship between the severity of a depolymerisation method and the prevalence of specific bonding motifs in the isolated technical lignins. Lastly, another emerging frontier of research, the catalytic upstream refining methods based on early-stage conversion of lignin, is presented and discussed.

The downstream processing section covers the catalytic valorisation of isolated lignin streams into commodity chemicals, fuels and, discussed to a far lesser extent in this review, materials. Firstly, some relevant market and economic considerations that underpin lignin valorisation are detailed. Subsequently, an array of 'mild' (oxidative, reductive, redox-neutral) and 'harsh' lignin depolymerisation strategies are described and compared.

The final section summarises the progress made in this field of research and proposes future directions for catalytic lignin valorisation research. An exhaustive coverage of all topics relevant to catalytic lignin valorisation is, indeed, impossible owing to the breadth of lignin research. Therefore, lignin analysis methods and characterisation of lignin products are discussed only succinctly. Furthermore, a detailed discussion of enzymatic and biological downstream processes is largely omitted.

2.2 Upstream Processing

2.2.1 Bioengineering of Lignins

To improve the economic feasibility of a biorefinery, biomass must be comprehensively converted into value-added products; this includes the lignin stream. The intricate connectivity (not only by physical arrangement but also *via* actual covalent bonding) between cellulose, hemicelluloses, and lignin poses a challenge for the direct enzymatic saccharification of cellulose into glucose or, for example, to improve the digestibility of forage crops for animal feed[41]. This difficulty has motivated plant biologists to modify the phenylpropanoid biosynthesis – a multi-step, multi-enzyme biosynthetic pathway for the preparation of nine-carbon propenylated *p*-hydroxyphenyl derivatives originating from the amino acid phenylalanine (or tyrosine) – in order to modify the molecular structure of lignin and/or the proportion incorporated into the plant cell wall.[11] Modifications to the phenylpropanoid pathway may exert changes to plant fitness because the branch-points of the pathway feed into a variety of other metabolic systems essential to plant growth and development. For a comprehensive discussion, the reader is directed to a recent review article.[11]

The majority of phenylpropanoid genetic strategies have been directed towards a decrease in lignin content across plant species, with research relating to biomass conversion being targeted at hardwoods,[42-44] softwoods,[45] monocots (grasses),[46-53] and dicots (including *Arabidopsis* and alfalfa/truncatula).[43,54-74] However, an increase in saccharification yield will not boost the economics of a biorefinery operation if the lignin fraction, at 15-30 wt% of dry biomass, becomes a more recalcitrant material.

In this section, recent and relevant genetic modifications of the lignin biosynthetic pathway are discussed, providing an overview of the impact of up- and down-regulation of an array of genes for enzymes involved in the biosynthesis of lignin building blocks on the lignin structure. A survey of current literature related to structural modifications of lignin demonstrates an almost limitless potential for improved utilisation of both the carbohydrate and lignin fractions of lignocellulosic biomass, *via* catalytic processing.[2] An ideal combination of genetic modifications would yield a plant with identical or improved growth compared to the wild-type. The lignin fraction does not necessarily have to be increased or reduced in quantity, but should be constructed in such a way as to facilitate chemical (or enzymatic) deconstruction under milder conditions than currently required, e.g., by incorporating a restricted subset of linkages or precursor units.[1] Bioengineering of lignin, therefore, may aim at enhancing the saccharification yield from biomass whilst simultaneously allowing for the improved valorisation of lignin *via* subsequent catalytic treatment.[1] Optimum conditions for any bioengineering strategy will be determined, at least in part, by the targeted products, and whether these target species evolve from the carbohydrate stream or the lignin stream.

2.2.2 The Phenylpropanoid Pathway

Figure 2.1 summarises the complete phenylpropanoid pathway, outlining enzymes directly involved in the biosynthesis of the prototypical lignin monomers. These monolignols, *p*-coumaryl alcohol, coniferyl alcohol, and sinapyl alcohol, are involved in lignification, the polymerization process that creates the lignin polymer, affording the so-called 'H', 'G' and 'S' units, respectively. The phenylpropanoid pathway starts with phenylalanine (Phe), but tyrosine (Tyr) may also be consumed in monocots.[75] Phenylalanine is first deaminated to cinnamate (by the enzyme phenylalanine ammonia-lyase, PAL), and cinnamate is then hydroxylated to *p*-coumarate (by cinnamate 4-hydroxylase, C4H). If tyrosine is used instead as the starting point, this two-stage enzymatic process is circumvented and Tyr is directly converted into *p*-coumarate *via* deamination (by tyrosine ammonia-lyase, TAL, but also by PAL which is not absolutely specific for Phe).[76]

At *p*-coumarate, the sequence of enzymatic reactions may diverge to afford either *p*-coumaroyl-CoA (by 4-coumarate: CoA ligase, 4CL) or caffeate *via* a second hydroxylation of the aromatic ring (C3H or C4H). In the normal monolignol biosynthetic pathway,

Figure 2.1: Summary of the phenylpropanoid pathway focusing on the formation of native lignin monomer precursors.[11,66] Marked intermediates (*) may be introduced as a monomer or used to create a new monomer that is used in lignification following genetic modification (see Figure 2.2). Enzymes are abbreviated as follows: phenylalanine ammonia-lyase (PAL); cinnamate 4-hydroxylase (C4H); tyrosine ammonia-lyase (TAL); 4-coumarate: CoA ligase (4CL); *p*-coumarate 3-hydroxylase (C3H); shikimate/quinate hydroxycinnamoyltransferase (HCT); cinnamoyl-CoA reductase (CCR); cinnamyl alcohol dehydrogenase (CAD); caffeoyl shikimate esterase (CSE); caffeic acid *O*-methyltransferase (COMT); caffeoyl-CoA *O*-methyltransferase (CCoAOMT); ferulate 5-hydroxylase (F5H); hydroxycinnamaldehyde dehydrogenase (HCALDH).

the *p*-coumaroyl-CoA is then converted into *p*-coumaroyl shikimic/quinic acid (by hydroxycinnamoyltransferase, HCT), or *via* reduction (cinnamoyl-CoA reductase, CCR) to *p*-coumaraldehyde, which may subsequently be reduced to *p*-coumaryl alcohol (cinnamyl alcohol dehydrogenase, CAD); *p*-coumaryl alcohol is incorporated into lignin to produce H units, which are usually found in low abundance.

Caffeate can also be converted into ferulate by methylation of the 3-hydroxyl group of the ring (caffeic acid *O*-methyltransferase, COMT) to produce ferulic acid and then feruloyl-CoA (by 4CL), which is more normally considered to arise directly from methylation of caffeoyl-CoA by CCoAOMT (Figure 2.1). Feruloyl-CoA is then subsequently reduced to coniferaldehyde (by CCR). Coniferaldehyde represents the branching point between the formation of the predominant G (coniferyl-alcohol-derived) and S (sinapyl-alcohol-derived) units. The hydroxylation of coniferaldehyde (by F5H) and subsequent methylation of the product (by COMT) constitutes the major pathway toward sinap-aldehyde. The final stage for the formation of both G and S units is the CAD-catalysed reduction of the aldehyde moiety to yield the corresponding primary alcohol. Conifer-aldehyde may be recycled back into the phenylpropanoid pathway *via* oxidation of the aldehyde to yield ferulic acid (by hydroxycinnamaldehyde dehydrogenase, HCALDH).

Although, in non-specialised literature, it is generalised that just the three monolignols are the building blocks of lignins, a number of alternate monomers may be naturally introduced into the lignin structure in normal wild-type plants or through their genetic modification – the latter, in which products of incomplete monolignol biosynthesis are incorporated into the lignin (and can often also be found at low levels in wild-type plants), is discussed in Section 2.2.3.

Natural alternate monomers can also include a number of structures that remain under-appreciated for their contributions to lignins in some plants. Of particular note are the acylated monolignols, monolignol acetates, *p*-hydroxybenzoates, and *p*-coumarates.[1] Confusion has arisen with these last two products that are often incorrectly quantified as H-lignin components. H-lignin units, by definition, result from the monolignol *p*-coumaryl alcohol. The monolignol conjugates, in contrast are monolignol (usually coniferyl and sinapyl alcohol) ester conjugates of *p*-hydroxybenzoic and *p*-coumaric acids. Although *p*-coumarate esters, in particular, derive from *p*-coumaroyl-CoA on the pathway, *p*-coumarate cannot be considered to be a monolignol, nor is it a lignin mono-mer. In all cases, the monolignol moiety of the conjugate has been found to couple into lignin in the usual manner, whereas the *p*-hydroxybenzoate and *p*-coumarate moieties do not, as they remain as free-phenolic pendant 'decorations' on the γ-OH groups of the C$_3$-sidechain of lignin's various units. The reason has been deduced to be the more facile radical transfer (to more stable G and S radicals) than radical coupling.[1,77-78] Notably, as pendant esters can occur at significant levels, and indeed may be some of the easiest and more valuable products to 'clip off' from various lignin streams, they must be seen as,

and are, part of the lignin. In spite of this, they must not be confused with the monomers that enter the radical coupling reactions that typify lignification and create the polymer backbone itself.

The radical coupling products from monolignol conjugates are structurally analogous to those from the monolignols themselves except in the case of their β–β coupling or their cross-coupling with a monolignol. In each case, novel tetrahydrofuran (THF) structures result in the lignin instead of the normal resinols; it is these structures that provide the evidence that acylated lignins derive from pre-acylated monolignols.[79-81] THF structures are present to the almost complete exclusion of the resinol moieties in maize, where essentially all of the β–β-coupling appears to be from sinapyl *p*-coumarate dimerization. Similarly, THF structures are dominant in particularly highly naturally acetylated lignins (such as in curauá) where the monomers are almost exclusively monolignol acetates.[80,82] A gene required for monolignol *p*-coumaroylation has been characterised,[83-86] but the genes for analogous *p*-hydroxybenzoylation and acetylation remain unknown.

Among other important natural monomers, as reviewed,[11,87-89] are: dihydroconiferyl alcohol in softwoods that, under the oxidative conditions of lignification, can also produce guaiacylpropan-1,3-diols;[90-92] tricin, a flavonoid from another pathway entirely, only recently identified in grasses.[80,93] In addition, as reviewed,[1,94] ferulates on arabinoxylans, and the dehydrodimers (and higher oligomers) that result from them, must also be considered lignin monomers in the broadest sense, as should the tyramine ferulates that are found incorporated into various of the Solanaceae species (e.g., tobacco, tomato).

Although a wealth of research has contributed to the collective knowledge of biochemical pathways of lignin and phenol derivatives in plants, the interplay between multiple genes (general and plant-specific) as well as the effects upon lignin biogenesis have only been partially elucidated.[8,11] In this regard, it is perhaps surprising for a pathway that was long ago considered to be fully described, that new enzymes and new pathways steps continue to emerge, for example, the CSE-catalysed conversion of caffeoyl shikimic or quinic acid to caffeic acid.[66]

2.2.3 Bioengineered Lignins

Following biosynthesis of the lignin building blocks, the lignin monomers are transported to the secondary plant cell walls, whereupon they are incorporated into the lignin macromolecular structure *via* laccase-/peroxidase-induced radical polymerisation reactions, affording several structural motifs (Figure 2.1).[41] The precise roles of laccases/peroxidases in the final polymerisation of lignin monomers are at present only partially understood.[41,61,64,70,124-128] Laccases, though capable of inducing the radical reactions for the polymerisation of lignin subunits, are many and varied. They perform several

functions in plant development, rendering the identification of lignin-specific laccases difficult.[125] Nevertheless, downregulation of various specific laccases has resulted in significantly altered lignification, implying that they certainly play a role in lignification.[61,129-130] Further investigation is also required to identify individual (or groups of) *peroxidases* involved in lignin biosynthesis.[8] For example, Peroxidase 4 was recently discovered to be involved in syringyl lignin formation in *Arabidopsis thaliana*,[70] but in a mutant, a decrease in the proportion of syringyl units was seen only under optimal lighting conditions, and was also dependent on the age of the plant. This finding highlights the complexity of the interplay of biotic or abiotic stress, and how genetically engineered plants sometimes do not develop the change expected because of factors not related to genetic improvement.[131] In this context, some attempts at determining holistic effects (i.e., encompassing bioengineering and an examination of the effects on other pathways, if not on external, 'ambient' factors) have been reported.[54,107,132]

Table 2.2 summarises contemporary research relating to genetic modifications of the phenylpropanoid pathway and effects on plant structure and saccharification yield.

In general, downregulation of the genes associated with enzymes responsible for the early steps of phenylpropanoid biosynthesis, i.e., for enzymes PAL, C4H and 4CL (Figure 2.1), results in decreased flux through the pathway, and consequently lowers lignin yields (#1,2-4). Although researchers long favoured this approach of producing less of the problematic component, plants require lignin, therefore adverse agronomic effects can result if the lignin reduction is too severe.[133]

PAL downregulation results in an over-accumulation of Phe. However, for *Arabidopsis thaliana* (#1), PAL down-regulation had no observable impact on the plant phenotype, despite a significant decrease in lignin content. Incorporation of Tyr, as an alternative starting point into the phenylpropanoid pathway, may explain this result.[75]

3-Hydroxylation of *p*-coumarate by C3H was originally thought to occur at either the acid or the CoA level, until researchers showed the presence of a new enzyme, HCT, in various plants that produce *p*-coumaroyl shikimic or quinic acid conjugates that are the preferred substrates of C3H. Following the hydroxylation, HCT was conjectured to return the product to the CoA level as caffeoyl-CoA. However, again the pathway appears to be more complex as another enzyme, CSE, is now firmly established in some plants as returning the product of the C3H reaction back down to caffeic acid, upon which 4CL must again act to produce the CoA derivative.

The advantage of discovering all of the genes associated with the expression of the enzymes in the biosynthesis of lignin building blocks is that there are now more ways to perturb the system. In general, however, the main result of downregulating HCT, C3H, or CSE is a relative increase in the H-unit level. Downregulation or deficiency of HCT (Figure 2.1, Table 2.2, #20-21) leads to a significant decrease in growth, a reduction in

Table 2.2: Summary of reported genetic modifications within the phenylpropanoid pathway and their effects on saccharification yield, total lignin content, lignin composition/structure (and/or the effect on metabolites) and plant phenotype; TG (transgenic), M (mutation), ND (not determined).

#	Species	Gene Alteration	T[a]	Compositional or Structural Change in Lignin or Metabolites	LC[b]	SY[c]	Phenotypic effect	Ref.
1	*Arabidopsis thaliana*	*PAL* deficient	M	Phe over-accumulation; S/G↑ Flavonol Glycosides↓	↓	ND	No change	[54]
2	*Brachypodium distachyon*	*PAL* down-regulation	TG	S/G↑; ferulate↓	↓	2×↑	Delayed development; root growth↓	[99]
3	*Capsicum annum, C. chinense* and *Solanum tuberosum*	*C4H* upregulation	TG	S/G↑	↓	ND	Curled leaves, dwarfism, or no change	[55]
4	*Arabidopsis ref3*	*C4H* deficient	M	S/G↑; New cinnamoylmalate	↓	ND	Dwarfism, male sterility, collapsed vasculature	[56]
5	*Populus alba x grandidentata*	*C3H* down-regulation	TG	H ~100×↑; S/G↓	50%↓	ND	No change	[100]
6	*Lolium perenne*	*CCR* down-regulation	TG	No change	↓	↑	No change	[101]
7	*Arabidopsis thaliana*	*CCR* deficient	M	Ferulic acid-coniferyl alcohol ether dimers in metabolites; sinapoyl malate ~4×↓	25-35%↓	ND	Dwarfism, delayed senescence	[102]
8	*Pinus radiata*	*CCR* down-regulation	TG	Increase of *p*-coumaroyl hexose, caffeic acid hexoside and ferulic acid hexoside; H↓ and G↓	*ca.* 50%↓	↑	ND	[67]
9	Maize	*CCR* deficient	M	H-units strongly decreased; S/G slightly↑	Slight↓	↑	No change	[103]
10	*Nicotiana tabacum*	*CCR* down-regulation	TG	S/G↑; β-O-4 units↓; introduction of ferulic acid and sinapic acid	↓	↑	Orange xylem; Less severe: no change; more severe: dwarfism, collapsed vessels	[104]
11	*Populus tremula x Populus alba*	*CCR* down-regulation	TG	Ferulic acid incorporated into lignin	5-24%↓	15%↑	Less severe: no change; More severe: dwarfism Orange xylem.	[105]
12	*Populus tremula x Populus alba*	*CCR* down-regulation	TG	Oligolignols↓	↓	~20%↑	Orange-coloured wood	[105-107]

[a] Type [b] Lignin content [c] Saccharification yield, measured at low conversion extent; yields at full conversion may not differ.[123]

#	Species	Gene Alteration	T[a]	Compositional or Structural Change in Lignin or Metabolites	LC[b]	SY[c]	Phenotypic effect	Ref.
13	*Medicago truncatula*	*CAD* deficient	M	~95% Sinapaldehyde- and coniferaldehyde-derived	Increase in wall-bound lignin moieties	ND	None at 22 °C; Dwarfed at 30 °C	43
14	*Maize*	*CAD* down-regulation	TG	S/G↓	No change	↑	No change	108
15	*Triticum sinskajae*	*CAD* down-regulation	TG	H↓; S/G↑	No change	ND	Slight dwarfism	109
16	*Brachypodium distachyon*	CAD deficient	M	Increase in β-O-4- and 4-O-5-coupled sinapaldehyde units; increase in free phenolic groups	↓	↑	No change	110
17	*Pinus taeda*	*CAD* deficient	M	Incorporation of coniferaldehyde and dihydroconiferyl alcohol; Increase in vanillin, ferulic acid, *p*-coumaric acid, coniferaldehyde and *p*-hydroxybenzaldehyde	↑	↑	Dark-brown wood	91,111
18	*Panicum virgatum*	*CAD* down-regulation	TG	Hydroxy-cinnamaldehydes↑	Lignin↓ and cutin↓	↑	No change	112
19	*Koshihikari x Chugoku 117 rice*	*CAD* deficient	TG, M	ND	↓	↑	No change	113
20	*Arabidopsis thaliana*	*HCT* deficient	M	H↑; S≈0; G≈0	↓	ND	Severe dwarfism	57
21	*Populus nigra*	*HCT* down-regulation	TG	H 17×↑	No change	ND	Dwarfism	114
22	*Medicago sativa*	*CCoAOMT* deficient	TG	Incorporation of 5OH-CA producing novel 5OH-G units as benzodioxanes	~20% decrease	~10% increase in cellulose	No change	42
23	*Brown midrib-3 Maize*	*COMT* deficient	M	S/G↓; incorporation of 5OH-CA producing benzodioxanes	↓	Improved	No change	115
24	*Arabidopsis thaliana*	*COMT* deficient	M	S/G↓; trimeric moiety 5OHG-5OHG-G; benzodioxane linkages	No change	ND	No change	58
25	*Saccharum officinarum cv. CP88-1762*	*COMT* deficient	M	S↓; *p*-coumarate (on lignin)↓	6-12%↓	28-32%↑	No change	116
26	*Arabidopsis thaliana*	*F5H* deficient	M	S 70–75%↓; G↑	No change	ND	Lack of 2° wall structure in inter-fascicular and xylem fibres	65
27	*Arabidopsis thaliana*	*F5H* overexpression	TG	~100% S (i.e., G↓, S↑)	↓	No change	Decreased plant stiffness	117-118

[a] Type [b] Lignin content [c] Saccharification yield, measured at low conversion extent; yields at full conversion may not differ.[123]

#	Species	Gene Alteration	T[a]	Compositional or Structural Change in Lignin or Metabolites	LC[b]	SY[c]	Phenotypic effect	Ref.
28	*Arabidopsis thaliana*	*F5H* deficient	M	~100% G (i.e., G↑, S↓)	No change	Decrease	Decreased plant stiffness	[117]
29	*Brassica napus*	*COMT, C4H, C3H, F5H*	TG	No change	26-40% decrease in the seeds	ND	No change	[102]
30	*Arabidopsis thaliana*	*F5H* up-regulation; *COMT* down-regulation	TG	Lignin >70% 5OH-CA-derived; ~90% benzodioxane units	↓	ND	Dwarfism; male sterility	[60,119]
31	*Arabidopsis thaliana*	*CCR* and *CAD* deficient	TG	Increase in interunit bonding; incorporation of coniferaldehyde, sinapaldehyde, ferulic acid	50%↓	↓	Dwarfism; male sterility	[62]
32	*Arabidopsis thaliana*	*CSE* deficient	M	H↑	↓	4×↑	No change	[66]
33	*Populus alba x grandidentata*	*FMT* introduced	TG	Ester linkages introduced into lignin backbone; S/G↑	Little change	78%↑	No change	[44]
34	*M. sativa*	*C3H* down-regulation	TG	H 65×↑	50%↓	ND	Dwarfed	[120]
35	*Populus tremula x alba*	*F5H* up-regulation	TG	97.4%S; (i.e., G↓, S↑)	Little change	Pulp yield higher, pulp brighter	No change	[121-122]

[a] Type [b] Lignin content [c] Saccharification yield, measured at low conversion extent; yields at full conversion may not differ.[123]

the lignin quantity, over-accumulation of flavonoids, and a predictable rise in the relative level of H-units. The *c3h* mutant of Arabidopsis, called *ref8*, is a particularly stunted plant that does not produce seed but has H-only lignin. Intriguingly, however, the agronomic issues do not arise from the change to H-lignin *per se* – co-downregulating a pair of mediator genes results in recovery of seed production as well as much of the dwarfing yet retains the novel high-H lignin characteristics.[134]

To proceed toward the monolignols, *p*-coumaroyl-CoA, feruloyl-CoA, and/or sinapoyl-CoA are first reduced to the corresponding aldehydes (*via* CCR). CCR-downregulation has attracted considerable interest (#6-12), particularly in Europe, as Arabidopsis and then poplar plants proved to be significantly more readily saccharifiable, and strikingly so even in the absence of a pretreatment.[105] Plants show a small growth penalty and have lower lignin levels, but the most intriguing characteristic was that ferulic acid, as a monomer, was shown to be incorporated (at low levels) into the lignins.[106-107] As the incorporation produced novel acetal branch-points in the polymer, and as acetals are readily cleaved with acid, the analysis of CCR-deficient plants have produced another strategy for engineering lignins that are easier to chemically degrade.

The enzymatic conversion of coniferaldehyde is an important branching point in the lignin biosynthetic pathway, leading to G-units (CAD), to S-units (F5H, COMT and CAD), or back to ferulic acid (HCALDH). The overexpression of F5H with a powerful lignin promoter (#27) leads to a lignin almost exclusively composed of S-units, whereas down-regulation or deficiencies in F5H (#28) results in a predominance of G-units.[117] However, in both cases in Arabidopsis, a decrease in plant stiffness, caused by the lack of secondary plant wall structure in the interfascicular and xylem fibres, was observed.[65] For lignins composed primarily of G-units, no change in overall lignin content was observed, yet the saccharification yield of the biomass decreased, indicating the formation of a more recalcitrant biomass.[117]

Two classes of *O*-methyltransferases, the so-called CCoAOMT and COMT enzymes (Figure 2.1), are involved in producing the 3- and 5-methoxyl groups on G and S monomers. 5-Hydroxyconiferaldehyde, when 5-*O*-methylation is deficient, reduces to 5-hydroxyconiferyl alcohol that is then integrally incorporated into lignins in COMT-deficient plants (#23-24). The resulting 5-hydroxyguaiacyl units react by typical 4–O–β-coupling with any of the hydroxycinnamyl alcohol monomers (the prototypical monolignols or further 5-hydroxyconiferyl alcohol), but the internal trapping of the intermediate quinone methide product by the novel 5-OH results in the formation of benzodioxane structures in the polymer.[11,92,135-139] Benzodioxane levels can be amplified through a combination of F5H upregulation and COMT downregulation. In Arabidopsis, the resulting plants may incorporate up to ~70% 5-hydroxyconiferyl alcohol monomer and produce benzodioxane levels of as high as 90% in the polymer (#30). However, the phenotypic outcome at this extreme level was abnormal plant growth.[60,119] CCoAOMT, invoked earlier in the pathway has a similar effect on guaiacyl units and results in the incorporation of caffeyl alcohol into lignin but only in softwoods (that do not make S-lignin);[140] attempts to even downregulate both OMTs (and various genes) in hardwoods, or dicots in general, have not produced any authentic evidence for caffeyl alcohol incorporation. Furthermore, other OMTs (or other genes besides those currently targeted) appear to be implicated as even strong downregulation of CCoAOMT and/or COMT results in the production of the normal G and S monolignols, albeit at a lower level.[141]

The downregulation of *CAD*, producing the CAD enzyme that is involved in the final step of production of all conventional lignin monomers, often results in the introduction of hydroxycinnamaldehydes into lignification, resulting in various types of atypical units in the lignin structure (#14-16, 18). Both coniferaldehyde and sinapaldehyde may be introduced into the lignin structure as monomers in their own right.[42,58,60,115] Particularly intriguing was the observation that coniferaldehyde will not, *in vitro* or *in vivo*, β–O–4-cross-couple with G units and is therefore poorly integrated into gymnosperm (G-only) lignins. In contrast, coniferaldehyde readily cross-couples with S units so it,

and sinapaldehyde that readily cross-couples with both G and S units, are well incorporated into dicot lignins. Recent CAD misregulation examples show just how high the level of non-canonical monomers can be tolerated in plants that grow more or less normally, at least under some conditions. A CAD-deficient mutant of *Medicago truncatula* has reportedly some 95% of its lignin derived from hydroxycinnamaldehydes.[43] In Arabidopsis, manipulation of the G and S monomer synthesis coupled with CAD deficiency has been examined, again producing plants that have essentially none of their lignin derived from the conventional monolignols, and plants that are derived almost solely from either coniferaldehyde or sinapaldehyde.[142]

Entirely new or non-traditional monomers can be utilised in lignification, resulting in novel structures in the lignin polymer. To be completely accurate, some of these are also found in normal wild-type plants at low levels (by sensitive analytical methods). For example, downregulation/suppression of C4H, C3H, CCR, COMT or CCoAOMT resulted in the incorporation of monomers other than the three H, G, or S monolignols into the lignin structure, regardless of the plant species. The nature of the monomers that are alternatively incorporated in the lignin structure vary between species, but include: ferulic acid;[67,102,104-105] coniferaldehyde;[43,62,111] sinapaldehyde;[43,110-111] 5-hydroxyconiferyl alcohol (5OH-CA),[42,44,58,115] caffeyl alcohol,[140,143] and monolignol ferulates.[44] In addition, various new products, or enhanced levels, arise in the extractable low molecular weight metabolites from actively lignifying tissues. Examples include sinapic acid,[104] *p*-coumaroyl hexose,[67] caffeic acid hexoside,[67] and various hydroxycinnamate esters.[56] The alternate monomers that have been found incorporated into the lignin structure are summarised in Table 2.3; the monomers and metabolites are summarised in Figure 2.2.

Inspired by three independent findings regarding lignin structure, namely that 1) ferulates were excellent lignin monomers and were implicated in monocot lignification, 2) monolignol conjugates were being used in lignification in certain natural plants, and 3) monolignol substitution was becoming increasingly evident with the study of transgenics, an attempt was made to 'redesign lignin for processing'.[1,44]

In preliminary model studies, it was estimated that with ~25% incorporation of monolignol ferulate conjugates, the alkaline pulping temperature could be decreased from 160-170 °C to 100 °C for the same degree of delignification.[1] At an incorporation level of ~65% (that is likely unattainable), the pulping process on the model system could operate at just 30 °C whilst maintaining equivalent lignin removal from the biomass.[1] The insertion of ester linkages into the lignin backbone may feasibly retain the lignin quantity whilst also maintaining the natural function. In a recent investigation,[44] it was estimated that cell wall lignin could be augmented with perhaps ~7-20% of its units derived from monolignol ferulates via a specific transferase enzyme, FMT. The genetically modified biomass exhibited increased delignification and higher fibre yields after mild alkaline pretreatments compared to the control. Coniferyl ferulate and sinapyl ferulate monomer

Table 2.3: Summary of various alternate monomers incorporated into lignin, and the mutation(s) responsible for their incorporation (Scheme 2).

#	Alternate Monomer	Effect on Lignin Structure	Gene Responsible
1	Ferulic acid	New acetal branch-points in lignin	*CCR*[67,102,104-105]
2	Sinapaldehyde	Sinapaldehyde integrally incorporated into polymer, enhanced unsaturation, and increased free-phenolics	*CAD*[43,110-111]
3	Coniferaldehyde	Coniferaldehyde integrated into polymer chain in G/S lignins only, enhanced unsaturation, increased free-phenolics	*CAD/CAD-CCR*[43,62,91,111]
4	5-Hydroxyconiferyl alcohol	Benzodioxane units in polymer; linear polymer if 100% 5OHCA	*COMT, F5H-COMT*[42,58,60,115]
5	Caffeyl alcohol	Benzodioxane units in polymer; linear polymer if 100% caffeyl alcohol	*CCoAOMT*[140,143]
6	Monolignol ferulates	Incorporation of ester linkages Into the polymer backbone	*Ferulate monolignol transferase*[1,44]

conjugates may be incorporated into the lignin macrostructure analogous to that of a dimer of G, S or H units (Figure 2.2b).

In certain instances, similar phenotypic characteristics may be exhibited by the same genetic mutation for different plant species; with *Nicotiana tabacum* (Table 2.2, #10)[104] and *Populus tremula x Populus alba* (#11)[105] severe downregulation of CCR results in dwarfed plants, for example. By contrast, the same genetic mutation can also have a profoundly different result depending on the selected plant type: for CAD-deficient *Pinus taeda* (#17),[111] a slightly higher quantity of lignin is observed compared to the wild-type, yet for CAD-deficient *Koshihikari x* Chugoku 117 rice (#19),[113] a decrease in lignin content occurred. In some cases in which the plant phenotype was not affected, the saccharification yield increased regardless of the lignin content.

2.2.4 Practical Challenges of Lignin Bioengineering

Currently, the majority of bioengineering strategies have been directed towards decreasing the lignin content in order to achieve higher saccharification yields/improved fermentability. However, to ensure economic feasibility of a biorefinery, the recalcitrance of the lignin fraction must also be considered.[1] In light of this consideration, preparation of lignin with a more chemically labile structure (e.g., by incorporating some ester bonds into the backbone of the polymer rather than dealing with the more recalcitrant ether linkages) is an interesting prospect (Figure 2.2b).
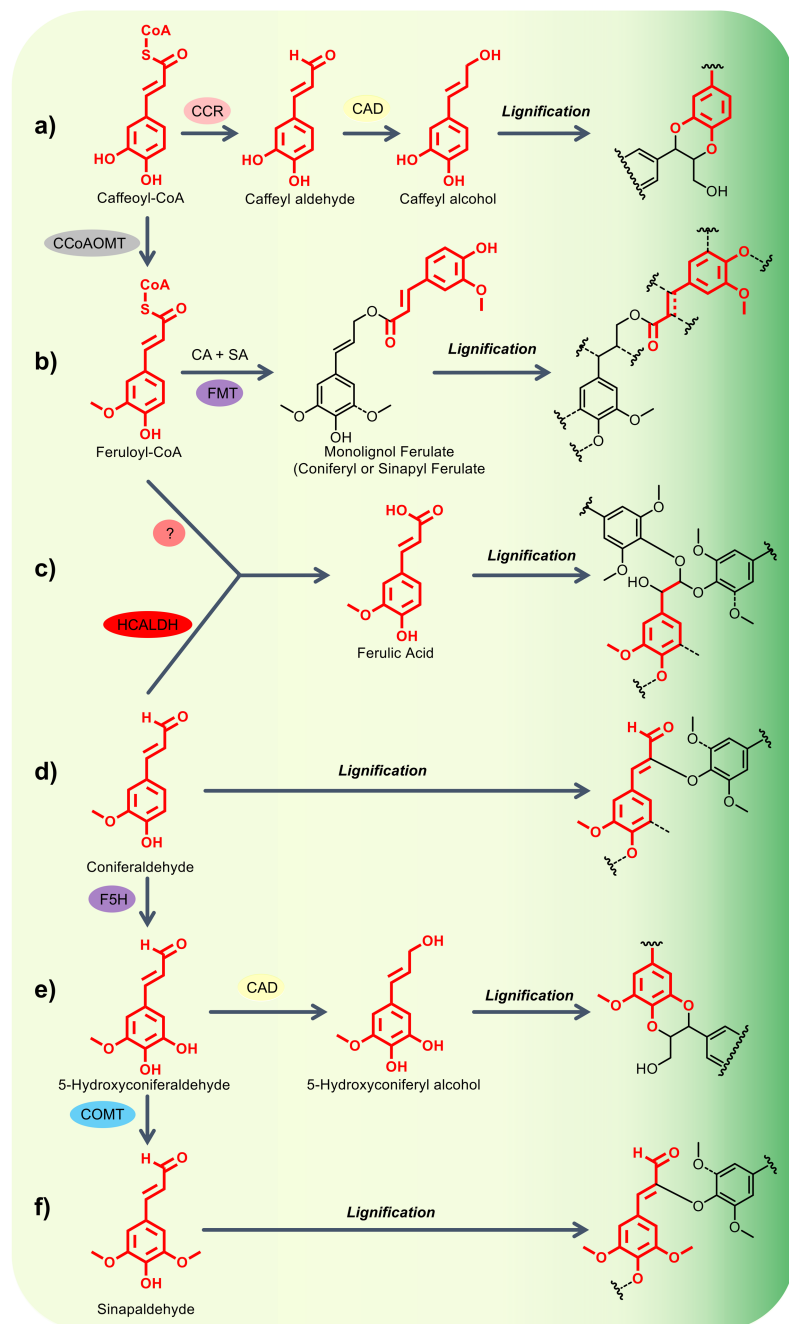
Figure 2.2: Incorporation of non-native monomers in the lignification process, *via* genetic modification to the phenylpropanoid biosynthetic pathway. The incorporation of new monomers (highlighted in red) by the same radical coupling modes gives rise to new structures in the lignin polymer (Table 2.3), mainly as a result of new opportunities for rearomatization of the intermediate quinone methides.

Research on plant improvement towards better lignin processing is a non-trivial task. One major challenge is the time required for production and growth of the biomass. For most softwoods and hardwoods, this is between 5 and 30 years.[131] To alleviate this limitation, the bulk of research on lignin bioengineering has been directed towards angiosperms with a shorter life cycle (e.g., the model dicot, *Arabidopsis thaliana* and, more recently, the model monocot, *Brachypodium distachyon*). Arabidopsis and Brachypodium are useful models of longer life-cycle analogues such as Poplar/Aspen and the commercially produced monocots (grasses), exhibiting many similar biochemical and genetic traits. Model plants are valuable for indicating possible directions for genetic alterations. Nevertheless, the strategies still need to be applied to the actual softwood or hardwood trees, or grasses, at some stage of the development, and it is crucial to not assume trait portability between gymnosperms, dicots, and monocots. Differences in the phenotypic behaviour of any one plant species may even vary according to whether the plants are grown in a greenhouse or in the field.[131] Application into readily transformable, moderately rapid growing and commercially important plants, is often via Poplar, Aspen, or Eucalypts (for hardwoods), and corn, barley, and switchgrass (for monocots); Loblolly and Radiata pine (*Pinus taeda*, *Pinus radiata*) are among the best for applications to softwoods, but the development remains difficult and slow.

Phenotypic alterations (i.e., changes in the morphology, in development, or behaviour) of a plant are common upon perturbing the phenylpropanoid pathway (although specific explanations for individual phenotypic changes are difficult to pinpoint). Dwarfism is typically accompanied by collapsed xylem vessels and, therefore, decreased water transport.[43,56-57,60,62,65,102,104-105,109,114] However, contrary to prior belief, over-accumulation of flavonoids is not necessarily associated with a decrease in plant growth.[13] The precise cause of dwarfism remains elusive.

The challenges associated with predicting plant physiology and long-term growth performance upon slight genetic modification has led to the proposal of using high-throughput multi-trait genetic modification. In this strategy, large numbers of genetically modified plants are screened for favourable growth traits at multiple stages during their life-cycle.[131] Plants are exposed to both biotic and abiotic stresses. Tolerant plants are carried on into further studies (assessed on the basis of growth, saccharifiability, and/or lignin composition) whilst non-tolerant plants are discarded. This method of high-throughput screening allows rapid identification of a plant with a lignin that can be chemically deconstructed. After this plant has been discovered, work may then be undertaken to try to identify the genetic changes responsible for the plant improvement. One high-throughput strategy for multi-trait genetic engineering, modified to include lignin screening, is illustrated in Figure 2.3.[131]

Immunostimulatory activities of different lignins depend on their structure, neutral sugar content, molecular weight, and degree of polymerisation.[144] Although research has
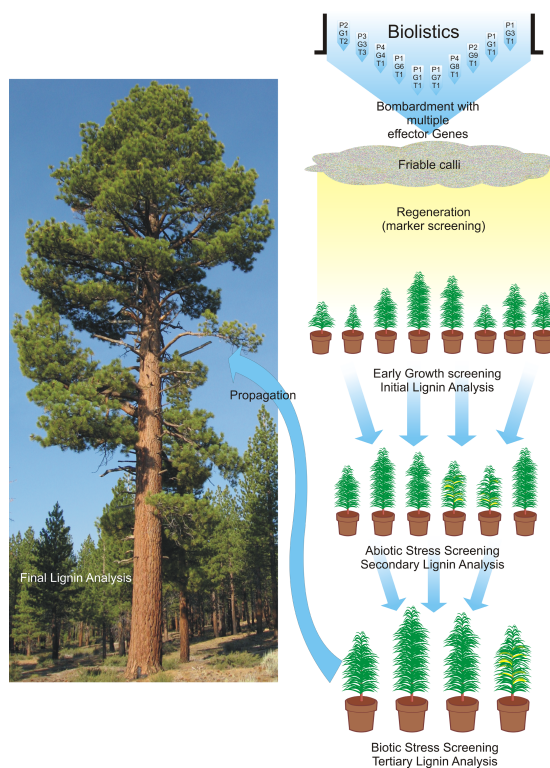
Figure 2.3: High-throughput multi-gene engineering scheme.[131] Final field trial stages are of critical importance to identify potential *environmental* impacts, (e.g., toxicity to insects, impact on soil chemistry). For a thorough review of environmental risk assessments for genetically-engineered trees, the reader is directed to other literature.[154] Adapted from *Plant Sci.*, 2013, **212**, 72-101.

been conducted on the response of lignin to abiotic stress (e.g., drought, salinity, wounding, low temperature, and UV-B radiation), these studies typically focused on how lignin quantity was affected and not on structural analysis of lignin, and therefore, there are several pending questions.[41] Abiotic stress directly impacts the formation of lignin *via* the phenylpropanoid and lignin biosynthetic pathways.[5,41,99,145-151] The response of these pathways to abiotic stresses is crucial for understanding the full biological role of lignin in the plant.[5,145] Effects of abiotic stress can be analysed either by individually introducing stresses e.g., growing the plant in a medium with high salinity),[150,152] or by monitoring how the plants perform in a greenhouse setting *vs*. in field trials.[153] Recent review literature provides a comparison of the impacts of biotic and abiotic stress on plant fitness when transferring from a controlled greenhouse environment to field trials.[131] However, even for non-transgenic tree varieties, it is hard to predict the behaviour and performance of the mature tree from greenhouse analyses.

To conclude, the rational incorporation of chemically-labile linkages into the chemical structure of lignin represents a promising area of future investigation. Furthermore, developments in 'high-throughput multi-gene engineering' will aid in identifying specific effective strategies to reduce the recalcitrance of the native lignin polymer. Notably, the wealth of variables associated with each stage of the valorisation stream (and difficulties associated with assigning the observed phenotypic changes to specific biotic or abiotic influences), in conjunction with the highly multidisciplinary nature of the research (from the initial introduction of the genetic mutation through to eventual chemical processing), render any bioengineering strategy challenging. In order to genetically engineer a more chemically deconstructible lignin whilst maintaining full functionality of the plant species, a combination of different types of expertise is required. To achieve this, long-term research objectives, funding security, and commitment from multiple complementary research teams are mandatory.

2.2.5 Structural Features of Native Lignins

Over the past three decades, plant biochemists have made significant progress in the understanding and manipulation of genes associated with the expression of enzymes involved in the phenylpropanoid biosynthetic pathway, enabling modification of the prevalence and nature of lignin's building blocks, thus altering the distribution of structural motifs or linkages as well as the content of lignin in the plant biomass. However, manipulation of the biosynthesis of lignin monomers is just one of many key variables of lignification (i.e., the polymerisation of phenylpropanoid units rendering native protolignins). In fact, the concentrations of monolignols are governed not only by their relative prevalence, following their biosyntheses, but also by the transport and diffusion of monomers to the secondary plant cell wall.[31] Moreover, other physical stress conditions (e.g., temperature, pressure, salinity and light) may dramatically affect lignification.[131] These variables may partially offset the anticipated benefits from genetic manipulation of the phenylpropanoid biosynthetic pathway.

The lignification process is induced by the action of peroxidase and laccase enzymes producing the corresponding phenolic radicals that undergo cross-coupling reactions to incorporate the monomer units into the growing lignin polymer. Certain peroxidases and laccases are believed to oxidise lignin oligomers directly.[155] In these instances, the reaction was suggested to involve a one-electron transport chain from the active site to the enzyme surface.[155-156] Despite the key roles of peroxidases and laccases in initiating the polymerisation, lignification *per se* is not an enzyme/protein-controlled process. In fact, lignification is a 'solution-like' chemical process, as evidenced by the lack of optical activity in native lignins.[155,157] This fact implies that lignification neither occurs in the proximity of an enantioselective enzyme cavity nor is affected by the chiral environment of the surrounding polysaccharides.

Although coupling of lignin monomers into the growing polymer is evidenced to take place in a combinatorial and non-stereospecific manner, i.e., lacking a specific sequence of monomers,[158] there is ample evidence for the cell's control of the composition and structure by altering monomer supply. It was long ago revealed that, in dicots, lignification proceeded from H to G to S (in overlapping regimes) with cell maturity.[159] More recently, under optimised conditions (pH 9, 488 nm excitation wavelength), fluorescence microscopy images were able to identify lignins at specific regions in Pine and Poplar cell structures that were likely enriched with G or H units.[160] An investigation of 25 Chinese hardwood biomass species demonstrated similar topochemical patterns of lignin whereby, e.g., in diffuse-porous hardwoods the vessel cell walls incorporated predominantly guaiacyl (G) lignin yet the fibres were primarily composed of syringyl (S) lignin.[161] Softwood lignins are predominantly G, although high-compression-wood zones are particularly H-rich.[162-163] There is little question that harsh and unselective delignification processes will dismantle any such arrangement of enriched domains in hardwoods, affording a more uniform distribution of units in the isolated technical lignins through the recombination of lignin fragments dissolved in the extraction liquor. However, the development of soft delignification methods may represent a novel but challenging strategy to explore for the selective extraction of (H-), G- or S-type units that has potential for reducing the costs associated with product separation in the catalytic downstream processing of lignin streams.

The advent of multidimensional NMR methods in the 1980s enabled easier characterisation of complex molecules, including lignins. Short-range ^{1}H–^{13}C correlation experiments, such as the now popular Heteronuclear Single Quantum Coherence (HSQC) experiment, have taken over from the traditional 1D ^{1}H and ^{13}C experiments that suffered from insufficient resolution to distinguish subtle structural details, and are now widely employed for the investigation of lignin composition and structure. The interested reader is referred to thorough recent review articles on the methodology, potential and limitations of NMR spectroscopy for the characterisation of lignin, even without requiring its isolation from the cell wall.[33-34] HSQC experiments have been instrumental in the identification and (approximate) estimation of the relative abundance of bonding motifs of the types **A**, **B**, **C**, **D** and **F** (Figure 2.4) and other structural elements that may occur both in untreated native lignins (e.g., spirodienone moieties, derived from β–1 coupling of a monolignol with a preformed β-ether unit),[164] and residual linkages in the depolymerised material.[165] Expansive literature, and two book chapters,[31,166] describe its application to deduce the changes in normal units and to elucidate and validate new products in the many transgenics.

Despite the obvious value of ^{1}H–^{13}C HSQC NMR spectroscopy for lignin characterisation, the information provided should not be over-interpreted. The difficulty of performing quantitative analysis is indeed an important limitation of HSQC NMR in general.
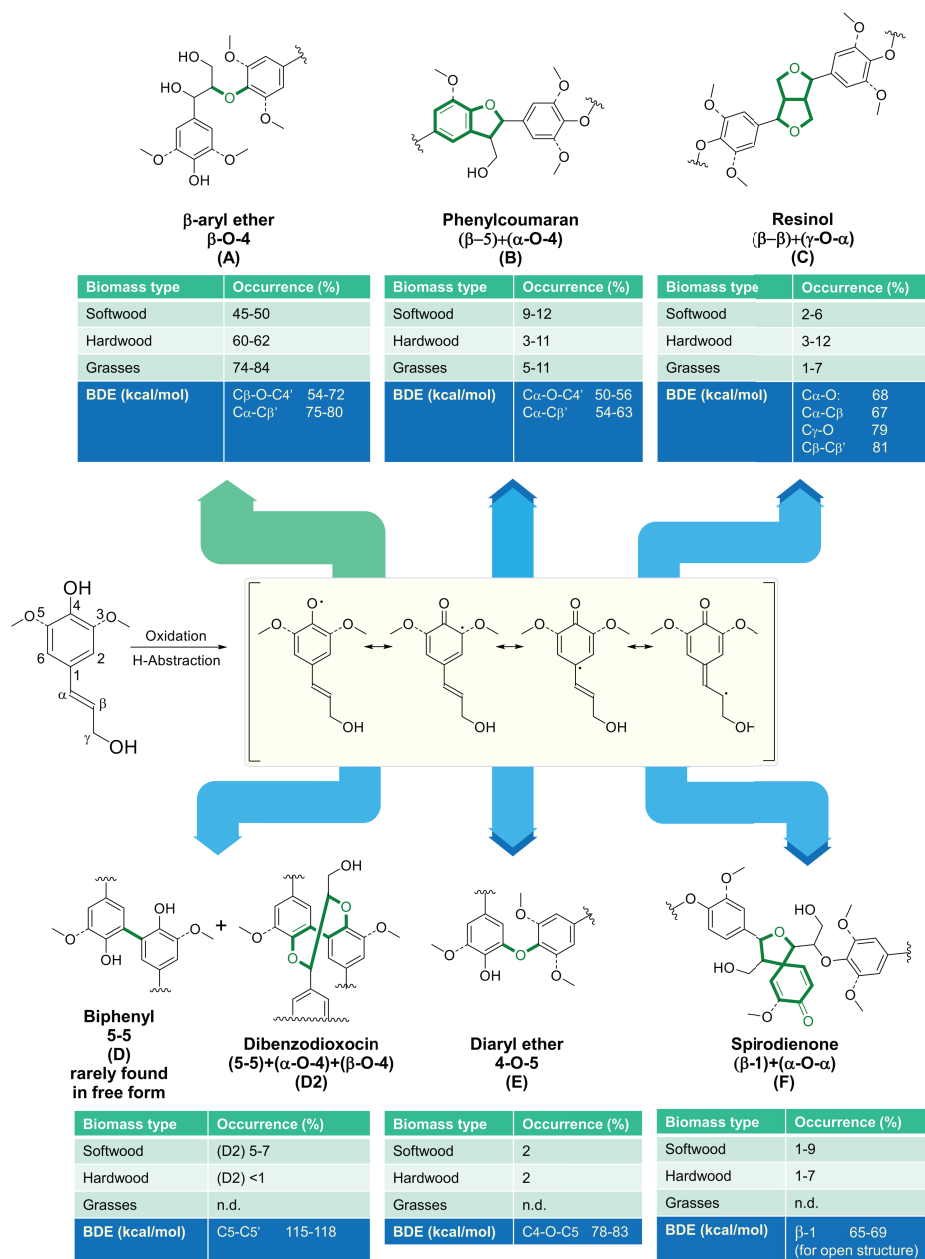
Figure 2.4: Diagram highlighting the bonding motifs and potential linkages as targets for depolymerisation (in green), % occurrence values from the literature, and bond dissociation energies for a range of commonly encountered linkages/bonding motifs in native lignins.[177-180,186-187] It is important to point out that many of these % occurrence values, although reported in the literature, are unlikely or even untenable: β–1 moieties likely do not exceed 1-2% of all structures; it is impossible to encounter 19-27% of 5–5-units in any lignin, and; the abundance of 4–O–5-linkages in softwoods is almost certainly much lower than the 4-7% claimed.

Semi-quantitative determination of integral ratios is, however, possible when the ^{1}H–^{13}C pairs are located in similar chemical environments, e.g., Cα–Hα signals for lignin side-chains or C2–H2/C6–H6 aromatic signals, because $^1J_{CH}$ assumes similar values under this condition.[165,167-168] The $^1J_{CH}$ dependence of polarisation transfer was previously an issue, with cross-peaks having different response factors. However, various adiabatic variants in particular minimise this problem. Indeed, progress has been achieved for quantitative HSQC NMR, using so-called QQ-HSQC and HSQC$_0$, with pulse sequences allowing better quantification of the identified functionalities.[169-171] However, these methods still fail for rapidly and differentially relaxing samples. For example, in lignins, correlation peaks from the more mobile endgroups, including the *p*-coumarates and *p*-hydroxybenzoates that adorn some lignin sidechains, relax much more slowly than those from units in the polymer backbone and are consequently overestimated by often large factors. Methods for overcoming such issues are still actively sought. Regardless, regular HSQC NMR experiments still offer highly valuable *semi-quantitative*, *relative* information on the linkage abundance, allowing for comparison of lignin structures and whole plant cell compositions.[167-168,172] It should also be noted that ^{31}P NMR provides quantitative data on the nature of the various OH groups in lignin, and is also capable of quantifying various of the interunit linkage types in lignins.[173]

The most common structural element in native lignins is the β-ether (usually indicated by the letter '**A**' in HSQC NMR studies of lignins, Figure 2.4), accounting for 50-80% or more of the measurable interunit linkage types. The *threo (syn)* and *erythro (anti)* forms of the arylglycerol-β-aryl ethers are present in amounts that reflect the kinetics of the proton-assisted rearomatisation of the quinone methide (by water); β-guaiacyl ethers form in approximately equal proportions, whereas β-syringyl ethers form with *erythro*-isomers predominating by ~3:1; in both cases the thermodynamic ratio is close to 50:50, indicating that lignification is not under thermodynamic control.[174-175] As for all the units in lignins, β-ether units do not possess any optical activity, implying that both the radical coupling itself and the addition of water to the quinone methide intermediate produce fully racemic products. Lignification is therefore concluded, as originally theo-rised,[176] to be simply a chemical reaction, independent of proteinaceous control.[155,158,168] DFT calculations performed on molecular models predicted values of bond dissociation energy (BDE) for the β–O–4 bond between 54 and 72 kcal/mol.[177-180] Notably, substitu-ent effects can have a significant impact on the BDE of a β–O–4 bond. For example, oxidation of the α-hydroxyl to a ketone was found to lower the BDE by 15 kcal/mol.[178]

A phenylcoumaran unit **B** has a five-membered ring that results from internal trapping of the intermediate quinone methide by the phenolic-OH following the β–5 coupling (Figure 2.4). Again it is racemic, but the ring-closure is *trans*-selective such that there is only a single isomer of the dimeric unit. DFT calculations predict the α–O–4 bond of phenylcoumaran molecular models to have a low value of BDE (50-56 kcal mol^{-1}),
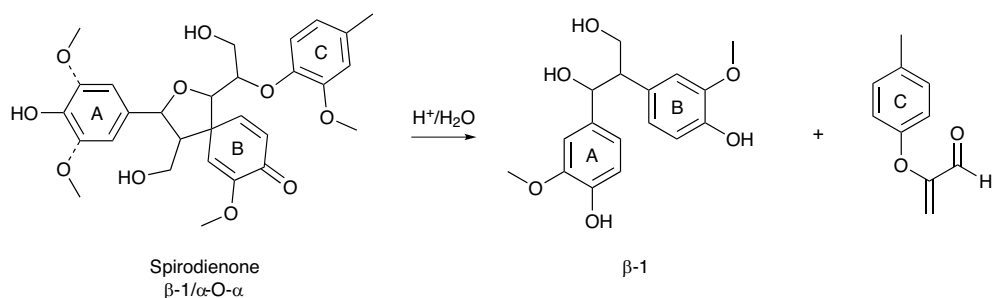
Figure 2.5: Degradation of (native) spirodienone structures under mildly acidic conditions.[164]

suggesting that these structural motifs can easily undergo radical cleavage under conditions of high severity.

Resinol structures **C** that are formed *via* β–β coupling, can only occur at the monomer stage, i.e., in dimerization or crossed dimerisation reactions. In fact, sinapyl alcohol produces syringaresinol as its only authenticated dimer in peroxidase-H_2O_2-catalyzed reactions. Structures **A** and **B** can also form directly from the coupling of coniferyl alcohol with another monolignol, but most of these structures in lignin arise from the more common monomer-oligomer cross-coupling reactions that extend the polymer chain.[155] Biphenyl linkages **D** from 5–5-coupling, that almost always result in dibenzodioxocin structures **D2** after addition of the next monolignol to the chain, are only obtained from the coupling of two preformed oligomers.[155]

In 2001, spirodienone bonding motifs ('**F**') were discovered in the structure of native lignins, shedding light on the divergence within the wood chemistry community regarding the occurrence and frequency of the β–1 linkage.[164] These spirodienone structures are particularly prone to undergo ring opening under mildly acidic conditions, leading to the formation of structures containing solely the β–1 linkage (Figure 2.5). The discovery of spirodienone structures through modern 2D NMR methods illustrates how challenging the structural elucidation of native lignins may be, as the native polymer is modified even by mild isolation methods.

It was recently suggested that the *thermodynamics* of the radical reactions leading to lignification may govern the selectivity to the formation of different bonding motifs in the native lignins (Figure 2.6). Dimerisation of lignols was explored by DFT calculations at the M06-2X/6-311++G(d,p) level of theory.[181] The formation of the β–O–4 linkage was predicted to be the most exothermic coupling reaction (for an H–H or G–G dimer, approximately 15 kcal/mol more favourable than the corresponding 4–O–5 linkage). This thermodynamic data concurs with the β–O–4 linkage being more abundant that 4–O–5 motifs. However, this prediction should not be taken as evidence that lignification is a thermodynamically controlled process. It is also important to bear in mind that
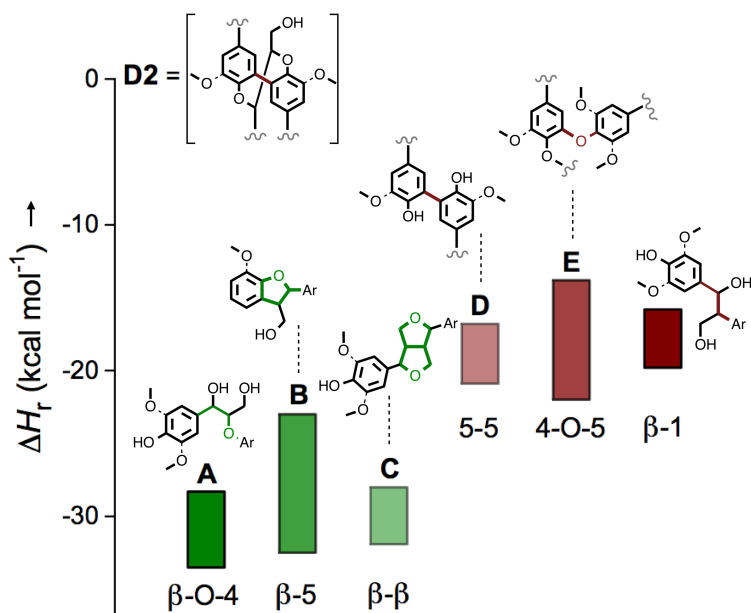
Figure 2.6: Calculated ΔH_r ranges for homo-coupling and cross-coupling reactions, yielding a variety of lignin linkages and bonding motifs (M06-2X/6-311++G(d,p) level of theory). Adapted with permission from *J. Phys. Chem. B,* 2012, **116**, 4760-4768.[181] Copyright 2012 American Chemical Society.

4−O−5 units are formed by coupling of oligomers, whereas lignification is mostly the result of sequential addition of monomers to the chain; the formation of β-ether units would therefore prevail over 4−O−5 counterparts, regardless of the thermodynamics. Most importantly, there is convincing evidence that the processes leading to the formation of lignin linkages are instead kinetically controlled, as previously noted.

From the DFT predictions, the enthalpy values for self-/cross-coupling reactions of lignols become gradually less exothermic values in the order: β−O−4 > β−β > β−5 >> 5−5 > β−1 > 4−O−5.[181] Not surprisingly, this ranking contradicts that originated from BDE values (Figure 2.4), giving the false impression that β−O−4 linkages would be the most stable against homolytic cleavage of the C–O bond. Notably, one should consider that the initial and final states for the studies on BDE and heat of dimerisation of lignols are not identical. Accordingly, these sets of theoretical predictions cannot directly be compared.

The absence, or at least extremely low abundance, of non-cyclic α−O−4 linkages, in addition to the discovery of eight-membered ring structures **D2**, constitute an important update to the classical models of lignin proposed by Nimz (1974)[182] and Adler (1977).[31,183] These dibenzodioxocin motifs became recognised as crucial branching points in native lignins.[184] However, various researchers have so far found evidence only for structures of

type **D2** in which the added monolignol unit remains free-phenolic (to form a 'U' type branch).[185] Although **D2** units could also implicate the joining of three chains, there is currently no evidence that **D2** units forms a true 'Y' branch. The same can be said for 5–O–4-units in lignins. If this is the case, then lignins must be thought of as essentially linear, and not branched to any significant degree. Indeed, although lignins are referred to as 'polymer networks', the quantity of condensed structures (i.e., aromatic units linked to others *via* their 3 or 5 ring positions in ways that form Y-type structures) occurring in native lignins is now understood to be very low,[184-185] which at least in part explains the ease of depolymerising native lignins. This observation is in strong contrast with technical lignins, for which prior upstream treatment often results in a highly condensed structure (as discussed in further detail later in this chapter).

The progress made in the identification of native substructures of lignin, elucidated largely by NMR methods and validated using synthetic model compound data, allows for accurate identification of specific linkages/bonding motifs occurring in lignins. It has been noted that 2D NMR is capable of pinpointing only a fraction of all the linkages because detection by HSQC is limited to C–H fragments *a priori*, with the technique being blind to other linkage patterns containing non-protonated tertiary or quaternary carbons, such as in 5–5 (biaryl) and 4–O–5 (biaryl ether) structures.[168] However, this is not actually true. Essentially all of the 5–5-linked units in native lignins are in the form of dibenzodioxocins **D2** that are easily seen, well dispersed and, in principle, quantified. Even the 4–O–5 structures leave signatures, because their C2–H2 and C6–H6 correlations are unique (at least in the G-only softwoods).

Finally, it is important to note that as polymer growth occurs, the likelihood of observing two identical lignin macromolecules becomes vanishingly small.[88,158] On this basis, the sequencing of lignin building blocks in a similar manner as performed for amino acid residues (in 'proteomics') is impossible and, in any case, of limited value for the design of catalytic lignin conversion processes. Strategies for lignin conversion ought to be designed bearing in mind the occurrence of linkage/bonding motifs rather than a specific macromolecular structure. Due to lignin's racemic nature, its complexity, and its largely unknown associations with other cell wall polymers many macromolecular aspects of the structure remain elusive.

2.2.6 Structural Features of Native Lignins

Native lignins undergo extensive chemical transformation as a result of pulping or pretreatment processes. The extent of structural modification hinges upon the process 'severity' (i.e., temperature and duration of cooking and concentration of pulping).[188-193] The abundance of different C–O and C–C linkages in technical lignins, therefore, are likely to differ substantially from those determined for the native lignin,[190,194] a realisation that

greatly impacts any choices for further depolymerisation. An example of the impact of pretreatment severity on the nature of the lignin isolated is shown in Figure 2.7, in which mild acetolysis produces a lignin high in β-ethers, whereas almost no native lignin identity remains following the harshest pretreatment.

Structural characterisation (*via* 2D NMR and/or chemical degradation methods, e.g., acidolysis, thioacidolysis, *etc.*) of the technical lignins before catalytic treatment, and any remaining technical lignin after catalytic treatment, must become common practice in this field. The effectiveness of a catalyst either for performing a particular chemical transformation or for the cleavage of a specific linkage can then be better assessed.[194] Such a strategy circumvents the difficulties associated with the limitations of simple model compounds. Indeed, these often offer a poor representation of the actual lignin structure (reactions on model compounds are discussed in greater detail later in this chapter), and such results can thus typically only with difficulty be extrapolated to 'real' lignins. Model compounds of high structural fidelity can nonetheless provide valuable insight and aid in the elucidation of changes in the lignin structure upon catalytic processing. For instance, in the oxidation of kraft lignin with DDQ, the characteristic resinol (from β–β-coupling) signal was found to disappear. The reaction performed on a model compound of appropriate complexity allowed for the identification of an unexpected pyron-4-one product.[196] It is also worth noting that model compounds can be particularly useful for screening for the best reactions and conditions. Thus, although there is no guarantee that a reaction that works well on a model compound will also perform well on an actual lignin sample, the converse is almost always upheld, i.e., it is almost universally true that little is to be expected of a reaction on lignin if that reaction does not perform well on a lignin model compound of sufficient fidelity.

The distinct bonding features of technical lignins are described in the following subsections, describing the predominant structural modifications brought about by kraft and organosolv processing and their implications for catalysis. Herein, emphasis is placed on these two specific pulping processes for two main reasons. Firstly, kraft pulping is operated on a large scale commercially, producing the largest volumes of lignin-containing streams.[197] In addition, the chemistry of organosolv pulping underpins the novel class of valorisation processes referred to here as 'Early-stage Catalytic Conversion of Lignins' (ECCL) or the 'Lignin-first' strategy.[198]

2.2.6.1 Kraft Pulping Process

Globally, the kraft process is the dominant technology of the pulp and paper industry. Approximately 130 million tons of kraft pulp are generated annually.[197] Surprisingly, this technology is one of the few persistent examples of a chemical organic process, performed at a million-ton-scale, that is stoichiometric and not catalytic. The kraft process
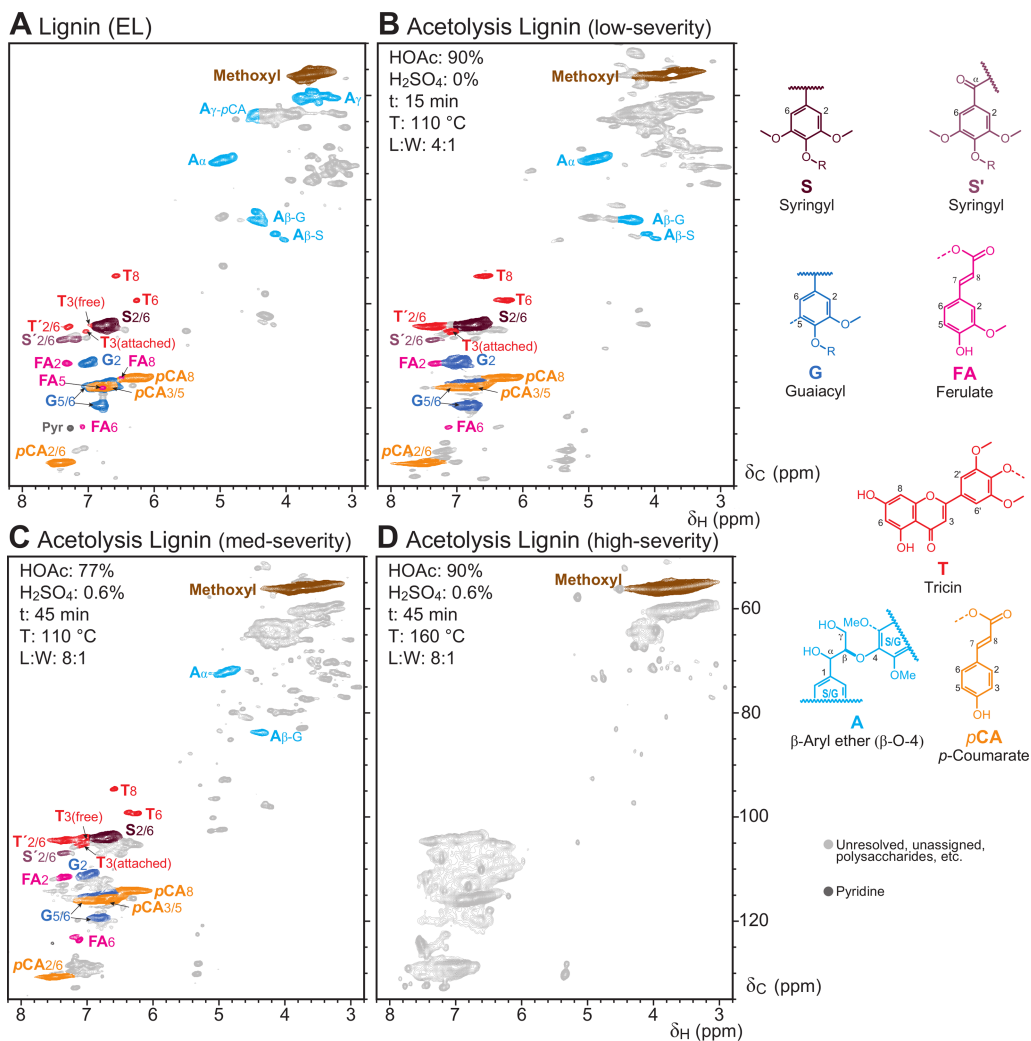
Figure 2.7: Influence of pretreatment severity on the nature of a processed lignin as revealed by HSQC NMR spectroscopy. Here, a comparison is drawn between A) a maize Enzyme Lignin (EL), isolated in the lab, with B-D) lignins that are precipitated from an acetosolv process,[195] in which acetic acid is the organic solvent. As can be seen by examining especially the β-ether **A** correlations (cyan) but also the general nature of the aromatics, the mild process in B) produces a rather native-like lignin, with β-ethers largely intact, and only a little 'distortion' of the aromatics; the 'lignin' does however contain significant levels of polysaccharide-derived material (as seen by the additional grey peaks). With the medium-severity treatment, which uses added mineral acid and a lower level of AcOH, β-syringyl ethers have disappeared, the β-ether level in general is lower, more tricin has detached from the polymer, and the aromatics are decidedly more complex. Under the highest severity conditions, in D), no recognizable structural features (other than methoxyl and general aromatic signals) are evident – it has no β-ethers. L:W = liquor to wood ratio. Contours in the NMR spectra, where they are sufficiently well resolved, are colour-coded to match the structures below; overlapping peaks are simply colored gray along with peaks from polysaccharides or other unidentified materials.

originated in 1879 in Danzig, Prussia (nowadays Gdańsk in Poland). It is so-named after the German word for 'strength', because of the superior resilience of the pulps *vs.* those obtained from the earlier soda and sulfite processes. The long-term success of the kraft process lies in the recyclability of the inorganic pulping agents ($Na_2S/NaOH$) and, more recently, in the efficient generation of electricity by the kraft recovery boiler.[197] In the boiler, the black liquor obtained from the pulping step (which contains the lignin fraction) is incinerated and Na_2S is regenerated ($Na_2SO_4 + 2C \rightarrow Na_2S + 2CO_2$), i.e., the lignin's carbon is employed as a reducing agent. The boiler produces high-pressure steam that powers turbo-generators.[197] Modern kraft mills generate a considerable electricity surplus, which is often sold back to the local electrical grid.[199] Considering the global scale of the process (incineration of lignin generates ~700 million tons of high-pressure steam per year),[200] kraft lignin actually constitutes one of the world's most important biofuels.[199] Notably, kraft lignin black liquor represents the largest share of renewable biofuel in the Finnish and Swedish energy matrices.[199]

Although kraft lignins currently constitute the largest lignin stream by volume, they are not available commercially in isolated form in the same abundance. This is because the black lignin liquor plays a key role as an internal energy supply and to recover the inorganics used in the pulping process. Nonetheless, the diversion of a fraction of kraft lignin away from fuel use and towards the production of bulk, specialty or fine chemicals may be economically viable if the price of a lignin-derived product exceeds the price of electricity, once all further downstream costs (i.e., for lignin isolation from the alkaline liquor, neutralisation, chemical transformation, product separation and purification) are accounted for. Despite recent advances, there are currently no widespread catalytic processes for the valorisation of kraft lignins into bulk or fine chemicals. This can at least partly be attributed to the highly complex and condensed nature of the kraft lignin, with a prevalence of highly recalcitrant linkages/bonding motifs in addition to a considerable sulfur content, an established catalyst poison. These properties of kraft lignins render them challenging feedstocks for downstream catalytic valorisation.

Delignification of wood fibres can be regarded as a heterogeneous process in which lignin is "peeled" away from the residual lignocellulosic matrix *via* lignin depolymerisation.[201] In the kraft process, the wood fibres are treated with 'white liquor' (a 1 mol L^{-1} NaOH and 0.25-0.70 mol L^{-1} Na_2S aqueous solution) at temperatures of 165-175 °C. The process is maintained at this maximum temperature for 1-2 h, depending on the type of wood feedstock, the desired extent of delignification, and the exact digestion temperature.[202] Throughout the pulping process, it is essential to ensure a liquor pH value >10, to avoid re-deposition of lignin residues onto the remaining cellulosic fibres.[203] The degradation and solubilisation of lignin fragments from Spruce wood into the cooking liquor, as a function of time and programmed temperature, is displayed in Figure 2.8a.[188] The quantification of β-ether units (as inferred from analytical acidolysis) of kraft lignin
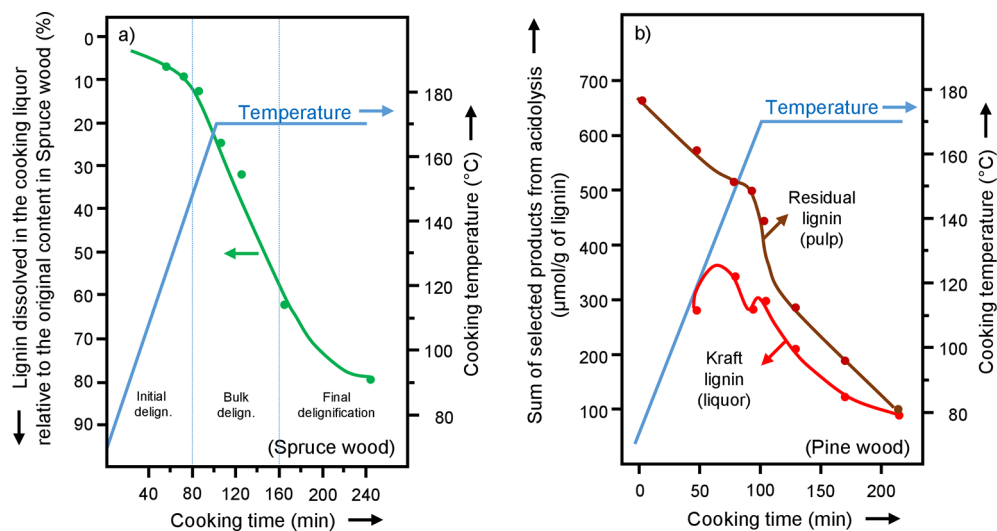
Figure 2.8: Reaction profiles for kraft delignification of two native softwood biomass feedstocks: (a) evolution of Spruce wood lignin into the liquor (green) as a function of cooking time and temperature, and; (b) the quantification of β-ethers in Pine wood lignin (quantified *via* analytical acidolysis), isolated from the liquor (light red) and residual lignin in the pulp (dark red), as a function of cooking time and temperature. For each graph, the programmed temperature (blue) increases steadily up to a fixed maximum of 170 °C.[188,190]

from Pinewood, both isolated from the liquor and residual in the pulp (functions of time and programmed temperature), are displayed in Figure 2.8b.[190]

The evolution of lignin into the liquor can be categorised into three approximate stages: *initial* (0-15%), *bulk* (15-60%) and *final* (60-90%) delignification (shown for Spruce kraft lignin in Figure 2.8a).[188] Analysis of the evolution of β-ether content in kraft lignins provides valuable insight into the design of future catalytic valorisation technologies. During initial delignification, the lignin dissolved in the liquor still has significant quantities of β-ether units (approximately half of that estimated for the residual lignin in the pulp).[193] On this basis, it is a reasonable assumption that the lignins following initial treatment will still exhibit good reactivity under mild conditions, as the subunits are linked largely *via* these relatively weak ether linkages. However, during the bulk delignification stage, the content of β-ethers drastically decreases for both the liquor-phase (kraft) and solid-residue lignins.[190,203-204] At the final delignification point, both lignins exhibit approximately one seventh the content of β-ethers present in the initial native lignin, as inferred from analytical acidolysis data.[190] Recent HSQC NMR characterisation confirmed some β–O–4 and other bonding motifs (e.g., phenylcoumaran (β–5) and resinol (β–β) structures) are still present in a kraft lignin, albeit indeed with very low abundance.[196]

a) Cleavage of non-phenolic β-ethers under alkaline conditions (slow reaction in both soda and Kraft processes)

Further degradation
(enol ether formation,
condensation, and several
other reactions)
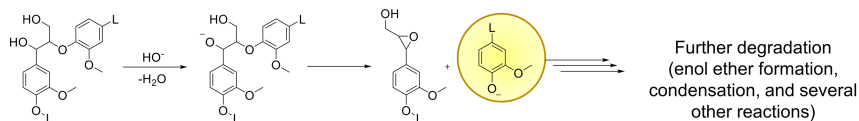
L: Lignin backbone

b) Cleavage of phenolic β-ethers under alkaline conditions
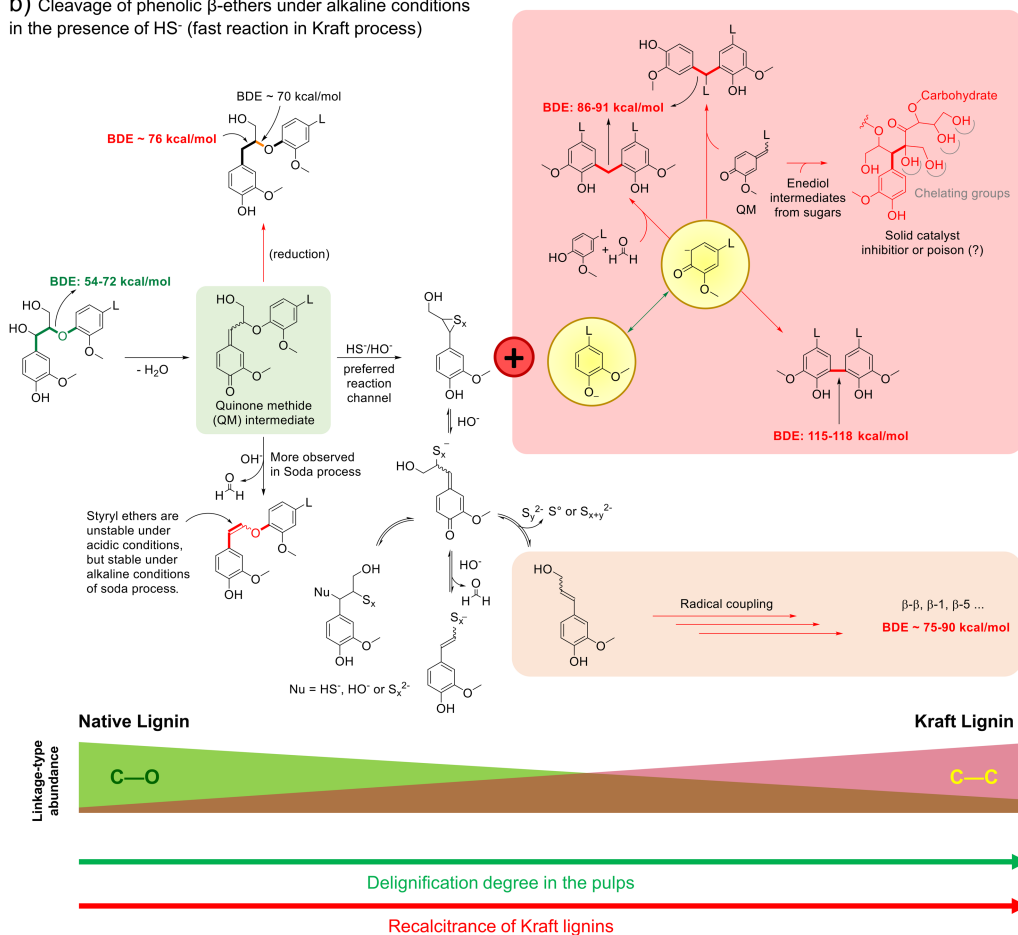in the presence of HS⁻ (fast reaction in Kraft process)

Figure 2.9: Reaction pathways for the conversion of β–O–4-rich native lignins to recalcitrant and highly-condensed/cross-linked kraft lignins *via* a quinone methide (QM) intermediate (shaded green). The kraft lignins are characterised by C–C linkages with high bond dissociation energies (~86-118 kcal/mol, shaded red).[203] For clarity, the scheme depicts only G-units.

β-Ether units predominate in native lignins. Therefore, a substantial level of research has been devoted to understanding the fundamental aspects of β-ether cleavage under the kraft processing conditions. Detailed information regarding the mechanisms involved

is contained in several recent book chapters.[203-204] Represented in Figure 2.9 is a network of reactions underpinning the formation of recalcitrant, highly-condensed and cross-linked (C–C) kraft lignin from native feedstocks rich in β-ether (C–O) linkages.

Kraft pulping shares one of its major depolymerising reactions with that of soda pulping, the cleavage of internal, non-phenolic β-ethers occurring in native lignins via an epoxide mechanism (Figure 2.9a). The second major depolymerising reaction, which is exclusive to the kraft process, involves the trapping of quinone methide (QM) intermediates in an essential step in the cleavage of free-phenolic β-aryl ethers, including those that get produced by these non-phenolic β-ether cleavage reactions (Figure 2.9b).[203,205] Under the conditions of the kraft process (HS⁻/OH⁻), the QM undergoes addition of nucleophilic HS⁻, followed by the elimination of a phenolate species via anchimeric assistance and formation of a thioepoxide.[203] This is the particular reaction that explains the improvement seen upon introduction of sulfide (and the HS⁻ produced during the process) to the earlier soda (NaOH-only) process. In soda pulping, the retro-aldol elimination of g-CH_2OH as formaldehyde from the QM occurs more frequently. Such a transformation leads to styryl ether (sometimes called by the less specific term, vinyl ether) structures that are quite stable under alkaline conditions (but are prone to hydrolysis under acidic conditions).[203] More importantly, the formaldehyde released in the soda process can react with any free-phenolic guaiacyl unit (at its 5-position) where subsequent *o*-QM formation and condensation at C5 with another phenolic unit can result in additional condensation producing diphenylmethane structures (Figure 2.9b shaded in red).[206]

The actual reactive species in kraft pulping is not the sulfide (di)anion, but rather the hydrosulfide anion, HS⁻, as noted above. Partial oxidation of HS⁻ generates polysulfide species (S_x^{2-}) that are assumed to promote one-electron transfer reactions.[204] However, the redox sulfur chemistry involved remains poorly understood. The sulfur-containing lignin species may undergo a variety of subsequent reactions, leading to deoxygenation of the alkyl side chain. Subsequent radical coupling with lignin-derived monomers partially regenerates oligomeric species (Figure 2.9, shaded in beige). Under the harsh conditions of the kraft process, the radical couplings are under thermodynamical control. Consequently, multiple alternate and highly stable C–C cross-linked structures (for example, β–β, β–1 and β–5) are formed, replacing the C–O bonds found in native lignins.[203,207]

Several investigations have demonstrated the kinetic resolution of β-ether diastereoisomers under kraft (or soda) processing conditions. As can be readily predicted from the anti-elimination mechanism in which the nucleophile, the –S⁻ on Cα, must attack from the opposite side of the O-aryl leaving group, the *erythro* isomers were found to be cleaved faster than *threo* isomers by studies performed on both model compounds and true lignocellulose.[188] As a result, *threo* isomers of the β-ether units will predominate in the residual kraft lignin.[188]
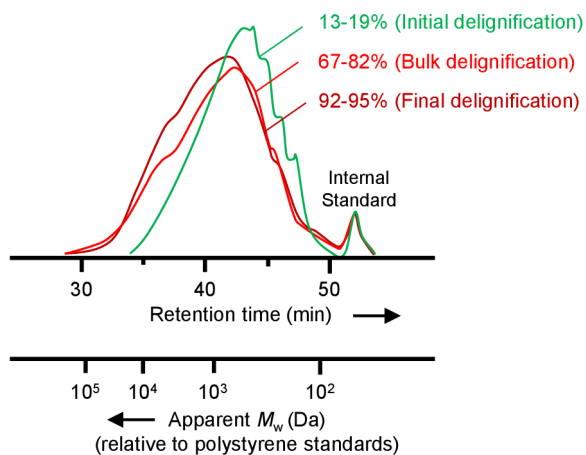
Figure 2.10: Superimposed Gel Permeation Chromatography (GPC) traces of the black liquor obtained following varying extents of delignification from Pine wood.[190]

The reduced β-ether structures, containing the deoxygenated α-CH$_2$ groups (Figure 2.9), are relatively stable under the kraft pulping conditions.[203] These structures are thus a valid target for catalytic processing *via* hydrogenolysis, as they are more refractory than the original β-ether units towards acid-catalysed hydrolysis. The high BDE values (~76 kcal mol^{-1}) for such deoxygenated bonding motifs (approximately 20 kcal mol^{-1} higher than the most labile β–O–4 linkages) suggest that they will be far more resistant to (homolytic) cleavage.[178]

Under the harsh conditions of the kraft process, the free-phenolic guaiacyl units are prone to undergo multifarious repolymerisation processes (Figure 2.9, region shaded in red).[203,205] Accordingly, there is a noticeable increase in molecular weight of lignin fragments in the liquor (i.e., those peeled from the lignocellulosic matrix) measured at the three stages (initial, bulk and final) of delignification (Figures 2.8 and 2.10).[191] As noted above, formaldehyde, liberated by the elimination of γ-CH$_2$OH groups, plays a critical role in the repolymerisation process but this formaldehyde elimination is markedly less problematic in kraft pulping than in the soda process.[203] In addition, lignin condensation reactions (some involving QM intermediates), the cross-condensation of lignin fragments with reducing sugar end groups on polysaccharide polymers, oxidative coupling of phenolic guaiacyl units forming biphenyl (5–5-linked) structures, and radical cross-coupling processes are also viable reaction channels creating refractory structural motifs.[203,207] Regardless of the exact mechanism, the repolymerised oligomeric and polymeric lignin fragments are characterised by very strong, highly recalcitrant C–C linkages (BDE: 70-118 kcal/mol).[178]

Repolymerisation of lignin fragments during the kraft process, therefore, poses not only *kinetic* challenges associated with catalysis, but also impedes the overall *thermodynamic* efficiency of downstream processing. In fact, the thermodynamic costs associated with breaking stable C–C bonds will invariably be ~30-60 kcal mol^{-1} higher (Figure 2.9) than those required for the cleavage of β-ether linkages in native lignins. Thereby, it is highly desirable to 'tune' the kraft process in order to avoid recondensation of the lignin fragments. Unfortunately, this is not a trivial task, due to the multitude and chemical variety of repolymerisation channels.[205] Alternatively, continuous extraction of monomeric and oligomeric species from the black liquor could be an effective strategy, and would alleviate problems associated both with the self-condensation of lignin and the condensation of lignin with hemicellulosic sugars.[208] The removal of soluble carbohydrates is also desirable so as to avoid problems in subsequent downstream processing. As a case in point, it was recently shown that the presence of carbohydrates in the feed exerts a negative impact on the HDO reaction of guaiacol, taken as a model compound for lignin-derived phenolics, over Ru/C catalysts.[209]

In conclusion, although modification of the already highly optimised kraft process is conceivable, it is important to consider that, at least at present, high-quality cellulose fibres remain as the primary target because of their value (kraft pulp global prices at 600-800 US$/ton as of January 2016).[210] Accordingly, a productive line of investigation would be to devise an optimised system for maximising both the cellulose pulp quality and the quality of lignin (i.e., improving its susceptibility towards mild downstream valorisation), rather than exclusively focusing on the development of improved catalysts for treatment of highly-condensed kraft lignins. In fact, most technologies for (reactive) lignocellulose fragmentation have been developed with maximisation of the potential of the cellulosic fibres in mind, with lignin considered mainly as a by-product, or worse, as a waste. However, there is a growing recognition that if future biorefining operations are to be commercially successful, valorisation also of the lignin fraction is mandatory.

2.2.6.2 Pulping with Organic Solvents: Organosolv Lignins

One of the serious drawbacks of kraft pulping is the emission of malodourous organosulfur compounds.[197,204] This problem has long motivated the search for more environmentally-benign alternatives. In this context, pulping with organic solvents was first reported in 1931 as an alternative to processes based on sulfurous chemicals.[211] At temperatures of ~180 °C, the treatment of wood chips in aqueous ethanol (1:1 vol/vol) was demonstrated to be effective at releasing a major fraction of lignin and hemicelluloses into the solution, enabling the isolation of high-purity cellulosic fibres.[211] Despite this valuable finding, pulping in organic solvents remained a dormant field until the late 1960s, after which research activity intensified.[212] At that time, the umbrella term 'organosolv' was established, in reference to the many variants of delignification processes performed in

organic solvents.[213] In this section, properties of organosolv lignins derived from treatment with and without added acid are discussed, owing to their importance for cellulosic biorefineries.[214-217] Organosolv processes performed under alkaline conditions have also been the focus of some investigations.[212] However, their chemical features are similar to those of aqueous alkaline processes (e.g., the soda process, Figure 2.9a).

Organosolv processes have been commercially evaluated at pilot-scale. One notable example is the Alcell process developed by *Repap Enterprises Inc.* (acquired by *UPM-Kymmene Corporation* in 2000). The demonstration plant yielded over 5,000 tons of pulp from various northern hardwood feedstocks, generating consistent data, and the process was considered competitive with established kraft pulping.[218] Despite the great potential of the more environmentally benign organosolv technology for pulping of lignocellulose, no process has yet survived longer than five years of operation at demonstration scale. Notably, as the installation of a kraft mill represents a multi-billion € investment, the replacement of well-established technology is difficult and requires regulation to change the global industry. Moreover, unlike the kraft process in which kraft liquor is incinerated to recover the inorganics, in the organosolv processes the incineration of the organosolv liquor is prohibitive as it destroys the organic solvents used in the pulping process. This makes solvent recovery, and therefore, lignin isolation mandatory. Recent optimisation of the Alcell process has centred on the pretreament of plant biomass for enzymatic saccharification of cellulose.[216,219-221] In this context, *Lignol Innovations Corporation* was the proprietor of an integrated process involving solvent pretreatment of lignocellulose, saccharification, fermentation, and product recovery procedure.[222] Once again, the process was not brought to commercialisation. Tentatively, one primary cause may be the relative lack of high-value applications to absorb the high-quality, sulfur-free isolated lignins, as suggested by techno-economic analyses recently performed on organosolv processes.[223-224]

A variety of viable organosolv solvent/water mixtures has emerged over the past 50 years. Typically, the organic solvent is a low-weight primary alcohol (e.g., methanol, ethanol), a cyclic ether (e.g., 1,4-dioxane, tetrahydrofurfuryl alcohol), a ketone (e.g., acetone), or a diol (e.g., ethylene glycol), in order to effectively dissolve the liberated lignin and hemicelluloses.[212] Low-molecular-weight alcohols are favoured for their high volatility, and their consequent ease of removal after cooking. For improved delignification of the pulps, the organic solvent/water mixture must exhibit a Hildebrand parameter (δ) of approximately 23 ± 2 MPa$^{1/2}$, which corresponds to the solvent parameter of lignin.[225] The organic solvent/water mixture plays at least two crucial roles in an organosolv process:[226-227] (1) the *impregnation* of the plant tissue (transferring the catalyst or reagent to the lignin through the polysaccharide matrix), and (2) the *transport* of the soluble lignin fragments from the matrix to the bulk solution.
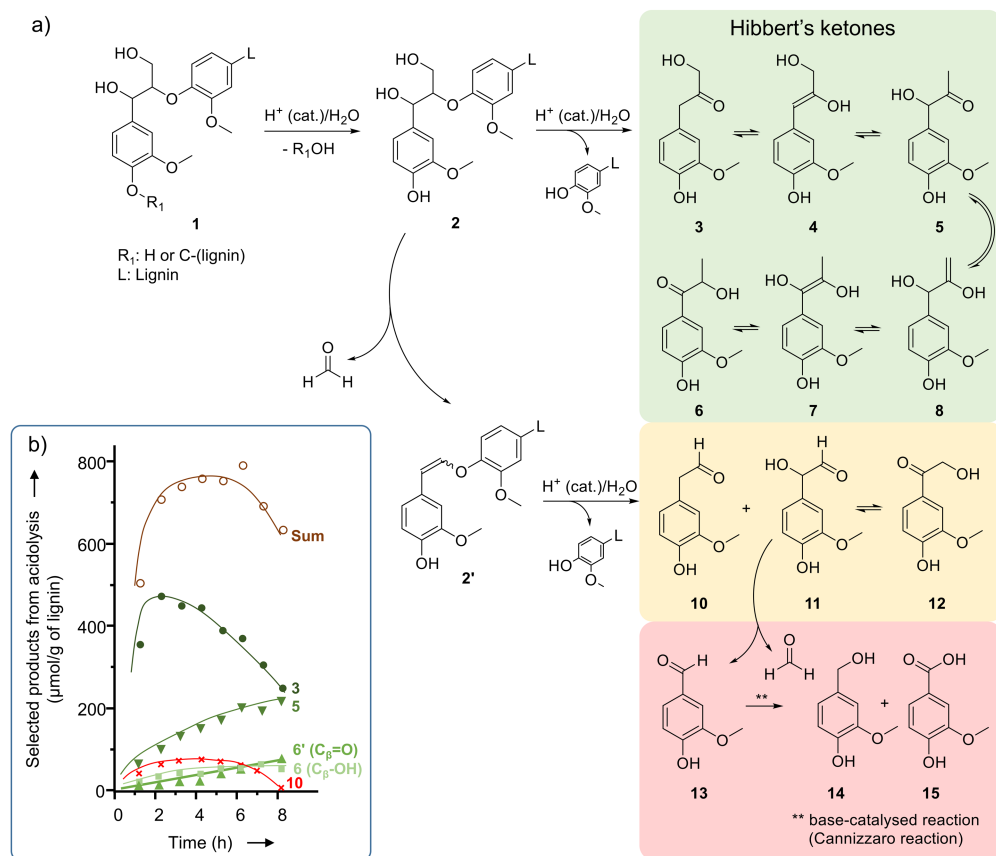
Figure 2.11: (a) Reaction channels (based on the acidolysis method) for the acid-catalysed depolymerisation/degradation of lignin under organosolv conditions, *via* 'Hibbert's ketone' intermediates;[205,228] (b) inset highlighting measured concentrations of sum and individual species along the pathway of acidolysis of milled wood lignin (Pine), as a function of reaction time. For clarity, the scheme depicts only G-units.

Typically, organosolv processes may operate at cooking temperatures of 180-195 °C, for a cooking duration of 30-90 min, an ethanol concentration of 35-70% (wt/vol), and a liquor-to-solid ratio ranging from 4:1 to 10:1.[212] Organosolv treatment typically results in extensive removal of lignin (>70%) with minimum loss of cellulose (<2%).[212] Variants of the organosolv process, performed with an added acid catalyst (e.g., HCl, H_2SO_4, oxalic acid, acetic acid, and formic acid) have been exploited for pretreatment of lignocellulose, in order to aid subsequent enzymatic saccharification of the cellulosic fraction.[212,228] Here, the pH of the organosolv liquor is typically between 2 and 4, and at temperatures of 140-190 °C the lignocellulosic matrix undergoes a solvolytic reaction leading to partial or full 'peeling' of hemicelluloses and extensive delignification. Again, cleavage of a fraction of the β-ether linkages is essential to the delignification process.[192]

A proposed reaction network for degradation of lignin under acidic conditions is shown in Figure 2.11.

The reaction network is derived from analytical acidolysis data of lignins and model compounds. Acidolysis enables the abundance of β-ether linkages to be semiquantified according to the known hydrolysis of arylglycerol-β-aryl ethers in the presence of HCl in 1,4-dioxane/water (9:1 vol/vol).[229] Such conditions resemble those used in some lignocellulose solvent pulping or acid treatment processes.[212] The sum of compounds **3**, **5**, **6**, **6'** and **10** (Figure 2.11b) is often used as the descriptor for β-ether abundance.

Recently, acidolysis of lignin β-ethers was revisited, in order to examine certain observed discrepancies in the rates of phenolic/non-phenolic β-ether hydrolyses (Figure 2.12).[230] Hydrolysis of non-phenolic model compounds (e.g., 1-phenyl-2-phenoxyethanol highlighted in black in Figure 2.12) was approximately two orders of magnitude slower than for corresponding phenolic analogue (shown in green or red in Figure 2.12), with 0.2 M aqueous H_2SO_4 at 150 °C. This observation similarly demonstrates the importance of selecting an appropriate lignin model compound for investigations regarding β-ether cleavage. Clearly, the lack of the phenol moiety renders β-ether species more recalcitrant and far less reactive towards hydrolysis. Therefore, it appears necessary for the model compound to incorporate a phenol or etherified phenol group *para* to the β-ether alkyl chain (representing a lignin monomer at the end of or inside a chain, respectively) in order for the model to accurately reflect the reactivity of the β-ether unit in a native or technical lignin.

The reaction pathways of phenolic/non-phenolic β-ether hydrolyses were similarly examined by using DFT calculations.[230] The predictions showed that both the cleavage of the ether linkage and elimination of the γ-CH_2OH group (as formaldehyde) are energetically feasible in the acidolysis of phenolic β–O–4 alkyl aryl ethers. With increasing acidity of the liquor, elimination of the γ-CH_2OH moiety (forming intermediate **2'** Figure 2.11a) begins to become the predominant mechanism; equimolar quantities of competing **2'** and intermediates **3-8** were formed by subjecting phenolic β-ether model compounds to 0.2 M aqueous H_2SO_4/150 °C conditions for 2 h.[230]

The *in situ* evolution of formaldehyde may facilitate repolymerisation (condensation) of lignin fragments, affording diphenylmethane structures. Critically, this side-reaction is pH dependent.[231] Repolymerisation occurs at an appreciable rate *outside* the pH window of 2-7. Therefore, for relatively mild acid-catalysed organosolv processes, formaldehyde-induced repolymerisation of phenolic fragments may play a less significant role as a repolymerisation channel, compared to kraft, soda or base-catalysed organosolv processes. However, experimental evidence supporting this assumption is still pending.

Importantly, compound **3** in Figure 2.11 belongs to a family of compounds known as 'Hibbert's ketones'. Intermediates **4-8** are formed *via* tautomerisation and hydride
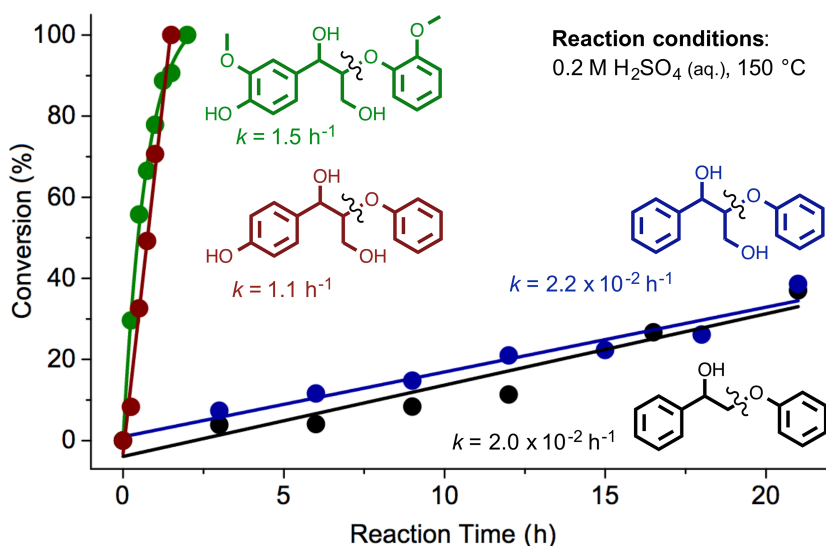
Figure 2.12: Graph highlighting relative rates of β-O-4 ether cleavage for phenolic and non-phenolic model compounds, under 0.2 M aqueous H_2SO_4/150 °C conditions. Adapted with permission from *ACS Sustain. Chem. Eng.*, 2014, **2**, 472-485.[230] Copyright 2014 American Chemical Society.

transfer. Tautomerisation of **3** may also convert the keto group into a γ-aldehyde group. The co-existence of all these species at varying equilibrium concentrations substantially increases the complexity of the system, with respect to elucidating either further depolymerisation or repolymerisation processes.[232]

Examining the acid-catalysed organosolv depolymerisation reaction network presented in Figure 2.11, it is apparent that the sum of products derived from the cleavage of β-ether structural motifs (Figure 2.11b) reaches a maximum shortly after one hour, whereupon it begins to steadily decrease in concentration. The disappearance of specific phenolic monomers represents a primary and recurring problem for cross-laboratory reproducibility of acidolysis experiments.[32,229] The duration of the acidolysis procedure should be optimised on a sample-by-sample basis, owing to the variability of lignin composition in terms of H, G, and S-units. Consumption of these intermediates occurs as a result of condensation reactions involving the Hibbert's ketones. In wood pulping, the condensation of lignin fragments can occur either with lignin still immobilised on the lignocellulose matrix or in solution involving the lignin fragments detached from the plant tissue. Therefore, condensation processes of this type occurring in lignocellulosic feedstocks will inhibit delignification.

Recently, the early-stage conversion of Hibbert's ketones through a Raney*-Ni-catalysed hydrogen-transfer reaction (using 2-propanol as a hydrogen-donor and solvent) was

shown to substantially suppress the repolymerisation processes.[198,233] As a result, the lignin stream was obtained as a viscous oil rather than a solid. Such hydrogen-transfer reactions are discussed in Section 2.7. More recently, the protection of the aldehyde intermediates as acetals (using a 1,2-diol, e.g., ethylene glycol as a protective group) confirmed the importance of stabilising these intermediates for improved mono-aromatics yields (from acidolysis of Walnut dioxosolv lignin using triflic acid as the catalyst).[234] These two pieces of evidence indicate that the fractionation of lignocellulosic biomass and valorisation of lignin can mutually benefit from a firmer understanding of the complex chemistry underpinning organosolv processes, and from trapping/passivating reactive intermediates. In addition to the reactivity of the lignin fraction, hemicelluloses undergo varying extents of hydrolysis during acid-catalysed organosolv processes. Ordinarily, removal of the organic solvent by distillation under reduced-pressure suffices to cause precipitation of water-insoluble lignin fragments, whilst hemicellulosic sugars and oligomers remain in the aqueous solution.[223] Nevertheless, distillation of the organic solvent is invariably an energy-intensive step.[224,235] The 'organocat' process seems to overcome this constraint, whereby fractionation of lignocellulose occurs *via* the initial oxalic/formic acid-catalysed shell-peeling of lignin and hemicelluloses, in a biphasic 2-methyltetrahydrofuran/water system.[236-237] Lignin and hemicellulosic fragments were thus immediately partitioned into organic and aqueous phases, respectively, upon liberation from the lignocellulose matrix. In this manner, the cellulose could be isolated as a pale yellow solid.[236-237]

Organosolv processes may also be performed in the absence of an added acid, with good delignification results (see Figure 2.7).[212,238-239] For such processes, the deacetylation of hemicelluloses suffices to bring about a pH decrease from 7 to *ca*. 4, initiating acid-catalysed solvolysis of the most labile β-ether linkages.[198] The proportion of hemicellulosic hydroxyl residues occurring as acetyl groups is approximately 1% in softwoods, and between 3 and 6% in hardwoods and perennial grasses. Due to the *in situ* evolution of acetic acid, the process may be regarded as autocatalytic.[239] Importantly, under close to pH-neutral conditions, lignin may undergo solvolysis *via* radical-type reactions, in addition to acid-catalysed transformations.[240]

Organosolv processing without added acid is often assumed to afford technical lignins retaining the majority of native β-ether linkages.[241] In this context, in the chemical literature dating from the 1960s to the mid-1990s, it had been assumed that cleavage of non-cyclic α−O−4 linkages was the primary explanation for solvolytic release of lignin fragments.[212,228,238,242] However, it is important to revisit these claims in light of the current understanding that α−O−4-type bonding motifs are cyclic and mostly associated with phenylcoumaran and dibenzodioxocin bonding motifs.[31,155] Therefore, the cleavage of uncommon or non-existent non-cyclic α−O−4 linkages should make a minimal contribution to lignin depolymerisation. Notably, full scission of true α−O−4-containing

bonding motifs should involve concomitant breaking of several other even stronger structural elements to result in depolymerisation. For instance, depolymerisation at phenylcoumaran motifs is only effective when both the α–O–4 (BDE = 50-56 kcal/mol)[180] *and* $C_α$–$C_β$ (BDE = 54-63 kcal/mol)[180] bonds are cleaved. Fragmentation of lignin at dibenzodioxocin linkages, as a result of cleavage of α–O–4 and β–O–4 bonds, will bring about a reduction in lignin branching (in the absence of recondensation). Furthermore, comprehensive lignin depolymerisation at dibenzodioxocin structural motifs also demands the breaking of strong and recalcitrant biphenyl 5–5 linkages (Figure 2.4) that are likely to persist following the relatively mild treatment conditions of an organosolv process with or without added acid catalysts.

Typically, the content of β–O–4 linkages can be assessed by analytical protocols based on chemical degradation (e.g., acidolysis, thioacidolysis, DFRC, and several other).[32,229] Unfortunately, there is little comparative data relating to the quantities of β–O–4 linkages remaining in lignin streams following various organosolv processes. In a standalone report of β-ether cleavage in an organosolv process with added acid, the abundance of remnant β-ethers in the isolated lignin was found to decrease dramatically in line with the delignification degree (*cf.* Figure 2.8b for kraft lignins). At 90% delignification, only one quarter of the original β-ether abundance remained in the isolated lignin – a value nearing those found for certain lignin streams from kraft pulping (at the final stage of delignification), where just 10-15% of bonding motifs can be inferred from the acidolysis products to be β-ethers.[190]

As will be described in further detail in section 2.3.2, the yield of monomers obtained from depolymerisation of lignin is often directly correlated with the abundance of β-ether units in the lignin stream. Considering that retained β-O-4 linkages in the isolated technical lignins are (likely) the most reactive motifs towards depolymerisation, and that some organosolv lignins show fractions of these linkages comparable to kraft lignins, the blanket assertion that organosolv lignins are always easier to depolymerise than lignin streams derived from kraft process is, therefore, an erroneous generalisation. It is thus crucial to know the severity of the organosolv process. Ultimately, if lignin valorisation is tenable, techno-economic modelling may be useful to determine if the added value in keeping the lignin's β-ethers can even offset a slightly lower sugar yield, i.e., whether the process can be better balanced for the value of all of the products. Similar caution should also be exercised for lignin-enriched residues obtained from enzymatic saccharification of pretreated lignocellulosic feedstocks. The chemical nature of these lignins will depend strongly on the severity of the pretreatment method undertaken to enable the enzymatic saccharification (e.g., the presence of added acids or bases, temperature or process duration). Therefore, drawing general conclusions regarding the reactivity of such lignin streams is not possible without a detailed and thorough analysis employing HSQC NMR and chemical degradation protocols for each such lignin stream.

2.2.6.3 Other Fractionation Methods Based on Acid Catalysis

In addition to the more mainstream lignocellulose fractionation processes (e.g., kraft and organosolv) described in some detail above, in recent years research attention has been directed toward novel fractionation methods.[201] Such methods typically target the isolation of pure cellulose, *via* controlled and mild delignification, for subsequent depolymerisation into glucose (saccharification), or perform the saccharification directly, obviating the need for enzymes. In contrast to the kraft process (and some organosolv processes) that expose the biomass to harsh, energy intensive conditions and generate waste streams, these novel approaches afford high yields of sugar monomers/dimers at low temperatures (100-180 °C) in the absence of costly and unrecyclable polysaccharidase enzymes.[201]

The isolation of pentose and hexose sugars from a packed bed of biomass (Corn stover, Maple wood, Loblolly Pine) has been recently demonstrated, by using the promoting effects of γ-valerolactone (GVL) for mild aqueous acid hydrolysis.[243-246] High selectivities to different sugars obtained under varying conditions were attributed to the more facile hydrolysis of hemicelluloses relative to cellulose. By introducing a temperature gradient to the acid-catalysed flow reaction, hemicelluloses were hydrolysed and isolated in an early fraction (~150-180 °C), and cellulose in a latter fraction (180-220 °C), enabling separation of xylose (the main monomeric sugar from hemicelluloses) and glucose (from cellulose). Removal of the GVL (e.g., by phase separation upon adding liquid CO_2 or NaCl), yielded a sugar stream concentrated at up to 127 g L^{-1} (i.e., 65 to 85% of the highest concentrations obtained by enzymatic hydrolysis).[247] The lignin fraction is also depolymerised in this process and can be separately isolated. As determined by 2D HSQC NMR, this lignin stream shows structural features similar to analytical lignins due to the low severity conditions employed for extraction (120 °C, 30 min, 80:20 wt% GVL:H_2O). As an example of upgrading the lignin, a two-stage hydrogenolysis process (first-stage: 10% lignin, 80% THF, 8.5% H_3PO_4 and 1.5% H_2O at 150 °C; second-stage: solvent is replaced by heptane and temperature increased to 250°C), over a Ru/C catalyst in an H_2 atmosphere was reported. Up to 48% of the carbon of the original lignin intake could be converted into mono-aromatics that could then be extracted into a heptane solution, with methanol acting as a capping agent to form carboxylate esters.[246]

Solvent-free, mechanocatalytic deep depolymerisation of polysaccharides has also been explored, beginning with either cellulose or crude lignocellulosic biomass.[248-254] Here, the mechanocatalytic treatment affords a water-soluble, depolymerised lignocellulose. The saccharification of the water-soluble products renders high sugar yields (e.g., 88-92% glucose, 3.5-8% cellobiose, 93-98% xylose relative to glucan and xylan fractions, respectively) and leads to the precipitation of lignin fraction as a sulfur-free solid.[248-250,252-254] The lignin fractions isolated from mechanocatalysis of different biomass species (Pine, Beech and Sugarcane bagasse) closely resemble the lignins obtained *via* organosolv

processes, as determined by HSQC NMR analysis.[249] Although mechanocatalytic processes are typically associated with the high energy costs for the ball-milling operation, the energy requirement per kg of biomass diminishes drastically upon scale-up from 1 g to 1 kg, demonstrating that this process might be suitable both energetically and economically.[253]

A further possibility is to employ protic ionic liquids (ILs) as ('catalytic') solvent, affording another variant of the organosolv process denoted the 'Ionosolv' process.[255-261] As cellulose is insoluble in the new protic ILs, the process contrasts starkly with earlier methods for acid-catalysed depolymerization of cellulose in dialkylimidazolium ILs.[262-267] Accordingly, the acidic solvent acts specifically on lignin and hemicellulose. Delignification of lignocellulosic biomass (*Miscanthus giganteus*) is achieved at 120 °C by the cleavage of β-ether units[268] employing, e.g., 1-butylimidazolium hydrogen sulfate or triethylammonium hydrogen sulfate, as a solvent.[255-261] The lignin fraction dissolves in these ILs, and can be precipitated by the addition of water. Adopting this procedure, it is possible to recycle the IL for successive fractionation cycles. Effective application of ILs towards biomass valorisation has been previously hindered by (amongst other reasons) the high costs of IL precursors and synthesis, the derivatising nature of the IL, and difficulties regarding the separation and recycling of the IL.[256,269-271] However, triethylammonium hydrogen sulfate shows production costs close to those of conventional organic solvents and can be recycled in the process.[259] Moreover, cellulosic fibres can be easily recovered by filtration as cellulose is insoluble in these ILs.

2.2.7 Early Stage Catalytic Conversion of Lignin

The Early-stage Catalytic Conversion of Lignin (ECCL) or "Lignin-first" strategy constitutes the backbone of emerging emerging technologies for lignin valorisation. ECCL involves the concurrent extraction and catalytic conversion of the lignin fragments released from plant biomass in a one-pot process. Employing heterogeneous catalysis in the fractionation of lignocellulose may fully alter the way that lignin is considered within current biorefinery schemes.[201,272] As illustrated in Figure 2.13, current research into lignin utilisation is mostly devoted to depolymerisation and upgrading of lignin wastes, which are unavoidably generated by wood pulping (kraft lignin and lignosulfonates) or cellulosic ethanol production. Strikingly, the emerging processes based on ECCL circumvent the inefficient sequence of depolymerisation (cleavage of weak C–O bonds), repolymerisation (formation of strong C–C bonds), and depolymerisation (through the cracking of C–C bonds formed in the previous step).

As described previously regarding the reactivity of lignins in both kraft and organosolv processes, β-ethers are the primary target for depolymerisation of native lignins. Research and development in catalytic upstream biorefining processes based on ECCL

have focused on chemical reduction of lignin fragments upon their removal from the lignocellulosic matrix. Such methods typically afford a highly-aromatic lignin-derived stream (whereby the most reactive functional groups have been deactivated through catalytic reduction, e.g., conversion of aldehydic intermediates into alcohols, and hydrodeoxygenation of ketones to methylene groups) and a holocellulose stream, as two distinct, stable and easily-separable fractions.[198] The two predominant approaches for such upstream catalytic processing of lignin under mild conditions are hydrogenation and deoxygenation reactions, using either a noble metal-supported catalyst[273-280] or inexpensive Ni catalysts (notably, Raney-Ni).[198,281-282]

ECCL performed on Birch wood sawdust (Ru/C catalyst, 3 MPa H_2, 250 °C) has been investigated as a method to tune the alcohol functional group content of lignin oils. The carbohydrate fraction is retained as a pulp that is conducive to further upgrading, and the lignin fraction is collected separately as a highly aromatic oil containing up to 50% of the carbon intake as mono-aromatics.[276] The synergistic use of Pd/C and Zn(II) (under an H_2 pressure of 3.8 MPa at a temperature of 225 °C) has been also demonstrated as an effective method for the depolymerisation of genetically modified Poplar wood lignin (rich in S-units), whilst retaining 95% of the carbohydrate fraction.[278] Increasing the proportion of S-units in the lignin structure resulted in a higher yield of cleavable linkages under low severity conditions, and a correspondingly higher yield of monomer aromatic compounds, which was also observed in the Ru/C system.[277-278] Three reasons were proposed for this result. First, higher-S lignins contain higher levels of β-ethers.
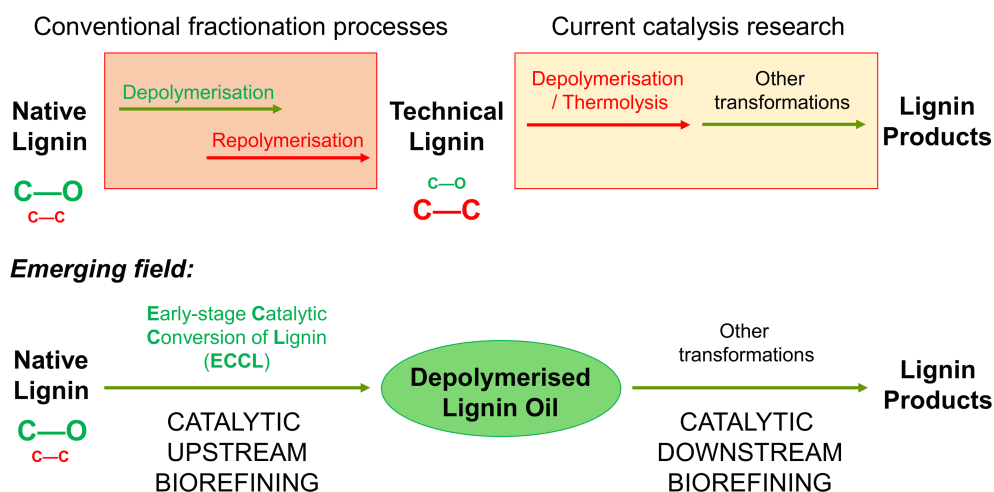

Figure 2.13: Process chains for valorisation of lignin isolated from conventional fractionation processes and from the emerging catalytic upstream biorefining processes based on Early-stage Catalytic Conversion of Lignin (ECCL).

Second, the high concentration of S-units minimises lignin re-condensation, due to a lack of unsubstituted positions *ortho* to the phenol on the syringyl moiety. The third reason is the relative scarcity of G-units, which reduces the complexity of the condensed units in lignin. There might also be reduced interconnectivity of the biopolymers within the lignocellulosic matrix, as G-units have been suggested to have a higher propensity to crosslink with hemicelluloses.[283] Catalytic delignification of high-S wood is one prime example of the potential of the combination of genetic engineering and upstream biorefining based on ECCL.

Employing gaseous molecular hydrogen (H_2) for hydrogenation places constraints on the process (e.g., reactor wall materials, solid feed systems, safety protocols). These limitations are circumvented by using a solvent capable of undergoing a hydrogen transfer reaction instead, for example secondary alcohols[198,281-282] or formic acid.[273-274,279] Hydrogen-transfer strategies of this type have been demonstrated as effective methods for upstream processing of lignocellulosic materials under conditions of lower severity (180-200 °C, autogeneous pressure),[233,284-285] when compared with aforementioned methods.

Importantly, to realise the full economic potential of a lignocellulose biorefinery that does not create unnecessary waste streams, the holocellulose fraction must also be valorised. Deconstruction of lignin may afford a solid carbohydrate pulp fraction, suitable either for undergoing full enzymatic hydrolysis into sugar monomers or for paper production (Figure 2.14).[198,275-278,282] Separation of the catalyst is important, so as to avoid contamination of the downstream products derived from the two streams. Furthermore, due to the strong possibility of poisoning by trace components in the lignocellulose feedstock, the catalyst must be relatively inexpensive. Recent investigations have centred on the use of Raney-Ni, a magnetic catalyst.[198,282] This property allows for facile separation of the catalyst from both lignin oil and holocellulose streams. Holocellulosic solids are obtained as predominantly catalyst-free solids that are highly conducive to further downstream treatment (Figure 2.14, picture A).

The liquid-phase extraction of lignin from Birch wood sawdust in alcoholic solutions has been reported, employing a Ni/C catalyst. Unfortunately, the recovered cellulose fraction could not be fully separated from the magnetic catalyst (Figure 2.14, picture B).[281] Moreover, in the characterisation of the lignin fraction extracted from Birch wood, just three products were identified by GC characterisation.[281] More recently, this catalyst system has been revisited by another research group,[286] who found the product mixture to be more complex than previously reported. Moreover, the product spectrum and yield were demonstrated to depend heavily on both catalyst loading and biomass type and origin.[286] Therefore, this example serves to reaffirm the need for standardised protocols for the analysis of lignin products.

Figure 2.14: Holocellulosic fractions derived from two different Ni-catalysed up-stream processes: (A) Raney˙Ni catalysed removal of lignin from Poplar wood chips (pulp conducive to further downstream processing[198]), and; (B) Ni/C catalysed removal of lignin from Birch wood saw dust (pulp not conducive to enzymatic hydrolysis[281]). Image A reproduced with permission from *Angew. Chem. Int. Ed.*, 2014, **53**, 8634-8639. Copyright 2014 John Wiley and Sons. Image B reproduced with permission from *Energ. Environ. Sci.,* 2013, **6**, 994-1007. Copyright 2013 Royal Society of Chemistry.

As will be discussed in the next sections, high temperatures (300-450 °C) and elevated H_2 pressures (MPa) are typically required for cracking the C–C bonds in technical lignins to produce low M_w products in heterogeneously catalysed processes.[287-288] Conversely, strategies based on ECCL benefit from the intrinsically high reactivity of native lignins compared to condensed, and therefore, recalcitrant technical lignins. Indeed, from the solvolytically released lignin fragments, the ECCL directly produces monophenols and small oligomers (M_w 100-400 Da).[198,277-278] Moreover, the lignin oil products that are obtained can be upgraded under conditions of low-severity similar to those employed in the conversion of phenolic model compounds of lignin and pyrolysis oil.[289-292] It is therefore clear that ECCL-based strategies hold great promise for future lignin research.

2.3 Downstream Processing of Isolated Lignin

2.3.1 Economic Considerations

When considering prospective applications of isolated lignin streams, the volume of lignin that such an application is able to absorb is of primary importance. Logically, where supply greatly exceeds demand, the large surplus will place a severe pressure on the market price, which may in turn put the profitability of the wider lignin valorisation process at risk. The glycerol market serves as an example of the disadvantages associated with dramatic oversupply. In fact, the prices of purified glycerol and crude glycerol were reduced by 50% and 80%, respectively, following the worldwide implementation of fatty-acid transesterification for biodiesel production.[293]

It has long been recognised that there is a need for *both* 'high-volume and low-value' and 'low-volume and high-value' applications in order to achieve full economic use of isolated lignins.[294-295] Seven categories of value-added products from lignin, initially proposed by Glasser about 30 years ago, still remain relevant to this day: (i) oil field chemicals; (ii) agricultural chemicals; (iii) asphalt extenders; (iv) carbon black; (v) adhesives; (vi) engineering plastics and (vii) specialty dispersants.[294]

Annually, more than 130 million tons of lignin are currently liberated in the paper-and-pulp industry, although at present only a very minor proportion is isolated and available.[295] This number rises significantly when biorefining for transportation fuels is taken into account. For example, a biorefinery process producing ethanol from corn-stover liberates approximately 0.5-1.5 kg of lignin per kg ethanol.[296] Taking into account that about 40% of the lignin-rich residue would suffice to cover the heat and power demand for bioethanol production (including biomass pretreatment and ethanol distillation), it is clear that lignins released from the production of cellulosic ethanol will add to the already enormous pile of under-utilised, technical lignins from kraft mills.

Vanillin, at present the only chemical commercially produced from lignin by oxidation of lignosulfonates, has a market volume of about 20,000 tons (Table 2.4).[297-298] With over 90% of the synthetic vanillin used today being mineral oil-derived, there is room for growth of lignin-derived vanillin, considered closer in flavour/taste than petrochemical guaiacol-derived vanillin. However, the limited total market volume does not suffice to absorb the entire lignin output from biorefineries. By contrast, phenol is produced in annual quantities of approximately 8 million tons, whilst the mixture benzene, toluene and xylenes (BTX, precursors for most petrochemical aromatics, Table 2.4), are produced at 80 million tons per year.[299] These markets hold the potential to employ a sufficiently large proportion of the lignin liberated from the paper-and-pulp and transportation fuel industries, so as to render the wider lignin valorisation process worthwhile.

Potential approaches to producing value-added products from lignin can be broadly divided into three sub-categories: (1) direct use or as precursor for material applications; (2) as a feedstock for (drop-in) transportation fuels and (3) as a raw material for commodity or high-value chemicals. Considering material use, the macroscopic or microscopic properties of the (technical) lignin macromolecule mixture must be acceptable without significant treatment, although some modifications may be exacted by physical or chemical treatment. In this manner, although the properties of the lignin here constrain the number of possible applications, no further depolymerisation is required and processing is simpler.

The application of lignin in phenol-formaldehyde resins is a typical example of this approach. Up to 50% of the phenol content in this material can be replaced by lignosulfonate, kraft, or organosolv lignin without significantly compromising properties of the

resin.[300-302] Similarly, kraft lignin may be oxypropylated and then used as a polyol component in the synthesis of rigid polyurethane foams.[303] Lignin may also be employed as a feedstock for high-quality carbon fibres, at present produced almost exclusively from poly(acrylonitrile).[29] Although this application is beset by problems associated with the necessity to melt-spin the precursor efficiently and rapidly convert it into carbon fibres at the carbonisation/graphitisation stage (requiring lignins with low polydispersity), there has nevertheless been considerable progress in this field.[304] More unusual applications include the incorporation of lignin in water-purification membranes,[305] as a composite in battery cathodes,[306] and as a starting material for the synthesis of highly porous carbon,[307] which, for example, may find application as anode materials in lithium-ion batteries.[308] For more information on the materials application of lignins, the reader is directed to recent reviews.[28,309-310]

Fuel production from lignin requires both further depolymerisation of the technical lignin, and subsequent upgrading of the phenolic stream. Lignin has both the highest energy density and the lowest oxygen content of the three major components of lignocellulosic biomass, rendering it an attractive starting material for the production of transportation liquid fuels. The primary goal is, therefore, to generate a relatively volatile fraction with reduced oxygen content, whilst simultaneously retaining the energy content and limiting the quantity of hydrogen required for the catalytic upgrading. Interestingly, complete reduction towards alkanes may not be necessary. Research on the combustion properties of lignin-derived small molecules suggests that cyclic alkyl alcohols and aromatic oxygenates could also find application as drop-in fuel components, particularly in gasoline and diesel blends.[311-313] However, this type of application is still in development, requiring further improvements to minimise soot and gas emissions.

Catalytic pyrolysis of biomass[314-317] and further catalytic upgrading of the pyrolysis oils[19,318-319] have been extensively studied, typically employing an acidic zeolite (e.g., H-USY and ZSM-5) catalyst. A large quantity of catalyst is typically required, making catalyst stability of paramount importance. Deactivation occurs *via* extensive coking, leading to pore-blockage and encapsulation of the active sites. Burning of the coke, followed by acid treatment, may partially restore activity.[320-321] Catalytic lignin pyrolysis efficiency will, in general, only be influenced to a limited extent by precise structural properties of the lignocellulosic feedstock. As the focus of this review is on a critical discussion about the relationships between lignin structure/bonding and susceptibility to valorisation through catalytic methods, catalytic pyrolysis strategies will therefore not be covered in further detail here and the reader is referred to other reviews (Table 2.1).

Catalytic depolymerisation in the liquid phase may provide more flexibility in terms of using lignin as a feedstock for both fuels and chemicals. Being the only primary component of lignocellulosic biomass containing aromatic subunits production of aromatic (bulk) chemicals has, from the start, been an obvious and attractive route for lignin

Table 2.4: Comparison of various potential products from lignin in terms of market volume, price and the maximum gravimetric yield from lignin, assuming a linear polymer of 'G' monomer units at 196 g mol^{-1}. Although market prices are in constant fluctuation, the data nevertheless serves to compare approximate sizes and yields of prospective lignin industries. Any residual carbon is assumed to be used for reforming to hydrogen.

Compound	Volume (10^3 kg y^{-1})	Price ($ kg^{-1})[a]	Max. Theoretical Yield from Lignin (wt%)	H$_2$ Produced (kg/kg product)	CO$_2$ Produced (kg/ kg product)
Benzene		1.49	40%	0.181	2.254
Toluene	80,000,000 (combined)	1.38	47%	0.088	1.433
Xylene		1.36	54%	0.019	0.829
Phenol	8,000,000	1.54	48%	0.172	1.871
Vanillin	~20,000	10-15	78%	0.066	0.579
4-Propylguaiacol	none	no (current) market	85%	-0.036	0.000[b]

[a] Benzene, toluene, xylene and phenol prices are FOB U.S. Gulf as of 30th October 2012. For reference, the oil price (WTI future for delivery December) was $85.66 on that date. [b] Excluding carbon sources required to produce external hydrogen.

valorisation (Table 2.4). There are multiple potential aromatic targets, differing in the degree of chemical complexity and (correspondingly) production volume. The simplest are BTX mixtures, which, as described previously, are an important feedstock for a wide array of petrochemical processes with a large market. Full hydrodeoxygenation of lignin streams to BTX may also facilitate the separation of products by fractional distillation as practiced in the oil refinery.[284] Despite the potential to absorb large quantities of technical lignin, BTX may not be the best target for lignin valorisation as chemicals. In the interest of atom-economy and energy efficiency,[322] approaches that fully hydrodeoxygenate biogenic molecules, rendering hydrocarbons as products, which again need to be oxidised to afford the desired end-products, should be considered as the preferred route in extreme cases only (i.e., to facilitate product separation,[284] or for a lack of any other route for the production of a desired chemical).[323] It has previously been recognised that redox-neutral reactions performed on plant carbohydrates are desirable so as to preserve the intrinsically high functionality.[322] A similar argument should be advanced for the valorisation of lignins.

For the BTX strategy, it remains to be seen if attractive price premiums can be realised. For example, in October 2012 the benzene price was $1.49 kg^{-1} (FOB USG), and the price of high-purity isolated lignin, though difficult to establish, is estimated at $0.25-0.50 kg^{-1}.[324] Nevertheless, it must be noted that, if lignin is idealised as a linear polymer of guaiacylglycerol ('G' units) with a monomer molecular weight of 196 g/mol, the maximum gravimetric toluene yield is just 40%. Although the remaining 60% weight can,

in principle, be employed towards the co-generation of (at least) methanol, additional expenditure associated with external reagents (i.e., hydrogen and protective groups) and other operating costs serve to drive down potential profit margins.

Notably, both the atom efficiency, energy efficiency and cost competitiveness of obtaining chemicals from lignin can be improved when higher value chemicals (e.g., phenol, cresols or adipic acid) can be directly obtained from lignin, circumventing the need to synthesise these compounds from the BTX mixture. Occupying positions further up the value chain are synthetic precursors for pharmaceutical, agrochemical or other specialty applications. In fact, such high-value precursors may be targeted in an initial mild lignin conversion strategy, prior to the application of harsher conditions in order to obtain higher-volume, lower-value bulk chemicals (e.g., BTX). In all discussions on chemicals production, it must be recognised that prices of bulk chemicals are strongly influenced by current oil prices and their price volatility, and therefore, the economic feasibility of any lignin-to-chemical pathway must be assessed with these factors in mind.

2.3.2 Catalytic Downstream Processing Strategies

As discussed in the previous sections, polymeric lignin streams vary widely in terms of their chemical nature. Some organosolv lignins, mainly those extracted without added acid catalysts,[192] may retain a considerable fraction of the original native β–O–4 linkages, as suggested by HSQC NMR analysis,[249,251] and evidenced by chemical degradation methods.[194] By contrast, for lignins from chemical pulping processes (e.g., kraft, soda lignins and lignosulfonates) β–O–4 linkages represent fewer than 10% of the connections.[190] In addition, extensive condensation of lignin fragments yields strong and recalcitrant carbon-carbon bonds. As a consequence of the highly varied and complex chemical/bonding properties of differing technical lignins, there is, unfortunately, no 'one-size-fits-all' solution for catalytic downstream processing of these polymeric technical lignin streams. Nevertheless, contemporary methodologies for lignin utilisation and valorisation can be broadly divided into two primary categories: (1) convergent approaches, and; (2) stepwise approaches (Figure 2.15).

Prior to individual discussions of the various depolymerisation strategies, it is valuable to consider the statistics of depolymerisation in order to estimate the maximum yields of mono-aromatics from lignins. Statistically, the release of a monomer from a finite polymeric chain containing cleavable and non-cleavable bonds involves the cleavage of two bonds.[325] Hence, the maximum yield of a monomer can be estimated by Eq. (1), as reported in ref. [326]:

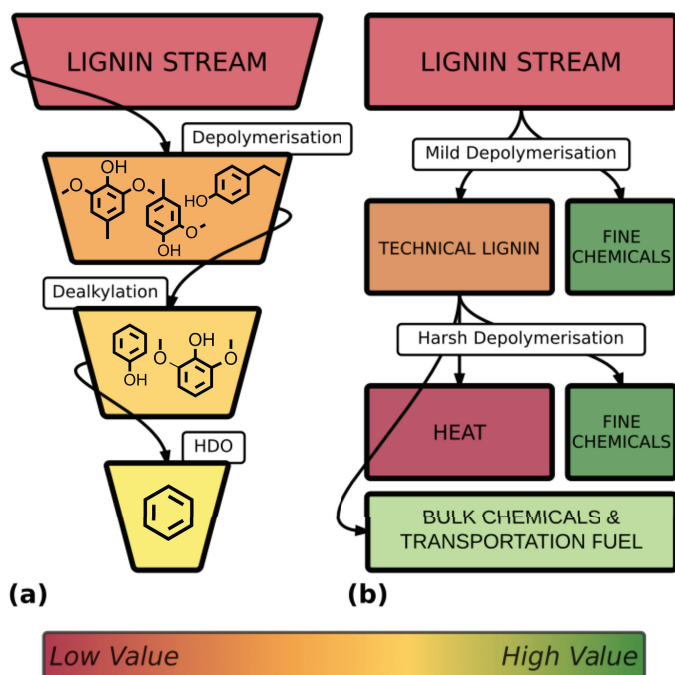$$Y = \frac{(n-2)P^2 + 2P}{n} \times 100 \tag{1}$$

Figure 2.15: Two alternate approaches to depolymerisation of low-value lignin streams: (a) a funneling scheme for convergent production, exemplified here for benzene, *via* depolymerisation-dealkylation-hydrodeoxygenation (HDO), or; (b) a stepwise approach whereby lignin is first depolymerised under mild conditions affording high-value fine chemicals, and residual technical lignin is then treated by more harsh depolymerisation conditions to afford fine/bulk chemicals and transportation fuels (and remnant material is used as fuel to heat/power the process). For the funneling scheme, downstream materials are not necessarily of higher value, although costs associated with *separation* are reduced.

In Equation 1 Y represents the sum of individual yields of mono-aromatics, n is the number of monomers occurring in the polymeric chain, and P corresponds to the fraction of cleavable bonds (e.g., for lignin, β–O–4 linkages). It has already been noted that upon increasing the polymeric chain to an hypothetically infinite value of n, the yield of monomers quickly converges to $Y \approx P^2$ already at $n \sim 10$.[326]

Figure 2.16 displays a graphical representation of the sum of individual yields of mono-aromatics compounds, obtained from the depolymerisation of an infinite chain of lignin, for various values of P, for which typical β–O–4 contents of several classes of lignin streams have been taken.

It is clear from Figure 2.16 that a high fraction of β–O–4 linkages (or other readily cleavable linkages) is essential to achieving high values of the sum of individual yields of mono-aromatics from lignins. Considering native lignins with P values in the range of 0.35 to 0.85, the theoretical mono-aromatics yields can be anticipated to be between 10

and 70%. This estimate agrees well with the fact that the catalytic upstream biorefining based on ECCL is conducive to afford high yields of monomer products.[198,273,278] Conversely, downstream treatment of technical lignins with *P* values lower than 0.2 (such as kraft and certain organosolv lignins) will lead to monophenol yields of less than 4% if only the easily cleaved bonds are targeted.[277] Notably, lignins derived from genetically engineered plants may hold the potential for even higher yield production of lignin mono-aromatics in catalytic upstream processes based on ECCL, as such native lignins may be tuned to *P* >0.85 (e.g., high-syringyl lignins).

Despite the many advances seen in catalytic depolymerisation, Figure 2.16 clearly illustrates that, under low-severity conditions, the transformation of technical lignins into a limited number of mono-aromatics at high yields is very challenging, owing to the structural complexity generated in the fractionation of lignocellulose. Therefore, successful valorisation of technical lignins will depend on addressing this challenge and making effective use of the structural diversity of the depolymerised products. Harsher methods will typically generate a mixture of compounds, adding the complication of product separation, which will take considerable effort, both in terms of energy as well as the
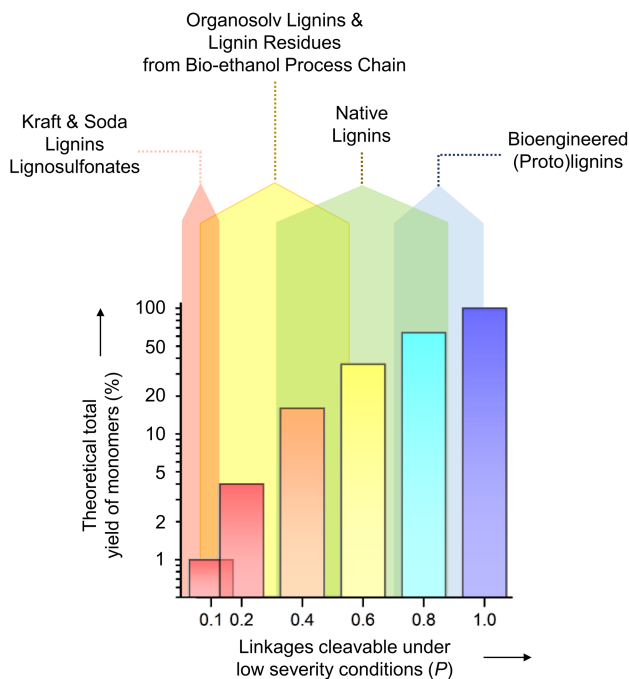

Figure 2.16: Graph representing equation (1) for various *P* values. For lignin with a *low* percentage of cleavable bonds, it is close to impossible to obtain high individual yields of products under low severity conditions. Lignin varieties with a *high* proportion of reactive linkages (β–O–4, or esters in genetically modified plants) are required for high-yield depolymerisation to be possible.

need for large distillation columns, or other separation setups. In fact, structurally similar compounds with comparable boiling points, such as alkylphenols, may not be readily separated by distillation. Alternatively, if the application allows, targeting instead a mixture of compounds with a well-defined specification in terms of macroscopic properties (e.g., analogous to petroleum-derived lubricants and fuels), might be a useful method to deal with this complexity and a means to valorise technical lignins.

An alternative strategy is to reduce the complexity of such a mixture of mono-aromatics and oligomers in subsequent processes that convert a large number of the different constituent components into the same, single target compound (or a limited number of them, Figure 2.15a). Such a convergent, funneling approach, schematically represented in Figure 2.15a, is also particularly well-suited to biological systems because catabolic pathways within microorganisms typically converge to a small number of metabolites. The selected, recent examples discussed below highlight the potential for the consolidation of bio- and chemocatalytic transformation as part of a convergent approach for the valorisation of lignin streams. As a thorough discussion of such biological methods goes beyond the scope of this review, the interested reader is directed towards an extensive review on this topic[327] and other key literature.[328-330]

The conversion of a mixture of lignin-derived phenols into polyhydroxy acids of various chain length was demonstrated by using *Pseudomonas putida*.[331] Employing a genetically-engineered strain instead, the wide range of lignin-derived aromatics present in the alkaline liquor obtained from a pretreatment of corn stover could be converted into *cis,cis*-muconic acid in high yield (67%). The *cis,cis*-muconic acid could then be easily hydrogenated to adipic acid, one of the monomers for Nylon-6,6.[332] The bioconversion of lignin-derived phenols thus markedly contrasts with (non-biological) lignin oxidation over chalcopyrite, whereby a mixture of acids with different carbon chain lengths is invariably obtained.[328]

The ability of a microorganism to degrade the macromolecular lignin polymer itself into smaller phenolic intermediates would bring considerable advantages. *Amycolatopsis sp.* and *Rhodococcus jostii* strains were found capable of both secreting laccases and peroxides (thus enabling the oxidative depolymerisation of lignin) and of catabolising the released phenolics, for example.[329] Employing these strains, a lignin conversion of up to 30 wt% could be achieved affording intracellularly-stored polyhydroxy acids or fatty acids. As the catabolic pathways of the stored products may also be further genetically modified, these bacteria represent excellent starting platforms for improved strains capable of producing other high-value products.

Alternatively, in a stepwise or cascade approach (Figure 2.15b), depolymerisation of technical lignins is conceived to occur gradually over several stages. Catalytic upstream biorefining methods based on ECCL may also be incorporated into such a cascade. The

initial mild depolymerisation step is designed so as to be highly selective to specific bonding motifs, targeting the production of highly-functionalised molecules (e.g., fine chemicals). The high value of the products may still ensure the economic feasibility of such an approach even when catalysts, reagents and separation of products obtained at low individual yields are accounted for. Nonetheless, the costs associated with costly reagents, (co)catalysts (e.g., TEMPO), molecular hydrogen and hydrogen donors, oxidants other than oxygen and (solvent-derived) capping agents will certainly impact the overall economics of the downstream processes. Indeed, similar to the efforts that are required (for example) in upscaling the synthesis of fine chemicals from laboratory to commercial scale, after the proof-of-principle technology has been established for promising mild lignin depolymerisation routes, considerable development efforts are still required to allow larger scale production, paying particular attention to the viability of employing certain chemicals, solvents and catalysts on a commercial scale.

In this context, the manufacture of vanillin lends valuable insight into the challenges associated with any industrial-scale lignin valorisation process.[297] The oxidation of spent sulfite liquor to generate vanillin was operated intensively throughout the 1960s, 1970s and 1980s. Despite a high value (historically $10-15 kg^{-1}) and an inexpensive catalyst, solvent and reagent (NaOH, water and oxygen, respectively), almost all liquor-to-vanillin plants had ceased production by the early 1990s. The low vanillin yield (2.5% at optimum condition) and large sodium hydroxide requirements resulted in the intolerably high generation of organic-containing 'caustic liquor' (~160 kg per kg vanillin), rendering the overall procedure costly and uncompetitive against then emerging petroleum-to-vanillin technologies. Only Borregaard Industries in Norway still operates a similar process, although run with a copper catalyst, which presumably significantly increases the efficiency and decreases the amount of waste. This example clearly urges researchers to also consider the use of their 'waste' streams when developing new lignin valorisation methods. Otherwise, novel technologies may share the same fate of most of the lignin-to-vanillin processes.

Critically, the residual lignin obtained from an initial mild depolymerisation step will invariably exhibit a larger fraction of resilient bonding motifs, compared to the starting material. Accordingly, in the cascade approach more severe downstream processing of the residual lignin stream may yield bulk chemicals (e.g., organic acids, phenolics, BTX) or additives to transportation fuels. Finally, any heavy residues that remain even after severe treatment may potentially be subjected to catalytic cracking, or substitute for the asphaltene fraction of crude oil, or be incinerated for the generation of heat and power. This combination of strategies ensures that the lignin feedstock is used to maximum benefit. The individual processing steps of such an approach must be designed in order to accommodate an increasingly degraded and condensed lignin structure, and to tolerate or separate impurities introduced in previous steps.

In light of the convergent and stepwise approaches, there is a clear requirement for a 'toolbox' of chemical lignin depolymerisation methods, under different severity conditions. In the following sections, multiple methods for the depolymerisation of lignin are discussed. Examples are subcategorised based on severity and selectivity of the procedures into so-called 'mild' procedures that target specific bonding motifs in lignins using highly selective catalysts and reagents; and 'harsher' procedures that use a regime in which concurrent thermal and catalytic reactions may take place. Selected examples are limited to those that specifically highlight the relationship between lignin structure and catalysis. Logically, this relationship is more difficult to assess under harsh depolymerisation conditions. In these instances, the discussion will also focus on other process variables (among others solvent effects and catalyst stability). Regardless of the somewhat artificial classification of the examples discussed based on process severity, the insight obtained from either category should be taken into account when devising new approaches to lignin depolymerisation.

2.3.3 Mild Depolymerisation Strategies

In recent years, an array of chemical depolymerisation methods has been developed that selectively target specific bonds within the lignin polymer,[232] the majority of which target the β-ethers. As already discussed, the generalisation that β–O–4 linkages constitute the predominant type in *all* varieties of isolated lignin is perhaps one of the major misconceptions that has unfortunately been propagated across the literature in this field. Logically, strategies that have proven effective for the cleavage of β–O–4 linkages in model compounds will not translate well into the processing of technical lignins that comprise little or none of this structural motif in their backbone. Nevertheless, conditions suitable for β–O–4 cleavage in model compounds are likely to translate well into the processing of some lignin varieties where a significant proportion of β–ether linkages has been left intact after upstream treatment. Selected pathways for the selective cleavage of β–ethers occurring in lignin (represented by a simple model compound) are summarised in Figure 2.17. For the strategies outlined below, attention is devoted primarily to providing an overview of methods available for mild depolymerisation rather than a detailed mechanistic description of the chemistry involved. For further mechanistic details, the reader is directed to a recent review article.[333]

2.3.3.1 Mild Oxidative Depolymerisation Pathways

Several oxidative routes have been reported targeting different end-products from lignin and are discussed in detail in a recent review article.[334] Indeed, a large number of these oxidation methods target the cleavage of the β-ethers, of which a number are discussed in this section. A chemoselective and organocatalytic method for the selective
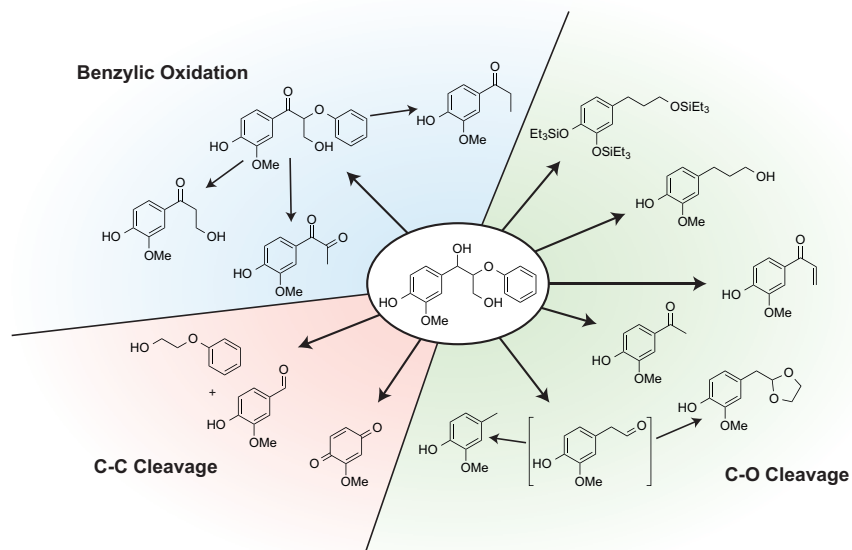
Figure 2.17: A variety of strategies for selective cleavage of the β–O–4 lignin linkages (represented by a simple dimer model compound), *via* C–O cleavage (green), C–C cleavage (red) and benzylic oxidation (blue).

oxidation of the secondary (benzylic) alcohol of lignin model compounds and *Aspen* lignin was demonstrated. The system employing a (2,2,6,6-tetramethylpiperidin-1-yl) oxyl (TEMPO) derivative, with HNO_3 and HCl, performed best under mild conditions (Figure 2.18a).[335] Moreover, models incorporating free phenolic groups (a functional group responsible for many of the difficulties encountered in oxidative lignin valorisation attempts), could be selectively oxidised. 2D HSQC NMR showed that the approach could be extended to Aspen lignin, with most of the S- and all of the G-units in Aspen lignin selectively converted into the corresponding benzylic ketones. As mentioned in the discussion on lignin structure, the C–O ether bond of the oxidised β–O–4 substructures is substantially weakened. Subsequent redox-neutral formic acid-mediated cleavage of the oxidised β–O–4 substructures led, in the absence of a reducing metal, to the formation of simple ketone, diketone and phenol derivatives as primary products (Figure 2.18a).[336] Extension of the strategy to an oxidised Aspen lignin (isolated *via* a mild cellulolytic enzyme protocol, and therefore, rich in β–O–4 linkages) also proved successful. A soluble fraction of low-molecular-weight aromatics was obtained, accounting for up to 61 wt% of the original lignin input, of which approximately 85% (i.e., 51 wt% based on original lignin input) could be identified, with the diketone products expected from the model compound studies making up the major fraction. By contrast, a lignin in which the secondary alcohol was not oxidised prior to the cleavage reaction, afforded
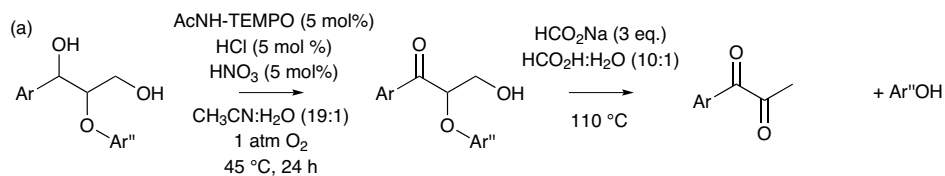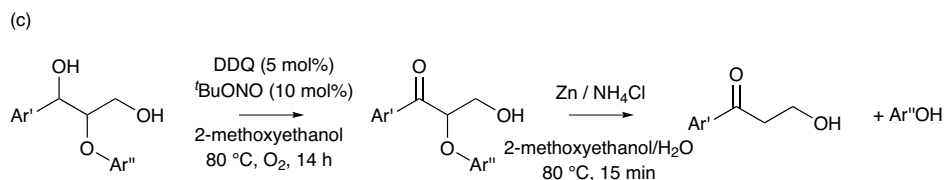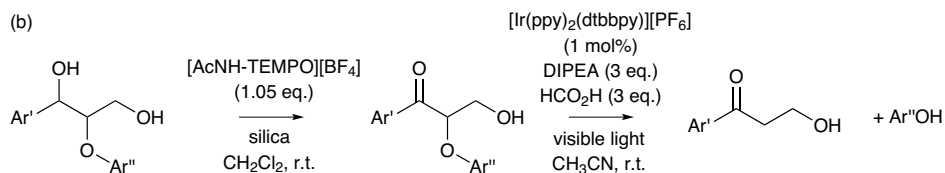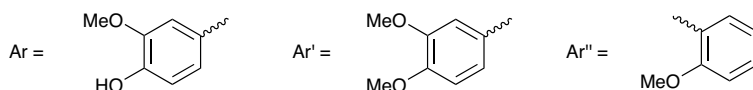
Figure 2.18: Mild oxidative pathways for cleavage of β-ether lignin model compounds, *via* selective oxidation of the secondary alcohol functional group. The 'Ar' groups represent simple aryl functionalities. For methods expanded to actual lignins, the results are indicated below the reaction scheme.

low monomer yields, highlighting the importance of generating the benzylic ketones to weaken the vicinal β–O–4 ether linkages and allow redox-neutral cleavage. Having established the proof-of-principle of stepwise oxidative activation/redox-neutral cleavage with this elegant approach, several practical aspects, including scalability, choice of solvent and chemicals used for the oxidation and cleavage steps and further reduction of the complexity of the product mixture obtained, now warrant further attention.

Along the same lines, a two-step lignin degradation strategy has been applied to a series of lignin model compounds. Selective oxidation of the benzylic alcohol was achieved using 'Bobbitt's salt' ([4-AcNH-TEMPO][BF$_4$]) followed by a reductive, photocatalytic cleavage step, rendering the overall process redox-neutral (Figure 2.18b).[337] The reductive cleavage of the oxidised β–O–4 moiety by single electron transfer was accomplished using a common photoredox catalyst, Ir(ppy)$_2$(dtbby)PF$_6$, operating under visible

light and employing a 3 equiv. of formic acid and the base *N,N*-diisopropylethylamine (DIPEA). As photocatalytic protocols can be expected to be less efficient for darkly coloured solutions, such as those expected for lignin streams (commonly varying from reddish brown to dark brown/black), reactions were also performed with the stepwise addition of a lignosulfonate material. In a batch reaction, the photocatalytic conversion suffered from ineffective radiation, but in a flow reactor the yields of mono-aromatic products were restored. Unfortunately, no mention of the fate of the lignosulfonate was made.[337] The viability of this photocatalytic strategy now needs to be demonstrated with actual lignin feeds. From an economic perspective it should be mentioned that while overall redox-neutral, the coupled two-step process still generates much stoichiometric waste. This, together with the costs associated with the expensive reagents and catalysts used remains to be addressed.

A third oxidation/cleavage strategy was applied to a dioxasolv *Birch* lignin, employing a DDQ/^{t}BuONO/O$_2$ system for the selective oxidation of the β-ether units at room temperature (Figure 2.18c).[325] For the processing of Birch lignin, an alternative solvent to that used in the selective cleavage of model compounds was required, an important, practical issue that is not to be underestimated. A mixture of 2-methoxyethanol/1,2-dimethoxyethane was found not only capable of dissolving the lignin feedstock, but also allowed for the catalytic DDQ reactions demonstrated on the model compounds. 2D HSQC NMR revealed a complete disappearance of the α-C-H cross-peak of the β–O–4 linkages, with a concomitant appearance of a signal associated with the oxidised linkage. A subsequent stoichiometric reduction using metallic zinc performed in the same pot yielded a monomeric syringyl-derived compound in 5 wt% isolated yield; it was also shown that the highly-functionalised 3-hydroxy-1-phenylpropan-1-one product provides many opportunities for further conversion into value-added fine chemicals (Figure 2.18c).[325] The production of this highly-functionalised derivative, and therefore, the possibility of generating high-value fine chemicals from this phenone product, may eventually justify the use of more expensive reagents and protocols, after which the remaining, lower-quality and lower-value condensed lignin could be further converted by harsher catalytic methods, i.e., by a cascading approach.

The same oxidation-cleavage reaction was applied to a β-ether polymer that included both G *and* S units, thus mimicking the structural complexity of lignin better than simple model compounds.[325] Similar polymeric lignin mimics have been employed in additional studies.[338-339] Furthermore, polymers of greater sophistication have been investigated, incorporating a combination of β–5, β–β and β–O–4 linkages, and with control over the S:G ratio.[340] It is anticipated that the use of such more advanced models, which incorporate more of the same bonding motifs as found in true lignin feedstocks, will offer further insight into the chemistry occurring in the actual lignin depolymerisation, and should be able to bridge the gap in terms of differences seen in reactivity

between simple model compounds and actual lignin macromolecules. Indeed, the drop in cleavage activity seen in going from dimeric models, to the polymer, to the actual lignin shows the difficulties that are generally faced in translating lab-based chemistry to real lignins. Importantly, though, as with the sodium formate/formic acid example, the main product obtained from lignin is the same as from the model compounds, which means that the chemistry on the lignin sample is well understood, allowing further optimisation.[272] The latter would entail an assessment of the solvents used, the stoichiometric reagents, co-catalysts and other additives, to improve the economic viability of such two-step, activation-before-cleavage strategies.

Mild oxidative selective cleavage of the carbon-carbon bond (rather than the carbon-oxygen) in the β-ether units represents an alternative route for lignin depolymerisation. A vanadium-oxo complex incorporating a dipicolinate ligand and a copper(I) chloride/ TEMPO system were compared alongside one another, with respect to the aerobic oxidation of a not quite authentic β-ether model compound 1-(3,5-dimethoxyphenyl)-2-(2-methoxyphenoxy)propane-1,3-diol (Figure 2.19).[341]

In the reaction with copper(I) chloride/TEMPO and molecular oxygen, a 56% combined yield of 3,5-dimethoxybenzaldehyde and 3,5-dimethoxybenzoic acid was obtained, with minimal α-ketone production. The vanadium system led not only to the corresponding α-ketone (oxidation) in the presence of oxygen but also carbon-carbon bond cleavage products were detected, albeit as minor products (<20% yield). In a later investigation employing a vanadium-oxo complex bearing 8-quinolinate ligands, similar selectivity to the α-ketone was observed (not shown in Figure 2.19).[342] Highlighting the importance of structural fidelity of model compounds, the use of a better analogue, a model compound with a phenolic hydroxyl group 1-(4-hydroxy-3,5-dimethoxyphenyl)-2-(2-methoxy-phenoxy)propane-1,3-diol led to carbon-carbon bond cleavage with the vanadium-oxo catalytic system, generating 3,5-dimethoxy-*p*-benzoquinone (Figure 2.19). Clearly, the oxidation selectivity is very sensitive to the choice of ligand structure, solvent and, most crucially, the model compound.[24]

Finally, the vanadium-quinolinato complex was shown to also affect the oxidation of an ethanosolv lignin isolated from mixed hardwoods. The reduction of molecular weight seen by GPC, was corroborated by the disappearance of characteristic cross-signals for β–O–4, β–5, β–β and dibenzodioxocin bonding motifs was detected by HSQC NMR[343] However, the formation of volatile aromatics was not assessed. Therefore, it is unclear how the chemistry seen with the model compounds translates to actual lignin oxidation.

Similar to the vanadium-catalysed example above, *p*-benzoquinones could also be obtained by the oxidation of 1-(4-hydroxy-3,5-dimethoxyphenyl)-2-(2-methoxyphe-noxy)propane-1,3-diol with a cobalt-Schiff base catalyst. Furthermore, partial loss of one of the ring methoxy substituent was also observed, suggesting both carbon-carbon
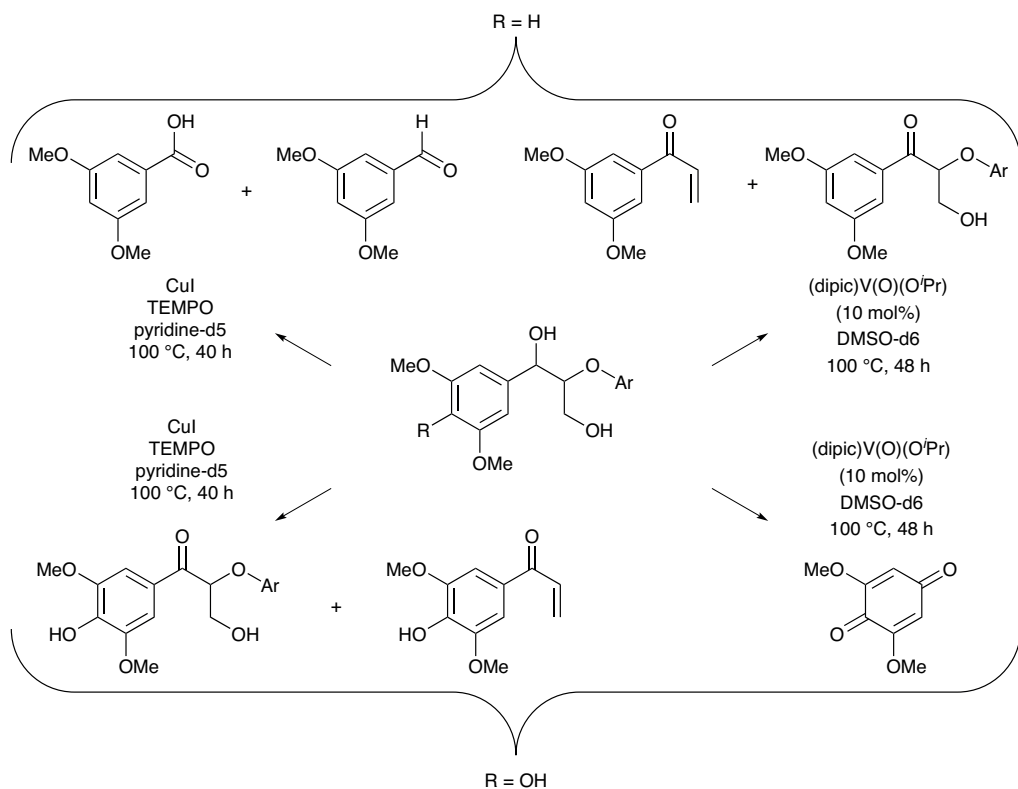
Figure 2.19: Mild oxidative pathways catalysed by a vanadium-oxo dipicolinate complex or CuI/ TEMPO, for cleavage of β–O–4-linked lignin model species: (a) 1-(3,5-dimethoxyphenyl)-2-(2-methoxyphenoxy)propane-1,3-diol, and (b) 1-(4-hydroxy-3,5-dimethoxyphenyl)-2-(2-methoxy-phenoxy)propane-1,3-diol.

and carbon-oxygen bond cleavage in the β–O–4 substructure.[344] A copper-catalysed oxidative process on the same model compound, by contrast, led primarily to an α-ketone.[345] These examples again outline the need of a careful choice of model compound and catalytic parameters, as the modification of a single substituent or metal complex can exert a profound influence on the predominant depolymerisation pathway(s).

Carbon-carbon bond cleavage via metal-free Baeyer-Villiger oxidation of 1-(3,4-dimethoxyphenyl)-2-(3-methoxy-5-propylphenoxy)propan-1-one with aqueous H_2O_2 in HCO_2H/CH_2Cl_2 was also demonstrated.[346] The C_α–C_β bond was successfully cleaved although only the 3,4-dimethoxybenzoic acid product could be isolated. The corresponding aldehyde and phenol fragments were presumed to undergo oxidative polymerisation reactions.

Vanadium- and copper-doped hydrotalcite materials were also found to depolymerise lignin under oxidative conditions,[347] whereby the hydrotalcite is believed to act as a reservoir for the release of homogeneous copper and vanadium species. Catalysts doped both with vanadium and copper gave rise to synergistic properties, and the depolymerisation of an organosolv lignin (extracted from Beech using mild water/ethanol conditions) led to a significant reduction in the apparent molecular weight (from 1100 to 300 Da, based on GPC analysis) in pyridine as solvent, under a 1.0 MPa pressure of O_2. HSQC NMR spectra revealed the full conversion of β-ether and resinol structures and *p*-hydroxycinnamyl alcohols. The low molecular weight fraction was assumed to consist of dimers or trimers, which was further supported by analysis by MALDI-TOF-MS, but these were not further isolated or identified. The reaction was also performed on kraft lignin, for which degradation of the β-ether units was also observed.

An iron(III) DABCO complex was recently reported to oxidatively cleave lignin using hydrogen peroxide as the oxidant in a DMSO/water solvent mixture.[348] A non-phenolic β-ether model compound was cleaved to afford guaiacol and veratraldehyde as the major products (in 47% and 46% maximum yield, respectively). The reaction is believed to proceed *via* a Fenton-type radical initiation mechanism, with DMSO providing reactive methyl radicals. However, using a model compound with a free-phenolic functionality the yield of guaiacol fell considerably (from 47 to 27%) and no veratraldehyde was detected. The system was subsequently applied to an organosolv lignin (isolated from Beech); HSQC NMR revealed cleavage of the β-ether units, accompanied by the disappearance of characteristic peaks for resinol and phenylcoumaran structures. GPC analysis also revealed a significant reduction of the molecular weight, but no monomeric products were isolated.

Some other recent developments in mild oxidative depolymerisation of lignin include direct photochemical oxidation[349] and radical oxidation performed in an ionic liquid solvent.[350] The former strategy was conducted on a β-ether model compound, which was cleaved by irradiation with visible light, in the presence of 10 mol% 1,4-hydroquinone and 2 mol% Cu/AlO(OH). This reaction afforded the corresponding benzaldehyde and phenol derivatives (albeit at low yields of 10-20%). The use of the ionic liquid 1-benzyl-3-methylimidazolium *bis*(trifluoromethanesulfonyl)imide as the reaction solvent was found to promote the generation of the hydroperoxyl radical (HOO·) under an oxygen atmosphere in a metal-free system. The cleavage of a β-ether model rendered high yields (*ca*. 80%) of the corresponding benzoic acid and phenol.[350] However, these novel methods have yet to demonstrate their applicability in lignin depolymerisation.

2.3.3.2 Mild Reductive Depolymerisation Pathways

The *tris*(perfluorophenyl)borane-catalysed reduction of an ether or alcohol with stoichiometric amounts of a hydrosilane is established organic synthetic methodology,[351-352] and has been recently applied to the reductive depolymerisation of lignin.[353] At room temperature, β-ether model compounds with increasing functionality could be effectively cleaved using excess triethylsilane in CH_2Cl_2 (Figure 2.20). The conversion of 2-phenoxy-1-phenylethanol resulted in triethyl(phenoxy)silane and triethyl(phenethoxy)silane in yields exceeding 90%, the latter compound being formed through the migration of the phenyl group. The corresponding alcohols could be obtained by acid-catalysed hydrolysis. Alternatively, phenylalkanes can be produced by extending the reaction time or adding extra equivalents of reducing agent. Notably, methoxy substituents are also converted into silyl ethers under the applied conditions. The commercially relevant silanes poly(methylhydrosiloxane) and tetramethyldisiloxane were identified as equally effective reducing agents for the reaction performed on simple β-ether model compounds.

This mild reductive triethylsilane method was subsequently implemented on formacell lignin derived from Black Poplar.[326] Four mono-aromatic compounds, representing both the silylated propanol and propane derivatives of guaiacol and syringol units, in net 20 wt% yield (i.e., accounting for weight added by silylation) relative to the input of lignin were isolated. Using lignin derived from the softwood Norway Spruce instead, a single silylated propylcatechol product could be obtained at a 21 wt% yield. Analysis of the residual lignin demonstrated that the β-ether units were fully converted by the reduction procedure. In addition, Pinewood lignin extracted by formacell, ethanosolv, methanosolv or acetosolv methods afforded 25, 18, 12 and 4 wt% yields of silylated phenols, respectively, offering a clear example of the influence of different upstream methods on the availability of labile β–ethers in the catalytic downstream processing of technical lignins.
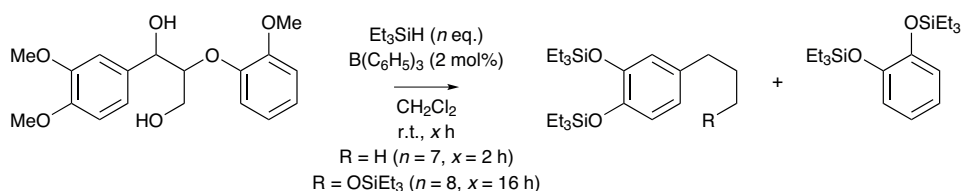
Multiple Formacell Lignins
G or S product depending on feedstock, R = H or R = OSiEt3 depending on conditions;
7-24% of hydrolysed alcohols isolated.

Figure 2.20: Mild reductive cleavage of a simple β-ether model compound, using excess triethylsilane and catalytic *tris*(perfluorophenyl)borane. For experiments with actual lignins, the results are indicated below the reaction scheme.

Hydrosilane loading offered control over selectivity to either the propane or propanol derivatives. Hydrolysis of each obtained triethylsilylated product finally enabled isolation of the corresponding catechol. Although high yields may be obtained by this depolymerisation pathway, the greater-than-stoichiometric use of a silylating agent would need to be addressed (e.g., by regeneration and/or recycling) for the operation of such a process on the large scale required for lignin processing.

2.3.3.3 Mild Redox-Neutral Depolymerisation Pathways

Redox-neutral methods for the depolymerisation of lignin under mild conditions have also been developed. Typically, the redox-neutral criterion can be achieved either by means of dehydrogenation of the lignin (or model) substrate itself, which provides the requisite H_2 for cleavage of the C–O ether (or other) bond, or through hydrolytic ether cleavage.

Redox-neutral cleavage of lignin model compounds has been reported with the use of vanadium Schiff-base complexes as catalysts.[354] A complex containing a sterically bulky tridentate ligand led to high conversion of 1-(4-ethoxy-3-methoxyphenyl)-2-(2-methoxyphenoxy)propane-1,3-diol, with good selectivity to the α,β-unsaturated ketone product 1-(4-ethoxy-3-methoxyphenyl)prop-2-en-1-one, the product of a formal elimination and dehydration reaction (Figure 2.21a). Mechanistic studies showed that for the reaction to proceed, a free α-hydroxyl group is required, whereas alkylation at the γ-OH exerts no effect on the reaction outcome.

The same vanadium complex was applied to the depolymerisation of organosolv lignins, extracted from *Miscanthus giganteus* using acetone, ethanol or 1,4-dioxane.[355] GPC results revealed a reduction in molecular weight of the lignins. The ethanosolv lignin underwent depolymerisation to a lesser extent compared to the other lignins studied. *O*-ethylation of the benzylic alcohol moiety in lignin during ethanosolv pulping[41] is responsible for this difference in reactivity, as a free α-hydroxy group is required for the catalytic reaction, in line with the model compound studies. This outcome clearly shows that solvent choice in upstream fractionation of lignocellulose carries implications for the efficiency of the catalytic downstream processing of the isolated lignin. Finally, 2D NMR experiments confirmed the disappearance of characteristic β-ether unit cross peaks in the treated lignins; units with other linkage types were largely unaffected by the depolymerisation procedure. However, the primary products observed were vanillin and syringaldehyde rather than the expected enone products. Further investigation is required in order to optimise the system and improve the yield of mono-aromatics. Solvent selection and possible derivatising effects are clearly important points to be further studied.

A redox-neutral, ruthenium-Xantphos-catalysed cleavage of β-ether units has also been demonstrated (Figure 2.21b);[338] 2-aryloxy-1-arylethanols were successfully cleaved to the corresponding phenols and acetophenones by employing 1 mol% $RuH_2(CO)(PPh_3)_3$ and 1 mol% Xantphos in toluene. The reaction was expanded to the synthetic β-ether polymer poly(4-hydroxy-1-phenethanol), yielding 4-hydroxyacetophenone in nearly quantitative yield. However, attempts to cleave models more similar to the actual lignin structural motifs afforded cleavage products only in low yield.[356] Instead, a double dehydrogenated substrate was found to have chelated to the ruthenium metal centre, inhibiting further catalytic activity. An acetylated keto-β-ether model on the other hand did undergo cleavage, yielding both the acetophenone and propiophenone, but also a large amount of condensation products. Preliminary small-scale experiments on an acetylated kraft lignin did seem to suggest cleavage of the lignin, but the products could not be unambiguously identified.[357]

Ruthenium-triphos complexes have also proved competent catalysts for the cleavage of 2-aryloxy-1-arylethanols.[358] Interestingly, when the triphos catalytic system was applied to the β-ether model 1-(3,4-dimethoxyphenyl)-2-(2-methoxyphenoxy)-propane-1,3-diol (Figure 2.21c), C_α–C_β carbon-carbon bond cleavage instead occurred, affording the corresponding benzaldehyde and 2-guaiacylethanol species;[359] a retro-aldol mechanism with internal hydrogen transfer was proposed. In analogy to the oxidative vanadium-catalysed cleavage, the examples of redox-neutral ruthenium catalysis demonstrate that alternative cleaving mechanisms at the β–O–4 linkage may occur upon *minor* modification of the model compound, catalyst properties or solvent.

Mild cleavage of β-ether units was reported with a heterogeneous palladium on carbon catalyst, generating the acetophenones and phenols.[274] A broad array of 2-aryloxy-1-arylethanol species could be cleaved using one equivalent of ammonium formate and 2.5 mol% of Pd/C at 80 °C, in a mixture of methyl *tert*-butylether and water in air, affording the corresponding acetophenone in >90% yield (Figure 2.21d). A model polymer, *poly*-(4-hydroxyphenyl)ethane-1,2-diol, could also be cleaved to obtain mono-aromatics in excellent yield. In analogy to the ruthenium-catalysed systems, the substituent at the γ-position has a profound impact on the reactivity. The cleavage of aryl glyceryl ethers was challenging, requiring excess ammonium formate and a second reaction step incorporating formic acid, leading to the reduced arylpropane and arylpropanol products (Figure 2.21d). The reaction likely proceeds by initial dehydrogenation at the benzylic alcohol to form a ketone, which is the species susceptible to hydrogenolysis (with ammonium formate acting as a hydrogen donor). The catalytic procedure was also performed on a dioxasolv lignin isolated from *Pinus sylvestris*; a modest reduction in molecular weight was observed by GPC, and HSQC NMR analyses demonstrated that 73% of the β-ether units (and certain ether resinol/coumaran units) were cleaved. Monomer
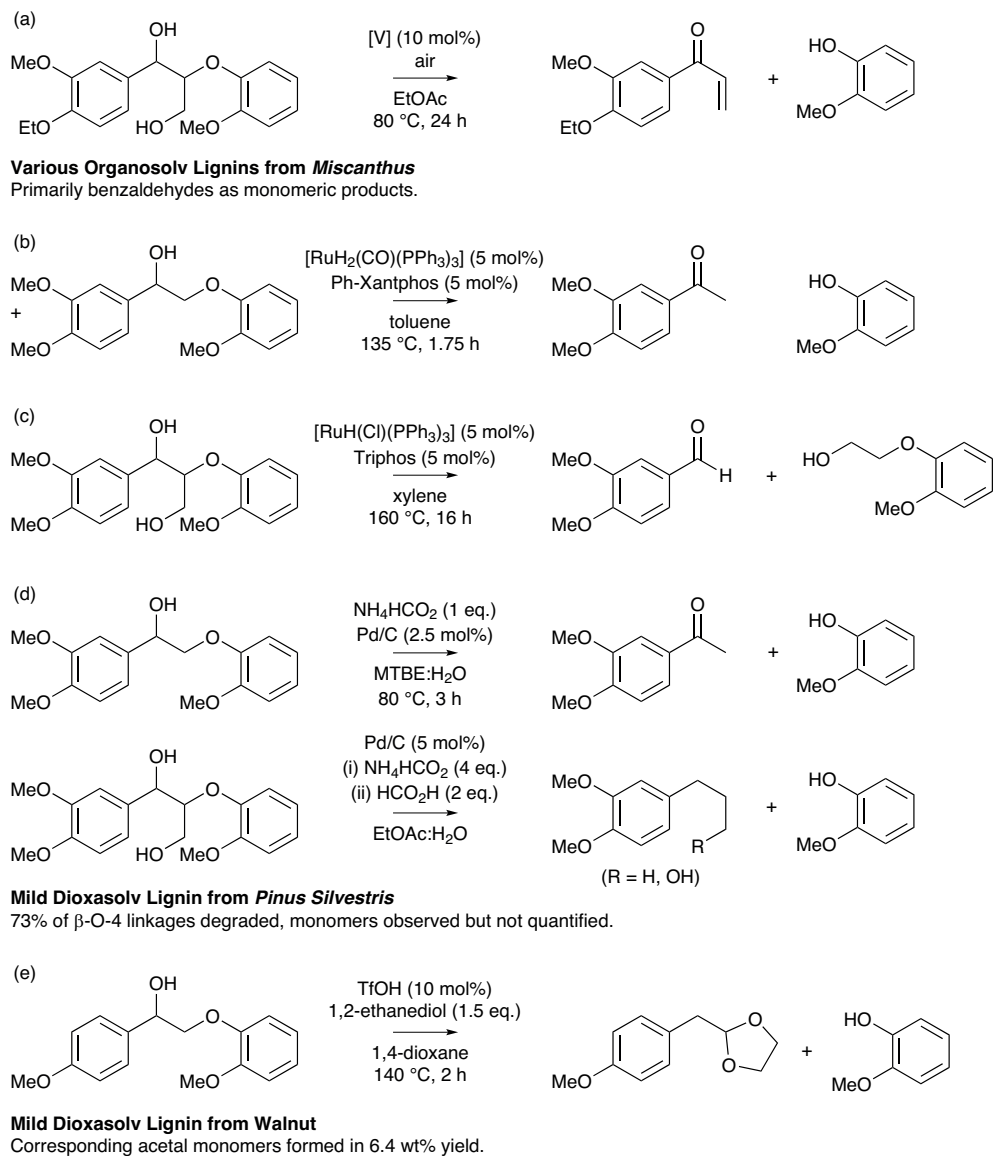
Figure 2.21: Select mild redox-neutral cleavage pathways, (a)-(e), for β-ether lignin model substrates. For experiments performed using actual lignins, the results are indicated below the reaction scheme.

products dihydroconiferyl alcohol and dihydro-*p*-coumaryl alcohol were detected by GC-MS, but not quantified.

Recent investigations of the acid-catalysed hydrolysis of a Dioxasolv walnut lignin have demonstrated the possibility of cleaving the aryl ether units, followed by reactive

'trapping' of the generated aldehydes in the form of a cyclic acetal, preventing the products from subsequent recondensation (Figure 2.21e).[234] Reaction of the simple β-ether model compound 2-phenoxy-1-phenylethan-1-ol with 10 mol% triflic acid in 1,4-dioxane at 140 °C in the absence of a trapping reagent yielded guaiacol in high yield, but 2-phenylacetaldehyde was only detected in small quantities, presumably lost to secondary aldol condensation reactions. Incorporating 1.5 equivalents of ethylene glycol, however, enabled isolation of the cyclic acetal in >90% yield. Alternatively, the intermediate may be trapped by *in situ* hydrogenation over Ru/C, although the product is a complex mixture of (semi-) hydrogenated and hydrogenolysed species. Furthermore, the aldehyde intermediate could be trapped by decarbonylation with $IrCl(cod)_2$ and PPh_3, which afforded toluene in 73% yield for the β-ether model compound. All three methods were further investigated for the depolymerisation of a dioxasolv lignin. Trapping of lignin-derived aldehyde products as acetals afforded a threefold increase in monomer yields relative to the control experiment, whereas hydrogenation improved the yield of monoaromatics by a factor of five. Decarbonylation demonstrated only a moderate increase in monoaromatics yield, however, which was attributed to the relatively slow rate of the iridium-catalysed reaction.

The aforementioned examples show that a broad array of mild oxidative, reductive, and redox-neutral pathways for the depolymerisation of β-ether lignin model compounds has emerged in the contemporary chemical literature. Moreover, several of these catalytic methods have been successfully applied to the treatment of lignin samples (typically organosolv lignins isolated under relatively mild conditions, and thus, assumed to still retain an appreciable fraction of the native β–O–4 linkages). Nevertheless, the examples also demonstrate that the modification of a single functional group (even when not in close proximity to the β–O–4 linkage), or modest changes to the catalytic system or process conditions, can result in pronounced changes in the chemistry observed and in the composition of the product mixture. Expectedly, neither (simple) model compounds nor synthetic β–O–4 polymers thus sufficiently represent the chemical complexity of the isolated technical lignins. Furthermore, economic constraints associated with the catalysts and reagents used have to be carefully considered with regard to large-scale industrial implementation. Finally, the extraction of limited amounts of high-value products should preferably be part of a cascade approach, in which the remnant lignin is also further valorised. To aid the latter, analytical data not only on the volatile or monoaromatic fraction, but also on the residual macromolecular components would provide valuable information on the action of homogeneous catalysts on the polymeric structure of lignin.

2.3.4 Harsh Depolymerisation Pathways

As discussed in the previous sections, the more reactive bonds (foremost, but not exclusively, β–ethers) will have already been cleaved to a significant extent for technical lignins. The 'toolbox' of mild and chemoselective catalytic cleavage methods (outlined in the previous sections) are, therefore, expected to prove largely ineffective for the depolymerisation and generation of value-added products from such refractory, degraded lignins. For highly condensed, technical lignins, effective depolymerisation requires more severe conditions (i.e., higher operating temperatures or pressures) as they are cross-linked by strong C—C bonds. The higher-severity conditions reduce the ability of the catalyst to steer selectivity to specific target molecules; instead, the production of a lignin oil with more complex chemical composition is typical. Accordingly, the criteria against which successful depolymerisation is measured are altered. The degree of deoxygenation, boiling point range, degree of (ring) saturation, and molecular weight distribution often constitute key final properties of the product mixture, and the harsh depolymerisation process may be then tailored to produce a range of compounds that collectively exhibit the desired physical and chemical characteristics for the intended application (e.g., fuels).

It may be feasible for lignin oils to be further refined into mixtures of value-added products, in analogy to the refining of crude oil, with eventual targets including BTX, phenols or cresols, which are employed as feedstocks to the chemical industry in sufficient volumes as to warrant large-scale production. The price of the catalysts and recyclability, the intrinsic cost of the solvent and loss due to evaporation, decomposition and inhibition of substrate and catalyst, the infeasibility of using costly stoichiometric reagents (e.g., protective groups) and the environmental burden of any waste material are all factors that will determine both the economic and environmental feasibility of any prospective process based on harsh lignin depolymerisation.

A typical approach for the depolymerisation of lignin under harsh conditions employs either an acid or a base catalyst, a supported metal catalyst with hydrogen transfer capability, or a combination of both, at temperatures of up to around 400 °C. Under these operating conditions, it is sometimes difficult to distinguish the contributions of catalytic and thermochemical reactions to the process outcome. Indeed, significant conversion of lignin is often observed without added catalyst under 'control' conditions. Solvents are typically water or lower alcohols, as well as phenols or even the products themselves in some cases. An external input of gaseous hydrogen may be employed in order to improve the catalytic activity for hydrogenolysis and carbonyl hydrogenation. Nonetheless, the reforming of the alcohol solvent is often sufficient to supply the process with molecular hydrogen at low levels so that saturation of the aromatic rings is minimised. This aspect is of critical importance if the production of BTX from aromatic-rich oils is desired. Alternatively, formic acid may be used as a hydrogen donor. Besides the

lignin-derived 'bio-oil', an insoluble 'char' is commonly obtained, and both water-soluble organics and gaseous products may evolve.

In the next sections, analytical techniques commonly employed for characterisation of lignin oils and selected harsh depolymerisation methods are briefly described. Regarding the characterisation of lignin products, the discussion is neither exhaustive nor intended to be a strict instruction towards or against specific analysis methods. Instead, it aims to offer some constructive suggestions regarding key considerations for the effective characterisation of (gaseous, liquid or solid) lignin products. Finally, selected recent methods for depolymerisation are highlighted, ordered so as to clearly indicate ways in which important and recurring aspects of harsh depolymerisation procedures can be addressed. Crucially, although the following sections centre around harsh depolymerisation methods, the discussion is also highly relevant to the milder methodologies described in the previous sections.

2.3.4.1 Characterisation of the Lignin Products

Thorough characterisation of the often highly complex lignin-derived products demands the use of a broad array of techniques for analysis of the liquid, solid and gaseous products obtained from lignin conversion. Regarding the liquid species, which are often the desired products obtained from mild or harsh depolymerisation methods, it should be noted that the terms 'lignin oil', 'bio-oil', 'product oil', and 'liquid product' are all equally ambiguous. Indeed, they may refer to a directly obtained liquid phase (after solids have been removed by filtration), via extraction into a solvent (commonly CH_2Cl_2 or EtOAc), or else through initial concentration by solvent removal. Although this seems to be merely a semantic problem, the lack of an unambiguous definition of the content of the liquid product (often quoted in wt% of the original lignin feedstock) hinders, to a certain extent, unbiased comparisons of the data. Residual solvent content in the oil, in particular water (3.3 wt% solubility in EtOAc at 20 °C), may lead to an overestimation of the yield. Conversely, prolonged solvent removal under rotary evaporation conditions may lead to an underestimation of the yield of liquid products, as lighter (more volatile) fractions are likely to be removed alongside the solvent.

Concerning the chemical composition of the liquid products, characterisation is most often performed by using Gas Chromatography coupled with Mass Spectrometry or Flame Ionisation Detection (GC-MS/GC-FID). While the former can aid in identification of volatile products, quantification should be done with the latter. However, the frequently encountered practice of analysing lignin oil samples without the addition of a standard, internal or external, for GC makes thorough and quantitative evaluation difficult. This is further compounded by the fact that authentic samples for calibration are not available commercially for many of the volatile lignin products, which must then

be (often laboriously) synthesized. Moreover, it must be recognised that the observed volatile compounds are often a poor representation of the net composition of the liquid products. In this context, Thermogravimetric Analysis (TGA) experiments of the liquid product, performed under an inert atmosphere (e.g., Ar, N_2) and at a low heating rate (e.g., 5-10 °C min^{-1}), are highly useful for estimating the fraction of volatile compounds at the injector temperature.[198]

As conventional one-dimensional GC techniques are actually not capable of fully resolving the individual components of the lignin oil, two-dimensional GC methods (e.g., GC×GC-MS/FID) are beneficial and strongly recommended. In GC×GC images, each volatile component can be grouped together with analogous, structurally related species. Furthermore, this analytical technique markedly improves both the resolution power and sensitivity, enhancing the capability for cross-checking against MS databases. Nonetheless, caution must be exercised when using the 'National Institute of Standards and Technology' (NIST) and Wiley libraries to identify the lignin products detected by (GCx)GC-MS. The libraries are a valuable yet non-exhaustive resource of structural information; products anticipated from lignin depolymerisation are often absent from the database, potentially leading to misinterpretation of the observed compounds (for example, peak assignments to unrealistic structural isomers).

As previously described, GC techniques are able to analyse only the volatile fraction of products in the lignin oil. However, the lignin oil will typically also contain non-volatile and higher-molecular-weight components. Therefore, characterisation by GC must be complemented by techniques that analyse the whole oil. Specifically, Gel Permeation Chromatography (GPC) offers an approximate indication of molecular weight and size distribution,[36] which may be compared against the determined quantities of volatile species. Noteworthy is the fact that, in GPC, the molecular weight is only indirectly inferred from the hydrodynamic volume of the analyte. Indeed, solvent effects and lack of suitable calibration standards seriously complicate molar mass determination. Cross-linking can significantly decrease the apparent molecular weight observed by GPC, for instance, whereas branching might have an opposite effect, with both effects not being captured by the linear polymers used for calibration. Unsurprisingly, molar mass determination of an Alcell hardwood lignin gave widely different results by small angle neutron scattering (26 kDa), GPC (3 kDa), and electrospray ionisation (ESI) mass spectrometry (18-30 kDa). In addition, the neutron scattering results suggested that the material is much denser than expected for a linear polymer. It was proposed that lignin in solution has a rather compact structure reminiscent of a hyperbranched polymer or nanogel. As such a compact structure has a rather small hydrodynamic volume it thus appears to be of low molecular weight in GPC, explaining the observed discrepancy.

Mass spectrometry coupled with Electrospray Ionisation (ESI-MS) is capable of resolving the complexity of the fraction of intermediate molecular weight (300-1500 Da),

which is particularly difficult to analyse.[318,362-363] Moreover, the use of multidimensional MS allows for structure elucidation from fragmentation patterns. Importantly, ESI-MS/MS offers the possibility for advanced quantitative analysis not only of this intermediate fraction, but of complex mixtures of lignin products in general. Nevertheless, the intermediate molecular weight fraction requires more attention. As the analytical challenges here are similar to those faced in the characterisation of the crude oil bitumen fraction,[364-365] analytical protocols used in this field may aid the analysis of lignin products in some instances.[277,366-369]

Some insight into the chemical reactivity and mechanisms underlying lignin depolymerisation may be gained from evaluation of the 'carbon balance' of the transformation. In this context, determination of the elemental composition of residual fractions (not simply the volatile fraction) in addition to the liquid products is mandatory. Elemental analysis is also widely employed for the characterisation of the liquid product, with (atomic) C/H and C/O indices offering valuable information on oxygen content (reduction of oxygen content is a common target in the catalytic upgrading of lignin), hydrogen consumption, and heating value. A graphical representation of changes in C/H and C/O values in a Van Krevelen plot might furthermore provide insight into which reaction types dominate (e.g. dehydration, reduction, etc.). Gravimetric and elemental analyses of the residual solids are essential to aid in understanding any repolymerisation processes. Moreover, the severe conditions of 'harsh depolymerisation' will likely generate a non-negligible fraction of gaseous products; compositional analysis (e.g., Micro-GC coupled with Mass Spectrometry) of the gas phase is, therefore, highly desired. Finally, the water-soluble organics are clearly more difficult to isolate and quantify. Accordingly, the determination of the total organic carbon is important for the proper assessment of the carbon balance.[370]

Comprehensive lignin product analysis thus requires a considerable research effort, yet is rewarded with valuable information. This is illustrated by an investigation of the oligomeric fraction of depolymerised EMAL lignin after a Pd/C catalysed hydrogenolysis procedure.[366] The obtained oil consisted of an approximately 1:1:2 mixture of mono-, di-aromatics and oligomers. After thorough extraction with diethyl ether, the higher molecular weight fraction was isolated and subjected to further analysis. With ESI-MS, trimers and tetramers were detected and, based on their molecular weight, were found to be mostly 4-propylguaiacol oligomers. HSQC and ^{31}P NMR further revealed the inter-unit linkages to be largely β–5, 5–5 and 4–O–5 linkages, with β–1 and β–β linkages present in small amounts. The dimeric and oligomeric fractions of the bio-oils obtained from the reactive fractionation of birch sawdust over a Ru/C catalyst were also extensively characterised.[277] Major dimeric products were found to have β–1 and β–5 linkages along with small amounts of 5–5 and 4–O–5 linkages. Surprisingly, β–β linkages, thought common in birch lignin, were not observed. Further HSQC analysis of the

oligomer fraction also confirmed these bonds to be prevalent in the higher molecular weight residual lignin. Interestingly, similar to the lignin oil fractionation noted above, a method was recently reported for separating five different technical lignins into fractions of varying molecular weight. ^{31}P NMR analysis on the separated fractions showed the lower molecular weight fractions to be less condensed.[368] The development of preparative liquid chromatography procedures or organic solvent nanofiltration,[367] followed by 2D NMR, would also be able to offer a further wealth of structural information. The insight that will be gained from these 'advanced' fractionation and analysis techniques could well provide valuable information for the design of novel lignin (cascade) depolymerisation strategies.

Notably, there is a pressing need within the catalysis community working on lignin for standardisation of analytical protocols, to allow for a proper comparison of (emerging) processes. To meet this requirement, a collaborative and multi-disciplinary approach between research groups is needed in order to translate the considerable number of analytical methods for lignin characterisation (developed by wood chemists) into standard protocols for the characterisation of lignin products obtained from catalytic reactions. Likewise, rational design and standarisation of 'work-up'/purification procedures is of paramount importance for effective comparison of processes for lignin depolymerisation.[371] A similar desire for a best-practices approach for the characterisation of bio-oils obtained from catalytic pyrolysis was recently proposed in a review.[369] Clearly, whilst the physical and chemical properties of the lignin products are influenced strongly by the choice of treatment, the methodologies for evaluation of their properties should be as consistent as possible across research laboratories.

2.3.4.2 Reactivity of Technical Lignins

Logically, the variety of structural motifs occurring in lignin streams, as a result of different sources and isolation methods, must be taken into account for the design of effective depolymerisation processes. Although it is tempting to directly compare different catalytic systems, this is often hampered by the fact that different lignin feedstocks have been employed. Indeed, for the mild methods, the relationship between available cleavable bonds and activity can more directly be established. For harsher depolymerisation methods, it is much more difficult to recognise such a relationship, given that multiple bonds may be cleaved both under catalytic and thermal control. A systematic comparison of different lignin sources in the same catalytic process is therefore highly valuable, but unfortunately, such literature is very scarce.

In one of the few examples, the depolymerisation of four lignin samples (i.e., soda wheat straw, AFEX wheat straw, organosolv Poplar, and ammonia Poplar), in the presence of Pt/Al_2O_3 catalysts at 300 °C in a methanol-water solvent (Figure 2.22), was compared.[194]
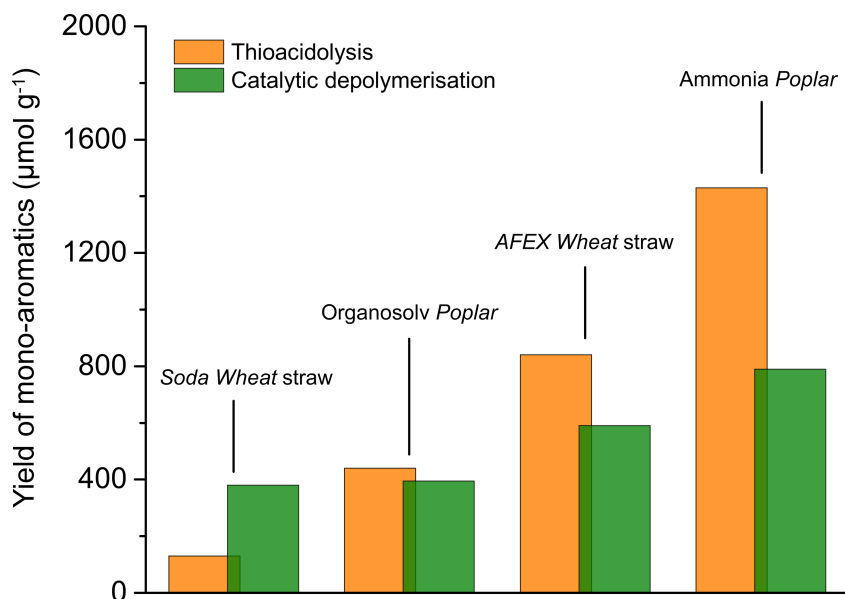
Figure 2.22: Comparison of lignin monomer yields *via* catalytic depolymerisation (green) *vs.* thioacidolysis (orange), of differing lignin samples, as a measure of degree of condensation.[194]

Interestingly, there is a good correlation between the relative yields obtained from the catalytic depolymerisation and analytical chemical degradation by thioacidolysis. This example suggests that the thioacidolysis method constitutes a useful, correlative approach for ranking lignin streams according to their potential for production of mono-aromatics products. This consideration is logical given that the thioacidolysis method is predicated on the cleavage of β-ether bonds. Regarding the lignin residues, GPC traces after reaction were similar for each lignin, suggesting convergence to a highly condensed lignin that is resistant to further depolymerisation.

It is often asserted that organosolv lignins are more amenable towards depolymerisation than those obtained from paper-mill operations. Nevertheless, the fraction of readily cleavable linkages (primarily β–O–4) in several types of technical organosolv lignins (mostly those obtained with added acid or base catalysts) has already been significantly reduced compared to the native lignin. An organosolv lignin may therefore sometimes resemble kraft lignin in recalcitrance. In some cases, organosolv lignins may in fact be even *more* difficult to cleave; the structural profiles of Organolsolv lignins obtained from the different severities of the 'same' organosolv process as shown in Figure 2.7 clearly illustrate this. Another example is provided by liquid-phase reforming of lignin using a Pt/γ-Al$_2$O$_3$ catalyst (with H$_2$SO$_4$ co-catalyst),[372] giving 18 wt% of mono-aromatics from kraft lignin compared to 9 wt% of mono-aromatics with an organosolv lignin. It remains to be verified whether the degree of condensation is responsible for the differences in yields obtained from the processing of the studied kraft and organosolv lignins. In any

case, it is not enough to assume that a process (or a process name) defines a lignin – the lignin must be profiled first to allow any understanding of a process that is applied to it.

Another example highlighting the influence of structure on depolymerisation is that of candlenut-derived lignin (*Aleurites moluccana*), catalysed by copper supported on a porous metal oxide catalyst under relatively mild conditions in methanol (140 °C, 40 bar H_2). This generated a series of 4-propylcatechol-type products in up to 64% monomer yields.[373] Compounds of this type have not been isolated from other lignins. Therefore, it is likely that the structure of the candlenut lignin differs from that in other feedstocks. As has been highlighted above in Section 2.2.3, homogeneous linear lignins derived solely from caffeyl alcohol or 5-hydroxyconiferyl alcohol have been recently discovered, attesting to this possibility.[143,374]

2.3.4.3 Solvents

Assumedly, the solubility of technical lignins is of critical importance for all catalytic depolymerisation methods, including harsh processes. Among other reasons, it has been demonstrated that insoluble lignin fractions may cause increased char formation during depolymerisation.[375] Lignin solubility is influenced, at least in part, by the structure and bonding properties of the macromolecules. At room temperature, isolated lignins that closely resemble native lignins (e.g., cellulolytic enzyme lignins, certain organosolv lignins) have low water solubility, and low solubility in pure polar organic solvents (e.g., ethanol, acetone, 1,4-dioxane), but moderate solubility in alkaline solutions, and may be completely soluble in mixtures of polar organic solvents and water that have the right solvent factor – 9:1 acetone:water and 96:4 dioxane water are established examples. By contrast, technical lignins (e.g., kraft lignin) are often comparatively insoluble in the same organic solvents or their mixtures with water.[372] Selected classes of imidazolium-derived ionic liquids (ILs) have shown capability for dissolving both lignin and lignocellulosic biomass itself (in sawdust form),[376-379] in particular those with strongly hydrogen-bonding basic anions to disrupt hydrogen bonding networks.[380-382] However, the often-associated high (aquatic) toxicities and other concerns associated with ILs still constitute barriers against their successful use in large-scale processes. For a more thorough discussion of lignin in ILs, the reader is directed to two recent review articles.[23,379]

Importantly, for any depolymerisation method, the actual solubility of lignin and solvent properties will markedly differ under process conditions from those determined at room temperature. At temperatures between 200 and 350 °C, under pressures higher than 10 MPa, many common solvents already experience near-critical, critical, or even supercritical conditions, causing the reaction medium to possess very distinguished properties. For instance, even water, a highly polar solvent, shows a substantial decrease in polarity under near-critical conditions. As a result, near-critical water is completely
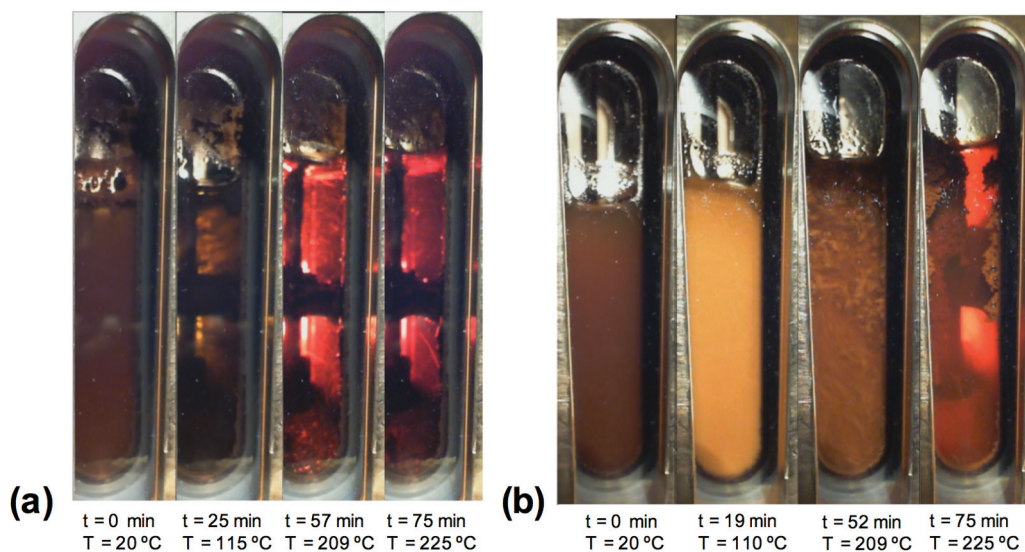
Figure 2.23. Images for dissolution of an organosolv lignin (a) and kraft lignin (b) (in water from 20 to 225 °C), taken in a high-pressure autoclave equipped with an optical window. Adapted with permission from *ChemSusChem,* 2011, **4**, 369-378.[375] Copyright 2011 John Wiley and Sons.

miscible with toluene.[383] Therefore, the assessment of the effects of lignin solubility upon the performance of catalytic depolymerisation must be performed under processing conditions, and not extrapolated from observations at room temperature.

Harsh depolymerisation methods are typically carried out in stainless steel pressure vessels. In this manner, the actual solubility of lignin (and the point at which solid residues begin to form) under such conditions is rarely known. However, the complete dissolution of an (initially insoluble) organosolv lignin at 115-130 °C under neutral aqueous conditions was demonstrated in a pressure vessel equipped with a glass window (Figure 2.23a).[375] By contrast, dissolution of a kraft lignin (Figure 2.23b) was accompanied by agglomeration of solids onto the window. Gas bubbles were observed from the agglomerates, suggesting formation of gaseous products. In a 1:1 water:ethanol mixture, both kraft and organosolv lignin were fully dissolved at 115 °C and agglomeration was completely supressed.[372]

Apart from the fact that solvents serve as media for dissolution of lignin (fragments), they also often react with the lignin or with itself and/or interact with the catalyst.[225] Regarding the former, side reactions of the solvent may generate a complex array of products. For example, in the reaction of a kraft lignin in the presence of a MoC catalyst and ethanol solvent (280 °C), an oil yield of 160 wt% was achieved, which includes a large amount of ethanol condensation products.[384] In the absence of lignin, however, yields of these products were far lower, suggesting that lignin itself plays a role in promoting

decomposition of the solvent. Solvent loss to side-products may impact the economy of the process, depending on the value and difficulty of separation of these products and the value of, and ability to recycle, the solvent. However, reactivity of the solvent can also be advantageous. Decomposition of alcohols or formic acid may be employed for *in situ* hydrogen formation, facilitating hydrogenolysis.[385] Furthermore, certain solvents may act as protective capping agents to prevent recondensation, or instead may even promote recondensation reactions, as described below.

Regarding the interactions between solvent and catalyst, in the hydrogenolysis of diphenyl ether (used as a model compound for recalcitrant ether structural motifs occurring in kraft lignins) catalysed by Raney®-Ni, strong inhibition was observed when performing the reaction in methanol or 1,4-dioxane, yet optimum reactivity was achieved in methylcyclohexane.[233] Inhibition was attributed to strong adsorption of the solvents onto the catalyst surface, blocking the active sites. Regardless of the fact that lignin is insoluble in methylcyclohexane at room temperature, an 81% conversion of organosolv lignin (isolated from Poplar without added acid) into soluble products (cyclohexanols and cycloalkanes) was achieved in the presence of Raney®-Ni at 300 °C under 70 bar H_2 (initial pressure measured at *r.t.*) for 8 h. Clearly, this example demonstrates that thermolysis of technical lignins in the liquid phase constitutes a key step that brings aromatic fragments into solution, and therefore, enables the action of solid catalysts. Thermolysis of technical lignins usually starts to be relevant and contribute to heterogeneously catalysed processes at temperatures between 200 and 250 °C. As lignin thermally decomposes at these temperatures, releasing soluble fragments into the reaction medium, its catalytic conversion can be performed even in solvents in which lignin is insoluble at room temperature (e.g., methylcyclohexane). This observation was recently confirmed by two other studies on reductive depolymerisation of lignin to cycloalkanes performed in hydrocarbon solvents.[386-387]

An interesting approach is to use the oil from a biomass liquefaction process itself as the solvent, as reported for a biomass liquefaction process in guaiacol which afforded excellent bio-oil (>93% carbon) yields.[388] Following the initial cycle, the produced oil was then used for subsequent biomass liquefaction and was demonstrated to be a still better solvent. Heavy fractions (>1 kDa) accumulated in the recycled oil, although this could be mitigated somewhat by selecting appropriate process parameters that balance the oil yield and the formation of heavy compounds.[389] Although fairly common in industry, this latter approach of employing the product as a solvent has so far been little explored with respect to catalytic lignin depolymerisation. Considering all the above examples, it is clear that the choice of solvent for a harsh lignin depolymerisation procedure is non-trivial.

Performing catalytic lignin depolymerisation in the absence of any solvent constitutes another attractive prospect.[390-392] The solvent-free hydrogenolytic depolymerisation of

a kraft lignin was recently explored, employing supported sulfided CoMo and NiMo catalysts under 100 bar H_2 at 350 °C.[393] Yields of CH_2Cl_2-soluble lignin oil increased when more basic catalyst supports were used. For instance, a NiMo catalyst supported on basic MgO-La_2O_3 afforded the highest monomer yield (26 wt%), with 4-alkylphenol compounds as the major constituents, as analysed by GC×GC-MS.

Solvent-free lignin depolymerisation may also be achieved by means of mechano-catalytic ball milling using basic catalysts. The concept was initially demonstrated on β-ether model compounds, employing 3.5 equivalents of NaOH (with Na_2SO_4 as a grinding auxiliary) and milling at 13.3 Hz to efficiently cleave the β–ethers.[394] Although guaiacol and syringol fragments could be isolated in good yields, the part of the model compound containing the propyl chain underwent several reactions, affording numerous unidentified products. Application of the procedure to an organosolv lignin from Beech wood enabled a considerable reduction in the content of β-ethers (analysed by HSQC NMR), although monomer isolation was not reported.[394]

2.3.4.4 Preventing Recondensation in Lignin Oils

It has long been recognised that the formation of reactive intermediates, particularly combinations of a phenol and aldehyde/ketone intermediate, leads to condensation and limits the efficacy of acid- or base-catalysed lignin depolymerisation procedures.[395] The repolymerisation channels are likely analogous to those previously described in the sections on isolation methods (Figure 2.11), whereby disappearance of β–O–4-containing fragments with the concomitant formation of a more recalcitrant lignin is observed. Correspondingly, there is a need to scavenge and 'deactivate' such reactive phenol, carbonyl and/or alkene functionalities in order to increase the yield of lignin oil. In one such strategy, a base-catalysed depolymerisation was performed with boric acid so as to convert the liberated phenols to the corresponding borate esters. The yield of bio-oil more than doubled to 52 wt%, relative to the standard NaOH-catalysed process.[395] As previously noted, for hydrogenolytic processes with added transition metal catalysts, removal of reactive functional groups is implicit, typically by hydrogenation of exposed carbonyl functional groups to the corresponding alcohols or alkanes. This is demonstrated by the depolymerisation of cellulolytic enzyme lignin from bamboo over a physical mixture of an acidic catalyst (ultrastable zeolite Y) and a hydrogenolysis catalyst (Raney®-nickel), using methanol as both the solvent and hydrogen donor.[396] Greatly improved bio-oil yields were obtained when the two catalysts were concomitantly used (28 wt%, *vs*. 3/13 wt% with only the acid/Ni catalyst);[396] the two catalysts thus appear to cleave different bonds in a complimentary manner.

The choice of solvent also has a profound influence on the propensity of depolymerised lignin oil to undergo recondensation. For example, the depolymerisation of lignin over
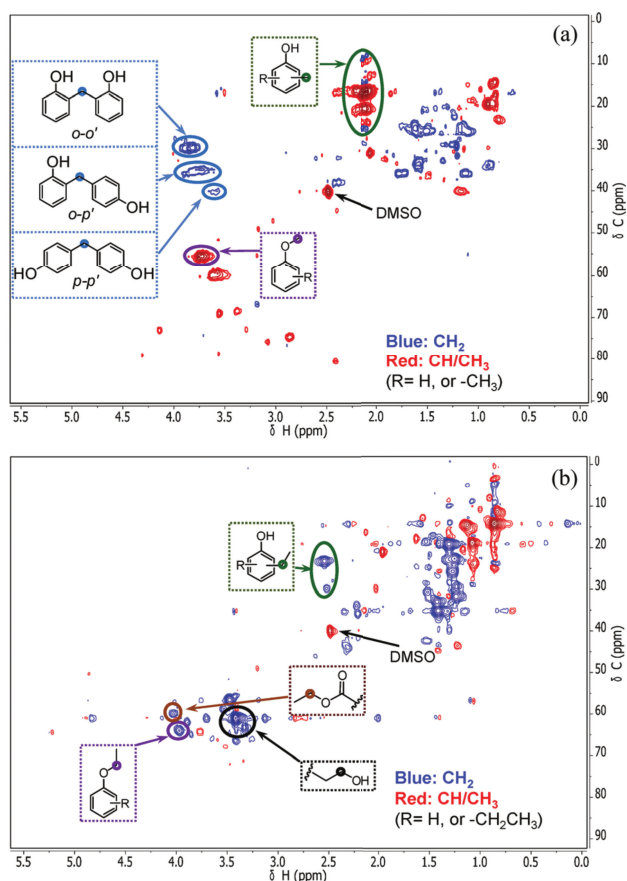
Figure 2.24: HSQC NMR spectra highlighting differences in reactivity of phenol in the presence of methanol (a) or ethanol (b) as solvent: with methanol, cross peaks corresponding to methylene bridges between phenol units are observed; with ethanol, C_2-alkylated phenols are instead visible. Adapted with permission from *Green Chem.,* 2015, **17**, 4941-4950.[288] Copyright 2015 Royal Society of Chemistry.

copper supported on (basic) porous metal oxides was initially reported in methanol.[397] However, a significant beneficial effect of using ethanol as a solvent was later discovered.[288,371] Indeed, ethanol may function as a 'capping agent' by ethoxylating reactive phenol moieties and preventing subsequent recondensation. HSQC NMR analysis of a Protobind-derived lignin oil, depolymerised in ethanol over the same catalyst at 300 °C, demonstrated extensive alkylation, with phenol-O alkylation preceding ring C-alkylation. Consequently, 17 wt% mono-aromatics and 73 wt% THF-soluble lignin oil were obtained under these conditions, whereas yields were limited to 6 wt% and 57 wt% in methanol.

Although methanol similarly demonstrates the ability to alkylate lignin fragments,[398] *in situ* formation of formaldehyde (from methanol) can occur, which undergoes condensation with phenols to form polymeric by-products. This phenomenon was clearly demonstrated by model reactions with phenol in either methanol or ethanol, highlighting the formation of diphenylmethanes in methanol, yet the formation of alkyl and alkoxyphenols in ethanol (Figure 2.24). Due to increased steric bulk, the alkyl-/alkoxyphenols are considerably less susceptible to recondensation. When employing a 1:1 methanol:ethanol solvent mixture, ethanol can furthermore 'scavenge' any methanol-derived formaldehyde and prevent condensation reactions with aromatic species. This effect is beneficial, as formaldehyde is also likely to form through the elimination of γ-CH$_2$OH groups on the propyl side-chain of phenolic lignin units. Building on this insight, further optimisation of the reaction conditions with actual Protobind lignin allowed the formation of 60 wt% alkylated mono-aromatics from lignin at 380 °C.

2.3.4.5 Catalyst Stability and Lignin Impurities

Sufficient catalyst lifetime is essential for economically viable lignin downstream processing. Nevertheless, information on catalyst stability/deactivation is limited to a select number of depolymerisation systems. The general challenges associated with the stability of heterogeneous catalysts under hydrothermal conditions[399] and specifically for the conversion of renewable feedstocks,[400] have been reviewed.

One of the most common supports for metal catalysts, γ-alumina, is known to undergo a phase transformation to boehmite in the presence of water.[401-402] Recently, catalyst stability was examined for liquid-phase reforming of lignin over a Pt/γ-Al$_2$O$_3$ catalyst.[403] In this study, it was found that catalyst deactivation occurred by the formation of boehmite, which encapsulates the metal particles, dramatically reducing the quantity of catalytic sites. In the presence of lignin-derived mono-aromatics (e.g., guaiacol), the transformation of γ-alumina into boehmite is inhibited by the coordination of phenolates onto the support surface. Lignin itself also has a great affinity for alumina, forming a coating and stabilising the textural properties of the catalyst support.

Impurities that occur in the lignin stream as a result of the lignin isolation procedure may also exert marked effects upon both reactivity and catalyst lifetime. No lignocellulose fractionation process is capable of yielding a lignin free from impurities (among others carbohydrates and ash). Despite the importance of thorough analysis of technical lignin impurities prior to subsequent catalytic downstream processing, such detailed characterisation is, unfortunately, often not presented in the literature. Residual sugars/carbohydrates are common impurities in lignin, particularly when milder fractionation procedures have been employed.[404] The instability of sugars under acidic or basic conditions may lead to the formation of furans or humins *via* dehydration reactions, which

can subsequently lead to catalyst deactivation by fouling/poisoning. Lignin and reactive carbohydrate fragments may also react, resulting in recondensation. Reforming of any sugars/carbohydrates present, on the other hand, may also reduce the demand for external hydrogen in hydrogenolysis/hydrogenation processes.

Recently, the influence of carbohydrate derivatives on catalyst performance was shown for the HDO of guaiacol catalysed by Ru/C.[209] Furfural and 5-hydroxymethylfurfural (5-HMF) strongly inhibited activity. At 270 °C and under 40 bar pressure of H_2, full conversion of guaiacol was observed after 1 h, reducing to just 30% in the presence of equimolar furfural. Supporting DFT calculations of the Ru(0001) surface highlighted that furfural and 5-HMF bind more strongly than guaiacol. In this manner, the reduced activity could be attributed to competitive adsorption at the active sites of the catalyst.

Residual (unsaturated) lipids may also be present in isolated lignins, and can influence catalyst performance through their olefinic and carboxylic acid functional groups. The former may lead to coking of a metal surface, the latter may coordinate to metal surfaces, potentially blocking active sites or promoting leaching of any active metal species.[405-406]

Elements and functional groups not present in the native lignocellulose may be introduced into the lignin stream as a result of the upstream fractionation treatment, foremost sulfur under kraft conditions (some sulfur impurities might originate from amino acid residues) and alkali/alkali earth metals (from inorganics used in the chemical pulping of wood). Sulfur acts as a poison for many transition metals, in particular those belonging to the platinum group in common use as lignin hydrogenolysis catalysts.[407] The precise mechanisms of sulfur poisoning in lignin valorisation processes, as well as the speciation and extent of incorporation of the sulfur in the lignin oil, are largely unknown. In general, predominantly sulfur-free isolated lignin feedstocks are probably desirable for most catalysts. Lignin desulfurisation or the use of a sulfur-tolerant catalyst[408] are alternative strategies for the treatment of lignins with a high content of sulfur-containing impurities. A Ni/C catalyst was, for example, demonstrated to be fairly robust against sulfur poisoning (using a sodium lignosulfonate feedstock in ethylene glycol at 200 °C and 50 bar of H_2).[408] In situ hydrodesulfurisation of the lignin feed was demonstrated by detection of H_2S in the gas phase. Nevertheless, catalytically inactive NiS was identified by powder X-ray diffraction, following the reaction. Interestingly, when typical cobalt-molybdenum or nickel-molybdenum sulfide catalysts are employed for lignin depolymerisation or the upgrading of a lignin oil by HDO, high sulfur content could actually be beneficial to retain the sulfided phase of the catalyst, preserving activity.

Where a solid acid (e.g., zeolite) catalyst is employed for downstream valorisation of lignin, the ion exchange of alkali (earth) metals with H^+ may bring about a decrease in acidity and, therefore, activity. This hypothesis was verified by the deactivation of mixed silica-alumina catalysts used for lignin depolymerisation in a solvent mixture

of water:methanol (1:5) at 250 °C.[409] Employing an organosolv lignin, catalytic performance could be maintained for at least three successive cycles, leading to *ca*. 60 wt% of chloroform-soluble oil. By contrast with a 'dealkaline' lignin, significant deactivation was already observed in the second cycle, halving the oil yield, which was attributed to the presence of small amounts of sodium (*ca*. 29 mg per g lignin) able to ion exchange with active sites of the solid acid catalysts. Impurities in the lignin feedstock following *upstream* treatment, therefore, may have a profound inhibiting influence on *downstream* catalytic procedures

2.3.4.5 Further Downstream Processing

The previous sections highlighted various mild and harsh depolymerisation routes for technical lignins. Nevertheless, the liquid products obtained from depolymerisation rarely already exhibit the desired properties, nor incorporate significant quantities of target species, for immediate utilisation in the intended applications. Therefore, catalytic upgrading processes are required for further chemical transformation to the desired products. Procedures typically focus on further reduction in the oxygen content *via* hydrodeoxygenation (HDO), and/or further cleavage within larger oligomeric fragments of the oil. HDO of liquid products from lignin and related model compounds is comprehensively described in recent review articles.[19,410-413] Here, the discussion is limited to an overview of general principles and selected examples that highlight recent significant advances and specific challenges associated with the treatment of actual depolymerised lignin streams (i.e., lignin oils).

HDO approaches may be broadly categorised into *direct* and *indirect* strategies. Direct strategies employ a catalyst for selective hydrogenolytic cleavage of carbon-oxygen bonds whilst avoiding (undesired) ring-hydrogenation reactions (useful for preparation of aromatics). Traditional catalysts are nickel- or cobalt-doped molybdenum sulfides (which enjoy widespread use in the petrochemical industry for the removal of sulfur from crude oil streams[410]). Heteroatom removal (deoxygenation or desulfurisation) is achieved *via* coordination to a catalyst sulfur vacancy, followed by hydrogenolysis of the carbon-heteroatom bond. Evolution of oxygen or sulfur as H_2O/H_2S then regenerates the active site. HDO typically proceeds more slowly than HDS owing to a stronger M–O bond *vs*. the analogous M-S bond. Acidic supports enhance the rate of HDO,[414] although *C*-alkylation of aromatic rings may also occur to some extent.[415] Coke formation on the catalyst (similarly related to support acidity) also significantly limits the lifetime of the catalyst;[412] alternative molybdenum/tungsten carbide[416] and metal phosphide[417-418] catalysts, that follow different deoxygenation mechanisms, have partially overcome this difficulty.

By contrast, *indirect* deoxygenation strategies employ hydrogenation catalysts to saturate the aromatic ring, thereby weakening the C–O bonds, which are subsequently cleaved *via* acid-catalysed dehydration. Typical catalysts contain noble metals (Pd, Pt, Ru, Rh) or Ni, supported on an acidic oxide or carbon.[19] Both the acidic *and* metal functionalities of the catalyst are critical.[419] Reaction of phenol in the presence of a Pd/C catalyst leads to the accumulation of cyclohexanone and subsequently cyclohexanol. However, in the presence of phosphoric acid, cyclohexanol rapidly dehydrates, rendering cyclohexene, which is also promptly hydrogenated to cyclohexane over the Pd/C catalyst. In several cases, the reaction of guaiacols proceeds *via* initial ring hydrogenation, followed by hydrolysis of the methoxy substituent to yield 1,2-cyclohexanediols, which again undergo dehydration and hydrogenation rendering cyclohexane. A zeolite-supported Ni catalyst demonstrated that both functions may be integrated into one material, and complex mixtures derived from biomass pyrolysis may be converted to alkanes.[420] In this context, Ni/Al-SBA-15 was recently demonstrated to be capable of hydrodeoxygenating an organosolv lignin with selectivity to cycloalkanes higher than 99%.[387] Owing to the similarities to hydrocarbons derived from petroleum, the lignin-derived alkanes could well be refined into drop-in fuels by subsequent conventional oil refinery processes. Moreover, in a broader perspective, this example highlight the importance of Al-SBA-15, as an acidic support alternative to zeolites or other acidic materials, for the HDO of phenolic streams.[387]

When arenes are desired, a supplementary *dehydrogenation* step is necessary following indirect deoxygenation. A mixture of Raney®-Ni and H-BEA-35 catalyst, with 2-propanol as a hydrogen donor dissolved in an aliphatic hydrocarbon as a solvent, effectively converted phenol to benzene *via* an indirect pathway.[284] By employing a liquid-phase transfer-hydrogen donor (2-propanol) instead of gaseous H_2, coverage of hydrogen on the nickel surface is significantly reduced, allowing for the dehydrogenation of cyclohexene intermediates to arenes as another potential route. The selectivity to arenes can therefore be fine-tuned by modification of the available hydrogen in the form of 2-propanol. This methodology is also applicable to complex pyrolytic bio-oils and organosolv lignins.

Examples of stepwise depolymerisation-HDO processes are known, and serve to highlight some of the challenges that occur for real lignin streams. In one approach, lignin oils were prepared by liquid phase reforming over a 1 wt% Pt on γ-Al$_2$O$_3$ catalyst, yielding 11%, 9% and 5% mono-aromatics for organosolv, kraft and sugarcane bagasse lignins, respectively.[421] The product mixture incorporated *mono-*, *bis-* and *tris-*oxygenated aromatics, consistent with abundances of coumaryl, guaiacyl and syringyl functionalities in the feedstock. Subsequent HDO, using a Mo$_2$C/C catalyst at 300 °C in dodecane, led to a monomer yield of 9% (of the original lignin feedstock) for an organosolv lignin, with a significant reduction in oxygen content. Interestingly, when beginning

with *bis*-oxygenated model compounds, *mono*-oxygenated intermediates accumulate first before oxygen-free products are formed, whereas mono-oxygenates did not accumulate with the lignin oils.[422] Complete deoxygenation of lignin-derived bio-oils is, however, still considerably more challenging than the conversion of oxygenated model compounds.

Birch wood sawdust was depolymerised *via* a hydrogenolysis procedure over a Pt/C catalyst, at 200 °C in a 1:1 water:1,4-dioxane mixture with 1 % phosphoric acid.[423] The product oil, extracted with cyclohexane, afforded a 46 wt% yield of propyl-/propanol-substituted mono-aromatics, and 12 wt% of di-aromatics. A second reaction step over Pd/C at 250 °C, using 5 wt% phosphoric acid in water, afforded alkanes in 94% yield (relative to former monomer yield, divided between C_8 (15%) and C_9 (85%) alkanes). The dimer fraction similarly yielded 82% of C_{14}-C_{18} alkanes. Methanol had been generated from hydrolysis of methoxy groups.

Effective hydrotreating of 4-(1-propyl)guaiacol to 4-(1-propyl)cyclohexanol over a ceria-supported nickel catalyst has been demonstrated.[424] The system was subsequently applied to a lignin-derived bio-oil, obtained by ECCL of Pine sawdust using Ru/C in methanol at 250 °C and 30 bar H_2. The oil incorporated ~12 wt% (relative to the lignin feedstock) of 4-(1-propyl)guaiacol, and minor quantities of related products (e.g., 4-ethylguaiacol, 4-(1-propyl)phenol). Subsequent hydrotreatment of the bio-oil (3 wt% Ni/CeO_2 catalyst, 40 bar H_2, 300 °C, 200 min) resulted in full conversion, rendering a 73% yield of the desired product, 4-propylcyclohexanol. Notably, reaction times required for full conversion were five times longer with the actual bio-oil, attributable to catalyst inhibition by some minor compounds. These results again illustrate that treatment of actual lignin is more challenging than reaction of simple model compounds.

2.4 Concluding Remarks

This chapter presented a critical assessment comparing various strategies for "beginning-to-end" lignin valorisation, with a focus on the literature published since 2010. This survey of the recent lignin chemical literature clearly highlights several recurring phenomena. Importantly, at least two general widespread misconceptions regarding lignin molecular structures and bonding must be amended. Firstly, the assertion that 'free' (acyclic) α−O−4 bonding motifs are present in the lignin macromolecules is now known to be incorrect, and it is understood that they are instead part of the '**D2**' cyclic dibenzodioxocin moieties. The second misconception is the common practice of assuming that the β−O−4 linkage is necessarily the most abundant linkage in all lignins, including industrial lignins. The prevalence of this bonding motif in native lignin varies from 35-85% depending on the plant type (hardwood, softwood, grass) and the exact species

of lignocellulosic feedstock. Furthermore, it must be acknowledged that the abundance of the β–O–4 linkages is influenced by a multitude of processing variables, including lignin bioengineering (i.e., the up-/down-regulation of specific enzymes of the phenylpropanoid pathway), any abiotic stress the plant encounters and, perhaps foremost, the severity of the conditions to which the lignin is exposed during any pretreatment or isolation process.

Clearly, the current lignin streams isolated *via* the kraft process exhibit a dramatically reduced quantity of the labile β-ether units. This principle will also hold true for certain organosolv processes, particularly those performed with added acid or base catalysts and those run with long residence times. It is therefore not always correct to assume that the kraft process must always generate a more recalcitrant and highly condensed lignin than organosolv (or other) processes. In general, lignin recalcitrance and degree of condensation will, to a large extent, be determined by residence time of the lignin fragments (released upon treatment of wood) in both the pulp and liquor. As a case in point, solution-phase lignins at the 'initial delignification' stage of kraft pulping are known to still retain a high proportion of the native β-ether moieties. Therefore, the continuous extraction of this kraft lignin stream may allow for improved ease of downstream valorisation.

To add to the chemical complexity of lignin, there is no *single* type of β-ether unit, rather, a variety of such units exhibiting calculated values of BDE in the range of 54-72 kcal/mol depending on the chemical nature of the surrounding H, G, S (and other) lignin units. Therefore, some types of β–O–4 linkages may not necessarily be more easily cleaved than the β–β or β–5 linkages. Under typical harsh conditions, chemical changes to the latter types of linkages are also expected, and therefore the fate of such linkages must be evaluated in more detail.

The bioengineering of lignins to afford a higher abundance of such readily cleaved linkages (e.g., β–O–4, β–β, or benzodioxane) may represent an effective strategy to improve catalytic lignin valorisation processes. It is possible to envision a 'cascading' scheme in which these linkages are sequentially cleaved or modified. However, the implications of any upstream modification for all downstream processes must be carefully evaluated, a research area that has so far been scarcely explored. As the properties of isolated lignin depends strongly upon the fractionation process, there is real need for the development of catalytic upstream processes based on ECCL benefiting from the remarkable features of bioengineered lignins. Without such progress, lignin bioengineering may play a limited role in improving the efficiency of catalytic downstream processing, as the fractionation step may destroy the structural features generated by bioengineering.

Perusal of the recent scientific literature shows that a wealth of oxidative, reductive and redox-neutral methods for mild depolymerisation has been developed for dimeric or

oligomeric lignin model compounds, and in selected cases also for lignin itself. It is noteworthy that, with several key exceptions, the optimum conditions for cleavage of model compounds do not translate well into those for real lignin depolymerisation reactions. Future investigations should therefore centre upon more complex models, or mixtures of models, that more accurately reflect the reactivity of lignin, and should apply the catalytic reactions to actual and well-characterised lignin feedstocks themselves. Advanced synthetic lignin-mimicking polymers are also particularly attractive in this sense, as they more accurately represent lignin than low-molecular-weight species and may allow bridging this gap.

Catalytic lignin depolymerisation methods employing costly and stoichiometric reagents ought to be avoided, or are only warranted if high value components can be extracted and if the remainder of the lignin can still be valorised by other means. By contrast, convergent approaches (for example lignin depolymerisation-hydrodeoxygenation) are likely to reduce the requirement for intermediate purification and separation stages.

The development of standardised analytical protocols for the characterisation of the starting feedstock and the generated bio-oil(s) are of utmost importance. Particular attention must still be devoted to the development of methods for the analysis of the structure of residual intermediate-molecular-weight fractions. Indeed, characterisation of such materials remains challenging. It is nevertheless evident that substantial progress has been made in developing depolymerisation methods that afford high yields of mono-aromatic compounds and liquid products. These emerging approaches often achieve this by inhibiting recondensation channels by the action of capping agents, solvents, catalytic trapping pathways, and careful tuning of reaction parameters.

It is of great importance for future research to consider other factors, for example the influence of lignin pretreatment methods on downstream catalytic processes, not simply in terms of the resulting lignin structure, but also with regards to any impurities that are imparted to the lignin stream. Such impurities, which can be very varied in nature, have been demonstrated to have a significant influence on the efficiency of depolymerisation. This influence is closely related to catalyst stability and the ability to recycle the catalyst during the long lifetimes that are required for actual commercial application.

Building upon the above conclusions and looking towards the future of lignin valorisation, effective and feasible catalytic valorisation strategies must consider every stage of the process stream, including contribution and expertise from a broad array of scientific disciplines. When designing lignin valorisation technologies, the volume of lignin that the envisaged application is able to absorb is of prime importance. Moreover, the size of the potential market and the price volatility of the targeted product are key considerations. In some circumstances, it will be appropriate to consider more than one possible target molecular and/or material. Advantages associated with a convergent

approach – whereby lignin fragments are 'funnelled' towards a limited, separable set of end products – or a stepwise, cascading approach – involving progressive production of high-value and low-value compounds – should be evaluated on a somewhat case-by-case basis. Integration of optimised catalytic lignin valorisation processes into existing cellulose-centred technologies is important in order for the concept of an integrated 'biorefinery' to be realised. As the majority of current biorefinery processes are primarily geared towards optimising sugar production, the (recondensed, and thus recalcitrant) technical lignin streams obtained are likely to require severe catalytic processing for their utilisation in the chemical and fuel industries. Future biorefineries ought to be designed with optimum valorisation of the whole biomass in mind, which potentially may lead to lignin streams more amenable to selective conversion (as with those obtained from the emerging catalytic treatments based on 'Early-stage Catalytic Conversion of Lignin', ECCL or 'lignin-first' strategies).

In conclusion, the high natural abundance, high carbon content and highly-functionalised nature of lignin render it an attractive feedstock for targeted valorisation to fuels, polymer composites, synthetic building blocks and valuable (e.g., pharmaceutical) precursors. At present, lignin is still heavily underutilised, being frequently employed simply as a low-grade fuel. With the emergence of evermore selective and tailored lignin valorisation processes and the growing ability to alter lignin structure in the growing plant, lignin-derived chemicals and materials may be expected to find increasingly widespread applications, opening up new avenues for the chemical and fuel industries.

2.5 References

1   J. Ralph, *Phytochem. Rev.,* 2010, **9**, 65-83.
2   R. Vanholme, B. Demedts, K. Morreel, J. Ralph, W. Boerjan, *Plant Physiol.,* 2010, **153**, 895-905.
3   R. Shi, Y.-H. Sun, Q. Li, S. Heber, R. Sederoff, V. L. Chiang, *Plant Cell Physiol.,* 2010, **51**, 144-163.
4   J.-K. Weng, C. Chapple, *New Phytol.,* 2010, **187**, 273-285.
5   J. C. Magalhaes Silva Moura, C. A. Valencise Bonine, J. d. O. Fernandes Viana, M. C. Dornelas, P. Mazzafera, *J. Integr. Plant Biol.,* 2010, **52**, 360-376.
6   Q. Zhao, R. A. Dixon, *Trends Plant Sci.,* 2011, **16**, 227-233.
7   C.-J. Liu, *Mol. Plant,* 2012, **5**, 304-317.
8   N. D. Bonawitz, C. Chapple, in *Annual Review of Genetics, Vol 44, Vol. 44* (Eds.: A. Campbell, M. Lichten, G. Schupbach), 2010, pp. 337-363.
9   Y. Mottiar, R. Vanholme, W. Boerjan, J. Ralph, S. D. Mansfield, *Curr. Opin. Biotechnol.,* 2016, **37**, 190-200.
10   H. Hatakeyama, T. Hatakeyama, in *Biopolymers, Vol. 232* (Eds.: A. Abe, K. Dusek, S. Kobayashi), Springer Berlin Heidelberg, 2010, pp. 1-63.
11   R. Vanholme, K. Morreel, C. Darrah, P. Oyarce, J. H. Grabber, J. Ralph, W. Boerjan, *New Phytol.,* 2012, **196**, 978-1000.
12   B. A. Simmons, D. Loqué, J. Ralph, *Curr. Opin. Plant Biol.,* 2010, **13**, 312-319.
13   N. D. Bonawitz, C. Chapple, *Curr. Opin. Biotechnol.,* 2013, **24**, 336-343.

14   M. P. Pandey, C. S. Kim, *Chem. Eng. Technol.,* 2011, **34**, 29-41.

15   J. Zakzeski, P. C. A. Bruijnincx, A. L. Jongerius, B. M. Weckhuysen, *Chem. Rev.,* 2010, **110**, 3552-3599.

16   P. Azadi, O. R. Inderwildi, R. Farnood, D. A. King, *Renew. Sustainable Energy Rev.,* 2013, **21**, 506-523.

17   S. Kang, X. Li, J. Fan, J. Chang, *Renew. Sustainable Energy Rev.,* 2013, **27**, 546-558.

18   C. Li, X. Zhao, A. Wang, G. W. Huber, T. Zhang, *Chem. Rev.,* 2015, **115**, 11559-11624.

19   M. Saidi, F. Samimi, D. Karimipourfard, T. Nimmanwudipong, B. C. Gates, M. R. Rahimpour, *Energ. Environ. Sci.,* 2014, **7**, 103-129.

20   Y. Zeng, S. Zhao, S. Yang, S.-Y. Ding, *Curr. Opin. Biotechnol.,* 2014, **27**, 38-45.

21   F.-X. Collard, J. Blin, *Renew. Sustainable Energy Rev.,* 2014, **38**, 594-608.

22   H. Lange, S. Decina, C. Crestini, *Eur. Polym. J.,* 2013, **49**, 1151-1173.

23   G. Chatel, R. D. Rogers, *ACS Sustain. Chem. Eng.,* 2014, **2**, 322-339.

24   S. K. Hanson, R. T. Baker, *Acc. Chem. Res.,* 2015, **48**, 2037-2048.

25   W. O. S. Doherty, P. Mousavioun, C. M. Fellows, *Ind. Crop. Prod.,* 2011, **33**, 259-276.

26   S. Laurichesse, L. Averous, *Prog. Polym. Sci.,* 2014, **39**, 1266-1290.

27   V. K. Thakur, M. K. Thakur, P. Raghavan, M. R. Kessler, *ACS Sustain. Chem. Eng.,* 2014, **2**, 1072-1092.

28   S. Sen, S. Patil, D. S. Argyropoulos, *Green Chem.,* 2015, **17**, 4862-4887.

29   D. Esposito, M. Antonietti, *Chem. Soc. Rev.,* 2015, **44**, 5821-5835.

30   E. Ten, W. Vermerris, *J. Appl. Polym. Sci.,* 2015, **132**, DOI: 10.1002/app.42069.

31   J. Ralph, L. L. Landucci, in *Lignin and Lignans*, CRC Press, 2010, pp. 137-243.

32   C. Lapierre, in *Lignin and Lignans*, CRC Press, 2010, pp. 11-48.

33   Y. Pu, S. Cao, A. J. Ragauskas, *Energy Environ. Sci.,* 2011, **4**, 3154-3166.

34   J.-L. Wen, S.-L. Sun, B.-L. Xue, R.-C. Sun, *Materials,* 2013, **6**, 359-391.

35   S. H. Ghaffar, M. Fan, *Biomass Bioenergy,* 2013, **57**, 264-279.

36   A. Tolbert, H. Akinosho, R. Khunsupat, A. K. Naskar, A. J. Ragauskas, *Biofuels, Bioprod. Biorefin.,* 2014, **8**, 836-856.

37   J. S. Lupoi, S. Singh, R. Parthasarathi, B. A. Simmons, R. J. Henry, *Renew. Sust. Energ. Rev.,* 2015, **49**, 871-906.

38   M. Thevenot, M.-F. Dignac, C. Rumpel, *Soil Biol. Biochem.,* 2010, **42**, 1200-1211.

39   T. D. H. Bugg, M. Ahmad, E. M. Hardiman, R. Rahmanpour, *Nat. Prod. Rep.,* 2011, **28**, 1883-1896.

40   T. D. H. Bugg, M. Ahmad, E. M. Hardiman, R. Singh, *Curr. Opin. Biotechnol.,* 2011, **22**, 394-400.

41   S. Bauer, H. Sorek, V. D. Mitchell, A. B. Ibáñez, D. E. Wemmer, *J. Agric. Food Chem.,* 2012, **60**, 8203-8212.

42   J. M. Marita, J. Ralph, R. D. Hatfield, D. J. Guo, F. Chen, R. A. Dixon, *Phytochem.,* 2003, **62**, 53-65.

43   Q. Zhao, Y. Tobimatsu, R. Zhou, S. Pattathil, L. Gallego-Giraldo, C. Fu, L. A. Jackson, M. G. Hahn, H. Kim, F. Chen, J. Ralph, R. A. Dixon, *Proc. Natl. Acad. Sci. U. S. A.,* 2013, **110**, 13660-13665.

44   C. G. Wilkerson, S. D. Mansfield, F. Lu, S. Withers, J. Y. Park, S. D. Karlen, E. Gonzales-Vigil, D. Padmakshan, F. Unda, J. Rencoret, J. Ralph, *Science,* 2014, **344**, 90-93.

45   A. Wagner, L. Donaldson, J. Ralph, in *Advances in Botanical Research. Lignins: biosynthesis, biodegradation and bioengineering, Vol. 61* (Eds.: L. Jouanin, C. Lapierre), Academic Press, Burlington, 2012, pp. 37-76.

46   L. Gallego-Giraldo, G. Shadle, H. Shen, J. Barros-Rios, S. Fresquet Corrales, H. Wang, R. A. Dixon, *Plant Biotechnol. J.,* 2015, DOI: 10.1111/pbi.12439.

47   H. L. Baxter, M. Mazarei, N. Labbe, L. M. Kline, Q. Cheng, M. T. Windham, D. G. Mann, C. Fu, A. Ziebell, R. W. Sykes, *Plant Biotechnol. J.,* 2014, **12**, 914-924.

48   H. Shen, C. R. Poovaiah, A. Ziebell, T. J. Tschaplinski, S. Pattathil, E. Gjersing, N. L. Engle, R. Katahira, Y. Pu, R. Sykes, *Biotechnol. Biofuels,* 2013, **6**, 71.

49   T. J. Tschaplinski, R. F. Standaert, N. L. Engle, M. Z. Martin, A. K. Sangha, J. M. Parks, J. C. Smith, R. Samuel, N. Jiang, Y. Pu, *Biotechnol. Biofuels,* 2012, **5**.

50   B. Xu, L. L. Escamilla-Treviño, N. Sathitsuksanoh, Z. Shen, H. Shen, Y. H. Percival Zhang, R. A. Dixon, B. Zhao, *New Phytol.,* 2011, **192**, 611-625.

51   C. Fu, J. R. Mielenz, X. Xiao, Y. Ge, C. Y. Hamilton, M. Rodriguez, F. Chen, M. Foston, A. Ragauskas, J. Bouton, *Proc. Natl. Acad. Sci. U.S.A.,* 2011, **108**, 3803-3808.

52   L. L. Escamilla-Treviño, H. Shen, S. R. Uppalapati, T. Ray, Y. Tang, T. Hernandez, Y. Yin, Y. Xu, R. A. Dixon, *New Phytol.,* 2010, **185**, 143-155.

53   H. Shen, M. Mazarei, H. Hisano, L. Escamilla-Trevino, C. Fu, Y. Pu, M. R. Rudis, Y. Tang, X. Xiao, L. Jackson, *Plant Cell,* 2013, **25**, 4342-4361.

54   A. Rohde, K. Morreel, J. Ralph, G. Goeminne, V. Hostyn, R. De Rycke, S. Kushnir, J. Van Doorsselaere, J. P. Joseleau, M. Vuylsteke, G. Van Driessche, J. Van Beeumen, E. Messens, W. Boerjan, *Plant Cell,* 2004, **16**, 2749-2771.

55   D. J. Millar, M. Long, G. Donovan, P. D. Fraser, A.-M. Boudet, S. Danoun, P. M. Bramley, G. P. Bolwell, *Phytochem.,* 2007, **68**, 1497-1509.

56   A. L. Schilmiller, J. Stout, J.-K. Weng, J. Humphreys, M. O. Ruegger, C. Chapple, *Plant J.,* 2009, **60**, 771-782.

57   X. Li, N. D. Bonawitz, J.-K. Weng, C. Chapple, *Plant Cell,* 2010, **22**, 1620-1632.

58   S. G. A. Moinuddin, M. Jourdes, D. D. Laskar, C. Ki, C. L. Cardenas, K.-W. Kim, D. Zhang, L. B. Davin, N. G. Lewis, *Org. Biomol. Chem.,* 2010, **8**, 3928-3946.

59   A. M. Patten, M. Jourdes, C. L. Cardenas, D. D. Laskar, Y. Nakazawa, B.-Y. Chung, V. R. Franceschi, L. B. Davin, N. G. Lewis, *Mol. Biosyst.,* 2010, **6**, 499-515.

60   R. Vanholme, J. Ralph, T. Akiyama, F. Lu, J. R. Pazo, H. Kim, J. H. Christensen, B. Van Reusel, V. Storme, R. De Rycke, A. Rohde, K. Morreel, W. Boerjan, *Plant J.,* 2010, **64**, 885-897.

61   S. Berthet, N. Demont-Caulet, B. Pollet, P. Bidzinski, L. Cezard, P. Le Bris, N. Borrega, J. Herve, E. Blondet, S. Balzergue, C. Lapierre, L. Jouanin, *Plant Cell,* 2011, **23**, 1124-1137.

62   J. Thevenin, B. Pollet, B. Letarnec, L. Saulnier, L. Gissot, A. Maia-Grondard, C. Lapierre, L. Jouanin, *Mol. Plant,* 2011, **4**, 70-82.

63   C. B. Sung, K. Si-Yong, B. Hyeun-Jong, L. Hyoun-Sub, P. Eui-Ho, B. Hanhong, *Res. J. Biotechnol.,* 2012, **7**, 23-33.

64   J. Herrero, A. Esteban-Carrasco, J. Miguel Zapata, *Plant Physiol. Biochem.,* 2013, **67**, 77-86.

65   D. Ohman, B. Demedts, M. Kumar, L. Gerber, A. Gorzsas, G. Goeminne, M. Hedenstrom, B. Ellis, W. Boerjan, B. Sundberg, *Plant J.,* 2013, **73**, 63-76.

66   R. Vanholme, I. Cesarino, K. Rataj, Y. Xiao, L. Sundin, G. Goeminne, H. Kim, J. Cross, K. Morreel, P. Araujo, L. Welsh, J. Haustraete, C. McClellan, B. Vanholme, J. Ralph, G. G. Simpson, C. Halpin, W. Boerjan, *Science,* 2013, **341**, 1103-1106.

67   A. Wagner, Y. Tobimatsu, G. Goeminne, L. Phillips, H. Flint, D. Steward, K. Torr, L. Donaldson, W. Boerjan, J. Ralph, *Plant Mol. Biol.,* 2013, **81**, 105-117.

68   M. B. Ali, D. H. McNear, Jr., *BMC Plant Biol.,* 2014, **14**.

69   J. Herrero, A. Esteban Carrasco, J. Miguel Zapata, *Plant Physiol. Biochem.,* 2014, **80**, 192-202.

70   F. Fernández-Pérez, T. Vivar, F. Pomar, M. A. Pedreño, E. Novo-Uzal, *J. Plant Physiol.,* 2015, **175**, 86-94.

71   H. Wang, Q. Zhao, F. Chen, M. Wang, R. A. Dixon, *Plant J.,* 2011, **68**, 1104-1114.

72   R. Zhou, L. Jackson, G. Shadle, J. Nakashima, S. Temple, F. Chen, R. A. Dixon, *Proc. Natl. Acad. Sci. U.S.A.,* 2010, **107**, 17803-17808.

73   Q. Zhao, L. Gallego-Giraldo, H. Wang, Y. Zeng, S. Y. Ding, F. Chen, R. A. Dixon, *Plant J.,* 2010, **63**, 100-114.

74   M. A. Naoumkina, Q. Zhao, L. Gallego-Giraldo, X. Dai, P. X. Zhao, R. A. Dixon, *Mol. Plant Pathol.,* 2010, **11**, 829-846.

75   F. Jansen, B. Gillessen, F. Mueller, U. Commandeur, R. Fischer, F. Kreuzaler, *Biotechnol. Appl. Biochem.,* 2014, **61**, 646-654.

76   T. Higuchi, Y. Ito, I. Kawamura, *Phytochem.,* 1967, **6**, 875-881.

77   R. Hatfield, J. Ralph, J. H. Grabber, *Planta,* 2008, **228**, 919-928.

78   U. Takahama, T. Oniki, H. Shimokawa, *Plant Cell Physiol.,* 1996, **37**, 499-504.

79   F. Lu, S. D. Karlen, M. Regner, H. Kim, S. A. Ralph, R.-C. Sun, K.-i. Kuroda, M. A. Augustin, R. Mawson, H. Sabarez, T. Singh, G. Jimenez-Monteon, S. Zakaria, S. Hill, P. J. Harris, W. Boerjan, C. G. Wilkerson, S. D. Mansfield, J. Ralph, *Bioenerg. Res.,* 2015, **8**, 934-952.

80   W. Lan, F. Lu, M. Regner, Y. Zhu, J. Rencoret, S. A. Ralph, U. I. Zakai, K. Morreel, W. Boerjan, J. Ralph, *Plant Physiol.,* 2015, **167**, 1284-1295.

81   F. Lu, J. Ralph, *Org. Biomol. Chem.,* 2008, **6**, 3681-3694.

82   J. C. del Río, J. Rencoret, G. Marques, A. Gutiérrez, D. Ibarra, J. I. Santos, J. s. Jiménez-Barbero, L. Zhang, A. n. T. Martínez, *J. Agric. Food Chem.,* 2008, **56**, 9525-9534.

83   R. A. Smith, E. Gonzales-Vigil, S. D. Karlen, J. Y. Park, F. Lu, C. G. Wilkerson, L. Samuels, J. Ralph, S. D. Mansfield, *Plant Physiol.,* 2015, **169**, 2992-3001.

84   D. L. Petrik, S. D. Karlen, C. L. Cass, D. Padmakshan, F. Lu, S. Liu, P. Bris, S. Antelme, N. Santoro, C. G. Wilkerson, *Plant J.,* 2014, **77**, 713-726.

85   S. Withers, F. Lu, H. Kim, Y. Zhu, J. Ralph, C. G. Wilkerson, *J. Biol. Chem.,* 2012, **287**, 8347-8355.

86   J. M. Marita, R. D. Hatfield, D. M. Rancour, K. E. Frost, *Plant J.,* 2014, **78**, 850-864.

87   R. Vanholme, K. Morreel, J. Ralph, W. Boerjan, *Curr. Opin. Plant Biol.,* 2008, **11**, 278-285.

88   J. Ralph, K. Lundquist, G. Brunow, F. Lu, H. Kim, P. F. Schatz, J. M. Marita, R. D. Hatfield, S. A. Ralph, J. H. Christensen, *Phytochem. Rev.,* 2004, **3**, 29-60.

89   W. Boerjan, J. Ralph, M. Baucher, *Annu. Rev. Plant Biol.,* 2003, **54**, 519-546.

90   J. Ralph, H. Kim, J. Peng, F. Lu, *Org. Lett.,* 1999, **1**, 323-326.

91   J. Ralph, J. J. MacKay, R. D. Hatfield, D. M. O'Malley, R. W. Whetten, R. R. Sederoff, *Science,* 1997, **277**, 235-239.

92   J. Ralph, C. Lapierre, J. M. Marita, H. Kim, F. Lu, R. D. Hatfield, S. Ralph, C. Chapple, R. Franke, M. R. Hemm, *Phytochem.,* 2001, **57**, 993-1003.

93   J. C. Del Río, J. Rencoret, P. Prinsen, A. n. T. Martínez, J. Ralph, A. Gutiérrez, *J. Agric. Food Chem.,* 2012, **60**, 5922-5935.

94   J. Ralph, M. Bunzel, J. M. Marita, R. D. Hatfield, F. Lu, H. Kim, P. F. Schatz, J. H. Grabber, H. Steinhart, *Phytochem. Rev.,* 2004, **3**, 79-96.

95   K. Osakabe, C. C. Tsao, L. Li, J. L. Popko, T. Umezawa, D. T. Carraway, R. H. Smeltzer, C. P. Joshi, V. L. Chiang, *Proc. Natl. Acad. Sci. U.S.A.,* 1999, **96**, 8955-8960.

96   J. Humphreys, M. Hemm, C. Chapple, *Proc. Natl. Acad. Sci. USA,* 1999, **96**, 10045-10050.

97   J. M. Humphreys, C. Chapple, *Curr. Opin. Plant Biol.,* 2002, **5**, 224-229.

98   L. Li, Y. Zhou, X. Cheng, J. Sun, J. M. Marita, J. Ralph, V. L. Chiang, *Proc. Natl. Acad. Sci. U.S.A.,* 2003, **100**, 4939-4944.

99   C. L. Cass, A. Peraldi, P. F. Dowd, Y. Mottiar, N. Santoro, S. D. Karlen, Y. V. Bukhman, C. E. Foster, N. Thrower, L. C. Bruno, O. V. Moskvin, E. T. Johnson, M. E. Willhoit, M. Phutane, J. Ralph, S. D. Mansfield, P. Nicholson, J. C. Sedbrook, *J. Exp. Bot.,* 2015, **66**, 4317-4335.

100   J. Ralph, T. Akiyama, H. D. Coleman, S. D. Mansfield, *Bioenerg. Res.,* 2012, **5**, 1009-1019.

101   Y. Tu, S. Rochfort, Z. Liu, Y. Ran, M. Griffith, P. Badenhorst, G. V. Louie, M. E. Bowman, K. F. Smith, J. P. Noel, A. Mouradov, G. Spangenberg, *Plant Cell,* 2010, **22**, 3357-3373.

102   M. M. Derikvand, J. B. Sierra, K. Ruel, B. Pollet, C.-T. Do, J. Thevenin, D. Buffard, L. Jouanin, C. Lapierre, *Planta,* 2008, **227**, 943-956.

103   B. Tamasloukht, M. S.-J. W. Q. Lam, Y. Martinez, K. Tozo, O. Barbier, C. Jourda, A. Jauneau, G. Borderies, S. Balzergue, J.-P. Renou, S. Huguet, J. P. Martinant, C. Tatout, C. Lapierre, Y. Barriere, D. Goffner, M. Pichon, *J. Exp. Bot.,* 2011, **62**, 3837-3848.

104   J. Piquemal, C. Lapierre, K. Myton, A. O'Connell, W. Schuch, J. Grima-Pettenati, A. M. Boudet, *Plant J.,* 1998, **13**, 71-83.

105 R. Van Acker, J.-C. Leple, D. Aerts, V. Storme, G. Goeminne, B. Ivens, F. Legee, C. Lapierre, K. Piens, M. C. E. Van Montagu, N. Santoro, C. E. Foster, J. Ralph, W. Soetaert, G. Pilate, W. Boerjan, *Proc. Natl. Acad. Sci. U. S. A.,* 2014, **111**, 845-850.

106 J. Ralph, H. Kim, F. Lu, J. H. Grabber, J. C. Leplé, J. Berrio-Sierra, M. M. Derikvand, L. Jouanin, W. Boerjan, C. Lapierre, *Plant J.,* 2008, **53**, 368-379.

107 J.-C. Leple, R. Dauwe, K. Morreel, V. Storme, C. Lapierre, B. Pollet, A. Naumann, K.-Y. Kang, H. Kim, K. Ruel, *Plant Cell,* 2007, **19**, 3669-3691.

108 S. Fornale, M. Capellades, A. Encina, K. Wang, S. Irar, C. Lapierre, K. Ruel, J.-P. Joseleau, J. Berenguer, P. Puigdomenech, J. Rigau, D. Caparros-Ruiz, *Mol. Plant,* 2012, **5**, 817-830.

109 A. A. Konovalov, I. K. Shundrina, E. V. Karpova, A. A. Nefedov, N. P. Goncharov, *Russ. J. Genet.,* 2014, **50**, 1161-1168.

110 M. B. d'Yvoire, O. Bouchabke-Coussa, W. Voorend, S. Antelme, L. Cezard, F. Legee, P. Lebris, S. Legay, C. Whitehead, S. J. McQueen-Mason, L. D. Gomez, L. Jouanin, C. Lapierre, R. Sibout, *Plant J.,* 2013, **73**, 496-508.

111 J. MacKay, T. Presnell, H. Jameel, H. Taneda, D. O'Malley, R. Sederoff, *Holzforschung,* 1999, **53**, 403-410.

112 A. J. Saathoff, G. Sarath, E. K. Chow, B. S. Dien, C. M. Tobias, *PLoS ONE,* 2011, **6**, e16416.

113 T. Ookawa, K. Inoue, M. Matsuoka, T. Ebitani, T. Takarada, T. Yamamoto, T. Ueda, T. Yokoyama, C. Sugiyama, S. Nakaba, R. Funada, H. Kato, M. Kanekatsu, K. Toyota, T. Motobayashi, M. Vazirzanjani, S. Tojo, T. Hirasawa, *Sci. Rep.,* 2014, **4**.

114 B. Vanholme, I. Cesarino, G. Goeminne, H. Kim, F. Marroni, R. Van Acker, R. Vanholme, K. Morreel, B. Ivens, S. Pinosio, M. Morgante, J. Ralph, C. Bastien, W. Boerjan, *New Phytol.,* 2013, **198**, 765-776.

115 S. E. Sattler, N. A. Palmer, A. Saballos, A. M. Greene, Z. Xin, G. Sarath, W. Vermerris, J. F. Pedersen, *Bioenerg. Res.,* 2012, **5**, 855-865.

116 J. H. Jung, W. Vermerris, M. Gallo, J. R. Fedenko, J. E. Erickson, F. Altpeter, *Plant Biotechnol. J.,* 2013, **11**, 709-716.

117 P. N. Ciesielski, M. G. Resch, B. Hewetson, J. P. Killgore, A. Curtin, N. Anderson, A. N. Chiaramonti, D. C. Hurley, A. Sanders, M. E. Himmel, C. Chapple, N. Mosier, B. S. Donohoe, *Green Chem.,* 2014, **16**, 2627-2635.

118 K. Meyer, A. M. Shirley, J. C. Cusumano, D. A. Bell-Lelong, C. Chapple, *Proc. Natl. Acad. Sci. U.S.A.,* 1998, **95**, 6619-6623.

119 J.-K. Weng, H. Mo, C. Chapple, *Plant J.,* 2010, **64**, 898-911.

120 J. Ralph, T. Akiyama, H. Kim, F. Lu, P. F. Schatz, J. M. Marita, S. A. Ralph, M. S. Reddy, F. Chen, R. A. Dixon, *J. Biol. Chem.,* 2006, **281**, 8843-8853.

121 S. K. Huntley, D. Ellis, M. Gilbert, C. Chapple, S. D. Mansfield, *J. Agric. Food Chem.,* 2003, **51**, 6178-6183.

122 J. J. Stewart, T. Akiyama, C. Chapple, J. Ralph, S. D. Mansfield, *Plant Physiol.,* 2009, **150**, 621-635.

123 N. Santoro, S. L. Cantu, C.-E. Tornqvist, T. G. Falbel, J. L. Bolivar, S. E. Patterson, M. Pauly, J. D. Walton, *Bioenerg. Res.,* 2010, **3**, 93-102.

124 A. Ros Barceló, *Protoplasma,* 1995, **186**, 41-44.

125 S. Berthet, J. Thevenin, D. Baratiny, N. Demont-Caulet, I. Debeaujon, P. Bidzinski, J.-C. Leple, R. Huis, S. Hawkins, L.-D. Gomez, C. Lapierre, L. Jouanin, in *Lignins: Biosynthesis, Biodegradation and Bioengineering, Vol. 61* (Eds.: L. Jouann, C. Lapierre), 2012, pp. 145-172.

126 Q. Zhao, J. Nakashima, F. Chen, Y. Yin, C. Fu, J. Yun, H. Shao, X. Wang, Z.-Y. Wang, R. A. Dixon, *Plant Cell,* 2013, **25**, 3976-3987.

127 S. Lu, Q. Li, H. Wei, M.-J. Chang, S. Tunlaya-Anukit, H. Kim, J. Liu, J. Song, Y.-H. Sun, L. Yuan, T.-F. Yeh, I. Peszlen, J. Ralph, R. R. Sederoff, V. L. Chiang, *Proc. Natl. Acad. Sci. U. S. A.,* 2013, **110**, 10848-10853.

128 C.-Y. Wang, S. Zhang, Y. Yu, Y.-C. Luo, Q. Liu, C. Ju, Y.-C. Zhang, L.-H. Qu, W. J. Lucas, X. Wang, Y.-Q. Chen, *Plant Biotechnol. J.,* 2014, **12**, 1132-1142.

129 S. Lu, Q. Li, H. Wei, M.-J. Chang, S. Tunlaya-Anukit, H. Kim, J. Liu, J. Song, Y.-H. Sun, L. Yuan, *Proc. Natl. Acad. Sci. U.S.A.,* 2013, **110**, 10848-10853.

130 I. Cesarino, P. Araújo, J. L. S. Mayer, R. Vicentini, S. Berthet, B. Demedts, B. Vanholme, W. Boerjan, P. Mazzafera, *J. Exp. Bot.,* 2013, **64**, 1769-1781.

131 J. G. Dubouzet, T. J. Strabala, A. Wagner, *Plant Sci.,* 2013, **212**, 72-101.

132 R. Dauwe, K. Morreel, G. Goeminne, B. Gielen, A. Rohde, J. Van Beeumen, J. Ralph, A. M. Boudet, J. Kopka, S. F. Rochange, *Plant J.,* 2007, **52**, 263-285.

133 S. L. Voelker, B. Lachenbruch, F. C. Meinzer, P. Kitin, S. H. Strauss, *Plant, Cell Environ.,* 2011, **34**, 655-668.

134 N. D. Bonawitz, J. Im Kim, Y. Tobimatsu, P. N. Ciesielski, N. A. Anderson, E. Ximenes, J. Maeda, J. Ralph, B. S. Donohoe, M. Ladisch, *Nature,* 2014, **509**, 376-380.

135 F. Lu, J. M. Marita, C. Lapierre, L. Jouanin, K. Morreel, W. Boerjan, J. Ralph, *Plant Physiol.,* 2010, **153**, 569-579.

136 K. Morreel, J. Ralph, F. Lu, G. Goeminne, R. Busson, P. Herdewijn, J. L. Goeman, J. Van der Eycken, W. Boerjan, E. Messens, *Plant Physiol.,* 2004, **136**, 4023-4036.

137 J. Ralph, C. Lapierre, F. Lu, J. M. Marita, G. Pilate, J. Van Doorsselaere, W. Boerjan, L. Jouanin, *J. Agric. Food Chem.,* 2001, **49**, 86-91.

138 J. M. Marita, J. Ralph, C. Lapierre, L. Jouanin, W. Boerjan, *J. Chem. Soc., Perkin Trans.* **1***,* 2001, 2939-2945.

139 L. Jouanin, T. Gujon, R. Sibout, B. Pollet, I. Mila, J.-C. Leplé, G. Pilate, M. Petit-Conil, J. Ralph, C. Lapierre, in *Plantation Forest Biotechnology in the 21st Century* (Eds.: C. Walter, M. Carson), Research Signpost, Kerala, India,, 2004, pp. 219-229.

140 A. Wagner, Y. Tobimatsu, L. Phillips, H. Flint, K. Torr, L. Donaldson, L. Pears, J. Ralph, *Plant J.,* 2011, **67**, 119-129.

141 L. Jouanin, T. Goujon, V. de Nadaï, M.-T. Martin, I. Mila, C. Vallet, B. Pollet, A. Yoshinaga, B. Chabbert, M. Petit-Conil, *Plant Physiol.,* 2000, **123**, 1363-1374.

142 N. A. Anderson, Y. Tobimatsu, P. N. Ciesielski, E. Ximenes, J. Ralph, B. S. Donohoe, M. Ladisch, C. Chapple, *Plant Cell,* 2015, **27**, 2195-2209.

143 F. Chen, Y. Tobimatsu, D. Havkin-Frenkel, R. A. Dixon, J. Ralph, *Proc. Natl. Acad. Sci. U.S.A.,* 2012, **109**, 1772-1777.

144 R. Tsuji, H. Koizumi, D. Aoki, Y. Watanabe, Y. Sugihara, Y. Matsushita, K. Fukushima, D. Fujiwara, *J. Biol. Chem.,* 2015, **290**, 4410-4421.

145 M. Cabane, D. Afif, S. Hawkins, in *Lignins: Biosynthesis, Biodegradation and Bioengineering, Vol. 61* (Eds.: L. Jouann, C. Lapierre), 2012, pp. 219-262.

146 J. Barros, H. Serk, I. Granlund, E. Pesquet, *Ann. Bot.,* 2015, **115**, 1053-1074.

147 J. Liu, A. Osbourn, P. Ma, *Mol. Plant,* 2015, **8**, 689-708.

148 M. Rossi, D. Trupiano, M. Tamburro, G. Ripabelli, A. Montagnoli, D. Chiatante, G. S. Scippa, *Planta,* 2015, **242**, 339-351.

149 A. Shafi, R. Chauhan, T. Gill, M. K. Swarnkar, Y. Sreenivasulu, S. Kumar, N. Kumar, R. Shankar, P. S. Ahuja, A. K. Singh, *Plant Mol. Biol.,* 2015, **87**, 615-631.

150 S. Srivastava, R. K. Vishwakarma, Y. A. Arafat, S. K. Gupta, B. M. Khan, *Physiol. Mol. Biol. Plants,* 2015, **21**, 197-205.

151 Y. Wang, Q. Wang, Y. Zhao, G. Han, S. Zhu, *Gene,* 2015, **566**, 95-108.

152 S. S. Lawson, C. H. Michler, *Transgenic Res.,* 2014, **23**, 817-826.

153 S. L. Voelker, B. Lachenbruch, F. C. Meinzer, S. H. Strauss, *New Phytol.,* 2011, **189**, 1096-1109.

154 H. Häggman, A. Raybould, A. Borem, T. Fox, L. Handley, M. Hertzberg, M.-Z. Lu, P. Macdonald, T. Oguchi, G. Pasquali, L. Pearson, G. Peter, H. Quemada, A. Séguin, K. Tattersall, E. Ulian, C. Walter, M. McLean, *Plant Biotechnol. J.,* 2013, **11**, 785-798.

155 Y. Barriere, J. Ralph, V. Mechin, S. Guillaumie, J. H. Grabber, O. Argillier, B. Chabbert, C. Lapierre, *C. R. Biol.,* 2004, **327**, 847-860.

156   L. Munk, A. K. Sitarz, D. C. Kalyani, J. D. Mikkelsen, A. S. Meyer, *Biotechnol. Adv.,* 2015, **33**, 13-24.

157   T. Akiyama, K. Magara, G. Meshitsuka, K. Lundquist, Y. Matsumoto, *J. Wood Chem. Technol.,* 2015, **35**, 8-16.

158   J. Ralph, G. Brunow, P. J. Harris, R. A. Dixon, P. F. Schatz, W. Boerjan, in *Recent Advances in Polyphenol Research, Vol. 1* (Eds.: F. Daayf, A. El Hadrami, L. Adam, G. M. Ballance), Wiley-Blackwell Publishing, Oxford, UK, 2008, pp. 36-66.

159   N. Terashima, K. Fukushima, L.-F. He, K. Takabe, in *Forage Cell Wall Structure and Digestibility* (Eds.: H. G. Jung, D. R. Buxton, R. D. Hatfield, J. Ralph), American Society of Agronomy, Crop Science Society of America, Soil Science Society of America, Madison,,**199**3, pp. 247-270.

160   L. Donaldson, *IAWA Journal,* 2013, **34**, 3-19.

161   J. Wu, K. Fukazawa, J. Ohtani, *Holzforschung,* 1992, **46**, 181-185.

162   L. Donaldson, A. Singh, in *Cellular aspects of wood formation*, Springer, 2013, pp. 225-256.

163   T. E. Timmel, *Compression wood in gymnosperms*, Springer Heidelberg, 1986.

164   L. Zhang, G. Gellerstedt, *Chem. Commun.,* 2001, 2744-2745.

165   M. Sette, H. Lange, C. Crestini, *Comput. Struct. Biotechnol. J.,* 2013, **6**, 1-7.

166   J. Ralph, J. M. Marita, S. A. Ralph, R. D. Hatfield, F. Lu, R. M. Ede, J. Peng, S. Quideau, R. F. Helm, J. H. Grabber, H. Kim, G. Jimenez-Monteon, Y. Zhang, H.-J. G. Jung, L. L. Landucci, J. J. MacKay, R. R. Sederoff, C. Chapple, A. M. Boudet, in *Advances in Lignocellulosics Characterization* (Ed.: D. S. Argyropoulos), TAPPI Press, Atlanta, GA, 1999, pp. 55-108.

167   S. D. Mansfield, H. Kim, F. Lu, J. Ralph, *Nat. Protocols,* 2012, **7**, 1579-1589.

168   J. Ralph, L. L. Landucci, *NMR of lignins*, CRC Press, 2010.

169   S. Heikkinen, M. M. Toikka, P. T. Karhunen, I. A. Kilpeläinen, *J. Am. Chem. Soc.,* 2003, **125**, 4362-4367.

170   K. Hu, W. M. Westler, J. L. Markley, *J. Am. Chem. Soc.,* 2011, **133**, 1662-1665.

171   K. Cheng, H. Sorek, H. Zimmermann, D. E. Wemmer, M. Pauly, *Anal. Chem.,* 2013, **85**, 3213-3221.

172   R. Samuel, M. Foston, N. Jaing, S. Cao, L. Allison, M. Studer, C. Wyman, A. J. Ragauskas, *Fuel,* 2011, **90**, 2836-2842.

173   D. S. Argyropoulos, in *Lignan and lignans: Advances in Chemistry* (Eds.: C. Heitner, D. R. Dimmel, J. A. Schmidt), CRC Press, Taylor & Francis Group, New York, 2010, pp. 245-265.

174   G. Brunow, O. Karlsson, K. Lundquist, J. Sipilä, *Wood Sci. Technol.,* 1993, **27**, 281-286.

175   J. Ralph, P. F. Schatz, F. Lu, H. Kim, T. Akiyama, S. F. Nelsen, *Hoboken, NJ: Wiley-Blackwell* 2009, 385-420.

176   K. Freudenberg, A. C. Neish, *Constitution and biosynthesis of lignin.* 1968.

177   S. Kim, S. C. Chmely, M. R. Nimlos, Y. J. Bomble, T. D. Foust, R. S. Paton, G. T. Beckham, *J. Phys. Chem. Lett.,* 2011, **2**, 2846-2852.

178   R. Parthasarathi, R. A. Romero, A. Redondo, S. Gnanakaran, *J. Phys. Chem. Lett.,* 2011, **2**, 2660-2666.

179   J. M. Younker, A. Beste, A. C. Buchanan, III, *ChemPhysChem,* 2011, **12**, 3556-3565.

180   J. M. Younker, A. Beste, A. C. Buchanan, III, *Chem. Phys. Lett.,* 2012, **545**, 100-106.

181   A. K. Sangha, J. M. Parks, R. F. Standaert, A. Ziebell, M. Davis, J. C. Smith, *J. Phys. Chem. B,* 2012, **116**, 4760-4768.

182   H. Nimz, *Angew. Chem. Int. Ed.,* 1974, **13**, 313-321.

183   E. Adler, *Wood Sci. Technol.,* 1977, **11**, 169-218.

184   K. Lundquist, J. Parkas, *Bioresources,* 2011, **6**, 920-926.

185   C. Crestini, F. Melone, M. Sette, R. Saladino, *Biomacromolecules,* 2011, **12**, 3928-3935.

186   T. Elder, *Energy & Fuels,* 2013, **27**, 4785-4790.

187   T. Elder, *Energy & Fuels,* 2014, **28**, 1175-1182.

188   K. P. Kringstad, R. Morck, *Holzforschung,* 1983, **37**, 237-244.

189   G. Gellerstedt, E. Lindfors, *Svensk Papperstidning-Nordisk Cellulosa,* 1984, **87**, R115-R118.

190   G. Gellerstedt, E. L. Lindfors, C. Lapierre, B. Monties, *Svensk Papperstidning-Nordisk Cellulosa,* 1984, **87**, R61-R67.

191 D. R. Robert, M. Bardet, G. Gellerstedt, E. L. Lindfors, *J. Wood Chem. Technol.,* 1984, **4**, 239-263.

192 S. K. Bose, R. C. Francis, *J. Pulp Pap. Sci.,* 1999, **25**, 425-430.

193 G. Gellerstedt, E.-L. Lindfors, *Holzforschung,* 1984, **38**, 151-158.

194 F. P. Bouxin, A. McVeigh, F. Tran, N. J. Westwood, M. C. Jarvis, S. D. Jackson, *Green Chem.,* 2015, **17**, 1235-1242.

195 G. Vázquez, G. Antorrena, J. González, S. Freire, *J. Wood Chem. Technol.,* 1997, **17**, 147-162.

196 F. Tran, C. S. Lancefield, P. C. J. Kamer, T. Lebl, N. J. Westwood, *Green Chem.,* 2015, **17**, 244-249.

197 M. Ragnar, G. Henriksson, M. E. Lindström, M. Wimby, J. Blechschmidt, S. Heinemann, in *Ullmann's Encyclopedia of Industrial Chemistry*, Wiley-VCH Verlag GmbH & Co. KGaA, 2014.

198 P. Ferrini, R. Rinaldi, *Angew. Chem. Int. Ed.,* 2014, **53**, 8634-8639.

199 J. Jönsson, K. Pettersson, T. Berntsson, S. Harvey, *Int. J. Energ. Res.,* 2013, **37**, 1017-1035.

200 H. Konnerth, J. Zhang, D. Ma, M. H. G. Prechtl, N. Yan, *Chem. Eng. Sci.,* 2015, **123**, 155-163.

201 R. Rinaldi, *Angew. Chem. Int. Ed.,* 2014, **53**, 8559-8560.

202 R. Patt, O. Kordsachia, R. Süttinger, Y. Ohtani, J. F. Hoesch, P. Ehrler, R. Eichinger, H. Holik, U. Hamm, M. E. Rohmann, P. Mummenhoff, E. Petermann, R. F. Miller, D. Frank, R. Wilken, H. L. Baumgarten, G.-H. Rentrop, in *Ullmann's Encyclopedia of Industrial Chemistry*, Wiley-VCH Verlag GmbH & Co. KGaA, 2000.

203 D. Dimmel, G. Gellerstedt, in *Lignin and Lignans*, CRC Press,, 2010, pp. 349-391.

204 M. Ek, *Pulping Chemistry and Technology, Vol. 2*, Walter de Gruyter, 2009.

205 R. B. Santos, P. Hart, H. Jameel, H. Chang, *BioResources,* 2013, **8**, 1456-1477.

206 B. C. Ahvazi, G. Pageau, D. S. Argyropoulos, *Can. J. Chem.,* 1998, **76**, 506-512.

207 F. S. Chakar, A. J. Ragauskas, *Ind. Crop. Prod.,* 2004, **20**, 131-141.

208 M. Alekhina, O. Ershova, A. Ebert, S. Heikkinen, H. Sixta, *Ind. Crop. Prod.,* 2015, **66**, 220-228.

209 A. A. Dwiatmoko, S. Lee, H. C. Ham, J.-W. Choi, D. J. Suh, J.-M. Ha, *ACS Catalysis,* 2015, **5**, 433-437.

210 Data obtained from http://www.foex.fi/PIX/pulp-paper/, accessed on 21st January 2016.

211 T. Kleinert, K. v. Tayenthal, *Angew. Chem.,* 1931, **44**, 788-791.

212 A. Johansson, O. Aaltonen, P. Ylinen, *Biomass,* 1987, **13**, 45-65.

213 T. N. Kleinert, US3585104 A.

214 X. J. Pan, C. Arato, N. Gilkes, D. Gregg, W. Mabee, K. Pye, Z. Z. Xiao, X. Zhang, J. Saddler, *Biotechnol. Bioeng.,* 2005, **90**, 473-481.

215 X. Pan, N. Gilkes, J. Kadla, K. Pye, S. Saka, D. Gregg, K. Ehara, D. Xie, D. Lam, J. Saddler, *Biotechnol. Bioeng.,* 2006, **94**, 851-861.

216 X. Pan, D. Xie, K.-Y. Kang, S.-L. Yoon, J. N. Saddler, *Appl. Biochem. Biotechnol.,* 2007, **137**, 367-377.

217 X. Zhao, K. Cheng, D. Liu, *Appl. Microbiol. Biotechnol.,* 2009, **82**, 815-827.

218 E. K. Pye, J. H. Lora, *Tappi J.,* 1991, **74**, 113-118.

219 J. Y. Zhu, X. Pan, R. S. Zalesny, Jr., *Appl. Microbiol. Biotechnol.,* 2010, **87**, 847-857.

220 J. Y. Zhu, X. J. Pan, *Bioresour. Technol.,* 2010, **101**, 4992-5002.

221 J. Wildschut, A. T. Smit, J. H. Reith, W. J. J. Huijgen, *Bioresour. Technol.,* 2013, **135**, 58-66.

222 Google Patents, search criterium: inassignee:"Lignol Innovations Ltd.", accessed on Sept 14, 2015.

223 J. Michels, K. Wagemann, *Biofuels, Bioprod. Biorefin.,* 2010, **4**, 263-267.

224 J. Viell, A. Harwardt, J. Seiler, W. Marquardt, *Bioresour. Technol.,* 2013, **150**, 89-97.

225 R. Rinaldi, in *Catalytic Hydrogenation for Biomass Valorization*, The Royal Society of Chemistry, 2014, pp. 74-98.

226 Y. A. Chirkova, A. E. Kreitus, *Polymer Science U.S.S.R.,* 1989, **31**, 2285-2291.

227 D. T. Balogh, A. A. S. Curvelo, R. Degroote, *Holzforschung,* 1992, **46**, 343-348.

228 T. J. McDonough, *Tappi J.,* 1993, **76**, 186-193.

229 K. Lundquist, in *Methods in Lignin Chemistry* (Eds.: S. Lin, C. Dence), Springer Berlin Heidelberg,, 1992, pp. 289-300.

230 M. R. Sturgeon, S. Kim, K. Lawrence, R. S. Paton, S. C. Chmely, M. Nimlos, T. D. Foust, G. T. Beckham, *ACS Sustain. Chem. Eng.*, 2014, **2**, 472-485.

231 E. Kumpinsky, *Ind. Eng. Chem. Res.*, 1995, **34**, 3096-3101.

232 P. J. Deuss, K. Barta, *Coord. Chem. Rev.*, 2015, **306**, 510-532.

233 X. Wang, R. Rinaldi, *Energ. Environ. Sci.*, 2012, **5**, 8244-8260.

234 P. J. Deuss, M. Scott, F. Tran, N. J. Westwood, J. G. de Vries, K. Barta, *J. Am. Chem. Soc.*, 2015, **137**, 7456-7467.

235 S. Laure, M. Leschinsky, M. Frohling, F. Schultmann, G. Unkelbach, *Cellul. Chem. Technol.*, 2014, **48**, 793-798.

236 T. vom Stein, P. M. Grande, H. Kayser, F. Sibilla, W. Leitner, P. Dominguez de Maria, *Green Chem.*, 2011, **13**, 1772-1777.

237 P. M. Grande, J. Viell, N. Theyssen, W. Marquardt, P. Dominguez de Maria, W. Leitner, *Green Chem.*, 2015, **17**, 3533-3539.

238 S. Aziz, K. V. Sarkanen, *Tappi J.*, 1989, **72**, 169-175.

239 G. C. Goyal, J. H. Lora, E. K. Pye, *Tappi J.*, 1992, **75**, 110-116.

240 K. Lundquist, J. Parkås, *J. Wood Chem. Technol.*, 2014, **35**, 3-7.

241 in *Top Value-Added Chemicals from Biomass, Volume II-Results of Screening for Potential Candidates from Biorefinery Lignin* (Eds.: J. E. Holladay, J. F. White, J. J. Bozell, D. Johnson), Pacific Northwest National Laboratory, 2007.

242 K. V. Sarkanen, in *Progress in Biomass Conversion, Vol. Volume 2* (Eds.: S. Kyosti V, T. David A), Elsevier, 1980, pp. 127-144.

243 J. A. Dumesic, A. D. Martin, J. S. Luterbacher, D. M. Alonso, US2015176090-A1; WO2015095399-A1.

244 J. Han, J. S. Luterbacher, D. M. Alonso, J. A. Dumesic, C. T. Maravelias, *Bioresour. Technol.*, 2015, **182**, 258-266.

245 J. S. Luterbacher, D. M. Alonso, J. M. Rand, Y. M. Questell-Santiago, J. H. Yeap, B. F. Pfleger, J. A. Dumesic, *ChemSusChem*, 2015, **8**, 1317-1322.

246 J. S. Luterbacher, A. Azarpira, A. H. Motagamwala, F. C. Lu, J. Ralph, J. A. Dumesic, *Energ. Environ. Sci.*, 2015, **8**, 2657-2663.

247 J. S. Luterbacher, J. M. Rand, D. M. Alonso, J. Han, J. T. Youngquist, C. T. Maravelias, B. F. Pfleger, J. A. Dumesic, *Science*, 2014, **343**, 277-280.

248 N. Meine, R. Rinaldi, F. Schüth, *ChemSusChem*, 2012, **5**, 1449-1454.

249 M. Käldström, N. Meine, C. Farès, R. Rinaldi, F. Schüth, *Green Chem.*, 2014, **16**, 2454-2462.

250 M. Kaldstrom, N. Meine, C. Fares, F. Schuth, R. Rinaldi, *Green Chem.*, 2014, **16**, 3528-3538.

251 M. Käldström, N. Meine, C. Fares, F. Schüth, R. Rinaldi, *Green Chem.*, 2014, **16**, 4994-4994.

252 F. Schüth, R. Rinaldi, N. Meine, M. Käldström, J. Hilgert, M. D. K. Rechulski, *Catal. Today*, 2014, **234**, 24-30.

253 M. D. K. Rechulski, M. Käldström, U. Richter, F. Schüth, R. Rinaldi, *Ind. Eng. Chem. Res.*, 2015, **54**, 4581-4592.

254 M. Käldström, R. Rinaldi, F. Schüth, N. Meine, DE102014102972-A1; WO2014139515-A2; WO2014139515-A3.

255 A. Brandt, M. J. Ray, T. Q. To, D. J. Leak, R. J. Murphy, T. Welton, *Green Chem.*, 2011, **13**, 2489-2499.

256 M. Schrems, A. Brandt, T. Welton, F. Liebner, T. Rosenau, A. Potthast, *Holzforschung*, 2011, **65**, 527-533.

257 P. Verdia, A. Brandt, J. P. Hallett, M. J. Ray, T. Welton, *Green Chem.*, 2014, **16**, 1617-1627.

258 L. Chen, M. Sharifzadeh, N. Mac Dowell, T. Welton, N. Shah, J. P. Hallett, *Green Chem.*, 2014, **16**, 3098-3106.

259 A. George, A. Brandt, K. Tran, S. M. S. N. S. Zahari, D. Klein-Marcuschamer, N. Sun, N. Sathitsuksanoh, J. Shi, V. Stavila, R. Parthasarathi, S. Singh, B. M. Holmes, T. Welton, B. A. Simmons, J. P. Hallett, *Green Chem.*, 2015, **17**, 1728-1734.

260 A. Brandt, R. J. Murphy, D. J. Leak, T. Welton, J. Hallett, WO2012080702-A2; WO2012080702-A3; CA2821403-A1; EP2652193-A2; CN103370469-A; US2014073016-A1.

261 J. P. Hallett, T. Welton, A. Brandt, WO2014140643-A1.

262 J. B. Binder, R. T. Raines, *Proc. Natl. Acad. Sci. U.S.A.*, 2010, **107**, 4516-4521.

263 H. F. N. de Oliveira, C. Fares, R. Rinaldi, *Chem. Sci.*, 2015, **6**, 5215-5224.

264 C. Li, Q. Wang, Z. K. Zhao, *Green Chem.*, 2008, **10**, 177-182.

265 C. Li, Z. K. Zhao, *Advanced Synthesis and Catalysis*, 2007, **349**, 1847-1850.

266 R. Rinaldi, N. Meine, J. vom Stein, R. Palkovits, F. Schüth, *ChemSusChem*, 2010, **3**, 266-276.

267 R. Rinaldi, R. Palkovits, F. Schüth, *Angew. Chem. Int. Ed.*, 2008, **47**, 8047-8050.

268 G. F. De Gregorio, T. Welton, J. P. Hallett, *Abstracts of Papers of the American Chemical Society*, 2014, **248**.

269 G. Ebner, S. Schiehser, A. Potthast, T. Rosenau, *Tetrahedron Lett.*, 2008, **49**, 7322-7324.

270 X. Wei, Z. Han, D. Zhang, *Carbohydr. Res.*, 2013, **374**, 40-44.

271 M. T. Clough, K. Geyer, P. A. Hunt, S. Son, U. Vagt, T. Welton, *Green Chem.*, 2015, **17**, 231-243.

272 P. C. Bruijnincx, B. M. Weckhuysen, *Nature Chem.*, 2014, **6**, 1035-1036.

273 M. V. Galkin, J. S. M. Samec, *ChemSusChem*, 2014, **7**, 2154-2158.

274 M. V. Galkin, S. Sawadjoon, V. Rohde, M. Dawange, J. S. M. Samec, *ChemCatChem*, 2014, **6**, 179-184.

275 W. Schutyser, S. Van den Bosch, T. Renders, T. De Boe, S. F. Koelewijn, A. Dewaele, T. Ennaert, O. Verkinderen, B. Goderis, C. M. Courtin, B. F. Sels, *Green Chem.*, 2015, **17**, 5035-5045.

276 S. Van den Bosch, W. Schutyser, S. F. Koelewijn, T. Renders, C. M. Courtin, B. F. Sels, *Chem. Commun.*, 2015, **51**, 13158-13161.

277 S. Van den Bosch, W. Schutyser, R. Vanholme, T. Driessen, S. F. Koelewijn, T. Renders, B. De Meester, W. J. J. Huijgen, W. Dehaen, C. M. Courtin, B. Lagrain, W. Boerjan, B. F. Sels, *Energ. Environ. Sci.*, 2015, **8**, 1748-1763.

278 T. Parsell, S. Yohe, J. Degenstein, T. Jarrell, I. Klein, E. Gencer, B. Hewetson, M. Hurt, J. I. Kim, H. Choudhari, B. Saha, R. Meilan, N. Mosier, F. Ribeiro, W. N. Delgass, C. Chapple, H. I. Kenttamaa, R. Agrawal, M. M. Abu-Omar, *Green Chem.*, 2015, **17**, 1492-1499.

279 M. Dawange, M. V. Galkin, J. S. M. Samec, *ChemCatChem*, 2015, **7**, 401-404.

280 M. V. Galkin, C. Dahlstrand, J. S. M. Samec, *ChemSusChem*, 2015, **8**, 2187-2192.

281 Q. Song, F. Wang, J. Cai, Y. Wang, J. Zhang, W. Yu, J. Xu, *Energy Environ. Sci.*, 2013, **6**, 994-1007.

282 P. Ferrini, R. Rinaldi, EP2891748-A1; WO2015104262-A1.

283 T.-T. You, L.-M. Zhang, S.-K. Zhou, F. Xu, *Ind. Crop. Prod.*, 2015, **71**, 65-74.

284 X. Wang, R. Rinaldi, *Angew. Chem. Int. Ed.*, 2013, **52**, 11499-11503.

285 J. Geboers, X. Wang, A. B. De Carvalho, R. Rinaldi, *J. Mol. Catal. A: Chem.*, 2014, **388-389**, 106-115.

286 I. Klein, B. Saha, M. M. Abu-Omar, *Catal. Sci. Technol.*, 2015, **5**, 3242-3245.

287 X. Wang, R. Rinaldi, *ChemSusChem*, 2012, **5**, 1455-1466.

288 X. Huang, T. I. Koranyi, M. D. Boot, E. J. M. Hensen, *Green Chem.*, 2015, **17**, 4941-4950.

289 C. Zhao, Y. Kou, A. A. Lemonidou, X. Li, J. A. Lercher, *Chem. Commun.*, 2010, **46**, 412-414.

290 H. Ohta, H. Kobayashi, K. Hara, A. Fukuoka, *Chem. Commun.*, 2011, **47**, 12209-12211.

291 R. Rinaldi, *Catalytic Hydrogenation for Biomass Valorization*, The Royal Society of Chemistry, 2014.

292 B. Güvenatam, O. Kurşun, E. H. J. Heeres, E. A. Pidko, E. J. M. Hensen, *Catal. Today*, 2014, **233**, 83-91.

293 F. Yang, M. A. Hanna, R. Sun, *Biotechnol. Biofuels*, 2012, **5**, 13-13.

294 *Chemical & Engineering News Archive*, 1984, **62**, 19-20.

295 Z. Strassberger, S. Tanase, G. Rothenberg, *RSC Adv.*, 2014, **4**, 25310-25318.

296 D. Humbird, R. Davis, L. Tao, C. Kinchin, D. Hsu, A. Aden, P. Schoen, J. Lukas, B. Olthof, M. Worley, D. Sexton, D. Dudgeon, *Process Design and Economics for Biochemical Conversion of Lignocellulosic Biomass to Ethanol: Dilute-Acid Pretreatment and Enzymatic Hydrolysis of Corn Stover*, Golden, Colorado, 2011.

297 M. B. Hocking, *J. Chem. Educ.*, 1997, **74**, 1055-1059.

298 M. M. Bomgardner, *Chem. Eng. News*, 2014, **92**, 10-14.

299 F. Cherubini, A. H. Strømman, in *Biofuels* (Eds.: A. Pandey, C. Larroche, S. C. Ricke, C.-G. Dussap, E. Gnansounou), Academic Press, Amsterdam, 2011, pp. 3-24.

300 M. Turunen, L. Alvila, T. T. Pakkanen, J. Rainio, *J. Appl. Polym. Sci.*, 2003, **88**, 582-588.

301 M. Wang, M. Leitch, C. Xu, *Eur. Polym. J.*, 2009, **45**, 3380-3388.

302 W. Zhang, Y. Ma, C. Wang, S. Li, M. Zhang, F. Chu, *Ind. Crop. Prod.*, 2013, **43**, 326-333.

303 Y. Li, A. J. Ragauskas, *J. Wood Chem. Technol.*, 2012, **32**, 210-224.

304 D. A. Baker, T. G. Rials, *J. Appl. Polym. Sci.*, 2013, **130**, 713-728.

305 L. Manjarrez Nevarez, L. Ballinas Casarrubias, O. Solis Canto, A. Celzard, V. Fierro, R. Ibarra Gomez, G. Gonzalez Sanchez, *Carbohydr. Polym.*, 2011, **86**, 732-741.

306 G. Milczarek, O. Inganäs, *Science*, 2012, **335**, 1468-1471.

307 M. Kijima, T. Hirukawa, F. Hanawa, T. Hata, *Bioresour. Technol.*, 2011, **102**, 6279-6285.

308 W. E. Tenhaeff, O. Rios, K. More, M. A. McGuire, *Adv. Funct. Mater.*, 2014, **24**, 86-94.

309 D. Stewart, *Ind. Crop. Prod.*, 2008, **27**, 202-207.

310 W.-J. Liu, H. Jiang, H.-Q. Yu, *Green Chem.*, 2015, **17**, 4888-4907.

311 M. Boot, P. Frijters, C. Luijten, B. Somers, R. Baert, A. Donkerbroek, R. J. H. Klein-Douwel, N. Dam, *Energ. Fuels*, 2009, **23**, 1808-1817.

312 L. Zhou, M. D. Boot, B. H. Johansson, J. J. E. Reijnders, *Fuel*, 2014, **115**, 469-478.

313 R. L. McCormick, M. A. Ratcliff, E. Christensen, L. Fouts, J. Luecke, G. M. Chupka, J. Yanowitz, M. Tian, M. Boot, *Energ. Fuels*, 2015, **29**, 2453-2461.

314 C. Amen-Chen, H. Pakdel, C. Roy, *Bioresour. Technol.*, 2001, **79**, 277-299.

315 D. Mohan, C. U. Pittman, P. H. Steele, *Energ. Fuels*, 2006, **20**, 848-889.

316 Q. Zhang, J. Chang, T. Wang, Y. Xu, *Energ. Convers. Manage.*, 2007, **48**, 87-92.

317 W. Mu, H. Ben, A. Ragauskas, Y. Deng, *Bioenerg. Res.*, 2013, **6**, 1183-1204.

318 B. C. Owen, L. J. Haupert, T. M. Jarrell, C. L. Marcum, T. H. Parsell, M. M. Abu-Omar, J. J. Bozell, S. K. Black, H. I. Kenttaemaa, *Anal. Chem.*, 2012, **84**, 6000-6007.

319 T. N. Pham, D. Shi, D. E. Resasco, *Appl. Catal. B: Environ.*, 2014, **145**, 10-23.

320 Z. Ma, J. A. van Bokhoven, *ChemCatChem*, 2012, **4**, 2036-2044.

321 E. F. Iliopoulou, S. Stefanidis, K. Kalogiannis, A. C. Psarras, A. Delimitis, K. S. Triantafyllidis, A. A. Lappas, *Green Chem.*, 2014, **16**, 662-674.

322 M. Dusselier, M. Mascal, B. Sels, in *Selective Catalysis for Renewable Feedstocks and Chemicals, Vol. 353* (Ed.: K. M. Nicholas), Springer International Publishing, 2014, pp. 1-40.

323 C. L. Williams, C.-C. Chang, P. Do, N. Nikbin, S. Caratzoulas, D. G. Vlachos, R. F. Lobo, W. Fan, P. J. Dauenhauer, *ACS Catal.*, 2012, **2**, 935-939.

324 R. J. A. Gosselink, *Lignin as a Renewable Aromatic Resource for the Chemical Industry*, PhD Thesis, Wageningen University, The Netherlands, 2011.

325 C. S. Lancefield, O. S. Ojo, F. Tran, N. J. Westwood, *Angew. Chem. Int. Ed.*, 2015, **54**, 258-262.

326 E. Feghali, G. Carrot, P. Thuery, C. Genre, T. Cantat, *Energ. Environ. Sci.*, 2015, **8**, 2734-2743.

327 T. D. H. Bugg, R. Rahmanpour, *Curr. Opin. Chem. Biol.*, 2015, **29**, 10-17.

328 R. Ma, M. Guo, X. Zhang, *ChemSusChem*, 2014, **7**, 412-415.

329 D. Salvachua, E. M. Karp, C. T. Nimlos, D. R. Vardon, G. T. Beckham, *Green Chem.*, 2015, **17**, 4951-4967.

330 Z. Mycroft, M. Gomis, P. Mines, P. Law, T. D. H. Bugg, *Green Chem.*, 2015, **17**, 4974-4979.

331 J. G. Linger, D. R. Vardon, M. T. Guarnieri, E. M. Karp, G. B. Hunsinger, M. A. Franden, C. W. Johnson, G. Chupka, T. J. Strathmann, P. T. Pienkos, G. T. Beckham, *Proc. Natl. Acad. Sci. U. S. A.*, 2014, **111**, 12013-12018.

332 D. R. Vardon, M. A. Franden, C. W. Johnson, E. M. Karp, M. T. Guarnieri, J. G. Linger, M. J. Salm, T. J. Strathmann, G. T. Beckham, *Energ. Environ. Sci.*, 2015, **8**, 617-628.

333   M. D. Kärkäs, B. S. Matsuura, T. M. Monos, G. Magallanes, C. R. Stephenson, *Org. Biomol. Chem.*, 2016, DOI: 10.1039/C1035OB02212F.

334   R. Ma, Y. Xu, X. Zhang, *ChemSusChem*, 2015, **8**, 24-51.

335   A. Rahimi, A. Azarpira, H. Kim, J. Ralph, S. S. Stahl, *J. Am. Chem. Soc.*, 2013, **135**, 6415-6418.

336   A. Rahimi, A. Ulbrich, J. J. Coon, S. S. Stahl, *Nature*, 2014, **515**, 249-252.

337   J. D. Nguyen, B. S. Matsuura, C. R. J. Stephenson, *J. Am. Chem. Soc.*, 2014, **136**, 1218-1221.

338   J. M. Nichols, L. M. Bishop, R. G. Bergman, J. A. Ellman, *J. Am. Chem. Soc.*, 2010, **132**, 12554-12555.

339   T. H. Parsell, B. C. Owen, I. Klein, T. M. Jarrell, C. L. Marcum, L. J. Haupert, L. M. Amundson, H. I. Kenttamaa, F. Ribeiro, J. T. Miller, M. M. Abu-Omar, *Chem. Sci.*, 2013, **4**, 806-813.

340   C. S. Lancefield, N. J. Westwood, *Green Chem.*, 2015, **17**, 4980-4990.

341   B. Sedai, C. Díaz-Urrutia, R. T. Baker, R. Wu, L. A. P. Silks, S. K. Hanson, *ACS Catal.*, 2011, **1**, 794-804.

342   S. K. Hanson, R. Wu, L. A. P. Silks, *Angew. Chem. Int. Ed.*, 2012, **51**, 3410-3413.

343   C. Díaz-Urrutia, W.-C. Chen, C.-O. Crites, J. Daccache, I. Korobkov, R. T. Baker, *RSC Adv.*, 2015, **5**, 70502-70511.

344   B. Biannic, J. J. Bozell, *Org. Lett.*, 2013, **15**, 2730-2733.

345   B. Sedai, R. T. Baker, *Adv. Synth. Catal.*, 2014, **356**, 3563-3574.

346   N. D. Patil, S. G. Yao, M. S. Meier, J. K. Mobley, M. Crocker, *Org. Biomol. Chem.*, 2015, **13**, 3243-3254.

347   J. Mottweiler, M. Puche, C. Räuber, T. Schmidt, P. Concepción, A. Corma, C. Bolm, *ChemSusChem*, 2015, **8**, 2106-2113.

348   J. Mottweiler, T. Rinesch, C. Besson, J. Buendia, C. Bolm, *Green Chem.*, 2015, **17**, 5001-5008.

349   L. J. Mitchell, C. J. Moody, *J. Org. Chem.*, 2014, **79**, 11091-11100.

350   Y. Yang, H. Fan, J. Song, Q. Meng, H. Zhou, L. Wu, G. Yang, B. Han, *Chem. Commun.*, 2015, **51**, 4028-4031.

351   W. E. Piers, in *Adv. Organomet. Chem., Vol. 52* (Eds.: R. West, A. F. Hill), Elsevier Academic Press Inc, San Diego, 2005, pp. 1-76.

352   A. Fedorov, A. A. Toutov, N. A. Swisher, R. H. Grubbs, *Chem. Sci.*, 2013, **4**, 1640-1645.

353   E. Feghali, T. Cantat, *Chem. Commun.*, 2014, **50**, 862-865.

354   S. Son, F. D. Toste, *Angew. Chem.*, 2010, **49**, 3791-3794.

355   J. M. Chan, S. Bauer, H. Sorek, S. Sreekumar, K. Wang, F. D. Toste, *ACS Catal.*, 2013, **3**, 1369-1377.

356   A. Wu, B. O. Patrick, E. Chung, B. R. James, *Dalton Trans.*, 2012, **41**, 11093-11106.

357   A. Wu, J. M. Lauzon, B. R. James, *Catal. Lett.*, 2015, **145**, 511-518.

358   T. vom Stein, T. Weigand, C. Merkens, J. Klankermayer, W. Leitner, *ChemCatChem*, 2013, **5**, 439-441.

359   T. vom Stein, T. den Hartog, J. Buendia, S. Stoychev, J. Mottweiler, C. Bolm, J. Klankermayer, W. Leitner, *Angew. Chem. Int. Ed.*, 2015, **54**, 5859-5863.

360   S. Dabral, J. Mottweiler, T. Rinesch, C. Bolm, *Green Chem.*, 2015, **17**, 4908-4912.

361   R. G. Harms, I. I. E. Markovits, M. Drees, h. c. m. W. A. Herrmann, M. Cokoja, F. E. Kühn, *ChemSusChem*, 2014, **7**, 429-434.

362   L. J. Haupert, B. C. Owen, C. L. Marcum, T. M. Jarrell, C. J. Pulliam, L. M. Amundson, P. Narra, M. S. Aqueel, T. H. Parsell, M. M. Abu-Omar, H. I. Kenttaemaa, *Fuel*, 2012, **95**, 634-641.

363   T. M. Jarrell, C. L. Marcum, H. Sheng, B. C. Owen, C. J. O'Lenick, H. Maraun, J. J. Bozell, H. I. Kenttaemaa, *Green Chem.*, 2014, **16**, 2713-2727.

364   A. G. Marshall, R. P. Rodgers, *Proc. Natl. Acad. Sci. U.S.A.*, 2008, **105**, 18090-18095.

365   A. A. Herod, K. D. Bartle, T. J. Morgan, R. Kandiyoti, *Chem. Rev.*, 2012, **112**, 3892-3923.

366   K. M. Torr, D. J. van de Pas, E. Cazeils, I. D. Suckling, *Bioresour. Technol.*, 2011, **102**, 7608-7611.

367   H. Werhan, A. Farshori, P. Rudolf von Rohr, *J. Membr. Sci.*, 2012, **423**–**424**, 404-412.

368   C. G. Boeriu, F. I. Fiţigău, R. J. A. Gosselink, A. E. Frissen, J. Stoutjesdijk, F. Peter, *Ind. Crop. Prod.*, 2014, **62**, 481-490.

369   R. H. Venderbosch, *ChemSusChem*, 2015, **8**, 1306-1316.

370   A. R. Ardiyanti, R. H. Venderbosch, W. Yin, H. J. Heeres, in *Catalytic Hydrogenation for Biomass Valorization*, The Royal Society of Chemistry, 2014, pp. 151-173.

371   X. Huang, T. I. Korányi, M. D. Boot, E. J. M. Hensen, *ChemSusChem*, 2014, **7**, 2276-2288.

372   J. Zakzeski, A. L. Jongerius, P. C. A. Bruijnincx, B. M. Weckhuysen, *ChemSusChem*, 2012, **5**, 1602-1609.

373   K. Barta, G. R. Warner, E. S. Beach, P. T. Anastas, *Green Chem.*, 2014, **16**, 191-196.

374   F. Chen, Y. Tobimatsu, L. Jackson, J. Nakashima, J. Ralph, R. A. Dixon, *Plant J.*, 2013, **73**, 201-211.

375   J. Zakzeski, B. M. Weckhuysen, *ChemSusChem*, 2011, **4**, 369-378.

376   Y. Pu, N. Jiang, A. J. Ragauskas, *J. Wood Chem. Technol.*, 2007, **27**, 23-33.

377   I. Kilpeläinen, H. Xie, A. King, M. Granstrom, S. Heikkinen, D. S. Argyropoulos, *J. Agric. Food Chem.*, 2007, **55**, 9142-9148.

378   P. Mäki-Arvela, I. Anugwom, P. Virtanen, R. Sjöholm, J. P. Mikkola, *Ind. Crop. Prod.*, 2010, **32**, 175-201.

379   A. Brandt, J. Grasvik, J. P. Hallett, T. Welton, *Green Chem.*, 2013, **15**, 550-583.

380   S. S. Y. Tan, D. R. MacFarlane, J. Upfal, L. A. Edye, W. O. S. Doherty, A. F. Patti, J. M. Pringle, J. L. Scott, *Green Chem.*, 2009, **11**, 339-345.

381   S. Singh, B. A. Simmons, K. P. Vogel, *Biotechnol. Bioeng.*, 2009, **104**, 68-75.

382   A. Brandt, J. P. Hallett, D. J. Leak, R. J. Murphy, T. Welton, *Green Chem.*, 2010, **12**, 672-679.

383   F. Kerton, R. Marriott, in *Alternative Solvents for Green Chemistry (2)*, The Royal Society of Chemistry, 2013, pp. 82-114.

384   R. Ma, W. Hao, X. Ma, Y. Tian, Y. Li, *Angew. Chem. Int. Ed.*, 2014, **53**, 7310-7315.

385   W. Xu, S. J. Miller, P. K. Agrawal, C. W. Jones, *ChemSusChem*, 2012, **5**, 667-675.

386   S. Kasakov, H. Shi, D. M. Camaioni, C. Zhao, E. Baráth, A. Jentys, J. A. Lercher, *Green Chem.*, 2015, **17**, 5079-5090.

387   X. Wang, R. Rinaldi, *Catal. Today*, 2016, DOI: 10.1016/j.cattod.2015.1011.1047.

388   G. van Rossum, W. Zhao, M. Castellvi Barnes, J.-P. Lange, S. R. A. Kersten, *ChemSusChem*, 2014, **7**, 253-259.

389   S. Kumar, J.-P. Lange, G. Van Rossum, S. R. A. Kersten, *Ind. Eng. Chem. Res.*, 2014, **53**, 11668-11676.

390   D. Meier, R. Ante, O. Faix, *Bioresour. Technol.*, 1992, **40**, 171-177.

391   A. Oasmaa, R. Alén, D. Meier, *Bioresour. Technol.*, 1993, **45**, 189-194.

392   A. Kloekhorst, J. Wildschut, H. J. Heeres, *Catal. Sci. Technol.*, 2014, **4**, 2367-2377.

393   C. R. Kumar, N. Anand, A. Kloekhorst, C. Cannilla, G. Bonura, F. Frusteri, K. Barta, H. J. Heeres, *Green Chem.*, 2015, **17**, 4921-4930.

394   T. Kleine, J. Buendia, C. Bolm, *Green Chem.*, 2013, **15**, 160-166.

395   V. M. Roberts, V. Stein, T. Reiner, A. Lemonidou, X. Li, J. A. Lercher, *Chem. Eur. J.*, 2011, **17**, 5939-5948.

396   Y. Jiang, Z. Li, X. Tang, Y. Sun, X. Zeng, S. Liu, L. Lin, *Energy & Fuels*, 2015, **29**, 1662-1668.

397   K. Barta, T. D. Matson, M. L. Fettig, S. L. Scott, A. V. Iretskii, P. C. Ford, *Green Chem.*, 2010, **12**, 1640-1647.

398   T. Voitl, P. Rudolf von Rohr, *ChemSusChem*, 2008, **1**, 763-769.

399   H. Xiong, H. N. Pham, A. K. Datye, *Green Chem.*, 2014, **16**, 4627-4643.

400   J. P. Lange, *Angew. Chem. Int. Ed.*, 2015, **54**, 13186-13197.

401   R. Rinaldi, F. Y. Fujiwara, U. Schuchardt, *Appl. Catal. A: Gen.*, 2006, **315**, 44-51.

402   R. Ravenelle, J. Copeland, A. Van Pelt, J. Crittenden, C. Sievers, *Top. Catal.*, 2012, **55**, 162-174.

403   A. L. Jongerius, J. R. Copeland, G. S. Foo, J. P. Hofmann, P. C. A. Bruijnincx, C. Sievers, B. M. Weckhuysen, *ACS Catal.*, 2013, **3**, 464-473.

404   R. Katahira, J. B. Sluiter, D. J. Schell, M. F. Davis, *J. Agric. Food Chem.*, 2013, **61**, 3286-3292.

405   S. A. W. Hollak, K. P. de Jong, D. S. van Es, *ChemCatChem*, 2014, **6**, 2648-2655.

406   D. A. Boga, F. Liu, P. C. A. Bruijnincx, B. M. Weckhuysen, *Catal. Sci. Technol.*, 2016, **6**, 134-143.

407   C. H. Bartholomew, *in Advances in Catalysis Volume 31 (Ed.: D.D. Eley), New York* 1982.

408   Q. Song, F. Wang, J. Xu, *Chem. Commun.*, 2012, **48**, 7019-7021.

409   A. K. Deepa, P. L. Dhepe, *ACS Catalysis*, 2015, **5**, 365-379.

410   E. Furimsky*, Appl. Catal. A: Gen.*, 2000, **199**, 147-190.

411   G. W. Huber, A. Corma*, Angew. Chem. Int. Ed.*, 2007, **46**, 7184-7201.

412   P. M. Mortensen, J. D. Grunwaldt, P. A. Jensen, K. G. Knudsen, A. D. Jensen*, Appl. Catal. A: Gen.*, 2011, **407**, 1-19.

413   A. H. Zacher, M. V. Olarte, D. M. Santosa, D. C. Elliott, S. B. Jones*, Green Chem.*, 2014, **16**, 491-515.

414   E.-J. Shin, M. A. Keane*, Ind. Eng. Chem. Res.*, 2000, **39**, 883-892.

415   A. Centeno, E. Laurent, B. Delmon*, J. Catal.*, 1995, **154**, 288-298.

416   A. L. Jongerius, R. W. Gosselink, J. Dijkstra, J. H. Bitter, P. C. A. Bruijnincx, B. M. Weckhuysen*, ChemCatChem*, 2013, **5**, 2964-2972.

417   K. Li, R. Wang, J. Chen*, Energ. Fuels*, 2011, **25**, 854-863.

418   H. Zhao, D. Li, P. Bui, S. Oyama*, Appl. Catal. A: Gen.* , 2011, **391**, 305-310.

419   C. Zhao, Y. Kou, A. A. Lemonidou, X. Li, J. A. Lercher*, Angew. Chem. Int. Ed.*, 2009, **48**, 3987-3990.

420   C. Zhao, J. A. Lercher*, Angew. Chem. Int. Ed.*, 2012, **51**, 5935-5940.

421   A. L. Jongerius, P. C. A. Bruijnincx, B. M. Weckhuysen*, Green Chem.*, 2013, **15**, 3049-3056.

422   A. L. Jongerius, R. Jastrzebski, P. C. A. Bruijnincx, B. M. Weckhuysen*, J. Catal.*, 2012, **285**, 315-323.

423   N. Yan, C. Zhao, P. J. Dyson, C. Wang, L.-t. Liu, Y. Kou*, ChemSusChem*, 2008, **1**, 626-629.

424   W. Schutyser, S. Van den Bosch, J. Dijkmans, S. Turner, M. Meledina, G. Van Tendeloo, D. P. Debecker, B. F. Sels*, ChemSusChem*, 2015, **8**, 1805-1818.

Part I

Depolymerisation of Lignin

Chapter 3

Tandem Catalytic Depolymerisation of Lignin by Water-Tolerant Lewis Acids and Rhodium Complexes

Abstract

Lignin could serve as an attractive renewable feedstock for the production of aromatic bulk and fine chemicals, provided that suitable depolymerisation procedures are developed. Here, a new strategy for the cleavage of the ether fragments within lignin is described, using water-tolerant Lewis acids such as $Sc(OTf)_3$ for hydrolysing the ethers and an *in-situ* generated rhodium bis-1,3-(diphenylphosphino) propane complex for decarbonylation of the generated aldehydes in a one-pot reaction. The latter step serves to scavenge the reactive aldehydes effectively, preventing the loss of monomers due to recondensation reactions without the need for any sacrificial reagents. The approach was first validated using model compounds for the β-O-4 linkage in lignin. Subsequent application of the procedure to poplar dioxasolv lignin showed a significant molecular weight reduction and afforded both decarbonylation products, as well as, rather surprisingly, *iso*-eugenol and 4-(1-propenyl)syringol. Crucially, product selectivity could be tuned by using metal triflates with different acid strengths: weak acids afforded 4-(1-propenyl)phenols and strong Lewis acids afforded 4-methylphenol decarbonylation products. The method was further shown to be broadly applicable to lignins from different biomass sources, thus also allowing the ratio of guaiacyl and syringyl products to be adjusted.

3.1 Introduction

As discussed in the previous chapters, the development of biorefineries for the production of renewable chemicals and fuels will require the valorisation of the complete biomass feedstock.[1] Lignin, which constitutes approximately 15-40% of plant biomass, is the only component of biomass of substantial abundance that is composed of aromatic substructures and would therefore be an ideal candidate for the production of aromatic bulk and fine chemicals.[2,3]

Lignin is an amorphous, heterogeneous polymer and has no single, well-defined structure. Native lignins, i.e. as found in the whole biomass, are derived from the radical coupling of the three monolignols coumaryl alcohol, coniferyl alcohol and sinapyl alcohol.[4] The ratio of the three monomers, often referred to as the S:G:H ratio, for the syringyl, guaiacyl and *p*-hydroxyphenyl-containing units, is highly dependent on the plant species. Grasses and softwoods are typically relatively rich in H and/or G, while hardwood species have a high S content. The monomers are connected via various different linkages in native lignin; most notable is the β-O-4 ether fragment, which may account for up to 60% of the linkages. Other common inter-unit linkages include the 4-O-5 ethers, as well as carbon-carbon bonds such as biphenyls (5-5), resinol structures (β-β) and phenylcoumarans (β-5).[5] Isolated (technical) lignins are almost invariably significantly changed in structure, as a (considerable) part of the ether bonds will already be cleaved during the isolation process and new carbon-carbon bonds will also have been formed, rendering those lignins more recalcitrant to further upgrading.[4] The amount of β-O-4 linkages in particular, may be severely reduced.

Upgrading of lignin for the production of chemicals requires selective depolymerisation of the polymer, which remains a considerable challenge. Many strategies have been developed in recent years, including the use of homogeneous catalysts under relatively mild conditions to selectively target specific bonds within the lignin (usually the β-O-4 linkage);[6] cleavage of such a linkage can be done either in an oxidative,[7-9] redox-neutral,[10,11] or reductive fashion,[12,13] and can provide access to product streams that contain a limited number of compounds, albeit often in moderate yield. For such approaches, it is of critical importance that the lignin has been isolated under sufficiently mild conditions to maintain a high abundance of the β-O-4 linkage. On the other hand, heterogeneous catalyst systems typically operate under much more severe conditions, i.e., in a regime allowing both thermochemical and chemocatalytic depolymerisation, affording high yields of lignin oils. However, such oils typically consist of a complex mixture of oxygenated aromatics.[14-18]

Depolymerisation by acid-catalysed hydrolysis of the ether linkages in lignin is one of the oldest methods for lignin depolymerisation.[19] The yields of monomeric aromatics obtained are typically very low, however, as the products formed by hydrolysis are rather
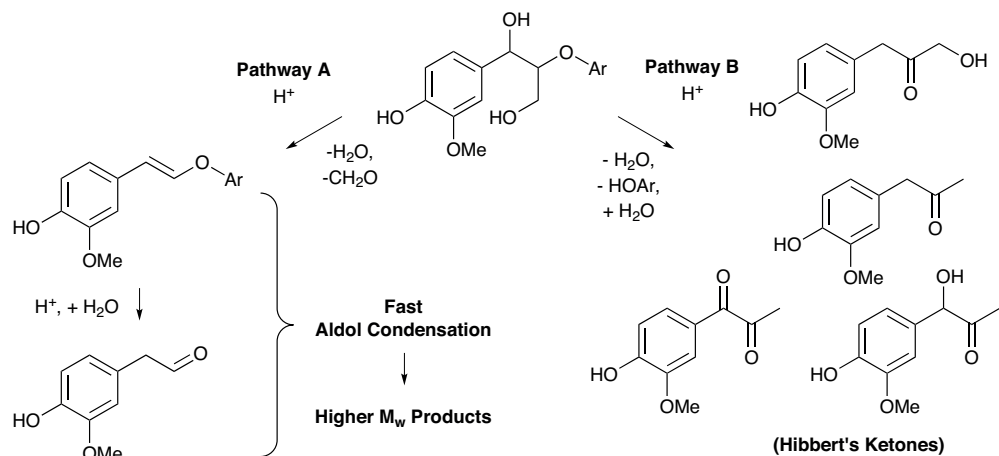
Figure 3.1: Two major pathways in acid-catalysed lignin degradradation. In pathway A, a dehydration and deformylation step leads to a two-carbon styryl ether, which can be hydrolysed to afford the corresponding aldehyde. The aldehydes and styryl ethers undergo fast aldol condensation, leading to the formation of higher molecular weight products. In pathway B, no deformylation takes place and after elimination of the phenol rapid isomerisation leads to a mixture of three-carbon products collectively known as Hibbert's ketones. Condensation of the phenolics generated through either pathway with liberated formaldehyde may provide an additional route to high molecular weight products.

susceptible to recondensation reactions, forming recalcitrant carbon-carbon bonds. Avoiding such consecutive reactions after depolymerisation highlights a second important challenge in any lignin valorisation strategy. An excellent example of the importance of control over recondensation reactions has been reported for the base-catalysed depolymerisation of Kraft lignin: using boric acid to trap generated phenolics as borate esters, the obtained monomer yield could be significantly increased.[20] In acid-catalysed hydrolysis, β-O-4 model compound studies revealed two pathways for cleavage (Figure 3.1).[6] In pathway A, both an acid-catalysed dehydration and deformylation takes place, to afford a two-carbon styryl ether. The styryl ether can then be hydrolysed to the corresponding aldehyde, but both aldehyde and styryl ether are highly susceptible to subsequent aldol condensation, affording higher molecular weight products.[21-23] In pathway B, no deformylation takes place and the analogous dehydration/hydrolysis sequence affords a ketone, which rapidly undergoes isomerisation to afford a mixture of products collectively known as Hibbert's ketones.[24] The latter are comparatively stable under acidolysis conditions. Experiments with actual lignin therefore showed that only the propyl-substituted products are found after acid hydrolysis, confirming fast condensation of the formed styryl ether and aldehyde intermediates.[24] Recent work by Deuss *et al.* elegantly demonstrated that this process could be limited by applying several trapping strategies in the triflic-acid catalysed depolymerisation of a walnut and a beech

dioxasolv lignin rich in β-O-4 linkages.[25] Trapping the reactive carbonyls produced *via* pathway A by (acid-catalysed) acetalisation was found to be most effective, tripling the amount of monomers that could be obtained.

The challenge is then to find a trapping strategy that simultaneously generates useful products. For maximum efficiency, such a strategy does not depend on using sacrificial trapping reagents, but preferably is catalytic. Catalytic decarbonylation is in that sense an interesting candidate, as it allows removal of the aldehyde function with simultaneous shortening of the propyl chain. In fact, many valuable aromatic products that can potentially be obtained from lignin do not bear a propyl substituent (including benzene, toluene and phenol), but rather have a shorter alkyl chain or none at all. Although this reaction was already described in the 1960's with a stoichiometric amount of Wilkinson's catalyst,[26] selective catalytic decarbonylation has remained challenging and only two systems are known to effect the reaction with reasonable efficiency.[27,28] Indeed, Deuss *et al.* also attempted trapping by decarbonylation as one of the strategies tested, but this had only limited success. The major problem was that the rate of decarbonylation was not sufficiently high to effectively compete with the condensation reactions.

Simultaneously, the work described here was undertaken, combining acid-catalysed hydrolysis of β-O-4 bonds in lignin with catalytic decarbonylation, but with water-tolerant Lewis acids of the M(OTf)$_3$ family (where M can be a group III or XII metal or lanthanide) as the acid catalyst. Such catalyst have gained attention in recent years for their ability to carry out a large number of reactions in aqueous media and other polar solvents, which are not possible with classical Brønsted acids.[29-32] In addition, recent work has also shown that they are quite effective in cleaving ether bonds in aqueous and other highly polar media.[33,34]

Efficient lignin depolymerisation by trapping of reactive intermediates by a tandem catalytic approach using a Lewis acid catalyst for hydrolysis and a rhodium-based decarbonylation catalyst is demonstrated here. With a combination of Sc(OTf)$_3$ and a rhodium catalyst prepared from [Rh(cod)Cl]$_2$ (cod = 1,5-cyclooctadiene) and dppp
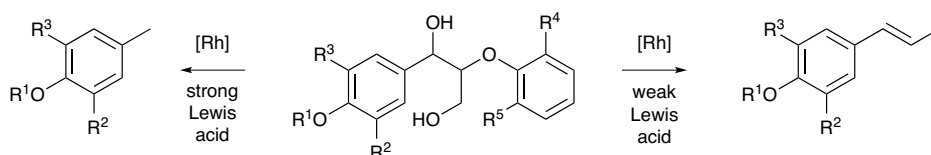

Figure 3.2: General strategy for the Lewis-acid catalysed cleavage of β-O-4 lignin fragments combined with rhodium-catalysed decarbonylation, exemplified here for a generalised model compound. The strength of the Lewis acid offers control over the cleavage pathway. (R^1 = H, Me; R^2, R^3, R^4, R^5 = H, OMe)

(1,3-bis(diphenylphosphino)propane), it is shown that acidolysis of the β-O-4 linkage in model compounds affords the corresponding decarbonylated 4-methyl substituted products. This chemistry is then successfully translated to a dioxasolv lignin isolated from poplar. Remarkably, with the poplar lignin the use of this catalytic system also enables a second trapping pathway, which leads to the formation of 4-(1-propenyl)phenols (Figure 3.2). These are valuable specialty chemicals and are ideally suited as a high-value/low-volume product from lignin. Crucially, we show that the trapping pathway can be selected by choice of the Lewis acid strength, thus allowing us to steer the outcome of the reaction to whichever of the two product classes is desired.

3.2 Results and Discussion

3.2.1 Hydrolysis/Decarbonylation of Model Compounds

To assess the suitability of a combined hydrolysis and decarbonylation approach for lignin depolymerisation, the tandem catalytic reaction was first attempted on model compounds representative of the β-O-4 fragment (Figure 3.3). Of the several metal triflates previously described as water-tolerant Lewis acids, scandium triflate was selected as it has been shown to cleave ether bonds in aqueous solution during delignification of wheat straw.[35] As decarbonylation catalyst the system reported by Madsen *et al.* was chosen, which can be conveniently prepared *in-situ* from an appropriate rhodium precursor and the 1,3-bis(diphenylphosphino)propane (dppp) ligand.[27] Whilst RhCl$_3$ was used as precursor, the actual active species was shown to be a rhodium(I) compound and we therefore opted to instead use the rhodium(I) precursor [Rh(cod)Cl]$_2$ (cod = 1,5-cyclooctadiene) to prevent the formation of HCl and consequent interference of Brønsted acid-catalysed reactions. A 9:1 mixture of 1,4-dioxane and water was selected as solvent for the reaction. The rhodium catalyst has previously been shown to be most active in polar solvents such as 1,4-dioxane and diglyme. At the same time, as a hydrolysis step is needed to cleave the β-O-4 ether, excess of water is required to ensure good hydrolysis activity. Although many transition metal complexes acting as catalysts are negatively impacted by the presence of water, this was not the case for the rhodium complex. The cleavage of the simple model compound **1a** was found to proceed very slowly at 175 °C, although at 200 °C (Table 3.1, #1) significant amounts of the expected hydrolysis/decarbonylation products phenol and toluene were formed. Indeed, the phenol is derived from the hydrolysis of the alkyl aryl ether and toluene from decarbonylation of 2-phenylacetaldehyde (**6a**). Although the latter was not observed as an intermediate in detectable amounts, a 12% yield of 2-phenylethanol was found, as well the dehydrogenated α-ketone starting material, suggesting that phenylacetaldehyde may also be hydrogenated if an appropriate hydrogen donor is available. Indeed, rhodium/dppp
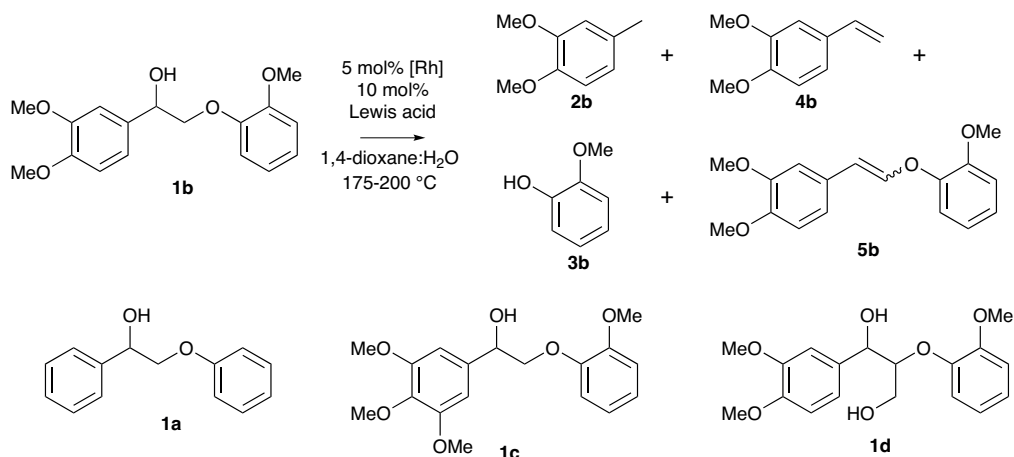
Figure 3.3: Tandem catalytic cleavage of β-O-4 model compound **1b** and major products observed. The cleavage of the other model compounds proceeds analogously.

Table 3.1: Results of the tandem catalytic cleavage of β-O-4 model compounds and major products observed.[a]

	β-O-4 model	Rh (mol%)	LA[b] (mol%)	T (°C)	Conv.[c] (%)	Yield (%)				
						2	**3**	**4**	**5**	**C**[d]
1	**1a**[e]	5	10	200	100	-	63	-	-	22
2	**1a**	5	10	200	57	24	47	-	2	-
3	**1b**	5	10	200	96	65	77	-	-	1
4	**1b**	5	10	175	99	37	81	-	-	17
5	**1b**	5	5	175	99	66	85	-	-	4
6	**1b**	5	2.5	175	92	36	41	3	44	-
7	**1b**	5	5[f]	175	99	84	5	-	-	31
8	**1b**	5	2.5[f]	175	98	45	61	-	25	-
9	**1c**	5	5	175	97	67	71	3	4	-
10	**1c**	5	2.5	175	39	7	12	8	16	-
11	**1d**	5	5	175	100	51	88	-	-	3

[a] Conditions: 2.4 mmol substrate, [Rh(cod)Cl]$_2$, 2 eq dppp, Sc(OTf)$_3$ (or In(OTf)$_3$) as listed; 175-200 °C, 2 h, 22 mL 9:1 1,4-dioxane:water; yields determined by GC-FID [b] Lewis acid [c] Conversion [d] Condensation products [e] No [Rh(cod)Cl]$_2$ [f] In(OTf)$_3$

complexes have previously been shown capable of catalyzing transfer hydrogenation.[36-38] In the absence of decarbonylation catalyst, the substrate is fully converted, but while a reasonable yield of phenol was obtained, neither toluene nor 2-phenylacetaldehyde was observed. Instead, higher boiling compounds were formed, which based on GC-MS data
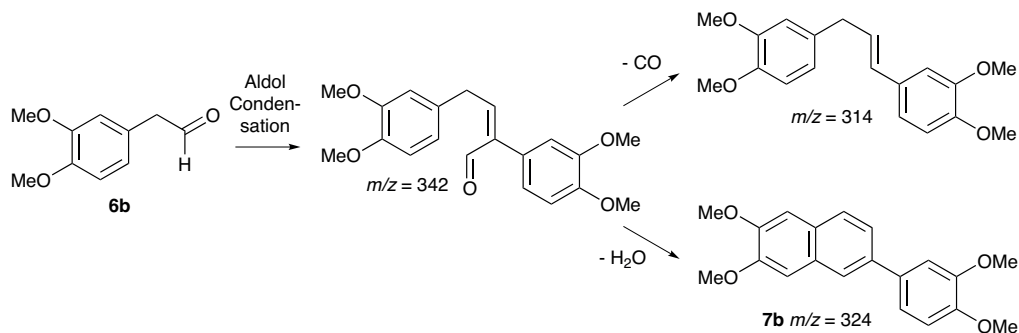
Figure 3.4: Formation of higher molecular weight condensation productions from homoveratryl aldehyde.

could be attributed to stilbenes and 2-phenylnaphtalene (**7a**). As scandium triflate is also an excellent catalyst for aldol condensations,[39,40] the latter is likely a product of the self-condensation of 2-phenylacetaldehyde (**6a**), followed by an intramolecular cyclisation. This clearly demonstrates the value of the tandem approach, in that the addition of the decarbonylation catalyst not only important to obtain the desired decarbonylated products, but also to rapidly remove the reactive aldehydes formed upon hydrolysis, thus preventing undesired side-reactions.

Compound **1a** provides a useful starting point in understanding the elementary reactions involved, but is also a rather poor model for the actual structure of lignin. The complexity of the model compounds was therefore gradually increased to assess the influence of functional group substitution on each of the catalytic steps. Thus, the cleavage of **1b** afforded both 4-methylveratrole (**2b**) and guaiacol (**3b**) in reasonable yield (Table 3.1, #3). Interestingly, **1b** could also be cleaved at 175 °C; whilst the excellent yield of guaiacol (81%) at this temperature indicated that hydrolysis was efficient, the much lower yield of 4-methylveratrole yield (38%) showed that decarbonylation was not. Supporting the idea that decarbonylation proceeds from the corresponding acetaldehyde, we were now able to observe homoveratryl aldehyde (**7b**) in about 1% yield. As with the Sc(OTf)$_3$-only reaction, the formation of higher molecular weight species was again observed at this temperature. Although the NIST library was not very helpful in their assignment, the peaks at m/z = 314, 324 and 342 were consistent with the product obtained from aldol self-condensation of homoveratryl aldehyde followed by either the decarbonylation or intramolecular cyclisation to give the biphenyl compound **7b**, analogous to the 2-phenylnaphtalene (**7a**) that was also observed on reaction of **1a** with only acid (Figure 3.4).[41]

These results thus imply that the kinetics of hydrolysis and decarbonylation are not sufficiently matched and that the decarbonylation catalyst cannot keep up with the amounts

of aldehyde generated at 175 °C. The amount of scandium triflate was therefore lowered (Table 3.1, #4-6). Indeed, using only 5 mol% of the Lewis acid, the 4-methylveratrole (**2b**) yield increased to 66%, with a concomitant drop in condensation products. Decreasing the amount of scandium triflate even further also decreased the amount of guaiacol formed, but proved very revealing mechanistically as it allowed for the observation of two other intermediates. The *cis* and *trans* styryl ethers (**5b**) are now detected, with the *cis* isomer being predominant. As the cleavage of the β-O-4 bond fragment under acidic conditions has been previously suggested to start by dehydration of the α-hydroxy functionality to form a styryl ether,[22,23] this is presumed to be an intermediate in the formation of the decarbonylation products. The formation of such styryl ethers as intermediates have also been observed previously in the base-[42] or methyldioxorhenium[43]-catalysed cleavage of β-O-4 models, where the *cis* isomer is predominant as well. To further confirm that **5b** is in fact an intermediate in the reaction, the reaction of **1b** with 2.5 mol% scandium triflate was monitored over time (Figure 3.5a). Indeed, rapid consumption of the starting material was observed, with concomitant formation of **5b**, followed by formation of both **2b** and **3b** with consumption of **5b**. The amount of homoveratryl aldehyde observed is lower than 1% at all times, showing the effectiveness of the rhodium decarbonylation catalyst even under such low aldehyde steady-state concentrations. The interplay between the Lewis acid and rhodium catalyst is also made clear
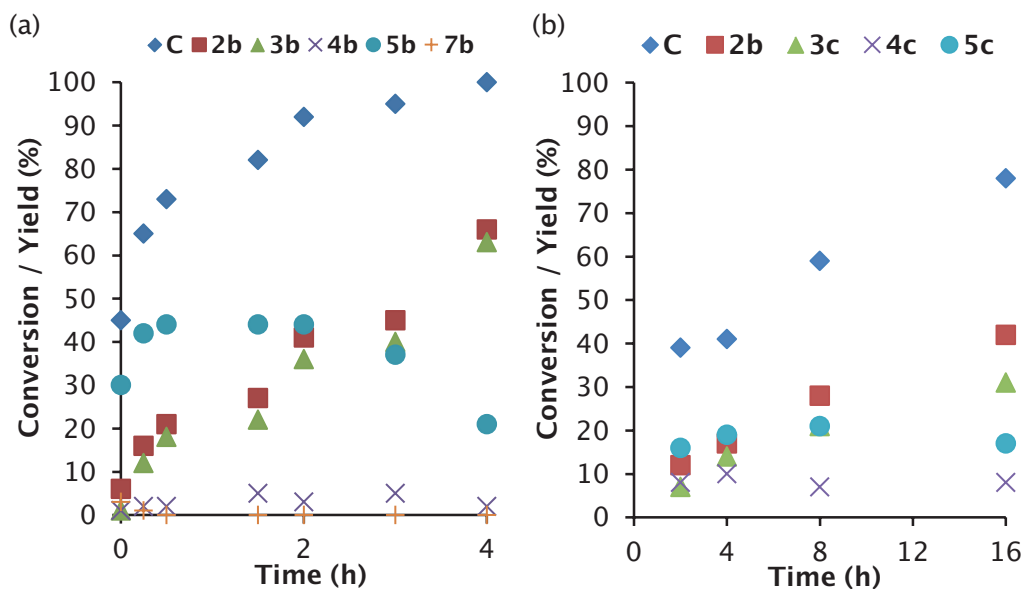

Figure 3.5: (a) The reaction profile of **1b** as function of time (determined through individual reactions) when using 2.5 mol% Sc(OTf)$_3$ shows the accumulation of **2b** as an intermediate. (b) Likewise, the consumption of **1c** is accompanied with the formation of **2c** as intermediate; the amount of styrene formed (**4c**) is constant in time.

by changing from Sc(OTf)$_3$ to In(OTf)$_3$ (Table 3.1, #7-8). As the latter is a stronger Lewis acid, hydrolysis is faster and a higher conversion and guaiacol (**3b**) yield is observed. However, aldol condensation of the intermediate aldehyde is also accelerated: the yield of decarbonylation products decreases and the amount of aldol condensation products increases. In light of the results obtained with **1c** and lignin (*vide infra*), it should already be noted that the formation of small amounts (ca 2%) of 3',4'-dimethoxystyrene (**4b**) in the experiments with 2.5 mol% Sc(OTf)$_3$ were also observed (Table 3.1, #6).

The use of **1c** as a model for the syringyl-containing β-O-4 linkages in lignin also afforded excellent conversion and good guaiacol (**3b**) and 3,4,5-trimethoxytoluene (**2c**) yields with 5 mol% Sc(OTf)$_3$ at 175 °C (# 9). However, upon lowering the amount of Sc(OTf)$_3$ to 2.5 mol% (#10) a conversion of **1c** of only 42% was obtained, with only 6% yield of 3,4,5-trimethoxytoluene (**2c**) and a 12% yield of the styryl ethers **5c**. Again, the formation of 7% of a styrene derivative (3,4,5-trimethoxystyrene, **4c**) was observed. Likely **1b** undergoes dehydration faster than **1c** because of the electron-withdrawing effect of the additional *meta* methoxy group, as this would destabilize the carbocation deriving from an E1 elimination mechanism.

The observation of styrene derivatives **4b** and **4c** from **1b** and **1c** respectively is quite remarkable and has not been reported before to the best of our knowledge. To get some insight into how these styrenes are formed, important also given the results obtained with lignin detailed below, the reaction of **1c** was also monitored at different reaction times (Figure 3.5b). As for **1b**, **1c** was observed to have been converted to the corresponding styryl ethers **5c**. Surprisingly the styrene derivative **4c** appears to be formed rapidly in the early stages of the reaction, but the amount of **4c** does not increase with time. Whether **4c** is formed directly from the β-O-4 model or from the styryl ether is unclear at this point; such a reaction nonetheless must involve a formal *hydrogenolysis* step to give **4c**. An alternative mechanism could be the formation of the styrene by transfer hydrogenation of the aldehyde (**6b/6c**) to give the corresponding alcohol, followed by an acid-catalysed dehydration step. However, the formation of styrene is favored in the presence of lower amounts of acid, which does not seem to be in agreement with such an indirect mechanism.

To mimic the glyceryl backbone of the β-O-4 linkage, the cleavage of model compound **1d** (a mixture of the *erythro* and *threo* isomers) was also studied. This compound was cleaved effectively as well and also resulted in the formation of guaiacol (**3b**) and the decarbonylation product 4-methylveratrole (**2b**), albeit with slightly lower yields. To arrive at the same products from **1d** as from ethanediol model **1b**, it is likely that the γ-carbonol group is eliminated as formaldehyde, which has been observed in acidolysis of lignin model compounds before.[22] The actual mechanism of formaldehyde elimination is still rather elusive; particularly whether elimination occurs prior to, simultaneous with or after the initial dehydration is unknown. Nevertheless, deformylation seems the
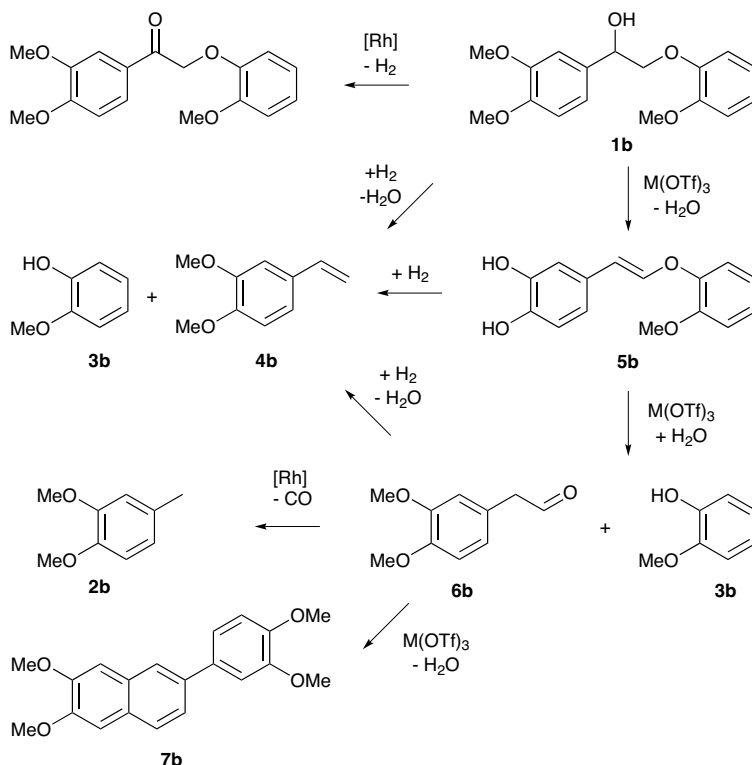
Figure 3.6: Proposed mechanism for the cleavage of β-O-4 models.

most likely operative route to allow decarbonylation to the methyl-substituted product. Notably, small amounts of **1-veratrylethanone** were also observed, where clearly the γ-carboninol has not been eliminated. As decarbonylation requires an initial oxidative addition into the aldehyde carbon-hydrogen bond, the rhodium catalyst is unreactive towards ketones and the resulting internal carbonyl functionality cannot be removed.[44]

Taken together, the results obtained with the ethanediol models provide detailed insight into the individual reactions taking place that lead to complete cleavage (Figure 3.6); whether in case of **1d** deformylation happens prior to or after dehydration is unclear. An initial Lewis acid-catalysed dehydration of the α-hydroxyl functionality forms a regioisomeric mixture of styryl ethers. Subsequent Lewis acid-catalysed hydrolysis of the styryl ether proceeds more sluggishly to afford the corresponding acetaldehyde. With a sufficiently active decarbonylation catalyst the corresponding methyl-substituted product is obtained, while in the absence thereof aldol condensation takes place instead. An alternative pathway (possibly originating from the styryl ether), leading to the formation of a styrene derivative instead, was also observed for the first time.

3.2.2 Depolymerisation of Poplar Dioxasolv Lignin

Having established that the combined hydrolysis/decarbonylation procedure, if properly matched, works well on β-O-4 model compounds, the approach was translated to actual lignin. As release of a monomer from the lignin polymer requires cleaving two bonds (one on each side for non-end group units) the maximum yield of monomers from a selective cleavage method is approximately quadratic with the fraction of cleavable bonds (see also the discussion in Chapter 2).[8,12] It is thus important to start with lignin that still contains a relatively high amount of targeted linkages. Lignin was therefore isolated from poplar sawdust, which was sourced from a local sawmill, using a mild, previously reported dioxasolv procedure.[8] The choice of solvent in this organosolv process is key, as the mechanism established for the model compounds mandates that the α-hydroxyl remains available. Alcohol-based organosolv processes would lead to ether formation by (partial) α-alkylation in the isolated lignin, limiting the required initial dehydration step, and are therefore not suitable.[45] The use of 1,4-dioxane for lignin isolation has the added advantage that the lignin obtained is actually soluble in (wet) 1,4-dioxane, the main solvent for the tandem reaction. GPC analysis of the isolated lignin showed a weight-average molecular weight (M_w) of $3.0 \cdot 10^3$ Da (0.1 wt% AcOH in THF as eluent, polystyrene as calibration standard; Figure 3.7). Elemental analysis revealed a H/C ratio of 1.22 and an O/C ratio of 0.41 (O by difference), while no sulfur and minimal (0.02 wt%) nitrogen impurities were found. Analysis of the dioxosolv lignin using HSQC NMR (Figure 3.8) showed the lignin to have 39 β-O-4, 3 β-5 and 5 β-β linkages per 100 aromatic units. The S:G:H ratio was determined to be 2.1:1.0:0.0; in addition 16 per 100 aromatic units of *p*-hydroxybenzoate were observed, which is typical for poplar.[46] Interestingly, the
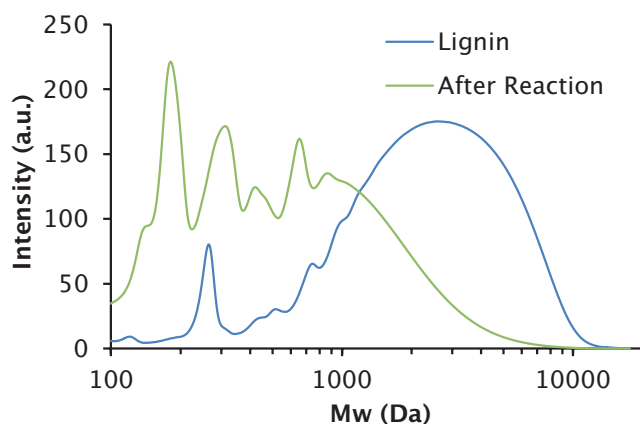

Figure 3.7: Molecular weight distribution of lignin before and after reaction, based on GPC data (reaction: 300 mg lignin, 0.060 mmol [Rh(cod)Cl]2, 0.240 mmol dppp, 0.120 mmol (ScOTf)3; 175 °C, 2 h, 22 mL 1,4-dioxane:water; GPC: 0.1% AcOH in THF eluent, polystyrene standards).

presence of Hibbert's ketone structures (Hk) was already noticed in the starting lignin: these structures were previously observed in various organosolv lignins.[47,48]

Depolymerisation of the isolated dioxosolv lignin was performed under similar conditions as the model compound experiments, with 300 mg lignin being used instead of

Figure 3.8: HSQC NMR spectra of poplar dioxasolv lignin before and the freeze-dried reaction mixture after reaction. After reaction both the signals for the β-O-4 and β-5 linkages have disappeared, demonstrating complete conversion of those ether fragments. Reaction conditions: 300 mg lignin, 0.060 mmol [Rh(cod)Cl]$_2$, 0.240 mmol dppp, 0.120 mmol (ScOTf)$_3$; 175 °C, 2 h, 22 mL 1,4-dioxane:water

2.4 mmol of model compound **1a**-**1d**. At 175 °C and equal molar amounts of rhodium and scandium triflate catalysts, a significant molecular weight reduction to 7.7 • 10^2 Da, was observed by GPC (Figure 3.7), with the GC and GC-MS chromatograms of the product mixture showing a very limited number of volatile products. The mixture was also analysed by GCxGC-MS (Figure 3.9) to check if the 1D GC methods accurately represent the complexity of the volatile fraction; this appeared to be the case. Generally, no char formation was observed (although a very small amount of dark precipitate would form upon standing of the reaction mixtures in air) and after reaction the reactor headspace contained ca. 0.5 bar of gas. Two of the major products were indeed the anticipated decarbonylation products, 4-methylguaiacol (**8a**) and 4-methylsyringol (**9a**), deriving from S and G units in the lignin, showing that the chemistry observed in the model compounds translates well to the actual lignin. Quite surprisingly, significant quantities of *iso*-eugenol (**8b**) and 4-(1-propenyl)syringol (**9b**) were also found, which presumably form analogously to the styrene derivatives mentioned above. Formation of such compounds have been observed previously in reactive organsolv pulping, although
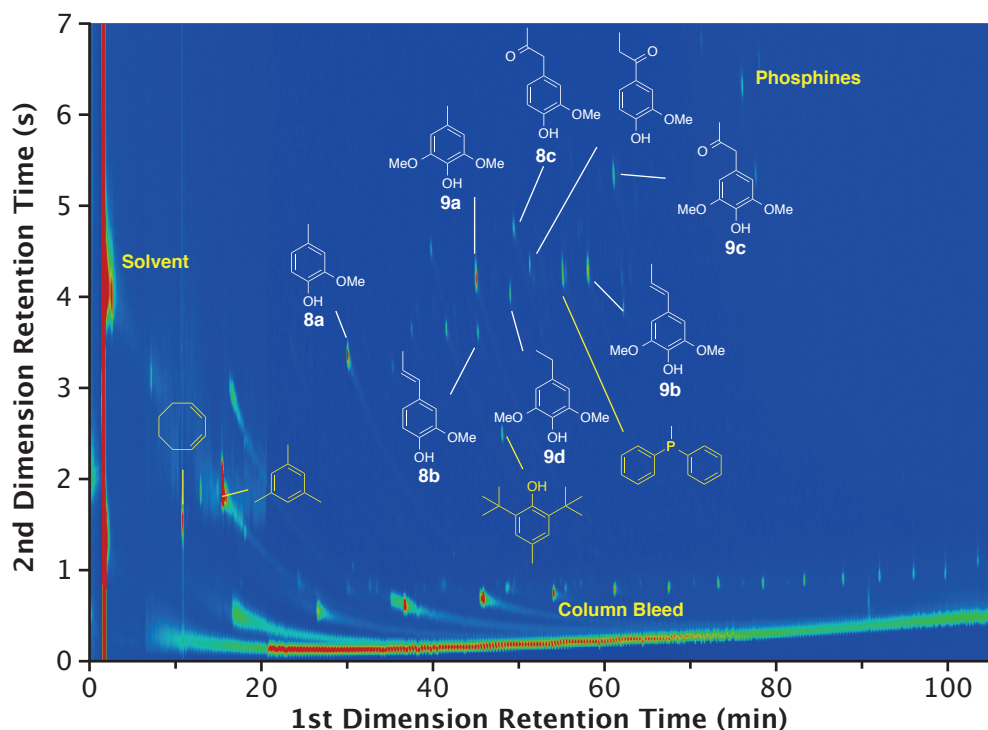
Figure 3.9: GCxGC-MS chromatogram of the volatile fraction after lignin depolymerisation. Lignin-derived products are indicated in white; non-lignin derived compounds in yellow and include 1,3-cyclooctadiene (from [Rh(cod)Cl]₂), BHT (stabiliser in 1,4-dioxane), mesitylene (internal standard) and phosphines deriving from the dppp ligand. Major peaks all correspond to peaks also seen and identified in the 1D GC(-MS) chromatograms.

they could not be obtained from isolated lignin.[49,50] Compounds identified in smaller amounts included 4-ethylguaiacol (**8d**), 4-ethylsyringol (**9d**), (4-guiacyl)acetone (**8c**) and (4-syringyl)acetone (**9c**) (Figure 3.10). A potential mechanism of formation for the latter two may involve the (transfer) hydrogenolysis of the terminal γ-hydroxyl of the original Hibbert's ketone. Combined, all identified monomers comprised 9.5 wt% or ca. 12 mol% of the original lignin intake. While this yield may initially seem somewhat limited, given the β-O-4 content of 39%, the actual maximum monomer yield is only 20 mol% (for a more expansive discussion of maximum monomer yields, see Chapter 2, Westwood *et al.*,[8] and Cantat *et al.*[12]). Thus, the amount of monomers listed accounts for 50% of the theoretical yield.

It is interesting to note that the monomeric products are comparatively richer in G (S:G ratio ca. 1.5:1) than the parent lignin. While this could reflect the increased reactivity of the guaiacyl units compared to the syringyl as was also observed in the model compounds **1a**-**1d**, extending the reaction time from 2 to 4 h did not afford more monomers. As the mass balance for the G-G model compound **1b** was slightly better than for the S-G model **1c** it is possible that the latter does undergo faster condensation reactions, leading to more higher-molecular weight products; indeed, slightly higher molecular weight product tails were also observed in the GPC after reaction of **1c**. Alternatively, it is possible that the S units are preferably tied up in more recalcitrant bond motifs, such as the β-β linkage. Analysis of the freeze-dried reaction mixture by HSQC NMR (Figure 3.8) revealed that the β-O-4 bonds present in the lignin were indeed successfully cleaved. Signals for the β-5 fragment also disappeared and the amount of β-β linkages was also significantly reduced, suggesting that at least the ether linkages in these fragments is susceptible to cleavage as well. Peaks corresponding to the epimerized β-β linkage were not observed.[51] As a control experiment, the depolymerisation of the lignin in the absence of the rhodium catalyst was attempted as well, however in this case no monomers were obtained and a large amount of dark precipitate had formed after the reaction. This further highlights the necessity of removal of the reactive carbonyl intermediates and the merit of the tandem catalytic conversion. In another control experiment with only the rhodium complex as catalyst, some monomer formation was observed (Table 3.2, #1). Possibly the rhodium complex itself is also able to act as a (weak) Lewis acid leading to some hydrolysis activity.[52]

3.2.3 Influence of the Lewis Acid

As quite a number of metal triflates can act as water-tolerant Lewis acids, Yb(OTf)$_3$, In(OTf)$_3$ and Ga(OTf)$_3$ were screened for activity in the coupled depolymerisation procedure as well. As it is not always certain if metal triflates act as true Lewis acids or as Brønsted acids after triflate hydrolysis, triflic acid (3 equivalents compared to the metal triflates) was also included. The GPC traces of the reaction mixture after
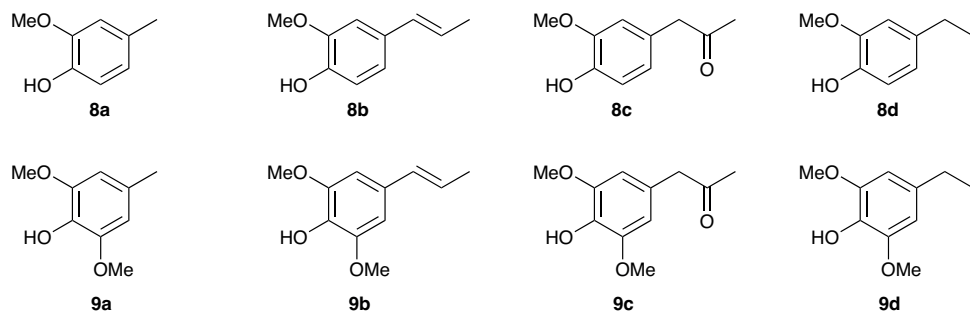
Figure 3.10: Major products obtained in the depolymerisation of poplar dioxosolv lignin.

Table 3.2: Results of the depolymerisation of lignin with differing (amounts of) Lewis acid and H_2O content[a]

	Acid (mmol)	H_2O (v%)	Monomer Yield (wt%)								
			8a	9a	8b	9b	8c	9c	8d	9d	Σ[b]
1	-	-	0.1	0.1	0.3	1.1	0.0	0.0	0.0	0.1	2.6
2	HOTf (0.360)	10	1.3	1.2	1.2	4.6	0.3	0.8	0.1	0.5	10.6
3	Yb(OTf)₃ (0.120)	10	1.7	1.5	1.0	4.6	0.4	0.9	0.1	0.6	11.4
4	Sc(OTf)₃ (0.120)	10	2.1	2.1	0.4	2.3	0.6	1.2	0.1	0.4	9.5
5	In(OTf)₃ (0.120)	10	2.6	2.4	0.2	0.4	1.0	1.7	0.1	0.9	9.7
6	Ga(OTf)₃ (0.120)	10	2.4	2.7	0.1	0.2	1.2	2.1	0.1	0.2	9.4
7	Sc(OTf)₃ (0.240)	10	2.0	2.2	0.1	0.7	0.7	1.5	0.1	0.3	7.9
8	Sc(OTf)₃ (0.060)	10	1.1	1.1	1.4	5.9	0.2	0.6	0.1	0.6	11.8
9	Sc(OTf)₃ (0.030)	10	0.6	0.6	1.9	7.1	0.0	0.4	0.1	0.4	12.1
10	Yb(OTf)₃ (0.030)	10	0.4	0.5	1.9	6.7	0.0	0.4	0.1	0.5	11.2
11	Yb(OTf)₃[c] (0.030)	10	0.6	0.6	2.0	7.2	0.0	0.4	0.2	0.7	12.4
12	Sc(OTf)₃ (0.120)	0	1.4	1.8	0.1	0.2	0.2	0.7	0.1	0.2	5.1
13	Sc(OTf)₃ (0.120)	5	1.9	2.1	0.5	2.6	0.4	0.9	0.1	0.4	9.1
14	Sc(OTf)₃ (0.120)	20	1.5	1.3	0.6	2.9	0.6	1.1	0.1	0.3	8.7

[a] Conditions: 300 mg lignin, 0.060 mmol [Rh(cod)Cl]₂, 0.240 mmol dppp, acid; 175 °C, 2 h, 22 mL 1,4-dioxane:water; yields determined by GC-FID [b] Sum of all identified monomers [c] 4 h reaction

depolymerisation did not prove very informative and under all conditions seem to converge to a similar weight distribution (Figure 3.11). On the other hand, comparison of the monomer yield (Table 3.2, #2-6) did reveal some interesting trends. Yb(OTf)₃ gave a relatively low amount of decarbonylation products (**8a**, **9a**), but a relatively large amount of 4-(1-propenyl)phenols (**8b**, **9b**) was found instead, with a high total amount of monomers. Conversely, with In(OTf)₃ or Ga(OTf)₃, the selectivity was found to be exactly opposite, whilst the amount of monomers was also somewhat reduced. If the
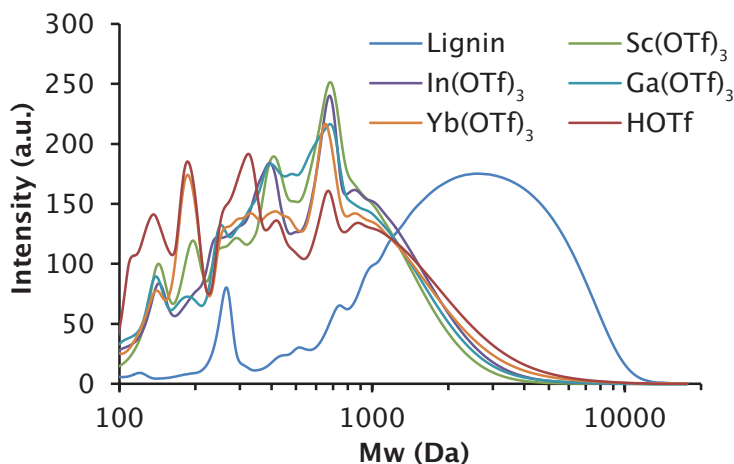
Figure 3.11: Molecular weight distributions from GPC data of reaction mixtures after depolymerisation with different acids.

acid strengths of the different metal triflates as measured by their hydrolysis constants (pK_h)[52] are considered, it is clear that the use of stronger acids leads to an overall increase in products derived from decarbonylation, whereas the weaker acids favor formation of the 4-(1-propenyl)phenols (Figure 3.12a). Triflic acid on the other hand showed an even greater preference for the formation of 4-(1-propenyl)phenols. If the reactivity of the metal triflates were solely based on their ability to generate Brønsted acids (i.e. by hydrolysis of the metal triflate bond), the triflic acid would be expected to act similar to the stronger Lewis acids instead. It is thus clear that the Lewis acids do not simply act as precursors for the Brønsted acids.

Likewise, variation of the amount of Lewis acid also significantly influences the outcome of the reaction (Table 2, #4,7-9). With larger amounts of Sc(OTf)$_3$, the relative yield of decarbonylation products was highest, while with lower Sc(OTf)$_3$ concentrations the 4-(1-propenyl)phenols were again formed as major product (Figure 3.12b). This is in line with the model compound studies and supports the notion that for both lignin and the model compounds the formation of the decarbonylation products proceeds through an identical mechanism: dehydration of the α-hydroxyl followed by styryl ether hydrolysis affords the aldehyde that is finally decarbonylated. The increase in decarbonylation products with more Lewis acid or a stronger one is then the result of faster styryl ether hydrolysis, as was also observed for the model compounds. On the other hand, with a weak acid the competitive (reductive) mechanism that leads to formation of the 4-(1-propenyl)phenols is apparently more favoured. In addition, this is in agreement with the model compound data where styrene derivatives were only observed with low amounts of scandium triflate. The selectivity differences between the
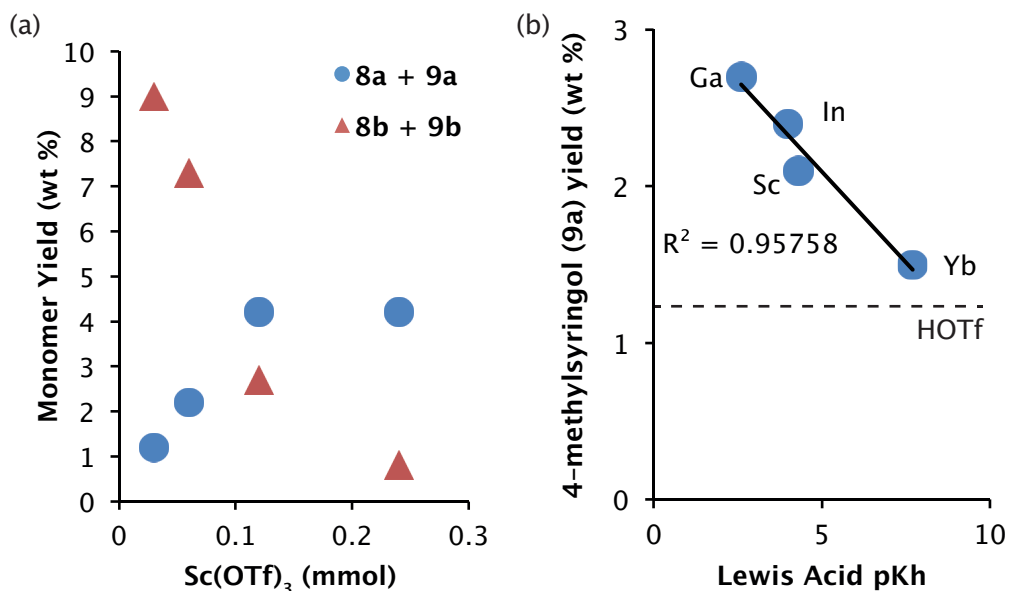
Figure 3.12: (a) Monomer yields for the 4-methylphenol decarbonylation products (**8a** + **9a**) or 4-(1-propenyl)phenols (**8b** + **9b**) as a function of the amount of scandium triflate employed, demonstrating the ability to tune product distribution by the amount of acid. (b) Correlation between the strength of the Lewis acid (as measured by the hydrolysis constant)[52] and the yield of 4-methylsyringol (**9a**).

guaiacyl and syringyl-derived products are also in agreement with what was observed in the model compounds: the former tend to form more decarbonylation products more rapidly, while the latter form more 4-(1-propenyl)phenols.

Variation of Lewis acid strength and amount thus allows control over product composition. Indeed, maximum yields of decarbonylation products (5.1 wt%) are obtained with the strongest Lewis acid gallium triflate. On the other hand, using only 0.030 mmol of scandium triflate the 4-(1-propenyl)phenol yield is the highest, with *iso*-eugenol (**8b**) and 4-(1-propenyl)syringol (**9b**) being obtained instead in an overall yield of 9.0 wt%. As weaker acids also give better selectivity towards to the latter products, use of a lower amount of ytterbium triflate (Table 3.2, #10) indeed affords a good yield of 4-(1-propenyl)phenols (**8b**, **9b**, total yield 8.6 wt%). However, since this is lower than obtained for scandium triflate, the strength and amount of acid may not be sufficient to push the reaction to completion under these mild conditions; indeed upon extending the reaction time to 4 h (#11) yields increased somewhat further, leading to both the highest yield of 4-(1-propenyl)phenols (9.2 wt%) as well as the highest overall monomer yield (12.4 wt%).

The influence of the amount of water added on the reaction was also assessed (Table 3.2, #12-14). Without added water the monomer yield decreased significantly and a large amount of dark precipitate was formed. Addition of just 5 vol% water significantly reduced the formation of precipitate as well as increased the monomer yield, which reaches a maximum at 10 vol% (standard conditions). While scandium triflate can act as a Lewis acid in water, this does not mean that water does not coordinate and does not inhibit Lewis acidity; added water is therefore expected to decrease the activity of the acid-catalysed steps. Nevertheless, increased monomer yields are observed as the added water also inhibits the acid-catalysed aldol condensation, which otherwise leads to the formation of higher molecular weight products (and precipitate). The rhodium-catalysed processes, unaffected by the water content, are then comparatively faster and can effectively scavenge the reactive aldehydes towards stable monomers.

3.2.4 Influence of Temperature and Catalyst Amount

To test for the optimal reaction conditions, both the temperature and catalyst amount were also varied (Table 3.3). Not surprisingly, decreasing the amount of catalyst resulted in lower overall monomer yields; analogously, the GPC traces of the reaction mixture also tended towards higher molecular weight products. Higher loadings than the standard 0.120 mmol did not increase the monomer yield, suggesting all cleavable bonds are already broken during the reaction at that loading; this is in agreement with the fact that no beneficial effect of increasing the reaction time was seen either. Elevating the temperature to 200 °C did result in a modest increase in monomer yield.

Table 3.3: Results of the depolymerization of lignin at varying temperatures and varying amount of catalyst.[a]

	T (° C)	Catalyst[b] (mmol)	Monomer Yield (wt%)								
			8a	9a	8b	9b	8c	9c	8d	9d	Σ[c]
1	175	0.030	1.4	1.3	0.1	0.5	0.2	0.6	0.1	0.2	4.4
2	175	0.060	2.2	2.0	0.3	0.9	0.6	1.4	0.1	0.3	7.9
3	175	0.120	2.1	2.1	0.4	2.3	0.6	1.2	0.1	0.4	9.5
4	175	0.240	2.2	2.1	0.3	1.7	0.5	1.2	0.1	0.5	8.8
5	150	0.030	0.2	0.2	0.0	0.4	0.0	0.3	0.0	0.0	1.0
6	188	0.030	1.6	1.6	0.1	0.5	0.2	0.7	0.0	0.2	4.9
7	200	0.030	1.7	1.8	0.1	0.4	0.2	0.8	0.1	0.3	5.5
8	150	0.120	0.9	1.0	0.4	2.1	0.0	0.5	0.0	0.0	5.5
9	200	0.120	2.2	2.3	0.5	2.6	0.7	1.3	0.1	0.5	10.6

[a] Conditions: 300 mg lignin; T, 2 h, 22 mL 1,4-dioxane:water; yields determined by GC-FID [b] Catalyst amount (0.5 eq [Rh(cod)Cl]2, 2.0 eq dppp, 1.0 eq Sc(OTf)3) [c] Sum of all identified monomers

3.2.5 Depolymerisation of Other Lignins

To demonstrate the general applicability of our tandem approach, reactions were performed as well on lignins isolated using the same dioxasolv procedure from spent brewer's grain and from pine sawdust, which are representative for grasses and softwoods, respectively. HSQC NMR analysis of the spent brewer's grain lignin revealed that it contained all three aromatic building blocks with an S:G:H ratio of 0.5:1.0:0.1 as well as *p*-coumarate, ferulate and tricin units, which are also common in grasses.[46,53] The β-O-4 content was determined to be 42 per 100 aromatic units, very similar to the poplar lignin. GPC analysis was also attempted, however, unlike with the poplar lignin, some material remained insoluble in the THF eluent, invalidating the analysis. In contrast with reactions performed with the poplar lignin, some dark precipitate did form in reactions with the spent brewer's grain lignin; the amount of monomers formed was also lower compared to poplar lignin. The distribution of products furthermore shifted (Table 3.4, #1); in accordance with the higher G content of the spent brewer's grain, a relatively larger amount of guaiacyl-substituted products were observed.

Analysis of the pine lignin revealed it to consist exclusively of G units, with 29 β-O-4, 12 β-5 and 4 β-β linkages per 100 aromatic units. Correspondingly, after reaction only guaiacyl-derived products are observed, further decreasing the complexity of the product mixture. The total monomer yield is lower than observed for the poplar lignin, which may be partially attributed to its lower β-O-4 content. On the other hand, at 5.1 wt% of 4-methylguaiacol (**8a**) the highest single product yield for a decarbonylation product is observed with this lignin. Consequently, the products of the lignin depolymerisation can be tuned in two dimensions (Figure 3.13): by selection of a biomass source with an appropriate S:G ratio and the appropriate (amount of) Lewis acid catalyst, any of the four major products can be specifically targeted.

As discussed in Chapter 2, reactive lignin upgrading directly on the biomass is an emerging field with considerable potential, as this avoids the cleavage of β-O-4 ethers and subsequent recondensation during the isolation, leading to a more recalcitrant lignin.[54] Given the quadratic relation between β-O-4 content and the potential yield of monomeric products, this allows high yields of small aromatics to be obtained.[55,56] The system described here seems ideally suited for such an approach, as the homogeneous nature of the catalysts enables good access to the insoluble biomass matrix; additionally if any reactive aldehydes are formed during such a 'pulping' step, these can be effectively removed by the rhodium catalyst, minimising the recondensation reactions that otherwise occur during lignin isolation. Reactions were therefore performed directly on the poplar sawdust, which was determined to have a Klason lignin content of 22.6%. To

Table 3.4: Results of the depolymerization of different lignins.[a]

Lignin	Monomer Yield (wt%)								
	8a	9a	8b	9b	8c	9c	8d	9d	Σ[b]
1 Spent Brewer's Grain	1.7	0.7	0.4	0.8	0.2	0.2	0.2	0.1	5.2
2 Pine	5.1	0.0	0.6	0.0	0.7	0.0	0.2	0.0	6.8
3 Poplar Sawdust	2.1	1.4	0.7	2.9	0.3	0.6	0.4	1.0	9.8
4 Poplar Sawdust[c]	2.4	1.6	0.3	1.4	0.0	0.6	0.2	0.6	7.1
5 Poplar Sawdust[d]	0.0	0.1	1.6	3.0	0.0	0.0	0.6	1.1	7.6

[a] Conditions: 300 mg lignin, 0.060 mmol [Rh(cod)Cl]$_2$, 0.240 mmol dppp, 0.120 mmol Sc(OTf)$_3$; 175 °C, 2 h, 22 mL 1,4-dioxane:water; yields determined by GC-FID [b] Sum of all identified monomers [c] Ga(OTf)$_3$ [d] 0.030 mmol Yb(OTf)$_3$, 4 h reaction

obtain a powder that disperses well in the 1,4-dioxane:water solvent, a mild ball milling pretreatment was employed, which generates a fine powder with high surface area without disrupting the lignin structure.[57]

Gratifyingly, under 'standard' conditions (i.e. 0.120 mmol rhodium complex, 0.120 scandium triflate, 175 °C, 2 h reaction time) and 2.0 g sawdust, lignin depolymerization products identical to those from the isolated lignins were also obtained. Some products derived from the sugar fraction, notably furfural and hydroxymethylfurfural were identified as well. Comparing the amount of monomers obtained from the whole biomass, the yield (accounting for the lignin content of the biomass) is comparable to what is observed for the isolated lignin (Table 3.4, #3-5). This is rather surprising, as part of the available β-O-4 are already expected to break and potentially condense into carbon-carbon bonds during the dioxosolv isolation procedure. The higher amount of β-O-4 fragments in the unprocessed biomass would be expected to translate to a larger amount of liberated monomers. One potential explanation for the similar monomer yield might be that smaller aromatic fragments also undergo condensation reactions with the liberated sugar (oligomers). Likewise, reducing sugars may act as an inhibitory competitive substrate for the decarbonylation reaction. As with the isolated lignin, changing the Lewis acid co-catalyst also allows tuning the obtained product distribution (Table 3.4, #3-5): using gallium triflate predominantly the decarbonylation products 4-methylguaiacol (**8a**) and 4-methylsyringol (**9a**) are observed; whereas with ytterbium triflate a larger amount of the 4-(1-propenyl)phenols are formed. In both cases the monomer yield is lower than observed for the isolated lignin, however. It is therefore clear that the interplay between the sugar fraction and the lignin during the reaction do have a pronounced effect on the eventual outcome.

3.3 Conclusions

In conclusion, the efficient tandem catalysis approach for cleavage of the β-O-4 fragments in lignin models and (isolated) lignins has been demonstrated, using a Lewis acidic metal triflate combined with a rhodium complex. Monomer yields in acid-catalysed lignin depolymerisation are typically limited by recondensation reactions of the liberated monomeric products, particularly aldehydes. The tandem catalytic approach serves to address this issue. The water-stable Lewis acid first catalyses the hydrolysis of β-O-4 aryl alkyl ethers, after which the liberated aldehydes are decarbonylated *in-situ* by the second, rhodium-based catalyst. Model compounds for the β-O-4 aryl alkyl ether not only allowed for the validation of this approach, but also provided mechanistic insight and proved instrumental to optimizing the interplay between the two coupled steps. Indeed, the anticipated decarbonylation products could be obtained in good yields when the speed of both reactions was appropriately matched. The overall mechanism was shown to go through the dehydration of the α-hydroxyl moiety, leading to a styryl ether. Metal triflate-catalysed styryl ether hydrolysis then leads to the formation of an aldehyde, which is readily decarbonylated by the rhodium complex.

The applicability of the tandem catalytic approach on a real lignin was subsequently demonstrated with lignin isolated from poplar using a mild dioxasolv procedure. In line with the results obtained in the model compound studies, the decarbonylation products 4-methylguaiacol (**8a**) and 4-methylsyringol (**9a**) were indeed formed from the lignin. Rather surprisingly, significant quantities of *iso*-eugenol (**8b**) and 4-(1-propenyl)syringol (**9b**) were found as well; these remarkable products presumably are formed *via* an alternative pathway, which must involve a formal hydrogenolysis of the ether bond. The selectivity towards either product family was shown to be strongly dependent on the amount and strength of the Lewis acid catalyst employed: the use of a stronger Lewis acid steered the reaction to afford primarily decarbonylation products, whereas a smaller amount of Lewis acid or a weaker one allows access to the 4-(1-propenyl)phenol products. The general applicability of the tandem procedure was also demonstrated on spent brewer's grain and pine lignin, which are representative for grasses and softwoods, respectively. By using a lignin with an appropriate S:G ratio and selection of the right Lewis acid, each of the four major products can then be specifically targeted. Finally, direct application of the tandem procedure to poplar sawdust also shows that separate isolation of the lignin is not required and reactions may be carried out directly on the biomass.

Thus, trapping of reactive intermediates in catalytic lignin depolymerisation is shown to be a very versatile approach and, in this particular case, also allows for a tuneable selectivity to each potential monomeric product. At the same time, a number of poignant questions remain. The cleavage of the β-O-4 aryl alkyl ethers to afford 4-(1-propenyl)
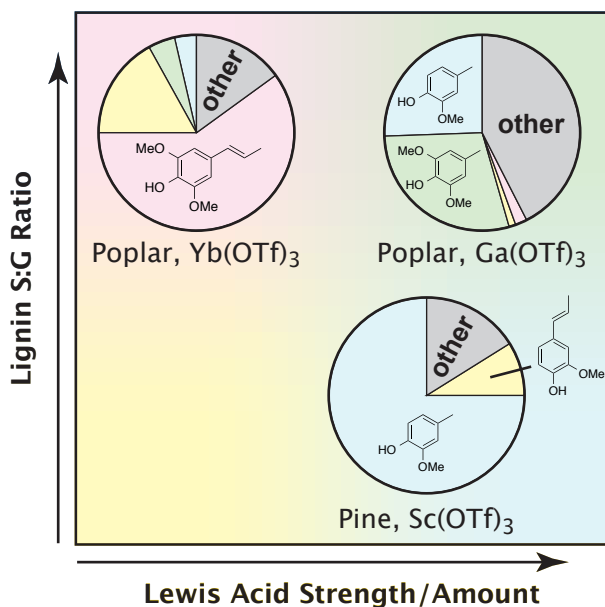
Figure 3.13: Product distributions for three protypical catalyst/lignin combinations demonstrating the ability to tune the product distribution of lignin depolymerisation. Use of lignin with an appropriate S:G ratio affords either S or G (**9** or **8**) products, whereas the choice of Lewis acid adjusts the selectivity between methylphenols (**a**) or 1-propenylphenols (**b**).

phenol is remarkable and requires further mechanistic study. Specifically, an important question is whether this reaction also proceeds through the styryl ether intermediate, as its hydrogenolytic cleavage would be a very useful, if unprecedented reaction. In addition, given the high content of β-O-4 aryl alkyl ethers available when the depolymerisation is carried out directly in the biomass, the yield of monomeric aromatics can likely be further improved. For this, it is important to assess how the carbohydrate matrix affects the tandem procedure and such insights will undoubtedly lead to further steps in the control of lignin depolymerisation with the new method.

3.4 Acknowledgements

3.5 Experimental

Materials. 1,4-dioxane (99+%, a.c.s. grade, Alfa Aesar), chloro(1,5-cyclooctadiene)rhodium(I) dimer (98%, ABCR), 1,3-bis(diphenylphosphino)propane (98%, ABCR), scandium(III) triflate (95%, Acros), indium(III) triflate (99%, ABCR), gallium(III) triflate (98%, ABCR) and ytterbium(III) triflate (98%, ABCR) were all used as received. Lignin model compounds 2-phenoxy-1-phenylethan-1-ol (**1a**),[10] 1-(3,4-dimethoxyphenyl)-2-(2-methoxyphenoxy)ethan-1-ol[10] (**1b**) and 1-(3,4-dimethoxyphenyl)-2-(2-methoxyphenoxy)propane-1,3-diol (**1d,** obtained as a 5:1 mixture of *erythro:threo*) were synthesised according to previously published procedure. Dioxasolv lignin was isolated from poplar sawdust (sieved through a 1 mm grid) according to a previously published procedure, affording 9 wt% of lignin.[8] Poplar sawdust used in reactions was Soxhlet extracted overnight, dried under vacuum, and ball-milled for 25 days at 60 rpm to afford a very fine powder.[57]

Physical Measurements. GC measurements were performed on a Varian GC equipped with a VF-5 ms capillary column and an FID detector. Mesitylene was used an internal standard; response factors were determined for all products for which reference materials were available, for other compounds these were extrapolated by number of carbon atoms from structurally similar compounds. GC-MS measurements were performed on a Shimadzu GC-2010 using a VF5-ms column, coupled to a Shimadzu GCMS-QP2010 mass spectrometer. 2D GC×GC-MS (1st column: VF-5ms 30 m, 0.25 mm ID, df 0.25 µm; 2nd column: VF-17ms, 1 m, 0.15 mm ID, df 0.15 µm) was performed in a GC-MS2010 Ultra (Shimadzu) equipped with a ZX1 thermal modulation system (Zoex). The temperature program started with an isothermal step at 40°C for 5 min. Next, the temperature was increased to 280°C by 2.5°C min^{-1}. The program finished with an isothermal step at 280°C for 5 min. The modulation applied for the comprehensive GC×GC analysis was a hot jet pulse (375 ms) every 7000 ms. The 2D chromatograms were processed with GC Image software (Zoex). GPC measurements were performed on a Polymer Labs GPC 50 system, equipped with a series of three PLGel Mixed-E columns and guard a guard column and using THF spiked with 0.1 vol% acetic acid as mobile phase. Detection was done with an external Knauer UV detector at 280 nm and molecular weight determinations were based on calibration with polystyrene standards.

NMR Measurements. NMR spectra were recorded on a Varian spectrometer operating at 400 MHz (^{1}H) or 100 MHz (^{13}C) in DMSO-d6 (unless mentioned otherwise) and referenced against the signal of the residual protio impurity of the solvent (^{1}H 2.50 ppm, ^{13}C 39.52 ppm). HSQC spectra were recorded on a Bruker Avance II 600 MHz spectrometer equipped with a 5 mm CPTCI ^{1}H-^{13}C/^{15}N/^{2}H cryogenic probe with z-gradients at 25 °C using the Q-CAHSQC pulse program.[58] Matrices of 2048 data points for the ^{1}H-dimension and 128 data points for the ^{13}C-dimension were collected with a relaxation delay of 6 s and spectral widths from 13 to -1 ppm and from 160 to 0 ppm for the ^{1}H and ^{13}C dimensions, respectively. The lignins and lignin products were dissolved in DMSO-d6 after overnight stirring (200 mg/750 µL) and chemical shifts were referenced to the solvent signal (2.50/39.5 ppm). The spectra were processed and analysed using MestReNova software. Prior to Fourier transformation, FIDs were apodised with a π/2 sine square bell function in both dimensions and zero-filled up to 512 points in the ^{13}C-dimension and 4096 points in the ^{1}H-dimension. A semi-quantitative analysis of the HSQC spectra was performed by integration of correlations peaks in the different regions of the spectra with MestReNova. The relative quantity of side chains involved in the interunit and terminal substructures was expressed

as a number per 100 aromatic units (S+G). In the aliphatic oxygenated region, interunit linkages were estimated from Cα–Hα correlations.

Catalytic Experiments. In a typical experiment, a 40 mL stainless steel Parr autoclave was charged with model compound (2.40 mmol), lignin (300 mg) or poplar sawdust (2.0 g), chloro(1,5-cyclooctadiene)rhodium(I) dimer (29.0 mg, 0.060 mmol), 1,3-bis(diphenylphosphino)propane (99.0 mg, 0.120 mmol), scandium(III) triflate (59.1 mg, 0.120 mmol) and 22 mL 9:1 1,4-dioxane:water mixture. After sealing, the autoclave was flushed three times with 50 bar argon and after release of pressure heated to the reaction temperature. After reacting for 2 hours, the heating mantle was removed and the reactor rapidly cooled with an ice-water bath. From the resulting solution was taken a 200 μL sample, which was concentrated *in vacuo* and redissolved in the GPC mobile phase for GPC analysis. To the remainder was added mesitylene and a 0.5 mL sample was passed over 0.5 g of silica gel padded with 0.2 g of magnesium sulphate to remove water and the inorganic compounds; organics were subsequently eluted with 3 mL ethyl acetate and analysed by GC and GC-MS. In so far possible, quantification was performed against authentic standards; if not response factors were determined by interpolating from known compounds.

2-bromo-3',4',5'-trimethoxyacetophenone. To 120 mL of ethyl acetate is added 40.3 g (180 mmol) of finely ground copper(II) bromide and brought to reflux. 3',4',5'-trimethoxyacetophenone (18.9 g, 90 mmol) was dissolved in 120 mL chloroform and added to the refluxing dark green copper(II) bromide suspension. After refluxing for 4 hours the suspension had turned brownish and HBr evolution ceased; the suspension was allowed to cool to room temperature and the solids removed by filtration. The filtrate was concentrated *in vacuo* to afford 22.8 g of brown oil that solidifies upon standing. The crude material was used directly in the subsequent step without further purification. ^{1}H NMR (CDCl$_3$): δ 7.24 (s, 2H), 4.41 (s, 2H), 3.92 (s, 9H).

2-(2-methoxyphenoxy)-1-(3,4,5-trimethoxyphenyl)ethan-1-one. The crude material from the previous step was dissolved in 250 mL acetone, to which was added 9.31 g (75 mmol) guaiacol and 11.3 g (81.8 mmol) potassium carbonate. The mixture was refluxed for 3 hours and after cooling to room temperature the solids were removed by filtration. Concentration of the filtrate afforded a yellow-brown solid, which was subjected to recrystallization from 5:1 ethanol:toluene, affording the title compound as 12.5 g (37.6 mmol, 42%) of yellow crystals. Analytical data was in agreement with literature. ^{1}H NMR (CDCl$_3$) δ 7.33 (s, 2H), 6.97 (dt, J = 8.6, 4.2 Hz, 1H), 6.91 (dt, J = 8.1, 1.0 Hz, 1H), 6.86 (dd, J = 4.6 Hz, 1.1 Hz, 2H), 5.26 (s, 2H), 3.92 (s, 3H), 3.90 (s, 6H), 3.87 (s, 3H). ^{13}C NMR (CDCl$_3$) δ 193.91, 153.27, 149.82, 147.50, 143.27, 129.89, 122.62, 120.96, 114.82, 112.24, 106.01, 72.54, 61.07, 56.41, 55.95.

2-(2-methoxyphenoxy)-1-(3,4,5-trimethoxyphenyl)ethan-1-ol. 2-(2-methoxyphenoxy)-1-(3,4,5-trimethoxyphenyl)ethan-1-one (11.4 g, 34.3 mmol) was added to a mixture of 250 mL tetrahydrofuran, 75 mL methanol and 75 mL methanol and gently heated to ca. 50 °C until all material had dissolved. Sodium borohydride (2.64 g, 96.8 mmol) was carefully added in small portions with vigorous gas evolution. After addition of all sodium borohydride, the mixture was stirred for another 2 hours and then quenched with 250 mL of saturated ammonium chloride solution. The organic layer was separated and the aqueous layer extracted three times with 100 mL ethyl acetate. The combined organic layers were washed with brine, dried with magnesium sulphate and concentrated *in vacuo* to afford 13.3 g of pale yellow oil. The compound was purified by silica gel column chromatography with a 1:1 ethyl acetate:hexanes mixture (Rf ~ 0.45) as eluent, to afford 9.00 g (27.0 mmol, 79%) of a colourless viscous oil, which

eventually crystallised as white needles. ^{1}H NMR (CDCl$_3$) δ 7.04 – 6.87 (m, 4H), 6.66 (s, 2H), 5.03 (dd, J = 9.2, 3.0 Hz, 1H), 4.18 (dd, J = 10.0, 3.0 Hz, 1H), 3.97 (dd, J = 10.0, 9.2 Hz, 1H), 3.89 (s, 3H), 3.87 (s, 6H), 3.84 (s, 3H). ^{13}C NMR (CDCl$_3$): δ 153.47, 150.27, 148.08, 137.72, 135.38, 122.78, 121.24, 116.28, 112.13, 103.34, 76.55, 72.59, 60.96, 56.26, 55.97; Elemental analysis calculated for C$_{18}$H$_{22}$O$_6$: C 64.66; H 6.63; found C 64.54 H 6.63.

3.6 References

1. Y. H. P. Zhang, *J. Ind. Microbiol. Biotechnol.*, 2008, **35**, 367–375.
2. A. J. Ragauskas, G. T. Beckham, M. J. Biddy, R. Chandra, F. Chen, M. F. Davis, B. H. Davison, R. A. Dixon, P. Gilna, M. Keller, P. Langan, A. K. Naskar, J. N. Saddler, T. J. Tschaplinski, G. A. Tuskan, and C. E. Wyman, *Science*, 2014, **344**, 1246843–1246843.
3. J. Zakzeski, P. C. A. Bruijnincx, A. L. Jongerius, and B. M. Weckhuysen, *Chem. Rev.*, 2010, **110**, 3552–3599.
4. F. S. Chakar and A. J. Ragauskas, *Ind. Crops Prod.*, 2004, **20**, 131–141.
5. J. Ralph, K. Lundquist, G. Brunow, F. Lu, H. Kim, P. F. Schatz, J. M. Marita, R. D. Hatfield, S. A. Ralph, J. H. Christensen, and W. Boerjan, *Phytochem. Rev*, 2004, **3**, 29–60.
6. P. J. Deuss and K. Barta, *Coord. Chem. Rev.*, 2016, **316**, 510-532.
7. S. K. Hanson and R. T. Baker, *Acc. Chem. Res.*, 2015, **48**, 2037–2048.
8. C. S. Lancefield, O. S. Ojo, F. Tran, and N. J. Westwood, *Angew. Chem. Int. Ed.*, 2015, **54**, 258–262.
9. A. Rahimi, A. Ulbrich, J. J. Coon, and S. S. Stahl, *Nature*, 2014, **515**, 249–252.
10. J. M. Nichols, L. M. Bishop, R. G. Bergman, and J. A. Ellman, *J. Am. Chem. Soc.*, 2010, **132**, 12554–12555.
11. S. Son and F. D. Toste, *Angew. Chem. Int. Ed.*, 2010, **49**, 3791–3794.
12. E. Feghali, G. Carrot, P. Thuéry, C. Genre, and T. Cantat, *Energy Environ. Sci.*, 2015, **8**, 2734–2743.
13. E. Feghali and T. Cantat, *Chem. Commun.*, 2014, **50**, 862–865.
14. J. Zakzeski, A. L. Jongerius, P. C. A. Bruijnincx, and B. M. Weckhuysen, *ChemSusChem*, 2012, **5**, 1602–1609.
15. Q. Song, F. Wang, and J. Xu, *Chem. Commun.*, 2012, **48**, 7019–7021.
16. R. Ma, W. Hao, X. Ma, Y. Tian, and Y. Li, *Angew. Chem. Int. Ed.*, 2014, **53**, 7310–7315.
17. K. Barta, T. D. Matson, M. L. Fettig, S. L. Scott, A. V. Iretskii, and P. C. Ford, *Green Chem.*, 2010, **12**, 1640–1647.
18. X. Huang, T. I. Korányi, M. D. Boot, and E. J. M. Hensen, *ChemSusChem*, 2014, **7**, 2276–2288.
19. E. Adler, *Wood Sci. Technol.*, 1977, **11**, 169–218.
20. V. M. Roberts, V. Stein, T. Reiner, A. Lemonidou, X. Li, and J. A. Lercher, *Chem. Eur. J.*, 2011, **17**, 5939–5948.
21. T. Yokoyama, *J. Wood Chem. Technol.*, 2014, **35**, 27–42.
22. L. H. Hoo, K. V. Sarkanen, and C. D. Anderson, *J. Wood Chem. Technol.*, 1983, **3**, 223–243.
23. T. Imai, T. Yokoyama, and Y. Matsumoto, *J Wood Sci.*, 2011, **57**, 219–225.
24. M. Kulka and H. Hibbert, *J. Am. Chem. Soc.*, 1943, **65**, 1180–1185.
25. P. J. Deuss, M. Scott, F. Tran, N. J. Westwood, J. G. de Vries, and K. Barta, *J. Am. Chem. Soc.*, 2015, **137**, 7456–7467.
26. J. Tsuji and K. Ohno, *Tetrahedron Lett.*, 1965, **6**, 3969–3971.
27. M. Kreis, A. Palmelund, L. Bunch, and R. Madsen, *Adv. Synth. Catal.*, 2006, **348**, 2148–2154.
28. E. P. K. Olsen and R. Madsen, *Chem. Eur. J*, 2012, **18**, 16023–16029.
29. G. K. S. Prakash, T. Mathew, and G. A. Olah, *Acc. Chem. Res.*, 2011, **45**, 565–577.
30. S. Kobayashi, *Eur. J. Org. Chem.*, 1999, **1999**, 15–27.
31. R. Ghosh, *J. Mol. Cat. A: Chem.*, 2007, **264**, 1–8.

32. S. Kobayashi, *Synlett*, 1993, **1994**, 689–701.

33. A. C. Atesin, N. A. Ray, P. C. Stair, and T. J. Marks, *J. Am. Chem. Soc.*, 2012, **134**, 14682–14685.

34. L. Yang, Y. Li, and P. E. Savage, *Ind. Eng. Chem. Res.*, 2014, **53**, 2633–2639.

35. S. Constant, C. Basset, C. Dumas, F. Di Renzo, M. Robitzer, A. Barakat, and F. Quignard, *Ind. Crops. Prod.*, 2015, **65**, 180–189.

36. A. M. D. Rocha Gonsalves, J. C. Bayón, M. M. Pereira, M. E. S. Serra, and J. P. R. Pereira, *J. Organomet. Chem.*, 1998, **553**, 199–204.

37. F. Hutschka, A. Dedieu, M. Eichberger, R. Fornika, and W. Leitner, *J. Am. Chem. Soc.*, 1997, **119**, 4432–4443.

38. O. Pàmies and J.-E. Bäckvall, *Chem. Eur. J.*, 2001, **7**, 5052–5058.

39. S. Kobayashi, I. Hachiya, H. Ishitani, and M. Araki, *Synlett*, 1993, **1993**, 472–474.

40. Shunpei Ishikawa, Tomoaki Hamada, and S. Kobayashi, *J. Am. Chem. Soc.*, 2004, **126**, 12236–12237.

41. G. Brunow and K. Lundquist, *Acta Chem. Scand.*, 1984, **B38**, 323–325.

42. S. Dabral, J. Mottweiler, T. Rinesch, and C. Bolm, *Green Chem.*, 2015, **17**, 4908–4912.

43. R. G. Harms, I. I. E. Markovits, M. Drees, M. Cokoja, and F. E. Kühn, *ChemSusChem*, 2014, **7**, 429–434.

44. P. Fristrup, M. Kreis, A. Palmelund, P.-O. Norrby, and R. Madsen, *J. Am. Chem. Soc.*, 2008, **130**, 5206–5215.

45. J. M. W. Chan, S. Bauer, H. Sorek, S. Sreekumar, K. Wang, and F. D. Toste, *ACS Catal.*, 2013, **3**, 1369–1377.

46. H. Kim and J. Ralph, *Org. Biomol. Chem.*, 2010, **8**, 576–591.

47. C. S. Lancefield, and N. J. Westwood, *Green Chem*, 2015, **17**, 4980–4990.

48. S. Constant, H. L. J. Wienk, A. E. Frissen, P. de Peinder, R. Boelens, D. S. van Es, R. J. H. Grisel, B. M. Weckhuysen, W. J. J. Huijgen, R. J. A. Gosselink, and P. C. A. Bruijnincx, *Green Chem, accepted for publication*.

49. M. V. Galkin and J. S. M. Samec, *ChemSusChem*, 2014, **7**, 2154–2158.

50. M. V. Galkin, S. Sawadjoon, V. Rohde, M. Dawange, and J. S. M. Samec, *ChemCatChem*, 2014, **6**, 179–184.

51. F. Tran, C. S. Lancefield, P. C. J. Kamer, T. Lebl, and N. J. Westwood, *Green Chem.*, 2015, **17**, 244–249.

52. S. Kobayashi and K. Manabe, *Acc. Chem. Res.*, 2002, **35**, 209–217.

53. J. C. del Río, J. Rencoret, P. Prinsen, Á. T. Martínez, J. Ralph, and A. Gutiérrez, *J. Agric. Food Chem.*, 2012, **60**, 5922–5935.

54. P. Ferrini and R. Rinaldi, *Angew. Chem. Int. Ed.*, 2014, **53**, 8634–8639.

55. S. Van den Bosch, W. Schutyser, R. Vanholme, T. Driessen, S. F. Koelewijn, T. Renders, B. De Meester, W. J. J. Huijgen, W. Dehaen, C. M. Courtin, B. Lagrain, W. Boerjan, and B. F. Sels, *Energy Environ. Sci.*, 2015, **8**, 1748–1763.

56. T. Parsell, S. Yohe, J. Degenstein, T. Jarrell, I. Klein, E. Gencer, B. Hewetson, M. Hurt, J. I. Kim, H. Choudhari, B. Saha, R. Meilan, N. Mosier, F. Ribeiro, W. N. Delgass, C. Chapple, H. I. Kenttämaa, R. Agrawal and M. M. Abu-Omar, *Green Chem.*, 2015, **17**, 1492–1499.

57. S. Wu and D. S. Argyropoulos, *J. Pulp Paper Sci.*, 2003, **28**, 235–240.

58. H. Koskela, I. Kilpeläinen, and S. Heikkinen, *J. Magn. Reson.*, 2005, **174**, 237–244.
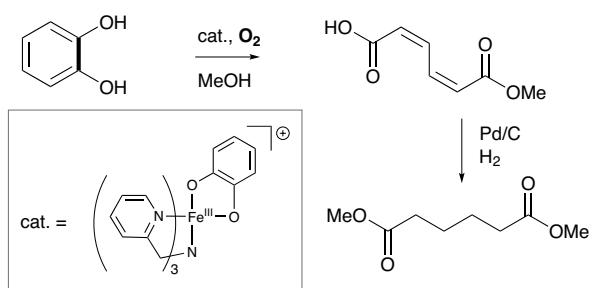
Part II

Iron-Catalysed Dioxygenation of Catechol

Chapter 4

Catalytic Oxidative Cleavage of Catechol by a Non-Heme Iron(III) Complex Complex as a Green Route to Dimethyl Adipate

Abstract

Catechol intradiol dioxygenation is a reaction that allows the selective cleavage of an aromatic carbon-carbon bond in 1,2-arenediols. In nature this reaction is catalysed by highly selective enzymes with iron(III) co-factors. Although synthetic iron(III) complexes have been studied as enzyme models, their catalytic application has been scarcely explored. This chapter describes how the catalyst system prepared *in-situ* from iron(III) salts, tris(2-pyridylmethyl)amine and base readily catalyses the intradiol dioxygenation of pyrocatechol in methanol selectively, to primarily afford the half-methyl ester of muconic acid. Dimethyl adipate is obtained by the subsequent, one-step catalytic hydrogenation/esterification, thus demonstrating a green route to this important nylon precursor.

The work described in this chapter was published in:

4.1 Introduction

The effective utilisation of lignin for the production of value-added bulk chemicals, requires not only depolymerisation of the macromolecule, but also further upgrading of the obtained oxygenated aromatics into the desired products.[1] To do so *oxidatively* may seem, at first glance, counterintuitive given that biomass is already highly oxygenated, but is still very relevant.

In the field of reductive lignin upgrading, considerable research is devoted to the hydro-deoxygenation (HDO) reaction, wherein oxygen functionalities are removed by catalytic reaction with molecular hydrogen or other hydrogen donors.[2] Indeed, a large body of work exists on the HDO of small oxygenated aromatics with various noble and non-noble metal catalysts;[3-8] there are also some examples that deal with actual lignin depolymerisation processes, although this is considerably more challenging and still far from actual application. If the goal is to obtain fuels, concomitant ring saturation by hydrogen is typically not an issue or even desirable, but for the production of chemicals retention of the aromatic ring is often preferred, which requires either selective catalysts[4,7] or careful engineering of the reaction conditions.[9] The targeted product can then be a valuable benzene-toluene-xylene (BTX) mixture, which can be easily separated further and serve as a feedstock for a large number of bulk chemical processes. A major advantage is then that further processing of the depolymerised lignin could proceed through existing petrochemical processes and infrastructure.

The subsequent process steps towards value-added chemicals are, however, often oxidative in nature, e.g. the oxidation of *p*-xylene to terephthalic acid,[10,11] the oxidation of cumene (from alkylation of benzene) to phenol and acetone[12] and the oxidation of cyclohexane (obtained by hydrogenation of benzene) to adipic acid.[13,14] It is then clear that a process based on the HDO of lignin oligomers is by definition rather circuitous and potentially wasteful as the feed is first reduced only to be oxidised again. However, if the functionalities already present in the oxygenated aromatics from lignin depolymerisation can be effectively leveraged, selective and mild oxidation to the desired bulk chemicals may be possible. The reduced number of process steps can then make sustainable chemicals derived from lignin more attractive not only from an environmental point of view, but also in terms of economics.

Given the inherent challenges of selective oxidation reactions, inspiration is frequently drawn from nature, which has developed a broad array of enzymes capable of performing oxidations, under mild conditions and with high substrate specificity, high conversions and high selectivity.[15-17] One particularly interesting class of enzymes is the *catechol dioxygenase* family, which catalyse key steps in biological catabolic pathways for dearomatisation.[18] Using only molecular oxygen as the oxidant, these enzymes selectively cleave an *aromatic* carbon-carbon bond of their catechol (1,2-benzenediol) substrates.
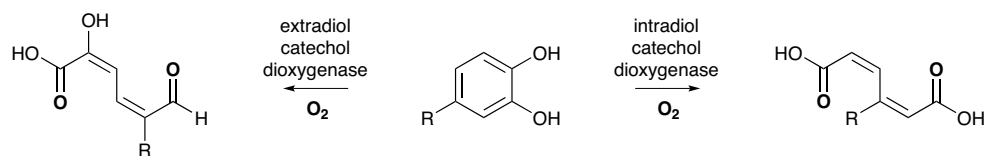
Figure 4.1: The intradiol catechol dioxygenases cleave the carbon-carbon of catechols between the diol functionality (right), whereas the extradiol catechol dioxygenases cleave the carbon-carbon bond adjacent to the diol functionality.

Based on their selectivity, two classes have been identified: the *intradiol dioxygenases* are characterised by a non-heme iron(III) active site and cleave the carbon-carbon bond between the hydroxyl functionalities (Figure 4.1); the *extradiol dioxygenases* feature a non-heme iron(II) active site and cleave a carbon-carbon bond adjacent to the hydroxyl functionality (Figure 4.1). In both cases, the catechol must bind the iron centre as a catecholate dianion before the reaction can occur. [19]

Biomimetic synthetic iron complexes have been developed with the purpose of understanding the chemistry of these systems. The first such complex was ferric nitrilotriacetate, which is capable of oxidizing 3,5-*tert*-butylcatechol to the corresponding intradiol dioxygenation products, albeit extremely slowly.[20] Further work, especially by the group of Que, led to the development of more active model complexes, with the most active complexes obtained with the tris(2-pyridylmethyl)amine (TPA) ligand.[21-23] Isolation and crystal structure determination of the complexes showed the catechol moiety to be bound to the iron centre as the dianion in a bidentate fashion, as in the enzymatic systems.[22,24,25]

Actual selective catalytic conversion of pyrocatechol has not been described so far, however. Such a route (Figure 4.2) may be very interesting in the context of biomass valorisation. Pyrocatechol, originally obtained by pyrolysis of wood, may for example also be obtained by depolymerisation of lignin or biological conversion of glucose.[26,27] At the same time, the intradiol dioxygenation product, *cis,cis*-muconic acid may be readily hydrogenated to adipic acid,[28-30] a bulk chemical produced on a million tonne per annum scale, primarily for the production of Nylon-6,6.
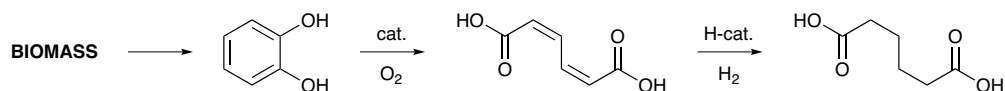

Figure 4.2: The route for valorisation of biomass proposed in this work: pyrocatechol is obtained by chemical or biochemical means from biomass; the pyrocatechol is the converted to *cis,cis*-muconic acid by an intradiol dioxygenation catatlyst; the formed *cis,cis*-muconic acid is then hydrogenated to obtain adipic acid.

In this chapter, the first example of the catalytic intradiol catechol dioxygenation of pyrocatechol using *in-situ* prepared iron(III) complexes of tris(2-pyridylmethyl)amine is described. The products of the reaction were identified and found to be exclusively derived from the intradiol dioxygenation reaction. Furthermore, using UV-Vis spectroscopy measurements, a gradual but reversible deactivation of the catalyst during the reaction was observed, which was connected to the reversible formation of μ-oxo iron dimer species. Finally, the product mixture obtained from the intradiol dioxygenation reaction can be convergently hydrogenated and transesterified to obtain the single product dimethyl adipate.

4.2 Results

Que et al. have reported the most active system for stoichiometric intradiol cleavage of the activated substrate 3,5-di-tert-butylcatechol to date, using the ligand tris(2-pyridylmethyl)amine (TPA).[22] We found that the dioxygenation of pyrocatechol (**1**) could be effected by 5 mol% of an iron(III) complex, prepared *in-situ* from iron(III) perchlorate, tris(2-pyridylmetyl)amine and two equivalents of piperidine (with respect to iron) as a base. Reactions were performed for 6 h in methanol under controlled air flow bubbling through the reaction mixture, at ambient pressure and at 50 °C.

The half-methyl ester of *cis,cis*-muconic acid (**2b**) was found as the major product (Figure 4.3), while minor products formed included the free acid (**2a**), half-catechol ester (**2c**) and *cis,trans* isomers of the above (**3a-c**), for a typical mole balance of 90%. Notably, all these products derive from the selective intradiol cleavage of catechol and may eventually be converted to dimethyl adipate (**5**) (*vide infra*). Products resulting from the extradiol cleavage of catechol were not observed, consistent with the selectivity previously reported for TPA-based iron complexes.[22]
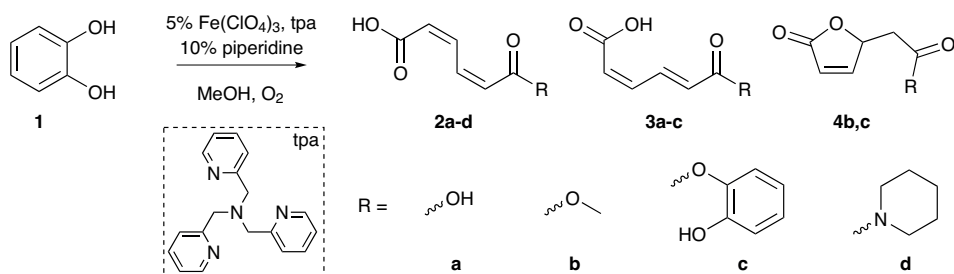

Figure 4.3: The intradiol dioxygenation of catechol (**1**) in methanol proceeds using an iron(III) complex as catalyst, prepared *in-situ* from iron(III) perchlorate, tris(2-pyridylmetyl)amine and two equivalents of piperidine. Products observed are derivatives of *cis,cis*-muconic acid (**3**), *cis,trans*-muconic acid (**4**) and muconolactone (**5**), which include free acids (**a**), methyl esters (**b**), catechol esters (**c**) and a piperidyl amide (**d**).
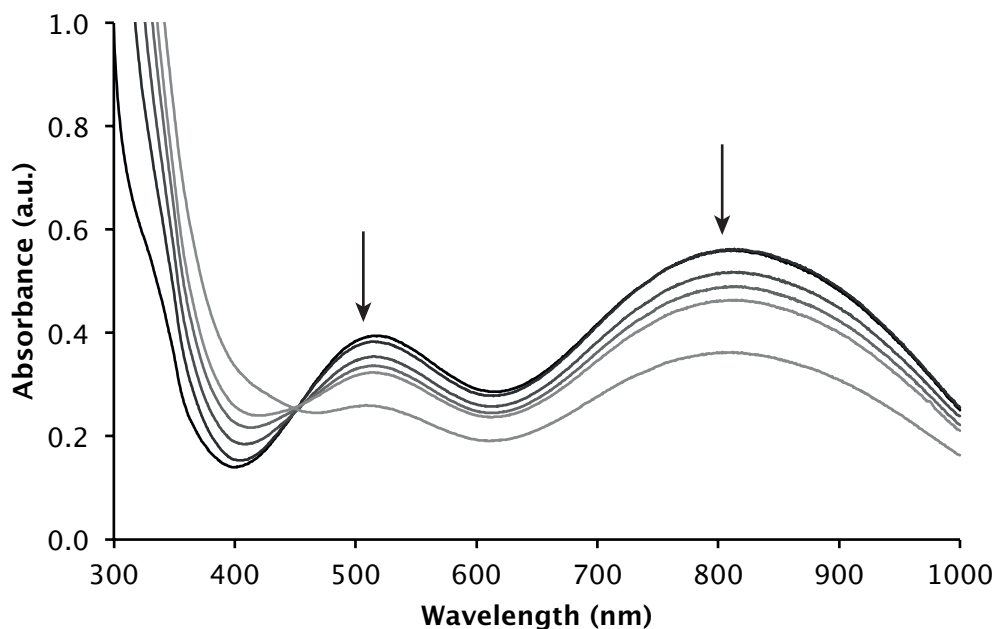
Figure 4.4: UV-Vis-NIR spectra of the diluted (20x) catalytic dioxygenation reaction mixture in time (lighter lines denote longer reaction time), using 5 mol% Fe(ClO$_4$)$_3$, 5 mol% TPA and 10 mol% piperidine. The bands at 518 and 812 nm are characteristic for [Fe(TPA)(catecholato)]$^+$ and remain even at the end of the reaction (conversion > 90%).

Solvolysis of the cyclic muconic anhydride, which is formed as the initial product of the dioxygenation reaction,[21,23,31] to obtain **2b** has been previously observed in methanol.[32,33] Catechol itself is apparently also a competent nucleophile for ring opening of the anhydride. Although catechol esters have not been previously reported as products of intradiol cleavage reactions, the previously reported experiments typically use a stoichiometric amount of the catechol at only 0.5 mM,[22] whereas in the catalytic runs reported here a concentration of 100 mM is used. The *cis,trans* isomers are not expected to directly result from the oxidative cleavage cycle, but rather result from a subsequent isomerisation step, which may proceed readily in solution and exclusively affords the isomer where the ester is in the *trans* position.[34-36] The 10% of original catechol intake that cannot be accounted for is possibly lost to the uncatalysed oxidation of catechol to 1,2-benzoquinone and subsequent condensation with catechol.[37-39]

UV-Vis-NIR spectra of diluted reaction mixtures show characteristic LMCT bands at 518 nm and 812 nm (Figure 4.4), confirming that the [Fe(TPA)(catecholato)]$^+$ complex[23,40,41] is formed and remains present throughout the reaction. The reaction rate was found to initially approximate 0th order in catechol, consistent with a mechanism in

Table 4.1: Results of the catalytic dioxygenation of catechol, using an *in-situ* prepared catalyst with different bases.[a]

| | | C^b | | | | 3a | 2c | 4b | MB^c | | TOF^e |
	Base	(%)	2a	2b	2d	3b	3c	4c	(%)	TON^d	(h^{-1})
1	1 eq piperidine	76	4	42	-	1	8	-	87	13	2.2
2	2 eq piperidine	92	5	48	-	2	13	-	89	16	2.7
3	4 eq piperidine	83	5	35	6	2	8	-	81	14	2.3
4	8 eq piperidine	78	4	15	11	3	4	-	63	9	1.4
5	2 eq NH$_4$OAc	94	6	48	-	4	11	-	86	15	2.5
6	2 eq 2,6-lutidine	90	6	49	-	4	10	-	89	16	2.7
7	2 eq DIPEA[f]	86	4	35	-	8	9	3	82	14	2.4
8	2 eq TBD[g]	88	4	40	-	7	12	2	89	16	2.6

[a] Conditions: 9.1 mmol catechol, 100 mL MeOH; iron precursor, 5 mol% Fe(ClO$_4$)$_3$, 5 mol% TPA and base (eq relative to Fe); 6 h, 50 °C, air flow at 1 atm [b] Conversion of catechol [c] Mole balance as moles of C$_6$ units found (including unconverted catechol) divided by starting amount of catechol as determined by ^{1}H NMR [d] Turnover number [e] Turnover frequency [f] Diisopropylethylamine [g] 1,5,7-Triazabicyclo[4.4.0]dec-5-ene

which oxygen insertion into the [Fe(TPA)(catecholato)]$^+$ complex is the rate-limiting step (as is further demonstrated in Chapter 6).[42]

Stoichiometric experiments have shown that addition of two equivalents of base relative to iron is required to deprotonate the catechol and form the [Fe(TPA)(catecholato)]$^+$ complex.[43] A systematic screening of bases showed that two equivalents is also the optimum for the catalytic reaction (Table 4.1). If more than two equivalents of base were used, UV-Vis-NIR spectra of these solutions (Figure 4.5) initially showed a strong absorption at 565 nm, which may suggest competitive coordination by the base. In addition, a new product, identified as the muconamide of piperidine (**3d**), was formed at higher base loadings.

Even though an acidic product is formed (pK_{a1} 3-4), the iron(III)-catecholato complex remained present in the reaction mixture even after multiple turnovers. As muconic acid is certainly a sufficiently strong acid to protonate piperidine (pK$_a$ 11.2), it seems likely that once all base has been protonated, muconate anions become the base that deprotonates the catechol, consistent with the remarkable stability of iron(III)-catecholato complexes.[44] This is further supported by the observation that the reaction still proceeded rapidly even when ammonium acetate is added as a base (Table 4.1, #5). Indeed, bases of different strengths (Table 4.1, #1-5) do not seem to significantly affect the activity. However, the use of diisopropylethylamine (DIPEA) or 1,5,7-triazabicyclo[4.4.0]dec-5-ene (TBD) resulted in formation of considerably more *cis,trans* isomers as well as two new
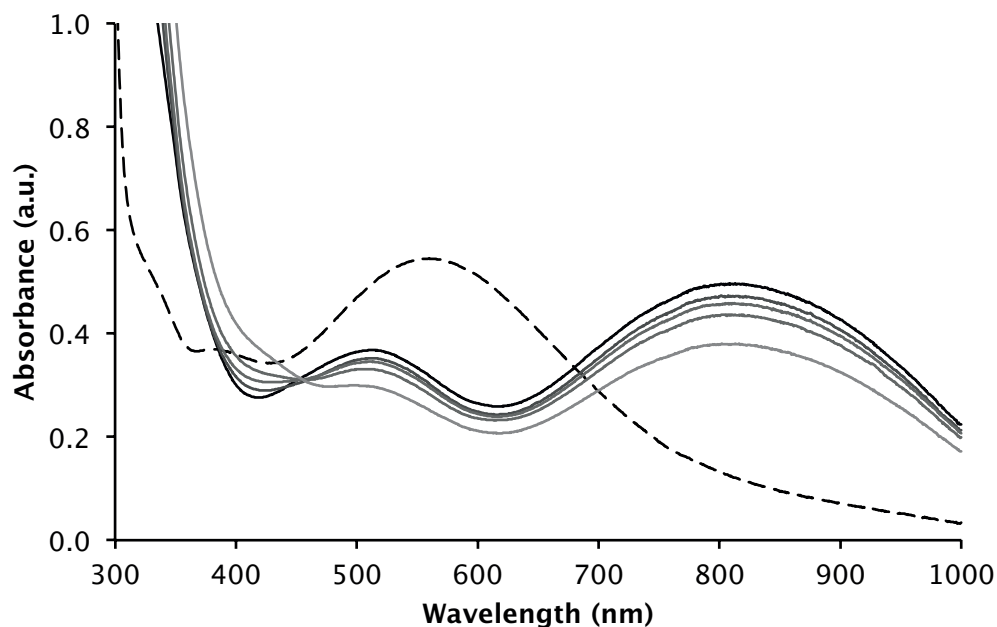
Figure 4.5: UV-Vis-NIR spectra of the diluted (20x) catalytic dioxygenation reaction mixture in time (lighter lines denote longer reaction time), using 5 mol% $Fe(ClO_4)_3$, 5 mol% TPA and 10 mol% piperidine. Initially (dashed line), a single absorption at 565 nm is evident, which as the reaction progresses is replaced by the typical absorption for $[Fe(TPA)(catecholato)]^+$.

products, which were identified as lactones of muconic acid (**4b**, **4c**). Both the isomerisation and lactonisation have previously been shown to be base-catalysed.[36,45]

Lower catalyst loading resulted in higher turnover frequencies (Table 4.2, #1-5), although presumably this is because in those cases the 0th order approximation is more valid. Running the reaction for 24 h at a 1.5 mol% Fe loading gives full conversion with a TON of 51. The use of ferric perchlorate or nitrate as the catalyst precursor expectedly gave similar results, as both salts have anions that are non-coordinating. Remarkably, even iron(III) acetylacetonate ($Fe(acac)_3$), despite its strongly bound acac anions, is able to form the catecholato complex and give considerable activity (Table 4.2, #7), with no additional base needed to be added to this reaction. Several of the stoichiometric intradiol dioxygenation reactions of (substituted) catechols use iron(III) chloride as the iron source,[32,46,47] but here low activity was observed with this precursor (Table 4.2, #6). Absorption bands at 518 and 812 nm in the UV-Vis-NIR spectrum (Figure 4.6) indicate $[Fe(TPA)(catecholato)]^+$ forms initially, but disappears with the formation of a new complex which absorbs at 420 nm, with a concomitant decrease in catalytic activity. Thus, while the active catecholato complex can apparently be formed from $[Fe(TPA)Cl_2]^+$, it appears that during the reaction another chloride-containing complex is formed,

Table 4.2 Results of the catalytic dioxygenation of catechol, using a catalyst system prepared *in-situ* from TPA and the listed iron precursors.[a]

			C^b (%)	2a	2b	3a 3b	2c 3c	4b 4c	MB^c (%)	TON^d	TOF^e (h⁻¹)
		Precursor									
1	0.7%	$Fe(ClO_4)_3$	18	2	12	-	3	-	102	25	4.2
2	2%	$Fe(ClO_4)_3$	50	3	27	-	7	-	94	21	3.4
3	5%	$Fe(ClO_4)_3$	92	5	48	2	13	-	89	16	2.7
4	10%	$Fe(ClO_4)_3$	100	3	44	8	16	-	87	8	1.3
5	5%	$Fe(NO3)_3$	88	6	49	2	11	-	91	14	2.3
6	5%	$FeCl_3$	30	2	12	-	2	-	88	4	0.7
7	5%	$Fe(acac)_3$[f]	73	4	21	15	5	8	85	11	1.8
8	1.5%	$Fe(ClO_4)_3$[g]	100	2	64	6	8	-	88	51	2.1
9	1%	**5**[h]	56	4	31	1	7	-	94	19	3.2
10	1%	μ-oxo[i]	51	4	30	1	5	-	94	18	2.9

[a] Conditions: 9.1 mmol catechol, 100 mL MeOH; iron precursor, TPA (1 eq) and piperidine (2 eq); 6 h, 50 °C, air flow at 1 atm. [b] Conversion of catechol [c] Mole balance as moles of C_6 units found (including unconverted catechol) divided by starting amount of catechol as determined by ¹H NMR [d] Turnover number [e] Turnover frequency [f] no base added [g] 24 h reaction [h] Compound isolated from a stoichiometric reaction using $Fe(ClO_4)_3$, TPA (1 eq) and base (2 eq) [i] $[Fe_2(TPA)_2(μ-O)(μ-OAc)](ClO_4)_3.2H_2O$

to which catechol can no longer coordinate. Based on the UV-Vis-NIR spectrum, several possibilities for the identity of this complex can be excluded, including $[Fe(TPA)Cl_2]^+$,[48] $[Fe_2(TPA)_2(μ-O)Cl_2]^{2+}$ [49] and catecholato complexes.[23] The iron complex could not be isolated from the reaction mixture in order to determine its identity, though.

With the other iron precursors the LMCT bands of the $[Fe(TPA)(catecholato)]^+$ complex were present throughout the reaction, but their intensity did decrease as the reaction progressed, as evident from Figure 4.4. As catechol is still available in the reaction mixture, this points at a gradual deactivation of the catalyst. Remarkably, addition of fresh catechol again led to an increase in intensity of the LMCT bands. This shows that while some decomposition of the active complex does seem to take place during the reaction, it appears to be largely reversible. As differric μ-oxo, μ-carboxylato complexes have been isolated as the product of the reaction in stoichiometric experiments with 3,5-di-*tert*-butylcatechol,[22] a similar complex was considered as the deactivation product here. Indeed, stoichiometric cleavage of catechol with iron(III) perchlorate, TPA and piperidine resulted in the precipitation of a brown microcrystalline material from solution. The UV-Vis-NIR of the material in acetone showed maxima at 693 nm, 490 nm and 457 nm, while the energy difference between the C=O asymmetric stretch (1608 cm⁻¹) and C=O symmetric stretch (1438 cm⁻¹) vibration modes was 170 cm⁻¹. Both spectral features are
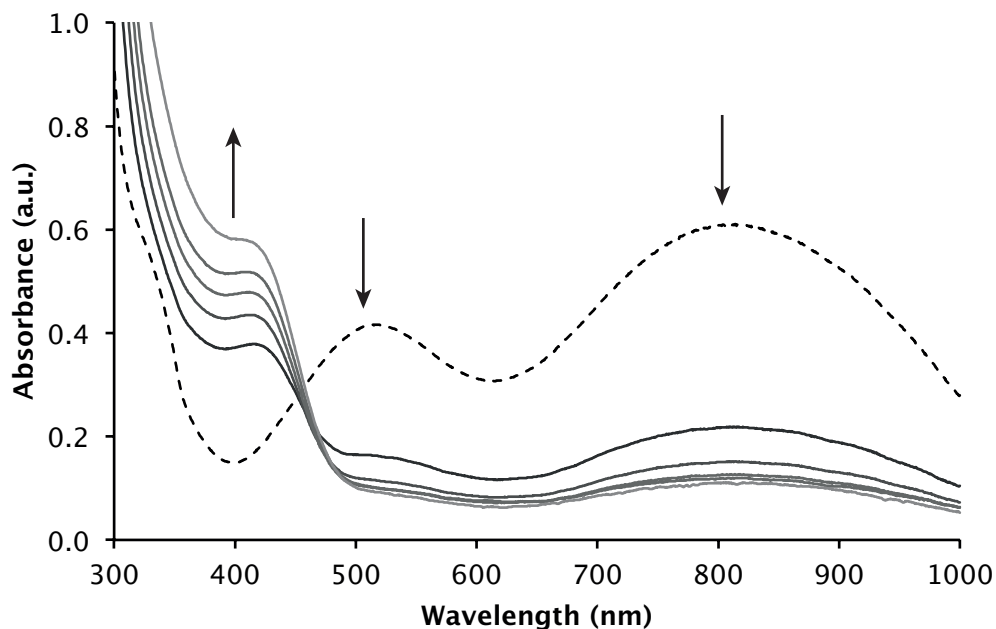
Figure 4.6: UV-Vis-NIR spectra of the diluted (20x) catalytic dioxygenation reaction mixture in time (lighter lines denote longer reaction time), using 5 mol% FeCl$_3$, 5 mol% TPA and 10 mol% piperidine. Initially (dashed line), the typical absorption for [Fe(TPA)(catecholato)]$^+$ is present, but a new adsorption rapidly appears at 420 nm with concomitant decrease of the 518 nm and 812 nm absorptions.

characteristic for a differric μ-oxo, μ-carboxylato complex, which was further confirmed by ^{1}H NMR showing rather narrow bands in the range between 20 - 0 ppm, rather than the broad bands expected for a mononuclear high-spin iron complex.[50] The bridging carboxylato group is likely provided by one of the muconate products formed.

In order to investigate the formation of the active catecholato catalyst from such a μ-oxo, μ-carboxylato species (Figure 4.7), which has previously been hypothesised,[51] [Fe$_2$(TPA)$_2$(μ-O)(μ-OAc)](ClO$_4$)$_3$.2H$_2$O (**5**) was prepared. Spectrophotometric titration of **5** in acetonitrile with catechol (Figure 4.8) clearly shows the appearance of the catecholato LMCT bands at the expense of the μ-carboxylato absorptions. Indeed, use of the differric μ-oxo, μ-carboxylato complexes as catalyst precursors resulted in a catechol dioxygenation reaction of similar activity and selectivity as with the *in-situ* prepared catalysts (Table 4.2, compare #2 with #9-10). To our knowledge, this is the first time that the formation of a μ-oxo, μ-carboxylato complex is shown to be reversible under reaction conditions in iron oxidation catalysis.

The product mixture of esters, acids and geometrical isomers obtained after the catechol dioxygenation at first sight looks rather complex, but this complexity can be
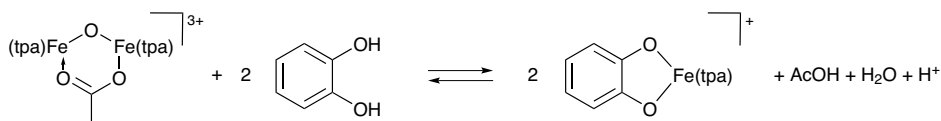
Figure 4.7: Reversible formation of the active [Fe(TPA)catecholato]⁺ complex from a μ-oxo, μ-acetato dibridged ferric complex.
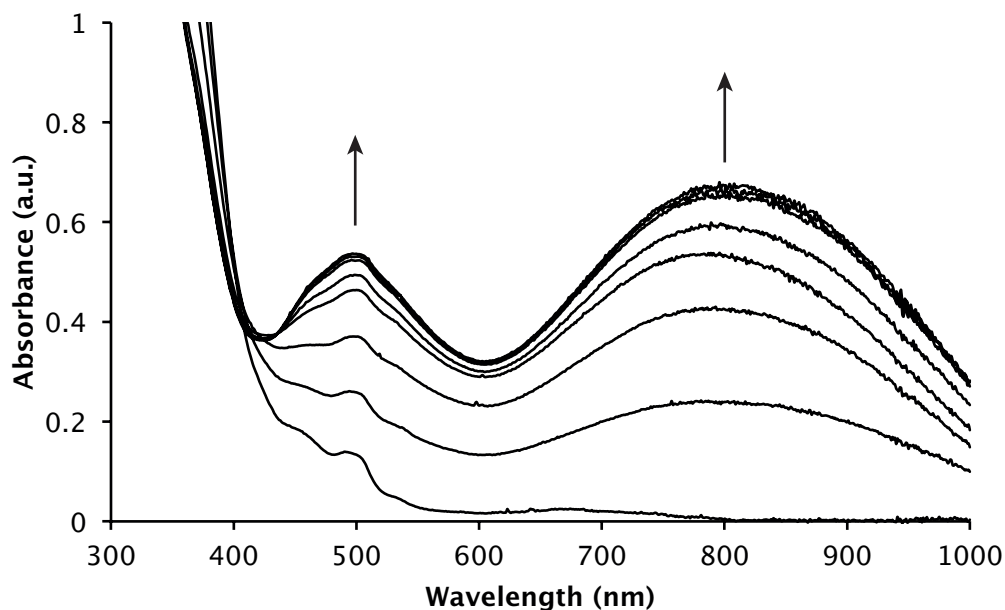

Figure 4.8: Spectrophotometric titration of a 0.2 mM solution of **5** in the presence of 0.2 mM piperidine in CH$_3$CN with addition of 0.5 eq of catechol in between spectra. The LMCT bands at 518 nm and 812 nm correspond to the formation of the [Fe(TPA)(catecholato)]⁺ complex.

readily resolved without any required product separation steps by a simple hydrogenation/transesterification reaction. Indeed, the product mixture could be convergently converted to the single end product dimethyl adipate, a monomer for nylon-6,6, by performing a transesterification of the product mixture simultaneously with hydrogenation. The isolated product mixture was hydrogenated over a Pd/C catalyst (1 atm H$_2$, 50 °C) in the presence of 10 mol% *p*-toluenesulphonic acid in methanol. Although the equilibrium position of adipic acid and its diester prohibits complete transesterification, dimethyl adipate was still isolated in 55% yield (based on original catechol intake). Most interestingly, isolation of the product mixture prior to hydrogenation/transesterification is not necessary, as the crude reaction mixture, *still containing the iron catalyst*, could be likewise converted to give dimethyl adipate in an isolated yield of 48%. These results show the excellent potential for the two-step synthesis of dimethyl adipate from

catechol, a route that does not require any intermediate purification steps. These promising results warrant further investigation, both to increase the somewhat modest activity of the iron catalyst and increase the yield of dimethyl adipate that is obtained. These topics are addressed in the next chapter.

4.3 Conclusions

The selective catalytic intradiol dioxygenation of catechol under mild conditions, using a catalyst prepared *in-situ* from ferric perchlorate, tris(2-pyridylmethyl)amine and base was demonstrated. The formation of μ-oxo, μ-carboxylato iron complexes was shown to be reversible under reaction conditions. Subsequent hydrogenation and esterification of the dioxygenation products using a Pd/C catalyst afforded pure dimethyl adipate in 55% isolated yield. Thus, a potentially sustainable, new route towards monomers for nylon-6,6 was demonstrated.

4.4 Acknowledgements

The CatchBio program is acknowledged for financial support.

4.5 Experimental

Physical Measurements. NMR spectra were recorded on a Varian spectrometer operating at 400 MHz (^{1}H) or 100 MHz (^{13}C) in DMSO-d6 (unless mentioned otherwise) and referenced against the signal of the residual protio impurity of the solvent (2.50 ppm). UV-Vis-NIR spectra were recorded on a Varian Cary 50 spectrometer using a quartz cuvette with 10.00 mm pathlength or on a Varian Cary 60 spectrometer using a dip probe (10.00 mm pathlength) and corrected for absorption by the solvent. IR measurements were carried on a Bruker Tensor-27 Fourier transform spectrometer equipped with a deuterated triglycine sulphate (DTGS) detector and ATR accessory (Pike Miracle, Pike Technologies) with a diamond crystal as the internal reflection element. GC-MS measurements were performed on a Shimadzu GC-2010 using a VF5-ms column, coupled to a Shimadzu GCMS-QP2010 mass spectrometer.

Chemicals. Tris(2-pyridylmethyl)amine[52] and [Fe$_2$(TPA)$_2$(μ-O)(μ-OAc)](ClO$_4$)$_3$.2H$_2$O[50] (**5**) were synthesised according to previously published procedures. Methanol (p.a. grade) was obtained from Merck and diethyl ether (p.a. grade) from Biosolve. All other chemicals were of reagent grade quality and were purchased from Sigma-Aldrich or Acros and used without further purification.

Catalytic Experiments. In typical catalytic experiment, a glass reactor with reflux condenser was charged with 100 mL methanol, 1.00 g (9.08 mmol) catechol and 1.00 g (5.37 mmol) of 1-dodecanol. Air was bubbled through the mixture through a glass frit at 170 mL/min and the reactor heated to 50 °C. Upon reaching reaction temperature, stock solutions of iron(III) perchlorate

nonahydrate (0.45 mmol), tris(2-pyridylmethyl)amine (0.45 mmol) and base (0.90 mmol) were injected, marking the start of the reaction. Samples were withdrawn during the reaction and reactions were run for 6 h. The withdrawn samples (1 mL) were diluted in 5 mL of 1 M HCl to dissociate the iron complexes and extracted 3 times with 5 mL diethyl ether. The combined organic layers were dried (MgSO$_4$), filtered and concentrated *in vacuo*. The residue was dissolved in DMSO-d6 and the products quantified as described below. Samples for UV-Vis spectroscopy (0.5 mL) were withdrawn, diluted in 9.5 mL of methanol and immediately measured.

Identification of Reaction Products. [1]H total correlation spectroscopy spectra with applied z-filter (zTOCSY) of selected samples were obtained. As zTOCSY gives cross-peaks for all ^{1}H peaks within the same spin system, this enabled grouping of peaks corresponding to a single muconate isomer and was used to identify the minor products. Based on ^{1}H NMR spectra of authentic samples and those previously reported in literature, assignments could be made for all products:

cis,cis-muconic acid (**2a**): ^{1}H NMR: ∂ 5.99 (2H, dd, 8.2 Hz, 2.2 Hz), 7.72 (2H, dd, J = 8.2, 2.2 Hz);

(2Z,4Z)-6-methoxy-6-oxohexa-2,4-dienoic acid[33,46] (**2b**): ^{1}H NMR: ∂ 3.68 (3H, s), 6.04 (2H, t, J = 11.2 Hz), 7.73 (2H, m); GC-MS (EI+): m/z 156 (M$^+$, 2%), 111 (M - COOH, 83), 97 (M - COOCH$_3$, 100);

(2Z,4Z)-6-(2-hydroxyphenoxy)-6-oxohexa-2,4-dienoic acid (**2c**): ^{1}H NMR: ∂ 6.08 (1H, d, J = 11.5 Hz)*, 6.32 (1H, d, J = 11.6 Hz), 6.75-7.10 (4H, m), 7.72 (1H), 7.91 (1H, t, J = 11.6 Hz), 8.25 (1H, ddd, J = 11.6, 11.7, 1.1 Hz), 9.78 (1H, s); GC-MS (EI+): m/z 234 (M$^+$, 7%), 125 (M - C$_6$H$_5$O$_2$, 29), 110 (M - C$_6$H$_4$O$_3$, 100), 83 (M - C$_8$H$_7$O$_3$, 54);

6-oxo-6-(piperidin-1-yl)hexa-2,4-dienoic acid (**2d**): ^{1}H NMR: ∂ 1.47 (2H, m), 1.58 (4H, m), 3.48 (4H, m), 5.83 (1H, dt, J = 11.4, 1.3 Hz), 6.50 (1H, dt, J = 11.5, 1.1 Hz), 7.05 (1H, td, J = 11.6, 1.1 Hz), 7.46 (1H, td, 11.7, 1.1 Hz);

cis,trans-muconic acid (**3a**): ^{1}H NMR: ∂ 5.99 (1H, dd, J = 8.0, 2.4 Hz), 6.20 (1H, d, J = 15.5 Hz), 6.81 (1H, t, J = 11.6 Hz), 8.20 (1H, ddd, J = 15.5, 11.6, 1.1 Hz); GC-MS: m/z 156 (M$^+$, 2%), 111 (M - COOH, 83), 97 (M - COOCH$_3$, 100);

(2Z,4E)-6-methoxy-6-oxohexa-2,4-dienoic acid[53] (**3b**): ^{1}H NMR: ∂ 3.71 (3H, s), 6.01 (1H, d, J = 11.3 Hz), 6.31 (1H, d, J = 15.6 Hz), 6.82 (1H, t, J = 11.6 Hz), 8.25 (1H, ddd, J = 15.6, 11.7, 1.1 Hz); GC-MS (EI+): m/z 156 (M$^+$, 2%), 111 (M - COOH, 83), 97 (M - COOCH$_3$, 100);

(2Z,4E)-6-(2-hydroxyphenoxy)-6-oxohexa-2,4-dienoic acid (**3c**): ^{1}H NMR: ∂ 6.08 (1H, d, J = 8.9 Hz)*, 6.54 (1H, d, 15.4 Hz), 6.75-7.10 (m, 5H), 8.39 (1H, ddd, J = 15.3, 11.5, 0.8 Hz), 9.74 (s, 1H); GC-MS (EI+): m/z 234 (M$^+$, 2%), 125 (M - C$_6$H$_5$O$_2$, 38), 110 (M - C$_6$H$_4$O$_3$, 100);

methyl 2-(5-oxo-2,5-dihydrofuran-2-yl)acetate[35,54] (**4b**): ^{1}H NMR: ∂ 2.62 (1H, dd, J = 16.5, 8.3 Hz), 2.96 (1H, dd, J = 16.5, 4.7 Hz), 5.41 (1H, m), 6.25 (1H, dd, 5.8, 2.0 Hz), 7.75 (1H, s)*;

2-hydroxyphenyl 2-(5-oxo-2,5-dihydrofuran-2-yl)acetate (**4c**): ^{1}H NMR: ∂ 2.94 (1H, dd, J = 16.7, 8.0 Hz), 3.21 (1H, dd, J = 16.7, 5.0 Hz), 5.52 (1H, m), 6.30 (dd, J = 5.7, 2.0 Hz), 6.76 - 7.12 (4H, m), 7.86 (1H, dd, J = 5.7, 1.5 Hz), 9.69 (1H, s);

* The multiplicity and coupling constants of these peaks were determined from the [1]H zTOCSY spectra, which were of limited resolution (4.7 Hz).

Product Quantification. Recorded ^{1}H NMR spectra were processed using MestreNova 7.1.2. Phase and baseline corrections were applied and characteristic muconic acid peaks were integrated and the integrals normalised to the 1-dodecanol triplet at 0.85 ppm. The response factor of catechol to 1-dodecanol was experimentally determined to be 0.979, whereas the response factor for muconic acid was determined to be 0.968. The latter value was used for all muconate

isomers. The overlapping peaks of **3a** and **3b** at 8.25 ppm were deconvoluted using MestraNova's GSD algorithm. The strongly overlapping peaks at 5.98 and 7.72 ppm could not be deconvoluted in this manner. To determine the contribution of **2a** to the 5.98 ppm peak, the known integral of **3a** was subtracted. To determine the contribution of **2b** to the 7.72 ppm peak, the known integrals of **2a** and **2c** were subtracted.

Single Turnover Experiment. Iron(III) perchlorate nonahydrate (496 mg, 0.96 mmol), tris(2-pyridylmethyl)amine (297 mg, 1.02 mmol), piperidine (173 mg, 2.02 mmol) and catechol (110 mg, 1.00 mmol) were dissolved in 30 mL of methanol. The intensely purple solution was exposed to an atmosphere of pure oxygen and allowed to stir gently for 16 h at room temperature. The formed precipitate was removed by filtration and washed with a small amount of methanol to obtain 194 mg of a brown microcrystalline solid.

Spectrophotometric Titration of 5 with Catechol. To a stirred solution of $[Fe_2(TPA)_2(\mu\text{-O})(\mu\text{-OAc})](ClO_4)_3.2H_2O$ (5 mL, 0.20 mM) in acetonitrile was added 20 μL of 50 mM piperidine solution in acetonitrile at room temperature. Catechol solution (50 mM) was added in steps of 10 μL. UV-Vis-NIR spectra of the solution were recorded between additions.

Hydrogenation/Transesterification of Isolated Product Mixture. A glass reactor with reflux condenser was charged with 100 mL methanol and 1.15 g (10.4 mmol) catechol and heated to 50 °C while bubbling air through the reaction mixture through a glass frit at 170 mL/min. Upon reaching reaction temperature, stock solutions of iron(III) perchlorate nonahydrate (0.14 mmol), tris(2-pyridylmethyl)amine (0.16 mmol) and piperidine (0.34 mmol) were added. After 24 h, the reaction mixture was concentrated *in vacuo* and the resulting dark oil partitioned over 100 mL 1M HCl and 75 mL diethyl ether. The organic layer was separated and the aqueous layer extracted twice with diethyl ether (75 mL). The combined organic layers were dried over $MgSO_4$, filtered and concentrated *in vacuo* to obtain 1.53 g of dark yellow oil, which solidified upon standing. The solid was dissolved in 50 mL of methanol and 5% wt Pd/C (55 mg) and *p*-toluenesulphonic acid monohydrate (195 mg, 1.03 mmol) were added. The mixture was heated to 50 °C under stirring and exposed to a H_2 atmosphere for 24 h. Afterwards, Pd/C was removed by centrifugation and filtration over a 0.4 μm PTFE filter. Pd/C was again extracted with 50 mL of methanol, centrifuged and filtered, after which the combined methanol solutions were concentrated *in vacuo*. The resulting oil was dissolved in 100 mL diethyl ether, which was subsequently washed with 100 mL saturated aqueous $NaHCO_3$, 100 mL 0.1 M NaOH solution and brine. The ethereal layer was dried ($MgSO_4$), filtered and concentrated *in vacuo* to obtain dimethyl adipate (1.00 g, 5.74 mmol, 55%) as a very pale yellow oil. ^1H NMR ($CDCl_3$): ∂ 1.61 (4H, m), 2.27 (4H, m), 3.61 (6H, s); ^{13}C NMR ($CDCl_3$): ∂ 24.38, 33.66, 51.52, 173.72; GC-MS (EI+): m/z 143 (M^+ - OCH_3, 59%), 114 (94), 111 (79), 101 (73), 59 (100), 55 (73).

Hydrogenation/Transesterification of Crude Reaction Mixture. A glass reactor with reflux condenser was charged with 100 mL methanol and 1.02 g (9.23 mmol) catechol and heated to 50 °C while bubbling air through the reaction mixture through a glass frit at 170 mL/min. Upon reaching reaction temperature, stock solutions of iron(III) perchlorate nonahydrate (0.17 mmol), tris(2-pyridylmethyl)amine (0.20 mmol) and piperidine (0.36 mmol) were added. After 24 h, the reaction mixture was transferred to a Schlenk flask and 5% wt Pd/C (50 mg) and *p*-toluenesulphonic acid monohydrate (180 mg, 0.95 mmol) were added. The mixture was heated to 50 °C under stirring and exposed to a H_2 atmosphere for 24 h. Afterwards, Pd/C was removed by centrifugation and filtration over a 0.4 μm PTFE filter. Pd/C was again extracted with 50 mL of

methanol, centrifuged and filtered, after which the combined methanol solutions were concentrated *in vacuo*. The resulting oil was dissolved in 100 mL diethyl ether, which was subsequently washed with 100 mL 1M HCl, 100 mL saturated aqueous NaHCO$_3$, 100 mL 0.1 M NaOH solution and brine. The ethereal layer was dried (MgSO$_4$), filtered and concentrated *in vacuo* to obtain dimethyl adipate (0.77 g, 4.42 mmol, 48%) as a very pale yellow oil. Analysis was identical to the experiment described above.

4.6 References

1   J. Zakzeski, P. C. A. Bruijnincx, A. L. Jongerius and B. M. Weckhuysen, *Chem. Rev.*, 2010, **110**, 3552–3599.

2   E. Furimsky, *Appl. Catal. A., Gen.*, 2000, **199**, 147–190.

3   E. Laurent and B. Delmon, *Appl. Catal. A., Gen.*, 1994, **109**, 77–96.

4   E. Laurent and B. Delmon, *Appl. Catal. A., Gen.*, 1994, **109**, 97–115.

5   X. Zhu, L. L. Lobban, R. G. Mallinson and D. E. Resasco, *J. Catal.*, 2011, **281**, 21–29.

6   C. Zhao, J. He, A. A. Lemonidou, X. Li and J. A. Lercher, *J. Catal.*, 2011, **280**, 8–16.

7   A. L. Jongerius, P. C. A. Bruijnincx and B. M. Weckhuysen, *J. Catal.*, 2012, **285**, 315–323.

8   Q. Bu, H. Lei, A. H. Zacher, L. Wang, S. Ren, J. Liang, J. Wei, Y. Liu, J. Tang, Q. Zhang and R. Ruan, *Bioresource Technology*, 2012, **124**, 470–477.

9   X. Wang and R. Rinaldi, *Angew. Chem. Int. Ed.*, 2013, **52**, 11499–11503.

10   P. Raghavendrachar and S. Ramachandran, *Ind. Eng. Chem. Res.*, 1992, **31**, 453–462.

11   R. A. F. Tomás, J. C. M. Bordado and J. F. P. Gomes, *Chem. Rev.*, 2013, **113**, 7421–7469.

12   R. J. Schmidt, *Appl. Catal. A., Gen.*, 2005, **280**, 89–103.

13   A. Castellan, J. C. J. Bart and S. Cavallaro, *Catal. Today*, 1991, **9**, 237–254.

14   F. Cavani and S. Alini, in *Sustainable Industrial Chemistry*, Wiley-VCH Verlag GmbH & Co. KGaA, Weinheim, Germany, 2009, pp. 367–425.

15   L. Que Jr. and R. Y. N. Ho, *Chem. Rev.*, 1996, **96**, 2607–2624.

16   B. Meunier, S. P. de Visser and S. Shaik, *Chem. Rev.*, 2004, **104**, 3947–3980.

17   L. Que Jr. and W. B. Tolman, *Nature*, 2008, **455**, 333–340.

18   F. H. Vaillancourt, J. T. Bolin and L. D. Eltis, *Crit. Rev. Biochem. Mol. Biol.*, 2006, **41**, 241–267.

19   T. D. H. Bugg, *Tetrahedron*, 2003, **59**, 7075–7101.

20   M. G. Weller and U. Weser, *J. Am. Chem. Soc.*, 1982, **104**, 3752–3754.

21   D. D. Cox and L. Que Jr., *J. Am. Chem. Soc.*, 1988, **110**, 8085–8092.

22   H. G. Jang, D. D. Cox and L. Que Jr., *J. Am. Chem. Soc.*, 1991, **113**, 9200–9204.

23   R. Yamahara, S. Ogo, H. Masuda and Y. Watanabe, *J. Inorg. Biochem.*, 2002, **88**, 284–294.

24   D. H. Ohlendorf, J. D. Lipscomb and P. C. Weber, *Nature*, 1988, **336**, 403–405.

25   M. W. Vetting and D. H. Ohlendorf, *Structure*, 2000, **8**, 429–440.

26   K. M. Draths and J. W. Frost, *J. Am. Chem. Soc.*, 1995, **117**, 2395–2400.

27   W. Li, D. Xie and J. W. Frost, *J. Am. Chem. Soc.*, 2005, **127**, 2874–2882.

28   K. M. Draths and J. W. Frost, *J. Am. Chem. Soc.*, 1994, **116**, 399–400.

29   J. M. Thomas, R. Raja, B. F. G. Johnson, T. J. O'Connell, G. Sankar and T. Khimyak, *Chem. Commun.*, 2003, 1126–1127.

30   X. She, H. M. Brown, X. Zhang, B. K. Ahring and Y. Wang, *ChemSusChem*, 2011, **4**, 1071–1073.

31   M. Costas, M. P. Mehn, M. P. Jensen and L. Que Jr., *Chem. Rev.*, 2004, **104**, 939–986.

32   G. Lin, G. Reid and T. D. H. Bugg, *J. Am. Chem. Soc.*, 2001, **123**, 5030–5039.

33   J. Tsuji and H. Takayanagi, *Tetrahedron*, 1978, **34**, 641–644.

34   J. A. Elvidge, R. P. Linstead, P. Sims and B. A. Orkin, *J. Chem. Soc.*, 1950, 2235.

35   D. W. Ribbons and A. G. Sutherland, *Tetrahedron*, 1994, **50**, 3587–3594.

36   S. Seltzer and J. Hane, *Bioorg. Chem.*, 1988, **16**, 394–407.

37   G. E. K. Branch and M. A. Joslyn, *J. Am. Chem. Soc.*, 1935, **57**, 2388–2394.

38   C. R. Dawson and J. M. Nelson, *J. Am. Chem. Soc.*, 1938, **60**, 245–249.

39   N. Schweigert, A. J. B. Zehnder and R. I. L. Eggen, *Environ. Microbiol.*, 2001, **3**, 81–91.

40   Y. Hitomi, M. Yoshida, M. Higuchi, H. Minami, T. Tanaka and T. Funabiki, *J. Inorg. Biochem.*, 2005, **99**, 755–763.

41   D. D. Cox, S. J. Benkovic, L. M. Bloom, F. C. Bradley, M. J. Nelson, L. Que Jr. and D. E. Wallick, *J. Am. Chem. Soc.*, 1988, **110**, 2026–2032.

42   V. Georgiev, H. Noack, T. Borowski, M. R. A. Blomberg and P. E. M. Siegbahn, *J. Phys. Chem. B*, 2010, **114**, 5878–5885.

43   M. Pascaly, M. Duda, F. Schweppe, K. Zurlinden, F. K. Müller and B. Krebs, *J. Chem. Soc., Dalton Trans.*, 2001, 828–837.

44   A. Avdeef, S. R. Sofen, T. L. Bregante and K. N. Raymond, *J. Am. Chem. Soc.*, 1978, **100**, 5362–5370.

45   B. M. Trost and P. G. McDougal, *J. Org. Chem.*, 1984, **49**, 458–468.

46   G. Lin, G. Reid and T. D. H. Bugg, *Chem. Commun.*, 2000, 1119–1120.

47   T. Funabiki, T. Yamazaki, A. Fukui, T. Tanaka and S. Yoshida, *Angew. Chem. Int. Ed.*, 1998, **37**, 513–515.

48   T. Kojima, R. A. Leising, S. Yan and L. Que Jr., *J. Am. Chem. Soc.*, 1993, **115**, 11328–11335.

49   R. E. Norman, R. C. Holz, S. Menage, L. Que Jr., J. H. Zhang and C. J. O'Connor, *Inorg. Chem.*, 1990, **29**, 4629–4637.

50   R. E. Norman, S. Yan, L. Que Jr., G. Backes, J. Ling, J. Sanders-Loehr, J. H. Zhang and C. J. O'Connor, *J. Am. Chem. Soc.*, 1990, **112**, 1554–1562.

51   W. O. Koch and H.-J. Krüger, *Angew. Chem. Int. Ed.*, 1995, **34**, 2671–2674.

52   G. J. P. Britovsek, J. England and A. J. P. White, *Inorg. Chem.*, 2005, **44**, 8125–8134.

53   M.-E. Martin, D. Planchenault and F. Huet, *Tetrahedron*, 1995, **51**, 4985–4990.

54   E. Quinoa, E. Kho, L. V. Manes, P. Crews and G. J. Bakus, *J. Org. Chem.*, 1986, **51**, 4260–4264.

Chapter 5

Sustainable Production of Dimethyl Adipate by Non-Heme Iron(III)-Catalysed Oxidative Cleavage of Catechol

Abstract

Adipic acid and its esters are important bulk chemicals whose principal use is in the production of the nylon-6,6 polymer. The novel sustainable route to dimethyl adipate, developed in the previous chapter, is further investigated here. An investigation of catalyst loading, temperature and oxygen pressure, allowed a turnover frequency of 120 h^{-1} to be obtained in the oxidative cleavage. The hydrogenation and transesterification of the muconic acid products were shown to proceed well over commercially available, supported catalysts. After vacuum distillation, dimethyl adipate could be isolated in 62% yield from catechol, thus demonstrating the improvements to this green and sustainable route to this important bulk chemical.
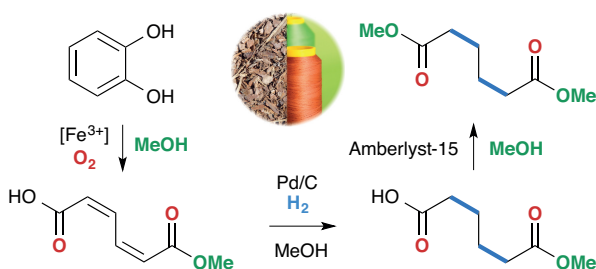
The work described in this chapter was published in:

5.1 Introduction

Adipic acid and its diesters are the most important carboxylic diacids produced in the chemical industry, with a production of approximately 2.8 million tonnes per year. The most important application is the production of the Nylon-6,6 polyamide, although other uses include synthesis of polyesters and polyurethanes, plasticisers in polyvinyl chloride and polyvinyl butyral and as additives in numerous other applications.[1]

The current industrial production of adipic acid (Figure 5.1) starts from oil-derived benzene, which is first hydrogenated to cyclohexane. Cyclohexane is typically oxidized by air to KA-oil, which is a mixture of cyclohexanol and cyclohexanone, over a cobalt catalyst.[2] As selectivity is inversely dependent on cyclohexane conversion, this reaction is typically run at low (4-8%) conversion and requires continuous distillation and recycling of cyclohexane.[3] Subsequent oxidation of the KA oil with nitric acid affords adipic acid, as well as a stoichiometric amount of nitrous oxide, a strong greenhouse gas.[4,5] There is considerable interest in novel processes for the production of adipic acid, both to abate waste emissions and to expand the feedstock to sustainable alternatives for benzene.

Van de Vyver and Román-Leshkov recently reviewed the development of novel catalytic processes for adipic acid production.[6] The most developed alternative to the current industrial production is the oxidation of cyclohexene with 30% hydrogen peroxide with a catalyst based on soluble tungstates, which was first reported by Sato *et al.*[7] Several routes starting from renewable substrates have also been reported, for example from 5-hydroxymethylfurfural[8], γ-valerolactone[9] and D-glucose[10]. In the latter, biochemical, route *E. Coli* strains were engineered to convert glucose into *cis,cis*-muconic acid, which could in turn be readily converted into adipic acid by catalytic hydrogenation. Lignin
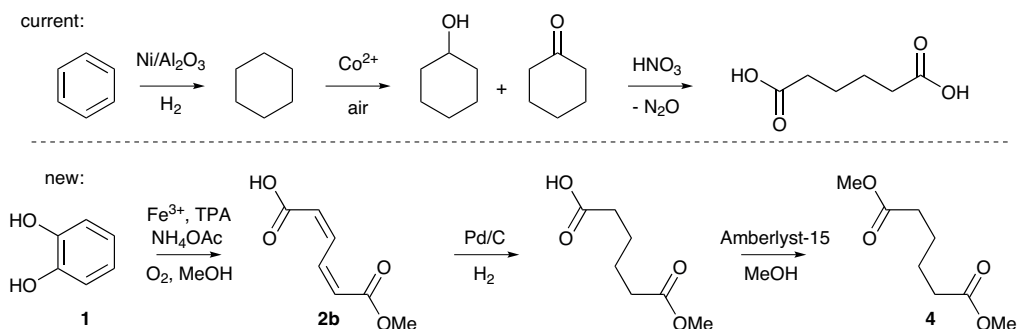

Figure 5.1: The current industrial production of adipic acid starts from benzene, which is hydrogenated to cyclohexane. Aerobic oxidation using a cobalt catalyst affords KA oil, which is oxidised by nitiric acid to adipic acid. The novel route described here starts from pyrocatechol, which is oxidized to the corresponding muconic acid by the iron catalyst. Subsequent hydrogenation and transesterification affords dimethyl adipate.

could also serve as a renewable resource for adipic acid production, as this renewable material is available at low-cost and in large quantities, but lignin-based routes are still largely unexplored.[11]

With lignin valorization in mind, catechol provides an interesting starting material. Indeed, guaiacols (i.e. catechol methyl ethers) are often reported as major products in lignin depolymerisation procedures[11-14] and hydrolysis may then afford the corresponding catechols.[15-18] In addition, lignin depolymerisation procedures that directly yield catechols have recently been reported.[19]

In the previous chapter, a selective catalytic system using an iron(III) tris(2-pyridylmethyl)amine (TPA) as catalyst was developed for the selective intradiol dioxygenation of pyrocatechol. This afforded a mixture of *cis,cis*-muconic derivatives, which could be further converted to dimethyl adipate by convergent hydrogenation and transesterification steps. While very selective, the activity of the iron oxidation catalyst was still rather modest. In addition the subsequent conversion steps were only superficially explored.

In this chapter, the further investigation into the catalytic intradiol dioxygenation of pyrocatechol is therefore described, which enabled a 35-fold improvement in the turnover frequency of the catalyst. The reaction was shown to proceed at catalyst loadings as low as 0.1 mol%, while an increase of reaction pressure and temperature significantly increased activity with retention of the excellent selectivity towards the desired oxidative cleavage products. Based on DFT calculations it is also shown that isomerisation of the products takes place as a secondary, uncatalysed, reaction through a lactonic transition state. Furthermore, the sequential, convergent hydrogenation and transesterification of the obtained product mixtures to dimethyl adipate was investigated, using compatible reaction conditions and recoverable catalysts, minimising the amount of work-up and isolation required in the reaction sequence.

Compared to the current industrial route, this new route is highly atom-efficient: water, rather than nitrous oxide, is the only stoichiometric by-product and only two equivalents of hydrogen (compared to three in the industrial process) are required to obtain the final adipates. In contrast to the high temperatures and pressures required for benzene hydrogenation in the conventional route, dearomatisation here proceeds oxidatively and as a result all reaction steps can be run at mild temperatures and pressures. Furthermore, the process uses largely non-toxic reagents and catalysts. The route thus provides a sustainable alternative to dimethyl adipate production.

5.2 Results

The dioxygenation of pyrocatechol (**1**) using an *in-situ* prepared iron(III) tris(2-pyridy-methyl)amine (TPA) complex (Figure 5.1) was investigated in a stainless steel batch autoclave equipped with reflux condenser to allow reactions to be run at elevated pressures and under continuous gas flow. In the previous chapter it was already demonstrated that the highest activities are obtained with iron(III) salts with non-coordinating anions, using mild bases; readily available iron (III) nitrate nonahydrate was therefore used as the iron source here. Variation of base concentration showed that the highest activity was obtained with two equivalents of base relative to the catalyst. In order to prevent undesirable side reactions, the (very) weak base ammonium acetate was employed. The TPA ligand is commercially available, but can also be conveniently prepared by a literature procedure.[29] In all oxidation chemistry, including industrially practiced processes such as the cyclohexane oxidation step of the current adipic acid process, one should be aware of the potential fire and explosion hazards that result from the use of oxygen and flammable organic compounds and solvents under pressure and elevated temperature. Therefore, all experiments were run using a 1:3 mixture of synthetic air and nitrogen, for a final oxygen concentration of 5 vol%. This is well below the limiting oxygen concentration for a methanol/oxygen system and thus outside the flammability range.[30]

A typical reaction proceeded for 4 h at 50 °C and 10 bar total pressure, using 0.5 mol% catalyst. Products were isolated from the reaction mixture by acidification with aqueous HCl to dissociate the iron complexes and subsequent extraction with diethyl ether. Under these conditions, six products were observed, which all derive from the selective intradiol dioxygenation of catechol and were found as products in Chapter 4 as well (Figure 5.2). Products that derive from ring cleavage with a different regioselectivity (i.e. extradiol dioxygenation) were not observed. Thus, given the convergent nature of the subsequent hydrogenation and esterification steps, all six products can be considered as desired, as they will all be converted to dimethyl adipate.

The cyclic muconic anhydride, which is the initial product of the intradiol dioxygenation reaction, is not directly observed.[25,28] Rapid nucleophillic attack by water, methanol or catechol affords, respectively, *cis,cis*-muconic acid (**2a**), its monomethyl ester (**2b**) and its catechol ester (**2c**). The major product observed in all cases is **2b**. At 96% conversion, a yield of 63% is observed, while yields of **2a** and **2c** are only 5% and 1% respectively. Isomerisation to the corresponding *cis,trans*-isomers (**3a-c**) is also observed, with a typical **2:3** ratio of 7:1.

The isomerisation of muconic acids has previously been proposed to proceed by intramolecular attack of the carboxylate moiety on the 1,3-diene to form a lactonic intermediate.[31,32] Given the rather mild conditions at which the reaction is performed, density functional theory (Amsterdam Density Functional, BP86 functional, TZP basis set)
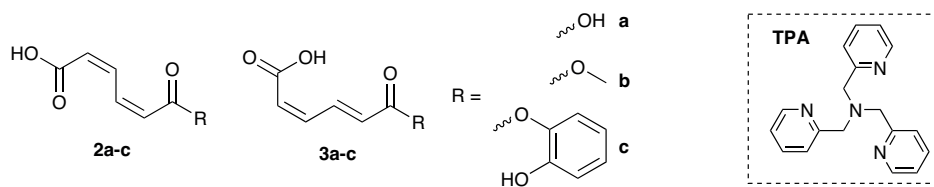
Figure 5.2: Products observed in the catalytic dioxygenation of catechol are derivatives of *cis,cis*-muconic acid (**2**) and cis,trans-muconic acid (**3**). The products include free acids (**a**), methyl esters (**b**) and catechol esters (**c**). The structure of the TPA ligand is given on the right.

was used to check if such a mechanism would be feasible under these reaction conditions. Geometry optimisation of the monomethyl muconate anion indeed gave minima for the *cis,cis* and *cis,trans* isomers. As expected, the *cis,trans* isomer is the thermodynamic end product having a free energy that was slightly lower than the *cis,cis* isomer by 2.4 kcal/mol. Interestingly, however, no stable lactonic intermediate could be found, but increased lactonic character of the muconic acid did lengthen the carbon-carbon double bond. Consequently, a lactonic transition state for the isomerisation could be optimised (Figure 5.3) with a free energy of 23.7 kcal/mol compared to the *cis,cis* isomer. This appears to be a reasonable activation barrier considering the relatively low *cis,trans* isomer yields that are observed. In the dioxygenation of substituted catechols, lactones have previously been observed as products,[26,33,34] although none were found under these

$\Delta G = 0.0$ kcal/mol $\Delta G = 23.7$ kcal/mol $\Delta G = -2.4$ kcal/mol
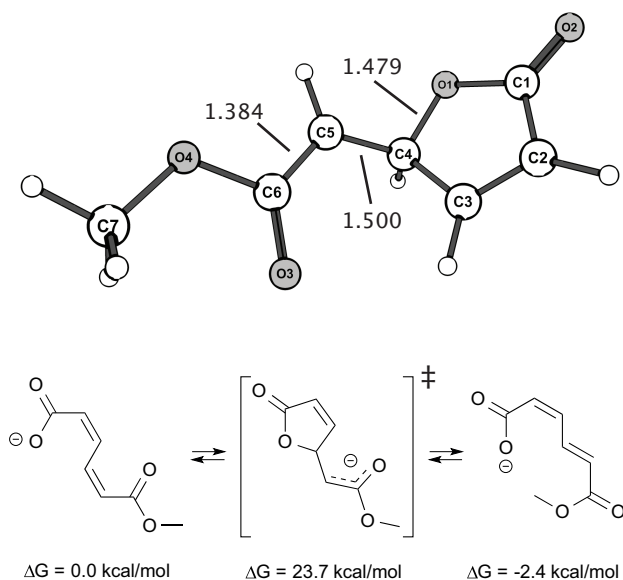
Figure 5.3: Transition state (top, selected bond lengths indicated) and mechanism (bottom) for double bond isomerisation in monomethyl muconate as revealed by density functional theory calculations.

Table 5.1: Results of the catalytic dioxygenation of catechol using different amounts of catalyst.[a]

	Cat.[b] (mol %)	C[c] (%)	TOF[d] (h⁻¹)	MB[e] (%)	Yield 2 + 3 (%)		
					a	b	c
1	0.1	12	27	99	1	10	< 1
2	0.5	43	20	98	4	33	2
3	0.5[f]	45	18	94	3	28	4
4	1.0	90	19	91	6	61	7
5	2.0	100	10	95	4	71	10
6	5.0	100	8	85	3	64	9

[a] Conditions: 27.2 mmol catechol, catalyst (1 eq $Fe(NO_3)_3$, 1 eq TPA, 2 eq NH_4OAc), 300 mL MeOH, 50 °C, 10 bar (5% O_2), 800 sccm gas flow, 4 h [b] Catalyst loading [c] Conversion [d] Turnover frequency [e] Mole balance as moles of C_6 units found (including unconverted catechol) divided by starting amount of catechol as determined by ^1H NMR [f] Using iron(III) oxalate and no NH_4OAc

conditions. The absence of a lactonic intermediate also explains why no lactone products are observed, as these might otherwise be formed simply by protonation of such an intermediate.

Under standard conditions, the six products and unreacted catechol accounted for 99% of the original catechol. Under more severe reaction conditions, we were unable to completely close the mole balance (as moles of C_6-units found, against the original intake of C_6 units) and ca. 5-15% of the original catechol intake was unaccounted for. To ensure all muconate products were completely extracted from the reaction mixture, the aqueous fractions were analysed by UV-Vis measurements after extraction. The muconate species have very intense absorption bands between 251 nm and 264 nm,[35] but no strong absorbances other than those from the TPA ligand could be observed. Having now excluded muconate losses due to the work-up procedure, the reduced mole balance was attributed to noncatalytic oxidation to 1,2-benzoquinone, as previously hypothesised. This highly unstable compound is known to undergo condensation reactions with catechol itself, forming poorly-defined, water-soluble oligomers, which are as a result not extracted and seen in our work-up procedure.[36-38]

5.2.1 Catalyst

As the intradiol dioxygenation was previously performed at a rather high catalyst loading of 5 mol%, it was interesting to see if the catalyst retained its activity at lower concentrations. Thus, the dioxygenation reaction was performed for 4 h of reaction time using loadings of 0.1 - 5 mol% catalyst at 50 °C and 10 bar total pressure (Table 5.1). At high catalyst loadings, the reaction proceeded with full conversion, while at lower catalyst loadings the turnover frequency increased up to 27 h⁻¹ at 0.1 mol%. As the catechol

intradiol dioxygenation proceeds approximately 0th order in substrate, the increase in turnover frequency presumably is the result of the 0th order approximation being more valid at low conversions, rather than a true activity increase. The product distributions are largely unaffected by the concentration of the catalyst.

To further simplify the system and reduce the environmental footprint by omitting the externally added base, the activity of an iron(III) salt with weakly basic counterions were also tested. As the first turnover produces muconate anions which then in turn act as base to continue the catalytic cycle, the basic counter ions merely are needed to initiate the catalytic cycle and a pKa ~ 3 of the conjugate acid should be sufficient. Thus, when performing the reaction using iron(III) oxalate (Table 5.1, #3) without any added base, an activity that was only slightly lower than with 2 eq. of NH_4OAc was obtained. The oxalate anions are also sufficiently basic to enable formation of the first catecholato complexes that initiate the catalytic cycle and also do not appear to significantly displace that catecholato moieties from the iron(III) centre.

5.2.2 Reaction Pressure

In order to increase the activity of the system, the influence of the total gas pressure (5 - 25 bar at 5 vol% oxygen) was also investigated, using 0.5 mol% catalyst at 50 °C (Table 5.2). An approximately linear increase of activity with pressure was observed, suggesting a first-order process in oxygen. This is consistent with the proposed mechanism for catechol intradiol dioxygenation that involves attack of oxygen on the active iron catecholato complex[39,40] and with the mechanistic work described in the next chapter. To exclude the influence of mass-transfer of oxygen into the liquid phase, which is also a first-order process, a control experiment with lower stirring rate was performed. The

Table 5.2: Results of the catalytic dioxygenation of catechol using different total pressures (5% O_2).[a]

	p[b] (bar)	C[c] (%)	TOF[d] (h[-1])	MB[e] (%)	Yield 2 + 3 (%) a	b	c
1	5	29	11	95	2	18	2
2	10	43	20	98	4	33	2
3	10[f]	56	23	93	4	37	4
4	15	73	31	94	6	51	5
5	20	88	36	87	6	63	3
6	25	97	37	77	8	66	< 1

[a] Conditions: 27.2 mmol catechol, 0.5 mol% catalyst (1 eq Fe(NO₃)₃, 1 eq TPA, 2 eq NH₄OAc), 300 mL MeOH, 50 °C, 800 sccm gas flow, 4 h [b] Pressure [c] Conversion [d] Turnover frequency [e] Mole balance as moles of C_6 units found (including unconverted catechol) divided by starting amount of catechol as determined by ¹H NMR [f] 400 rpm stirring

similar activity that was observed, together with the intrinsic low oxygen conversion (ca. 3%) in the experimental conditions, make it seem reasonable to assume that we are not working under mass-transfer limited conditions and that the pressure-dependent data represent the actual, expected order in oxygen. As with the catalyst loading, no significant changes in product distribution are observed with increasing pressure, which is also expected, as **2** and **3** are products of secondary reactions.

5.2.3 Reaction Temperature

The influence of temperature (30 °C - 80 °C) on the reaction was investigated at 10 bar total pressure (5% O_2) and 0.5 mol% catalyst (Table 5.3). As observed previously for the influence of catalyst loading and pressure, no significant changes in product selectivity were observed. Activities clearly increase with increasing temperature, although the mole balances do decrease somewhat with increasing conversion.

At first glance, the observed activities appear to increase approximately linearly with temperature, which is attributed to the rather narrow absolute temperature interval which was measured. To better interpret the dependence of the rate as a function of temperature, the data was plotted in the form of the Eyring-Polanyi equation (Eq 1, Figure 5.4):

$$\ln \frac{k}{T} = -\frac{\Delta H^{\#}}{R}\frac{1}{T} + \ln \frac{k_b}{h} + \frac{\Delta S^{\#}}{R} \tag{1}$$
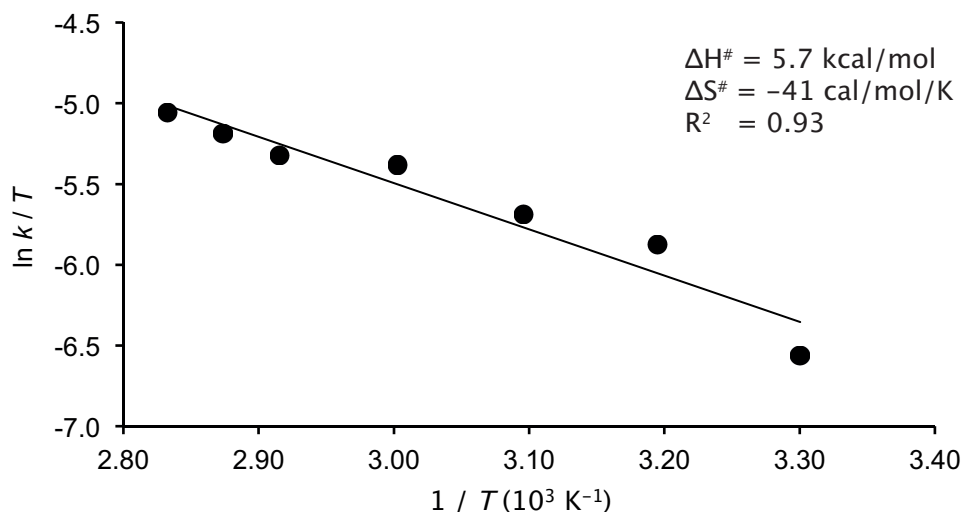
Figure 5.4: Temperature dependence of the reaction rate of catechol intradiol dioxygenation expressed as an Eyring-Polanyi plot and the derived thermodynamic parameters.

Table 5.3: Results of the catalytic dioxygenation of catechol using different temperatures.[a]

	T^b (° C)	C^c (%)	TOF^d (h^{-1})	MB^e (%)	Yield 2 + 3 (%)		
					a	b	c
1	30	21	8	94	1	14	0
2	40	45	16	91	3	25	4
3	50	43	20	98	4	33	2
4	60	75	28	84	4	45	5
5	70	84	30	76	7	53	0
6	75	96	35	76	6	62	2
7	80	96	40	87	8	69	3
8	80^f	63	120	86	4	41	2

[a] Conditions: 27.2 mmol catechol, 0.5 mol% catalyst (1 eq $Fe(NO_3)_3$, 1 eq TPA, 2 eq NH_4OAc), 300 mL MeOH, 10 bar (5% O_2), 800 sccm gas flow, 4 h [b] Temperature [c] Conversion [d] Turnover frequency [e] Mole balance as moles of C_6 units found (including unconverted catechol) divided by starting amount of catechol as determined by ^1H NMR [f] 0.1 mol% catalyst, 25 bar pressure

From the slope and intercept, the standard enthalpy and entropy of activation were determined to be 5.7 kcal/mol and -41 cal mol^{-1} K^{-1}, respectively. The large negative entropy of activation can be attributed to the binding of oxygen to the active catalyst complex, which is also not very favourable in terms of enthalpy and is thus an important limiting factor in the reaction rate. This high $\Delta S^{\#}$ is also in good agreement with the computational study of this system as described in Chapter 6, where an entropy of activation of -43 cal mol^{-1} K^{-1} was found. Nevertheless, increasing the temperature from 30 °C to 80 °C afforded a five-fold increase in the reaction rate.

5.2.4 Improved Conditions

Having investigated catalyst loading, pressure and temperature separately, appropriate parameters were selected for obtaining maximal activity in the system. Combining a low catalyst loading (0.1 mol%) with high pressure (25 bar) and high temperature (80 °C), a TOF of 120 h^{-1} and a turnover number of 480 (Table 3, #8) could be attained, which is a 35-fold improvement over the best results reported in Chapter 4.

5.2.5 Hydrogenation and Transesterification

For the investigation of the subsequent hydrogenation and transesterification steps to obtain dimethyl adipate, product mixtures were prepared from 3 g of catechol, using a standard oxidative cleavage condition, i.e. 4 h reactions with 0.5 mol% catalyst at 25 bar pressure and 80 °C to ensure full conversion of catechol. After isolation, a mixture of products is obtained as a solid in 85% yield (assuming an average molecular weight of
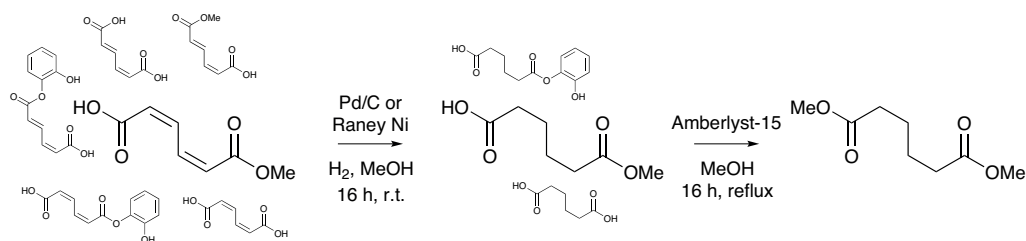
Figure 5.5: Reaction scheme for the hydrogenation and (trans)esterification of muconates derived from catechol intradiol dioxygenation, showing the convergent nature of the transformations.

156.14), with full conversion and **3b** as the dominant product. As the hydrogenation and transesterification step converge all products to dimethyl adipate, no further separation of the products is required nor performed.

The hydrogenation reaction (Figure 5.5) was investigated using commercially available catalysts. Raney® nickel is a cheap and readily available hydrogenation catalyst, although often elevated temperatures and hydrogen pressures are necessary to obtain good activity. Nevertheless, the mixtures were hydrogenated over Raney® nickel at very mild conditions (16 h, 1 bar H_2, room temperature), although some half-hydrogenated muconic acid products (including the 3-ene isomer) were identified based on their ^{1}H NMR signals. After simple filtration to remove the catalyst, the ^{1}H NMR signals of the products were found to be extremely broad, suggesting the presence of paramagnetic species, possibly as Ni^{2+} carboxylates, in the sample. An additional acid wash step was thus required to obtain a clean hydrogenated mixture, after which the adipates were isolated in 57% yield.

A commercial palladium on carbon catalysts also readily hydrogenates the muconic acid mixture under the same mild conditions. Reflecting the higher activity of carbon-supported palladium, only fully hydrogenated products were obtained in near quantitative yield. As no half-hydrogenated products are observed in this case, this method is preferred for the hydrogenation. Nevertheless, in an industrial setting where more severe conditions to reach full conversion would not be limiting, the use of cheaper Raney® nickel may be viable.

The transesterification of the hydrogenated acid mixture with methanol was in the previous chapter successfully performed using *p*-toluenesulphonic acid as catalyst. Using a commercially available heterogeneous solid acid catalyst (Amberlyst-15) in refluxing methanol both free acids and catechol esters could be (trans)esterified, to obtain dimethyl adipate. Purification by vacuum distillation (14 mbar, 80-105 °C) then affords highly pure dimethyl adipate in 62% overall yield. Analysis of the tarry distillation residue showed significant quantities of dimethyl adipate to be still present, which could not be recovered given the rather small scale on which the distillation was performed.

Furthermore, the distillation residue still contained the catechol liberated by transesterification of the catechol esters, which thus in principle could be recycled for another oxidation reaction.

Consequently, the main losses in the conversion of catechol to dimethyl adipate using our three-step route seem to occur by the radical oxidation of catechol during the first oxidation step, while hydrogenation and transesterification occur essentially quantitatively. Better recovery of the dimethyl adipate during the final step is rather a technical problem, which should be easily solved by better design of the distillation setup.

5.3 Conclusions

The catalytic dioxygenation of catechol to derivatives of *cis,cis*-muconic acid using 5% oxygen in nitrogen, using a catalyst prepared *in situ* from iron(III) nitrate, tris(2-pyridylmethyl)amine and ammonium acetate was demonstrated. The reaction was shown to proceed at catalyst loadings as low as 0.1 mol% and activity was shown to be approximately linear with respect to oxygen. Investigating the temperature dependence of activity, a high entropy of activation was found, consistent with the need of oxygen to bind the active iron(III) catecholate complex. Nevertheless, an increase in temperature from 30 °C to 80 °C afforded a five-fold increase in reaction rate and a turnover frequency of 120 h^{-1} could be obtained.

Subsequent hydrogenation and transesterfication of the afforded muconic acid mixtures proceeded efficiently over commercially available hydrogenation and solid acid catalysts. After vacuum distillation, pure dimethyl adipate could be recovered in 62% yield from the catechol starting material, thus demonstrating a sustainable synthesis of this high volume Nylon monomer.

To further improve dimethyl adipate yields, it will be important to reduce the amount of catechol lost to the non-productive radical oxidation. In addition, efficient separation and recycling of the iron catalyst, for example by heterogenisation, will enable a truly sustainable method for the production of dimethyl adipate.

5.4 Acknowledgements

5.5 Experimental

Materials. Catechol (99+%) and iron(III) nitrate nonahydrate (98+%) were purchased from Acros. Ammonium acetate (HPLC grade) was obtained from Fisher Scientific. Iron(III) oxalate hexahydrate, 1-dodecanol (98%), Raney® nickel (Raney® 4200), palladium supported on carbon (5% wt Pd) and Amberlyst-15 (dry, acid form) were obtained from Sigma Aldrich. Methanol (p.a. grade) was obtained from Merck. Compressed air (4.0) and nitrogen (5.0) were obtained from Linde Gas. All chemicals were used as received. Tris(2-pyridylmethyl)amine was synthesised according to a previously published procedure[29] and crystallised from boiling hexanes.

Physical Measurements. NMR spectra were recorded on a Varian spectrometer operating at 400 MHz (^{1}H) or 100 MHz (^{13}C) in DMSO-d6 (unless mentioned otherwise) and referenced against the signal of the residual protio impurity of the solvent (2.50 ppm). GC-MS measurements were performed on a Shimadzu GC-2010 using a VF5-ms column, coupled to a Shimadzu GCMS-QP2010 mass spectrometer.

Catalytic Studies. Catalytic oxidation reactions were carried out in a fed-batch 500 mL stainless steel autoclave reactor setup (Autoclave Engineers SA182-F316, rated up to 254 bar at 450 °C). Gas inlet was controlled by Brooks mass flow controllers and gas outlet by a needle valve to maintain a constant pressure. The effluent gas was cooled by a reflux condenser in order to minimise solvent losses.

In a typical experiment, the autoclave was charged with catechol (3.00 g, 27.2 mmol), aliquots of stock solutions of iron(III) nitrate (0.136 mmol), tris(2-pyridylmethyl)amine (0.136 mmol) and ammonium acetate (0.272 mmol), 1-dodecanol as internal standard (3.00 g, 16.1 mmol) and methanol (300 mL). The autoclave was sealed, purged with nitrogen and heated to a stable operating temperature. Oxygen was introduced by mixing compressed air with nitrogen (800 sccm gas flow, 5 vol% oxygen), marking the start of the reaction. After 4 h, gas flow was switched to pure nitrogen and the reactor was cooled to room temperature. A 1 mL sample was partitioned over 5 mL 1 M HCl and 5 mL diethyl ether. The organic layer was separated and the aqueous phase extracted two more times with 5 mL diethyl ether. The combined organic layers were dried over magnesium sulphate, filtered and concentrated *in vacuo*. The residual oil was dissolved in DMSO-d6 and analysed by NMR spectroscopy. Products were quantified by their previously identified characteristic chemical shifts. Turnover frequencies were determined by taking the total molar yield of intradiol cleavage and dividing by catalyst amount and reaction time. The k values (for use in the Eyring-Polanyi equation) were obtained by dividing the turnover frequency (in s^{-1}) by the oxygen concentration, which based on Henry's law and the solubility of oxygen in methanol was assumed to be 0.5 mM at 10 bar total pressure.[41]

Products for further hydrogenation and transesterification were prepared as above (at 80 °C and 25 bar pressure), but 1-dodecanol was omitted from the reaction mixture. After reaction, the methanol solution was concentrated to ca. 75 mL and partitioned over 100 mL 1 м HCl and 100 mL diethyl ether. The organic layer was separated and the aqueous phase extracted two more times with 100 mL diethyl ether. The combined organic layers were dried over magnesium sulphate, filtered and concentrated *in vacuo* to obtain 3.86 g of brown oil, which solidified upon standing.

In a typical hydrogenation experiment, the brown solid (3.86 g) obtained as above was dissolved in 50 mL methanol in a Schlenk flask under argon atmosphere. Palladium on carbon (5 wt% Pd,

0.203 g) was added and the flask brought at 1 bar hydrogen pressure by use of a gas balloon. After stirring for 16 h, the Pd/C catalyst was removed by centrifugation and filtration. The solution was concentrated *in vacuo* to obtain 3.82 g of brown oil, which based on the ^{1}H NMR spectrum consists exclusively of hydrogenated products.

In a typical transesterification experiment the oil as obtained above (3.82 g) was dissolved in 50 mL methanol. Amberlyst-15 (0.516 g) was added and the mixture refluxed for 22 h under nitrogen atmosphere. After cooling, the Amberlyst beads were removed by filtration and the solution concentrated to obtain abrown oil, which based on the ^{1}H NMR spectrum contained predominantly dimethyl adipate. Fractional vacuum distillation (14 mbar, 87 °C - 110 °C) afforded dimethyl adipate (2.92 g, 17.2 mmol, 62%) as a pale yellow oil: ^{1}H NMR: ∂ 3.58 (6H, s), 2.31 (4H, m), 1.52 (4H, m); ^{13}C NMR: ∂ 173.2, 51.16, 32.90, 23.86; GC-MS: m/z 143 (38), 114 (74), 111 (48), 101 (59), 59 (100), 55 (79). ^{1}H NMR analysis of the tarry distillation residue showed that it still contained a significant quantity of dimethyl adipate.

Computational Methods. Density functional theory (DFT) calculations were performed with the Amsterdam Density Functional (ADF 2013.01) package[42-44], using the BP86 functional[45,46] and the triple zeta slater orbital basis set with polarisation functions (TZP) that is included with ADF.[47] Energies were corrected for solvation using the conductor-like screening model (COSMO)[48] and for dispersion interactions using Grimme's DFT-D3 dispersion correction[49] with Becke-Johnson damping.[50] All structures were subjected to geometry optimizations without any constraints followed by a full analytical frequency calculation. All reported structures were characterized by no (minima) or one (transition states) imaginary frequencies. Energies reported are Gibbs free energies at 25 °C relative to the monomethyl *cis,cis*-muconate anion.

5.6 References

1   F. Cavani and S. Alini, in *Sustainable Industrial Chemistry*, Wiley-VCH Verlag GmbH & Co. KGaA, Weinheim, Germany, 2009, pp. 367–425.

2   A. Castellan, J. C. J. Bart and S. Cavallaro, *Catal. Today*, 1991, **9**, 237–254.

3   V. Hessel, I. Vural Gürsel, Q. Wang, T. Noël and J. Lang, *Chem. Eng. Tech.*, 2012, **35**, 1184–1204.

4   A. Castellan, J. C. J. Bart and S. Cavallaro, *Catal. Today*, 1991, **9**, 255–283.

5   R. A. Reimer, C. S. Slaten, M. Seapan, M. W. Lower and P. E. Tomlinson, *Environ. Prog.*, 1994, **13**, 134–137.

6   S. Van de Vyver and Y. Roman-Leshkov, *Catal. Sci. Technol.*, 2013, **3**, 1465–1479.

7   K. Sato, M. Aoki and R. Noyori, *Science*, 1998, **281**, 1646–1647.

8   M. Faber, US Patent 4,400,468, 1983.

9   P. K. Wong, C. Li, L. P. Stubbs, M. van Meurs, D. G. Anak Kumbang, S. C. Y. Lim, and E. Drent, International Patent Application WO 2012/134397 A1, 2012.

10   K. M. Draths and J. W. Frost, *J. Am. Chem. Soc.*, 1995, **117**, 2395–2400.

11   J. Zakzeski, P. C. A. Bruijnincx, A. L. Jongerius and B. M. Weckhuysen, *Chem. Rev.*, 2010, **110**, 3552–3599.

12   V. M. Roberts, V. Stein, T. Reiner, A. Lemonidou, X. Li and J. A. Lercher, *Chem. Eur. J.*, 2011, **17**, 5939–5948.

13   J. Zakzeski, A. L. Jongerius, P. C. A. Bruijnincx and B. M. Weckhuysen, *ChemSusChem*, 2012, **5**, 1602–1609.

14   Q. Song, F. Wang, J. Cai, Y. Wang, J. Zhang, W. Yu and J. Xu, *Energy Environ. Sci.*, 2013, **6**, 994–1007.

15   A. Baeyer, *Chem. Ber.*, 1875, **8**, 153–155.

16   W. H. Perkin, *J. Chem. Soc., Trans.*, 1890, **57**, 587–589.

17   S. B. Waghmode, G. Mahale, V. P. Patil, K. Renalson and D. Singh, *Synth. Commun.*, 2013, **43**, 3272–3280.

18   H. D. Dakin, H. T. Clarke and E. T. Taylor, *Org. Synth.*, 1923, **3**, 28.

19   K. Barta, G. R. Warner, E. S. Beach and P. T. Anastas, *Green Chem.*, 2014, **16**, 191–196.

20   T. D. H. Bugg, *Tetrahedron*, 2003, **59**, 7075–7101.

21   F. H. Vaillancourt, J. T. Bolin and L. D. Eltis, *Crit. Rev. Biochem. Mol. Biol.*, 2006, **41**, 241–267.

22   M. Costas, M. P. Mehn, M. P. Jensen and L. Que Jr., *Chem. Rev.*, 2004, **104**, 939–986.

23   P. C. A. Bruijnincx, G. van Koten and R. J. M. Klein Gebbink, *Chem. Soc. Rev.*, 2008, **37**, 2716.

24   M. W. Vetting and D. H. Ohlendorf, *Structure*, 2000, **8**, 429–440.

25   D. D. Cox and L. Que Jr., *J. Am. Chem. Soc.*, 1988, **110**, 8085–8092.

26   W. O. Koch and H.-J. Krüger, *Angew. Chem. Int. Ed.*, 1995, **34**, 2671–2674.

27   R. Yamahara, S. Ogo, H. Masuda and Y. Watanabe, *J. Inorg. Biochem.*, 2002, **88**, 284–294.

28   H. G. Jang, D. D. Cox and L. Que Jr., *J. Am. Chem. Soc.*, 1991, **113**, 9200–9204.

29   G. J. P. Britovsek, J. England and A. J. P. White, *Inorg. Chem.*, 2005, **44**, 8125–8134.

30   H. F. Coward and G. W. Jones, *Bureau of Mines Bulletin*, 1952, **503**, 1–154.

31   B. M. Trost and P. G. McDougal, *J. Org. Chem.*, 1984, **49**, 458–468.

32   S. Seltzer and J. Hane, *Bioorg. Chem.*, 1988, **16**, 394–407.

33   M. G. Weller and U. Weser, *J. Am. Chem. Soc.*, 1982, **104**, 3752–3754.

34   M. Pascaly, M. Duda, F. Schweppe, K. Zurlinden, F. K. Müller and B. Krebs, *J. Chem. Soc., Dalton Trans.*, 2001, 828–837.

35   J. A. Elvidge, R. P. Linstead, P. Sims and B. A. Orkin, *J. Chem. Soc.*, 1950, 2235.

36   G. E. K. Branch and M. A. Joslyn, *J. Am. Chem. Soc.*, 1935, **57**, 2388–2394.

37   C. R. Dawson and J. M. Nelson, *J. Am. Chem. Soc.*, 1938, **60**, 245–249.

38   N. Schweigert, A. J. B. Zehnder and R. I. L. Eggen, *Environ. Microbiol.*, 2001, **3**, 81–91.

39   Y. Hitomi, M. Yoshida, M. Higuchi, H. Minami, T. Tanaka and T. Funabiki, *J. Inorg. Biochem.*, 2005, **99**, 755–763.

40   M. Higuchi, Y. Hitomi, H. Minami, T. Tanaka and T. Funabiki, *Inorg. Chem.*, 2005, **44**, 8810–8821.

41   C. B. Kretschmer, J. Nowakowska and R. Wiebe, *Ind. Eng. Chem.*, 1946, **38**, 506–509.

42   C. F. Guerra, *Theor. Chem. Acc.*, 1998, **99**, 391–403.

43   G. te Velde, F. M. Bickelhaupt, E. J. Baerends, C. Fonseca Guerra, S. J. A. van Gisbergen, J. G. Snijders and T. Ziegler, *J. Comp. Chem.*, 2001, **22**, 931–967.

44   ADF2013, SCM, Theoretical Chemistry, Vrije Universiteit, Amsterdam, The Netherlands, http://www.scm.com

45   J. Perdew, *Phys. Rev. B*, 1986, **33**, 8822–8824.

46   A. D. Becke, *Phys. Rev. A*, 1988, **38**, 3098–3100.

47   E. Van Lenthe, *J. Comp. Chem.*, 2003, **24**, 1142–1156.

48   C. C. Pye and T. Ziegler, *Theor. Chem. Acc.*, 1999, **101**, 396–408.

49   S. Grimme, J. Antony, S. Ehrlich and H. Krieg, *J. Chem. Phys.*, 2010, **132**, 154104.

50   S. Grimme, S. Ehrlich and L. Goerigk, *J. Comp. Chem.*, 2011, **32**, 1456–1465.

Chapter 6

Experimental and Computational Evidence for the Mechanism of Catechol Dioxygenation by Non-Heme Iron(III) Complexes

Abstract

The iron(III)-catalysed catechol intradiol dioxygenation developed in the previous chapter is a remarkable reaction. The mechanism of dioxygen activation of this system is however controversial. Using a combination of kinetic measurements and computational modelling of multiple iron(III) catecholato complexes, the catechol cleavage mechanism is elucidated. Oxygen binds the iron centre by partial dissociation of the substrate from the iron complex. The formed iron(III) superoxide complex subsequently attacks the carbon atom of the substrate via a rate-determining C–O bond formation step. The mechanism explains the effect of ligand and substrate structure on activity and is therefore relevant for the development of novel catalysts and improved understanding of the related enzymes.
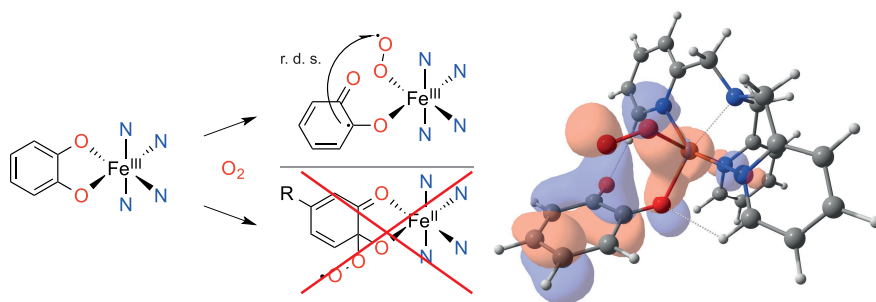
The work described in this chapter was published in:

6.1 Introduction

Enzymatic oxidation of catechols is a key step in catabolic pathways for the decomposition of aromatics. Three classes of enzymes are known: catechol oxidases oxidise the substrate to the corresponding quinone in a two-electron process at a copper active site. Extradiol dioxygenases feature an iron(II) active site and insert molecular oxygen adjacent to the hydroxyl functionalities to afford muconic semialdehydes. Intradiol dioxygenases, finally, cleave the C-C bond between the two hydroxyl functionalities of catecholic substrates, to yield derivatives of *cis,cis*-muconic acid.[1-4] The latter reaction has been shown to proceed at a mononuclear iron(III) centre with molecular oxygen as the oxidant.[5-7] Bio-inspired iron(III) complexes featuring various tetradentate donor ligands, of which tris(2-pyridylmethyl)amine (TPA) is the most active, were also found capable of selective intradiol catechol dioxygenation.[8-10] Such systems do not only provide additional insight into the enzymatic processes, but are also useful for the biodegradation of (chlorinated) aromatic compounds[11,12] and, as we have described in the previous chapters, may provide a sustainable, catalytic route for the production of the nylon feedstock adipic acid.

The catalytic mechanism of both the enzymes and biomimetic compounds is currently surrounded by major controversies due the fact that most oxygen-bound intermediates have a short lifetime and have not been trapped or characterised experimentally. Currently, two proposed mechanisms seem to support experimental product distributions and isotope effects: dioxygen can attack the substrate directly and subsequently react via a Criegee rearrangement or, alternatively, bind the iron(III) center prior to substrate attack and O–O bond homolysis (Figure 6.1).[13]
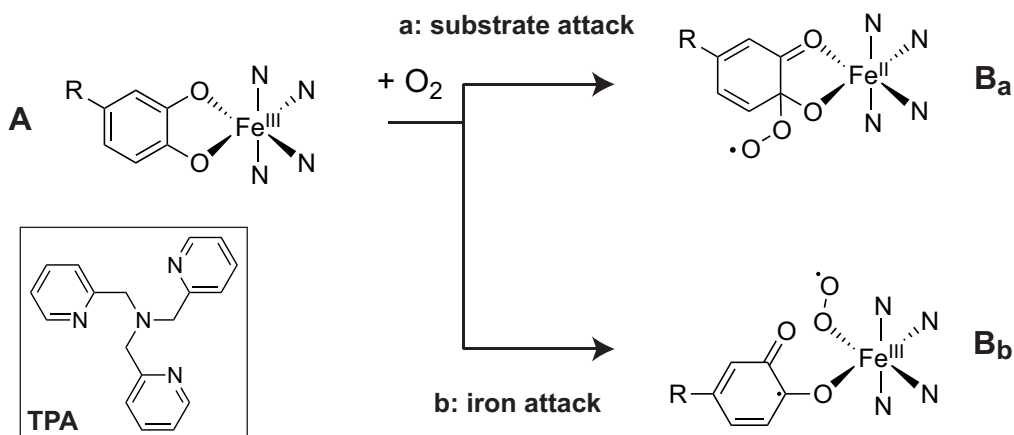

Figure 6.1: Two mechanistic possibilities of oxygen attack on an iron(III)-catecholato complex, the key step in intradiol dioxygenation.

The 'substrate activation' mechanism was first proposed by Que *et al.*[8,14] to explain the reactivity of (coordinatively saturated) catecholato complexes towards oxygen. A partial reduction of the catecholate to a semiquinone radical was suggested to enable direct electrophilic attack by oxygen on the substrate (pathway *a* in Figure 6.1). Such a mechanism would explain the persistence of the iron(III) state during reaction that is seen by EPR and accounts for the observation that even coordinatively saturated bio-inspired complexes show oxidative cleavage activity. Interestingly, the enzyme (1*H*)-3-hydroxy-4-oxoquinaldine 2,4-dioxygenase catalyses intradiol dioxygenation *without* the use of a transition metal co-factor by direct attack of molecular oxygen on the substrate,[15] which would support a mechanism analogous to pathway *a*. However, more recently an 'oxygen activation' mechanism has been proposed,[16,17] wherein oxygen must first bind to the iron(III) center instead (pathway *b* in Figure 6.1). Better understanding of this key mechanistic step and the function of the metal centre in catalysis will improve our understanding of the enzymatic reactions and allow for the development of more active bio-inspired systems. Therefore a detailed combined experimental and computational study was conducted, which provides evidence that oxygen binds the iron centre prior to substrate activation and that the rate-determining step involves C–O bond formation.

6.2 Results

To elucidate the catalytic mechanism and, in particular, the nature of the dioxygen binding step, kinetic measurements for stoichiometric intradiol dioxygenation by *in-situ* prepared iron(III) complexes were performed. Pseudo first-order rate constants (Table 6.1) could be conveniently obtained by monitoring the decay of the catecholate-to-iron charge transfer band at ca. 800 nm (Figure 6.2). Iron complexes were prepared with TPA and the novel TPA-derivative tris(4-chloro-2-pyridylmethyl)amine (Cl$_3$-TPA) and

Table 6.1: Spectroscopic data of *in-situ* prepared iron(III) catecholate complexes and corresponding rate constant for catechol dioxygenation.

Ligand	Catechol	λ_{max1} (nm) [a]	λ_{max2} (nm) [a]	k (s^{-1} M^{-1})
TPA	4-bromo	791 (3300)	502 (2300)	0.0262
TPA	4-chloro	791 (3100)	500 (2100)	0.0336
TPA	4-fluoro	810 (2900)	496 (1900)	0.293
TPA	pyro	804 (2600)	510 (2000)	0.221
TPA	4-methyl	843 (2900)	537 (2100)	3.85
TPA	4-*tert*-butyl	866 (3200)	538 (2200)	3.41
Cl$_3$-TPA	4-chloro	827 (2900)	516 (2100)	0.0550
Cl$_3$-TPA	pyro	834 (2700)	537 (2200)	0.330

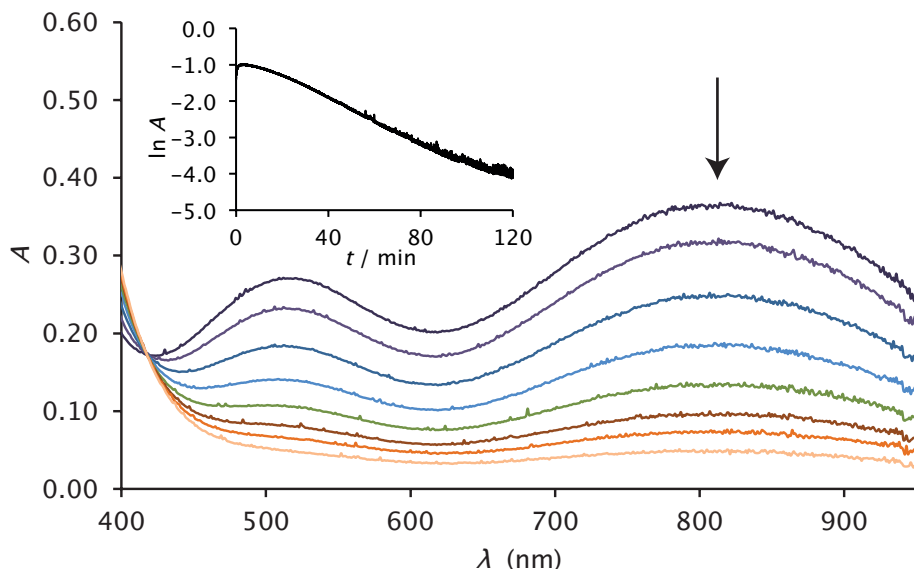[a] Extinction coefficients (M^{-1} cm^{-1}) in parentheses.

Figure 6.2: UV-Vis spectra of the iron(III) TPA catecholato complex, showing a decrease in intensity of the charge transfer bands over time (inset: ln A at 804 nm vs. time).

p-substituted catechols. As also previously observed, complexes of more electron-donating catechols and more electron-withdrawing ligands were more active.[9,16,17]

A Hammett analysis of the rate data already provided initial mechanistic information (Figure 6.3). As the reaction may proceed at the carbon atom *meta* or *para* to the substituent, fits were first attempted against both parameters σ_m and σ_p^+,[18] with the latter giving a considerably better fit. The ambiguity of the *meta* and *para* positions in this system, however, requires scaling of the resonance and field components of the Hammett parameter using the Swain-Lupton parameters for *para* substituents.[18,19] An excellent fit is obtained with a value of $\alpha = 1.14$, indicating a slightly stronger inductive effect than expected for a pure *para* substituent. The strongly negative value of the reaction constant $\rho = -4.33$ indicates a transfer of negative charge away from the catecholate moiety in the rate-determining step, which implies that the rate-determining step involves an electrophilic attack of oxygen on the catecholate moiety. However, this information alone does not allow one to discriminate yet between pathways *a* and *b*.

To gain better understanding of the mechanism of catechol intradiol dioxygenation by the iron(III) complexes, a set of density functional theory (DFT) calculations were ran following methods previously tested and benchmarked on analogous systems.[20,21] Geometry optimisation of the iron(III) catecholato complex (**⁶A**) revealed carbon-oxygen bond lengths of 1.34 Å and 1.35 Å, which are consistent with the reported crystal
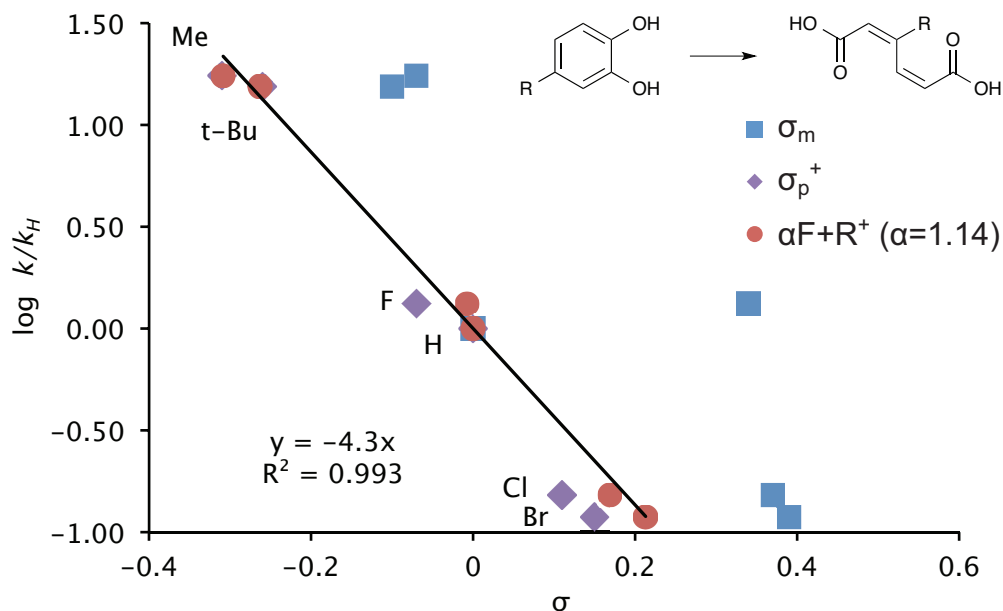
Figure 6.3: Hammett plot for the rate of intradiol dioxygenation by the iron(III) TPA complex with different catechols, using different Hammett parameters: for *meta* substituents (blue square), *para* substituents (purple diamond) and using a scaled field and resonance effect with the Swain-Lupton equation[18,19] ($\alpha = 1.14$) (red dots). With the latter, an excellent fit is obtained.

Table 6.2: Spins and charges on the iron (TPA) catechol complexes.

	Mulliken Spin				Natural Charge			
	Fe	TPA	Cat	O_2	Fe	TPA	Cat	O_2
^6A	4.05	0.12	0.82		1.23	0.71	-0.94	
^4B_a	3.79	0.07	0.13	-0.98				
^4B_b	3.62	0.22	0.51	-1.35	1.05	0.66	-0.36	-0.35
$^4B_b'$	3.98	0.09	0.43	-1.51				
$^4TS1_b$	3.07	0.13	0.14	-0.34	0.95	0.91	-0.28	-0.59
^4C_b	2.74	0.13	0.12	0.01	0.88	1.01	-0.19	-0.69
$^4C_b'$	2.60	0.12	0.15	0.13				
	Fe	TPA	CatO	=O	Fe	TPA	CatO	=O
^4C_b	2.739	0.133	0.093	0.036	0.879	1.006	-0.530	-0.354
$^4TS2_b$	3.017	0.144	-0.445	0.285				
^4D_b	3.099	0.100	-0.781	0.581				
$^4TS3_b$	1.401	-0.089	0.902	0.785				
^4E_b	2.622	-0.096	-0.010	0.485				
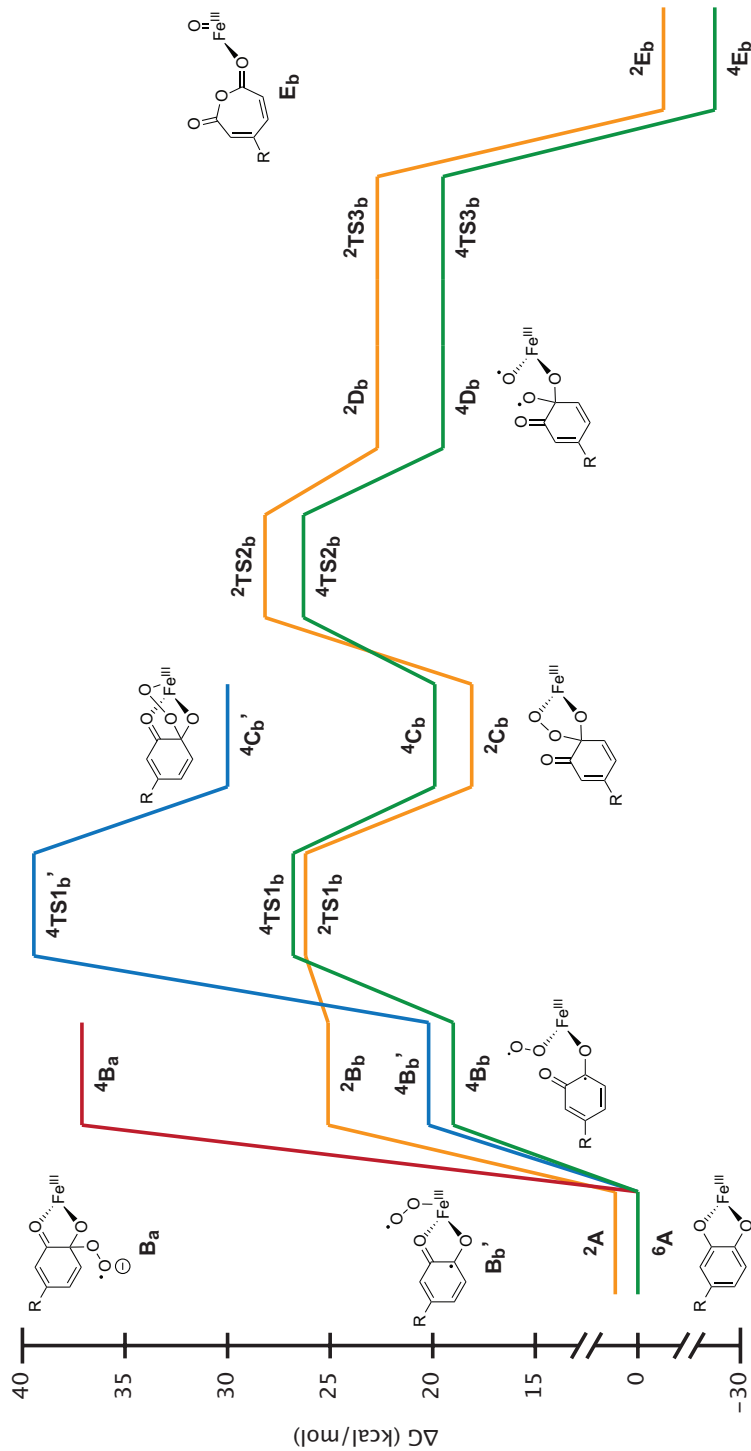
Figure 6.4: Free energy landscape for the dioxygenation of catechol (R = H) by the iron(III) complex of TPA. The pathway with direct substrate attack by oxygen (red) was found to be inaccessible. Oxygen attack on the iron center was found to be more favourable if the substrate (quartet: green, doublet: yellow), rather than the ligand (blue), partially dissociated.

structure coordinates.[22] The sextet spin state was found to be the electronic ground state at room temperature, with the doublet (^{2}**A**) state being more stable at 0 K. This is in excellent agreement with the experimentally observed spin-crossover behavior.[23] While there is significant spin density on the catecholate moiety (0.82, Table 6.2), it is primarily located on the oxygen atoms, originating from a covalent interaction between the catecholate π^* and iron t_{2g} orbitals. Thus, based on the bond lengths and spin densities, the catecholate moiety does not appear to have the semiquinone character that is required for pathway *a*.

We then focused on the relative energies of oxygen adducts **B**$_a$ and **B**$_b$ (Figure 6.4) and ran geometry optimisations for all low-lying spin states (i.e., doublet, quartet and sextet). Importantly, no stable local minimum could be found on any of the spin state surfaces for structure **B**$_a$ as all attempts relaxed to structure **A** (and unbound oxygen) instead; attempts to attain a minimum starting from structures further on in the mechanism likewise failed (Figure 6.5) As a last resort, constrained geometry optimisation with fixed C–O distance converged to a structure that was >30 kcal/mol higher in energy than ^{6}**A**. In addition to structure **B**$_b$, we also considered a complex with the catecholate bound bidentately and TPA as a tridentate ligand (**B**$_b$'). In the quartet spin state, both **B**$_b$ and **B**$_b$' could be located and characterised as a high-spin iron(III) center anti-ferromagnetically
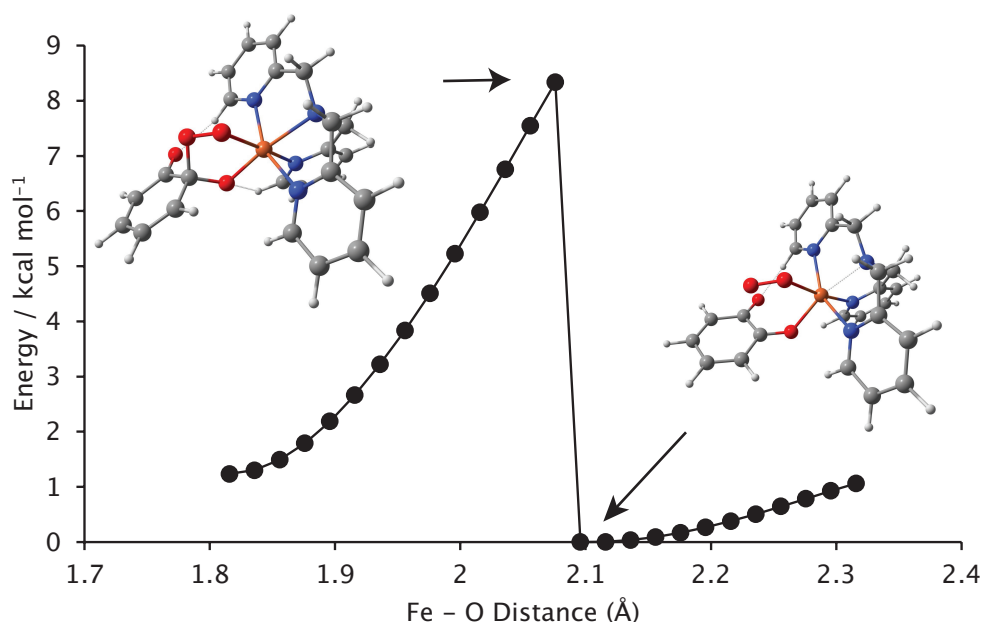

Figure 6.5: Increasing the Fe-O distance from ^{4}**C**$_b$ causes an increase in energy until ca. 2.09Å, where the most stable configuration is that the C-O bond between the catecholate and oxygen is broken, i.e. the ^{4}**B**$_b$ intermediate. Based on the principle of reversibility, this indicates that oxygen must first bind the iron center, before attack on the catecholate ring can occur.
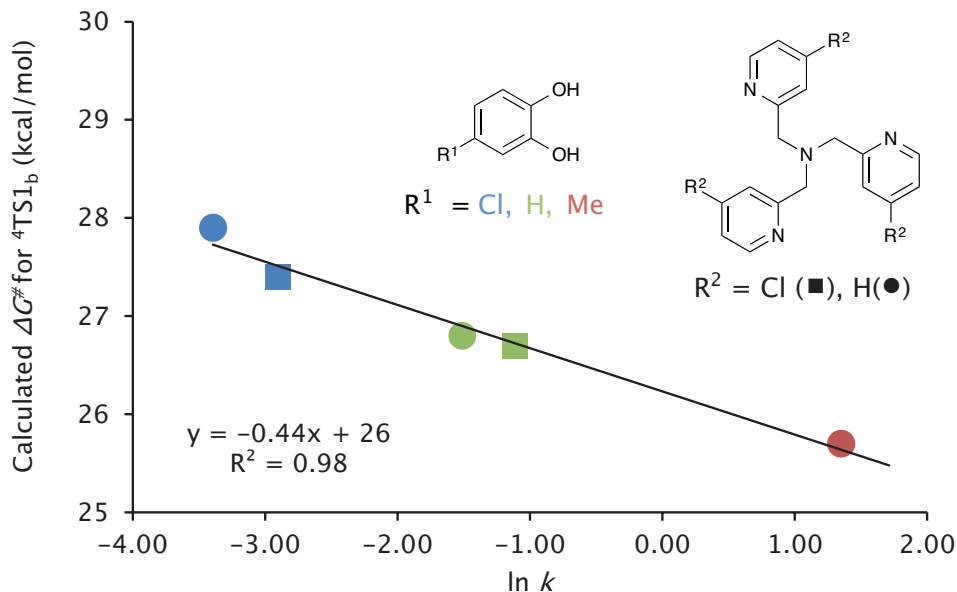
Figure 6.6: Excellent agreement is obtained between the natural logarithm of the experimentally determined rate constant and the calculated energy barrier.

coupled to a superoxide. As these states were found to be very close in free energy (within 1 kcal/mol), the activation barriers of C–O bond formation (**TS1**) leading to the peroxo-bridged intermediates **C**, were investigated for both, see Figure 6.4. Rather surprisingly, the transition state (26.8 kcal/mol vs. 39.2 kcal/mol) and peroxo intermediate (19.9 kcal/mol vs. 30.0 kcal/mol) were both found to be considerably more favourable if the catecholate was dissociated. Peroxo-bridged intermediates analogous to **C** have been proposed before in the catalytic cycles of catechol dioxygenases and other non-heme iron enzymes[24,25] and may undergo O–O bond homolysis. Homolytic O–O bond cleavage can indeed proceed through transition state ⁴**TS2** (26.3 kcal/mol) to form radical intermediate (⁴**D**) on the quartet spin state surface. The subsequent rearrangement to form the muconic anhydride product ⁴**E** via ⁴**TS3** then proceeds essentially barrierless. A similar mechanism can also occur on the doublet spin state surface, although the total barrier is higher.

Consequently, based on the computational results, the rate-determining step is predicted to involve ⁴**TS1** at 26.8 kcal/mol. Although this is somewhat high for the experimental rate constant of 0.2 M^{-1} s^{-1} it is likely that the entropic contribution for oxygen binding is systematically overestimated in our calculation. Having ⁴**TS1** as rate-determining step nevertheless is in agreement with the experimental results from the Hammett analysis, as it involves the electrophilic attack of oxygen on the catecholate moiety. To test

this hypothesis, the intermediates and transition states in the early part of the mechanism with other *p*-substituted catechols and/or TPA ligands were optimised as well. A comparison of the natural logarithm of the pseudo-first order rate constants with the calculated barrier ^{4}**TS1** shows an excellent correlation between the two (Figure 6.6), suggesting that our proposed mechanism is indeed valid.

Intermediates ^{4}**B**$_b$ and ^{4}**C**$_b$ seem to be key to improved understanding of the reactivity of the iron(III) catecholato complexes. Both intermediates retain a distorted octahedral coordination environment around the iron centre, with the dissociated catecholate arm stabilised by hydrogen bonding to an adjacent pyridine donor (Figure 6.7). Oxygen is bound *trans* to a pyridine *N* donor and already points at the reactive catecholate carbon in ^{4}**B**$_b$ (carbon-oxygen distance 2.505 Å). Interestingly, the catecholate moiety has been oxidised at this point to a semiquinone, as indicated by the shortening of one of the carbon-oxygen bonds to 1.27 Å, the decrease in natural charge as well as the observation that spin density is located primarily on the carbon atoms. The charge distribution, as well as the differences in charge between the different complexes (Figure 6.8), shows the oxidant to be not iron, but oxygen, which is reduced to a superoxide stabilised by σ-donation to the iron centre. To accommodate this formally spin-forbidden reaction, the iron centre acts as a buffer, accepting (down-spin) electron density from the catecholate in its t_{2g}-symmetry orbitals, while mixing up-spin density from the e_g orbitals into the oxygen π*. Such a transfer mechanism has been previously proposed by Solomon *et al.* for the enzymatic mechanism.[26] As the semiquinone π and oxygen π* orbitals now both are singly occupied and have good overlap, the carbon-oxygen bond can
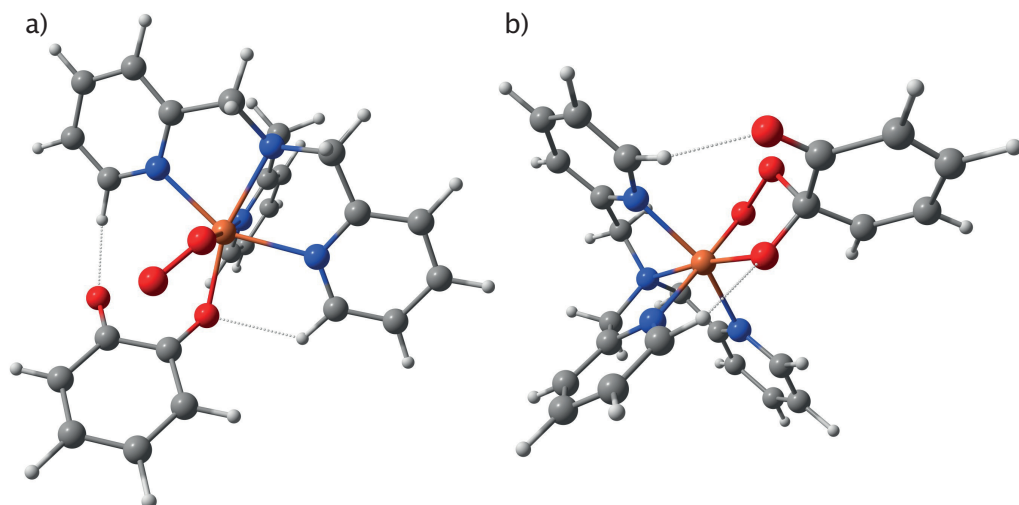

Figure 6.7: Geometry optimised structures of (a) ^{4}**B**$_b$ and (b) ^{4}**C**$_b$. Hydrogen bonding interactions are indicated with dotted lines.
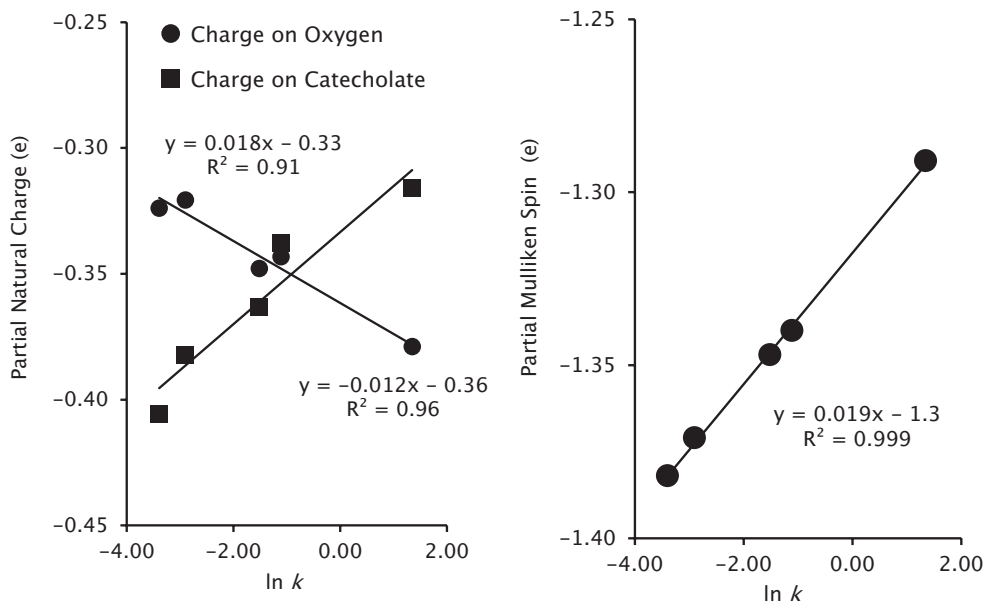
Figure 6.8: (left) Correlation between the natural logarithm of the rate constant against the charge on oxygen in $^4\mathbf{B_b}$. As the negative charge on oxygen increases, the negative charge on catecholate decreases, suggesting oxygen is reduced by the catecholate species, rather than the iron centre. (right) Correlation between the natural logarithm of the rate constant against the spin on oxygen in $^4\mathbf{B_b}$, indicating the importance of the reduction of oxygen by the catecholate moiety.

subsequently be formed by recombination of the anti-parallel electrons to obtain $^4\mathbf{C_b}$. In line with the principal role of iron as an electron buffer, its spin state has changed from a sextet state in $^6\mathbf{A}$ to a quartet state in $^4\mathbf{C_b}$. The electron transfer mechanism is schematically depicted in Figure 6.9.

Given the mechanism proposed, the influence of the substrate on reactivity can be clearly understood in terms of the energy level of the frontier catecholate π orbital, facilitating electron transfer away from the more electron-rich substrates. The influence of the ligand on the cleavage rate has, on the other hand, often been linked to the iron centre's Lewis acidity[9,11] for which the λ_{max} of the CT bands of the catecholato complexes were taken as a measure.[27] However, based on this mechanism the net electron transfer to or from iron is actually quite limited. Instead, the ligand field must be able to stabilise the quartet spin state to facilitate the oxidation of the catechol moiety by oxygen. Indeed, the symmetry of the TPA ligand is such that π-backbonding with all three pyridine donors involves only a single t_{2g} orbital, consequently lowering the energy of the quartet state. This increased backbonding is clearly strongest in the pyridine donor *trans* to oxygen, for which the Fe-N bond distance decreases from 2.14 Å to 2.00 Å going from $^6\mathbf{A}$ to $^4\mathbf{C_b}$. As this backbonding interaction will be stronger for more electron-withdrawing ligands,
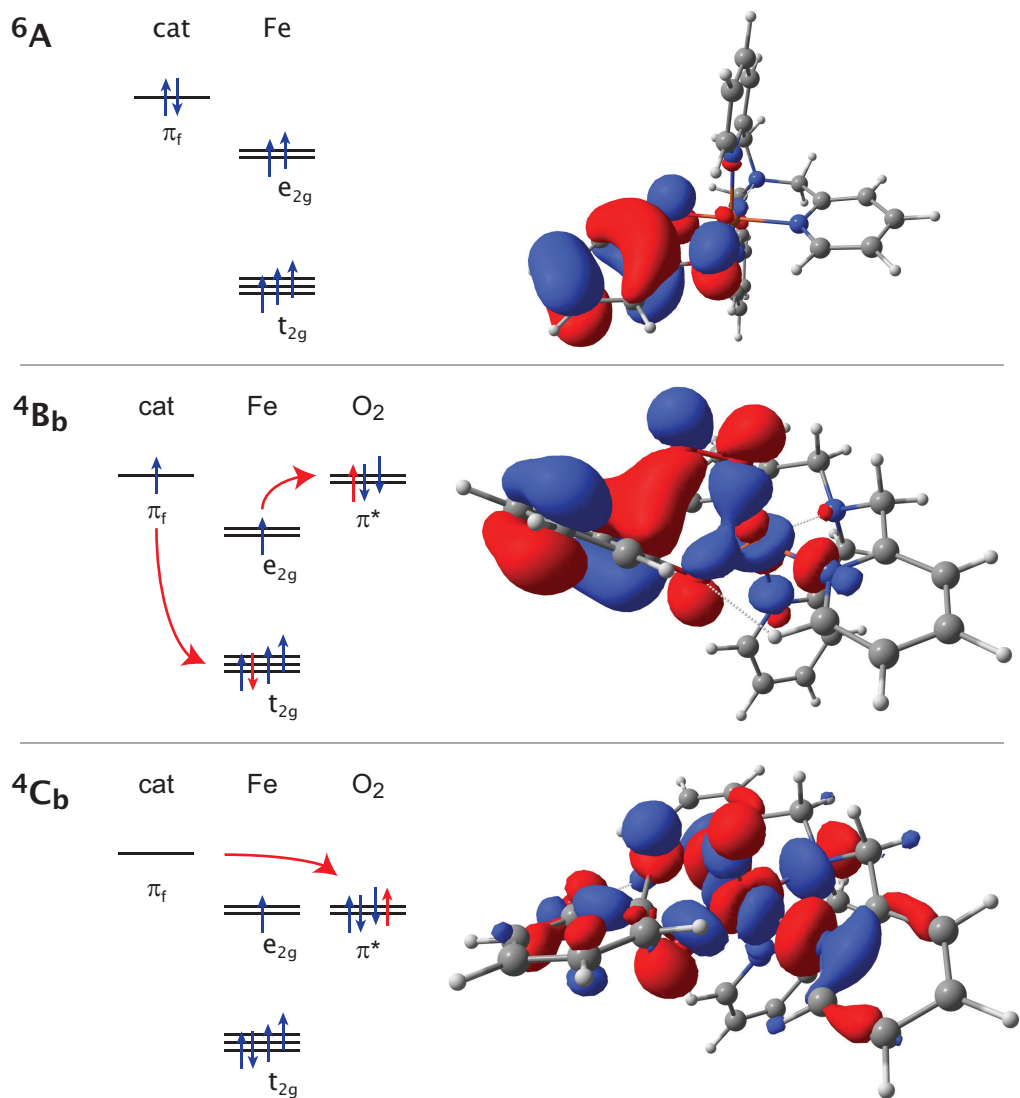
Figure 6.9: Simplified orbital diagrams of the states ^{6}A, ^{4}B$_b$ and ^{4}C$_b$. Red arrows indicate the electron transfers involved in their formation. Isosurfaces of the up-spin HOMOs are shown on the right.

the previously noted relationship between Lewis acidity of the iron centre and activity holds only for sets of ligands which have the same symmetry.[28,29] Thus, these results also provide insight into why ligands such as bispicen and bispidine, which at first sight might have electronic properties that seem well-suited for the reaction, show little intra-diol dioxygenation activity.[30,31] As evident from the crystal structures of the iron-cate-cholate complexes of these ligands (Figure 6.10), oxygen must bind *trans* to an aliphatic amine, if a similar mechanism is active. These aliphatic amine donors are clearly worse
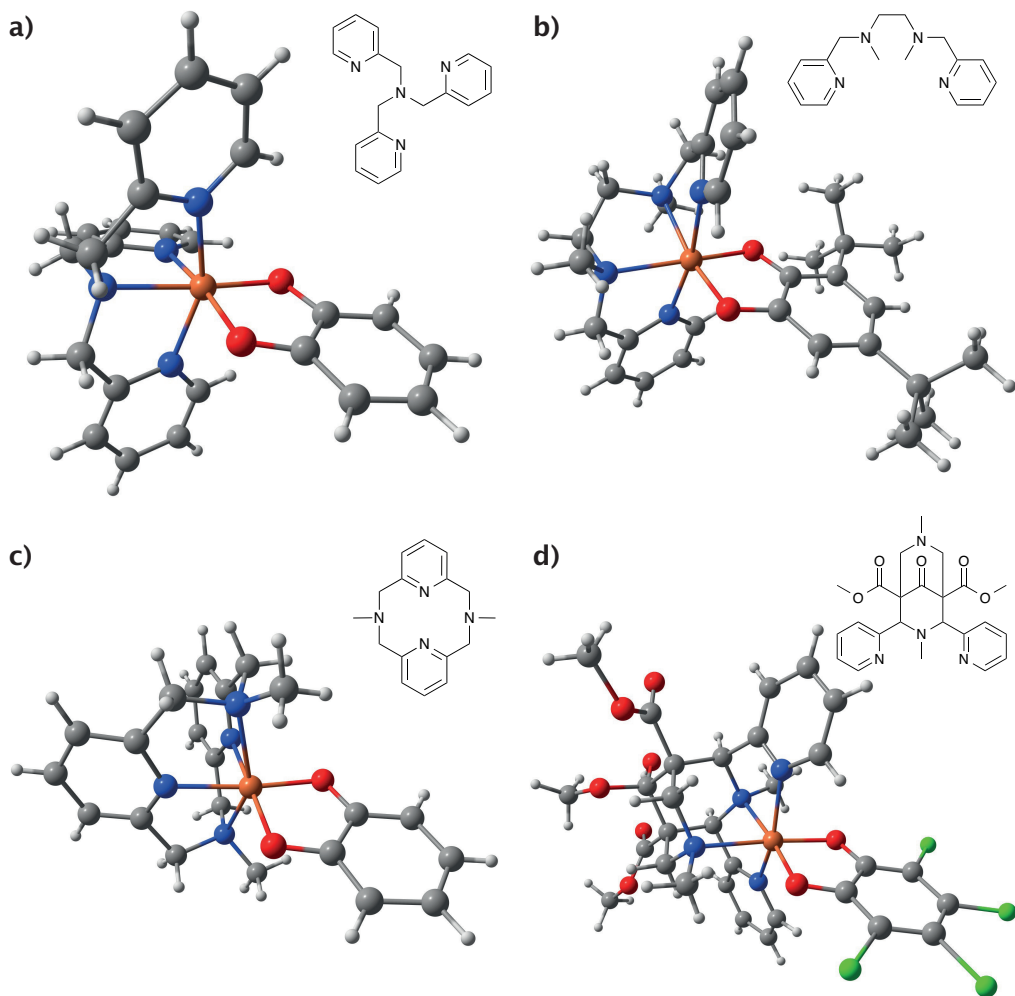
Figure 6.10: Structures of different ligands and three-dimensional structure of their iron (III) catecholate complexes based on reported crystallographic data: a) tris(2-pyridylmethyl-amine) (TPA)[23], b) Bispicen-derivative N,N'-Dimethyl-N,N'-bis(2-pyridylmethyl)-ethane-1,2-diamine (bispicMe₂en)[30], c) N,N'-Dimethyl-2,11-diaza[3.3](2,6)pyridino-phane[28], d) Bispidine[31]. In ligands **a** and **c**, dissociation of a catecholate arm can generate a binding site for oxygen trans to a pyridine donor and the combined π-backbonding interaction of the pyridine donor and oxygen stabilises the quartet state. On the other hand, in ligands **b** and **d**, oxygen must bind trans to an aliphatic amine, which shows no backbonding and thus also does not stabilise a quartet spin state.

ligands in terms of backbonding and in this geometry are unable to stabilise the quartet state. Furthermore, with bispicen[30] the two pyridine donors positioned *cis* to oxygen have their rings rotated 90° with respect to each other, and as a result the interaction with iron will involve two separate t$_{2g}$ orbitals, further reducing the stability of the quartet

state. This interpretation is further supported by an azacyclic system[28] (see Figure 6.10c) that shares the same *N* donor functionalities, but reacts two orders of magnitude faster. In this system, oxygen must bind *trans* to one of the pyridine donors, and the pyridine donors have the correct symmetry for interacting with a single t_{2g} orbital, enabling better stabilisation of the quartet state. Other peculiar features which have been previously observed in intradiol dioxygenation by non-heme iron(III) complexes can also now be better understood based on these mechanistic results. For instance, if both *N*-methyl groups in the azocyclic system were replaced by hydrogens,[32] its reactivity increased by two orders of magnitude. The increase in activity can now be attributed to more facile catechol dissociation, as the free N-H groups are significantly better hydrogen bond donors than the pyridine hydrogens in TPA. The influence of the ease of catechol dissociation is also evident from the unusually low reactivity of 3,6-di-*tert*-butylcatechol towards dioxygenation by the iron(III) TPA complex. Presumably, the bulky *tert*-butyl groups hinder the rotation of the catecholate moiety that is necessary to enable oxygen binding.[16]

Given that the electron-transfer mechanism found here is very much in agreement with the one previously suggested by Solomon *et al.*[26] for the enzymatic system, it seems likely that there are important similarities in the enzymatic and 'bio-mimetic' mechanisms, despite the obvious structural differences. As in this work, geometry optimisation on a small model of the enzyme-substrate-oxygen adduct did yield two $^4\mathbf{C_b}$-like intermediates, with partially dissociated catecholates. The obtained ligand fields were square pyramidal rather than octahedral, which would also assist in stabilisation of the quartet state. A previous hybrid DFT study on protocatechuate 3,4-dioxygenase[24] reported an oxygen-bound intermediate very similar to $^4\mathbf{B_b}'$ (i.e. a superoxide with catechol bound as a dianion) and a subsequent high barrier for bridging peroxide formation, as in this work. To obtain a reasonable barrier, a spin-crossover to the sextet state was proposed. However, as iron still had a free coordination site for oxygen, a mechanism wherein catechol dissociates was not considered. The importance of the second-shell residues for the reactivity in the native enzymes has been well-documented[24,33] and stabilisation of the dissociated catecholate in a $^4\mathbf{B_b}$-like intermediate may well be facilitated by strong hydrogen bonding with e.g. Arg-221 in 1,2-catechol dioxygenase.[34] Finally, it should be noted that the barrier for subsequent homolytic cleavage was found to be only 0.5 kcal/mol lower than carbon-oxygen bond formation, which was found to be rate determining. To obtain substantially more reactive systems, it is therefore necessary to address both steps, which is challenging as they have contrasting electronic requirements. This appears to be elegantly solved by the enzyme as a tyrosine ligand, which dissociates upon substrate binding, is thought to recoordinate further down the catalytic cycle.[25] If this occurs after the bridging peroxide formation, a more electron-rich iron centre is formed, facilitating the subsequent homolytic cleavage. These features will need to be further investigated in the actual enzymatic systems to confirm this hypothesis.

6.3 Conclusions

In conclusion, experimental rate data combined with DFT results allowed proposed mechanisms for catechol intradiol dioxygenation by non-heme iron(III) complexes with TPA-derived ligands to be discriminated. Based on these results, oxygen first coordinates to the ferric centre at a vacant site generated by partial dissociation of the catecholate substrate, which is simultaneously oxidised to a semiquinone by oxygen, with the iron centre acting as an electron buffer. The subsequent carbon-oxygen bond formation is then rate-determining. The mechanism provides a good explanation for both the effect of substrate and ligand electronic structure on reactivity. Undoubtedly the mechanistic insight provided will assist in the design of more active catechol intradiol dioxygenation mimics.

6.4 Acknowledgements

6.5 Methods

6.5.1 Experimental

Physical Measurements. NMR spectra were recorded on a Varian spectrometer operating at 400 MHz (^{1}H) or 101 MHz (^{13}C) and referenced against the signal of the residual protio impurity of the solvent. UV-Vis-NIR spectra were recorded on a Varian Cary 50 spectrometer using a quartz cuvette with 10.00 mm path length or on a Varian Cary 60 spectrometer using a dip probe (10.00 mm path length) and corrected for absorption by the solvent. Elemental analysis was performed by Mikroanalytisch Laboratorium Kolbe, Mülheim an der Ruhr, Germany.

Chemicals. Tris(2-pyridylmethyl)amine[35], 4-chloro-2-piconaldehyde[36] and 2-aminomethyl-4-chloropyridine[37] were prepared according to previously published procedures. Methanol (p.a. grade) was obtained from Merck. All other chemicals were purchased from commercial suppliers (Sigma-Aldrich, Acros or TCI Europe) and used as received.

Tris-(4-chloro-2-pyridylmethyl)amine. To a stirred solution of 2-aminomethyl-4-chloropyridine (309 mg, 2.17 mmol) in 50 mL anhydrous dichloromethane under argon atmosphere, was added sodium triacetoxyborohydride (1400 mg, 6.61 mmol). The suspension was cooled to 0 °C by an ice bath and 4-chloro-2-piconaldehyde (607 mg, 4.25 mmol) was added. The solution was stirred for 16 h and gradually warmed to room temperature. Saturated aqueous sodium bicarbonate solution (50 mL) was carefully added and the biphasic system stirred for 30 minutes. The

organic layer was separated and the aqueous layer extracted twice with 50 mL dichloromethane. The combined organic layers were dried over magnesium sulphate and the solvent removed *in vacuo* to give a brown oil. Purification by silica gel column chromatography (eluent 100:7:1 dichloromethane/methanol/25% ammonia in water, R_f 0.4) afforded the title compound as a pale yellow oil (277 mg, 0.70 mmol, 32%). ^{1}H NMR (CDCl$_3$) ∂ 8.44 (d, *J* = 5.4 Hz, 3H), 7.53 (d, *J* = 2.1 Hz, 3H), 7.18 (dd, *J* = 5.4, 2.0 Hz, 3H), 3.95 (s, 6H); ^{13}C NMR (CDCl$_3$) ∂ 160.22, 150.14, 144.99, 123.74, 122.96, 59.92; Anal. calcd for $C_{18}H_{15}Cl_3N_4$: C 54.91; H 3.84; Cl 27.02; N 14.23; found: C 54.81 H 3.91 Cl 26.97 N 14.23.

Determination of UV-Vis Absorption Maxima. To a stirred solution of methanol (10 mL) were added aliquots of stock solutions of iron(III) nitrate nonahydrate (3.00 mM, 1.00 mL, 3.00 μmol), ligand (3.00 mM, 1.00 mL, 3.00 μmol), triazabicyclodecene (3.00 mM, 2.00 mL, 6.00 μmol) in methanol. Subsequently, a stock solution of excess catechol (300 mM, 1.00 mL, 300 μmol) was added, causing the solution to turn intensely purple. A UV-Vis absorption spectrum (400 – 1100 nm) was recorded immediately thereafter.

Determination of the Rate Constants. To a stirred solution of methanol (10 mL) were added stock solutions of iron(III) nitrate nonahydrate (3.00 mM, 1.00 mL, 3.00 μmol), ligand (3.00 mM, 1.00 mL, 3.00 μmol), triazabicyclodecene (3.00 mM, 2.00 mL, 6.00 μmol) in methanol, which were all previously saturated with air. Subsequently, a stock solution of catechol (3.00 mM, 1.00 mL, 3.00 μmol, previously saturated with air) was added, causing the solution to turn intensely purple. The absorbance of the lower energy charge transfer band (λ_{max} between 791 nm and 866 nm depending on the complex) was monitored until no further change was observed. The absorbance decay was fit to the equation:

$$A = (A_0 - A_{inf})e^{-k_{obs}t} + A_{inf}$$

Where A_0 is the absorbance at t = 0 and A_{inf} is the absorbance at t = ∞. The pseudo-first order rate constant k was obtained by dividing k_{obs} by the oxygen concentration of air-saturated methanol (2.1 mM).[38] All reported values are the average of three independent measurements.

6.5.2 Computational Methods

Density functional theory (DFT) calculations were performed using the *Gaussian '09* software package[39], using the spin-unrestricted B3LYP* hybrid density functional[40,41], which has been optimised for transition metal centres in different spin states. Geometry optimisations were performed with the Los Alamos LANL2DZ[42] basis set with a ten electron core potential on iron and a 6-311G[43,44] basis set explicitly set on all other atoms (basis set BS1). Subsequent single point calculations were performed using a triple-zeta LACVP3* basis set on iron and the 6-311+G* on all other atoms (basis set BS2) and included the effect of the solvent using the continuously polarisable conductor model (C-PCM)[45,46] implemented in Gaussian using the UA0 atomic radii and appropriate parameters for methanol (dielectric constant of 32.613). Reported relative free energies include the electronic energy of the BS2 single point calculations, corrected with zero point and thermal energies and entropy from the BS1 frequency calculation at 298.15 K and 1 atm pressure and in addition included Grimme's dispersion correction (DFT-D3).[47]

All structures were subjected to geometry optimisations without any constraints followed by a full analytical frequency calculation. All reported structures were characterised by no (minima)

or one (transition states) imaginary frequencies. Transition states for the complex with TPA and catechol were found by a potential energy scan over the reaction coordinate, followed by a full transition state optimisation starting from the structure with the highest energy in the potential energy scan. Local minima were fully relaxed structures on the potential energy surface and optimised without constraints. The appropriate substituents of the TPA ligand were replaced in the transition states of the Fe/TPA/catechol complexes and reoptimised.

Partial atomic charges of selected complexes were calculated using the NBO program[19] as implemented in Gaussian '09.

6.6 References

1   T. D. H. Bugg, *Tetrahedron*, 2003, **59**, 7075–7101.

2   M. Costas, M. P. Mehn, M. P. Jensen and L. Que Jr., *Chem. Rev.*, 2004, **104**, 939–986.

3   F. H. Vaillancourt, J. T. Bolin and L. D. Eltis, *Crit. Rev. Biochem. Mol. Biol.*, 2006, **41**, 241–267.

4   S. P. de Visser and D. Kumar, Eds., *Iron-Containing Enzymes*, Royal Society of Chemistry, Cambridge, 2011.

5   O. Hayaishi, M. Katagiri and S. Rothberg, *J. Am. Chem. Soc.*, 1955, **77**, 5450–5451.

6   D. H. Ohlendorf, J. D. Lipscomb and P. C. Weber, *Nature*, 1988, **336**, 403–405.

7   E. I. Solomon, T. C. Brunold, M. I. Davis, J. N. Kemsley, S.-K. Lee, N. Lehnert, F. Neese, A. J. Skulan, Y.-S. Yang and J. Zhou, *Chem. Rev.*, 2000, **100**, 235–350.

8   H. G. Jang, D. D. Cox and L. Que Jr., *J. Am. Chem. Soc.*, 1991, **113**, 9200–9204.

9   R. Yamahara, S. Ogo, H. Masuda and Y. Watanabe, *J. Inorg. Biochem.*, 2002, **88**, 284–294.

10   P. C. A. Bruijnincx, G. van Koten and R. J. M. Klein Gebbink, *Chem. Soc. Rev.*, 2008, **37**, 2716.

11   T. Funabiki, T. Yamazaki, A. Fukui, T. Tanaka and S. Yoshida, *Angew. Chem. Int. Ed.*, 1998, **37**, 513–515.

12   A. Alfreider, C. Vogt and W. Babel, *Appl. Environ. Microbiol.*, 2003, **69**, 1372–1376.

13   T. D. H. Bugg, in *Iron-Containing Enzymes*, eds. S. P. de Visser and D. Kumar, Royal Society of Chemistry, Cambridge, 2011, pp. 42–66.

14   D. D. Cox and L. Que Jr., *J. Am. Chem. Soc.*, 1988, **110**, 8085–8092.

15   A. Hernandez-Ortega, M. G. Quesne, S. Bui, D. P. H. M. Heuts, R. A. Steiner, D. J. Heyes, S. P. de Visser and N. S. Scrutton, *J. Biol. Chem.*, 2014, **289**, 8620–8632.

16   Y. Hitomi, M. Yoshida, M. Higuchi, H. Minami, T. Tanaka and T. Funabiki, *J. Inorg. Biochem.*, 2005, **99**, 755–763.

17   M. Higuchi, Y. Hitomi, H. Minami, T. Tanaka and T. Funabiki, *Inorg. Chem.*, 2005, **44**, 8810–8821.

18   C. Hansch, A. Leo and R. W. Taft, *Chem. Rev.*, 2002, **91**, 165–195.

19   C. G. Swain and E. C. Lupton, *J. Am. Chem. Soc.*, 1968, **90**, 4328–4337.

20   R. Latifi, M. A. Sainna, E. V. Rybak-Akimova and S. P. de Visser, *Chem. Eur. J.*, 2013, **19**, 4058–4068.

21   M. G. Quesne, R. Latifi, L. E. Gonzalez Ovalle, D. Kumar and S. P. de Visser, *Chem. Eur. J.*, 2014, **20**, 435–446.

22   A. J. Simaan, M.-L. Boillot, R. Carrasco, J. Cano, J.-J. Girerd, T. A. Mattioli, J. Ensling, H. Spiering and P. Gütlich, *Chem. Eur. J.*, 2005, **11**, 1779–1793.

23   A. J. Simaan, M.-L. Boillot, E. Rivière, A. Boussac and J.-J. Girerd, *Angew. Chem. Int. Ed.*, 2000, **39**, 196–198.

24   T. Borowski and P. E. M. Siegbahn, *J. Am. Chem. Soc.*, 2006, **128**, 12941–12953.

25   M. Xin and T. D. H. Bugg, *J. Am. Chem. Soc.*, 2008, **130**, 10422–10430.

26   M. Y. M. Pau, M. I. Davis, A. M. Orville, J. D. Lipscomb and E. I. Solomon, *J. Am. Chem. Soc.*, 2007, **129**, 1944–1958.

27   D. D. Cox, S. J. Benkovic, L. M. Bloom, F. C. Bradley, M. J. Nelson, L. Que Jr. and D. E. Wallick, *J. Am. Chem. Soc.*, 1988, **110**, 2026–2032.

28   W. O. Koch and H.-J. Krüger, *Angew. Chem. Int. Ed.*, 1995, **34**, 2671–2674.

29   M. Pascaly, M. Duda, F. Schweppe, K. Zurlinden, F. K. Müller and B. Krebs, *J. Chem. Soc., Dalton Trans.*, 2001, 828–837.

30   P. Mialane, L. Tchertanov, F. Banse, J. Sainton and J.-J. Girerd, *Inorg. Chem.*, 2000, **39**, 2440–2444.

31   P. Comba, H. Wadepohl and S. Wunderlich, *Eur. J. Inorg. Chem.*, 2011, **2011**, 5242–5249.

32   N. Raffard, R. Carina, A. J. Simaan, J. Sainton, E. Rivière, L. Tchertanov, S. Bourcier, G. Bouchoux, M. Delroisse, F. Banse and J. J. Girerd, *Eur. J. Inorg. Chem.*, 2001, **2001**, 2249–2254.

33   P. C. A. Bruijnincx, M. Lutz, A. L. Spek, W. R. Hagen, G. van Koten and R. J. M. Klein Gebbink, *Inorg. Chem.*, 2007, **46**, 8391–8402.

34   M. W. Vetting and D. H. Ohlendorf, *Structure*, 2000, **8**, 429–440.

35   G. J. P. Britovsek, J. England and A. J. P. White, *Inorg. Chem.*, 2005, **44**, 8125–8134.

36   US Patent 7,078,419

37   S. Negi, M. Matsukura, M. Mizuno, K. Miyake and N. Minami, *Synthesis*, 2000, **1996**, 991–996.

38   C. B. Kretschmer, J. Nowakowska and R. Wiebe, *Ind. Eng. Chem.*, 1946, **38**, 506–509.

39   Gaussian 09, Revision D.01, M. J. Frisch, G. W. Trucks, H. B. Schlegel, G. E. Scuseria, M. A. Robb, J. R. Cheeseman, G. Scalmani, V. Barone, B. Mennucci, G. A. Petersson, H. Nakatsuji, M. Caricato, X. Li, H. P. Hratchian, A. F. Izmaylov, J. Bloino, G. Zheng, J. L. Sonnenberg, M. Hada, M. Ehara, K. Toyota, R. Fukuda, J. Hasegawa, M. Ishida, T. Nakajima, Y. Honda, O. Kitao, H. Nakai, T. Vreven, J. A. Montgomery Jr, J. E. Peralta, F. Ogliaro, M. J. Bearpark, J. Heyd, E. N. Brothers, K. N. Kudin, V. N. Staroverov, R. Kobayashi, J. Normand, K. Raghavachari, A. P. Rendell, J. C. Burant, S. S. Iyengar, J. Tomasi, M. Cossi, N. Rega, N. J. Millam, M. Klene, J. E. Knox, J. B. Cross, V. Bakken, C. Adamo, J. Jaramillo, R. Gomperts, R. E. Stratmann, O. Yazyev, A. J. Austin, R. Cammi, C. Pomelli, J. W. Ochterski, R. L. Martin, K. Morokuma, V. G. Zakrzewski, G. A. Voth, P. Salvador, J. J. Dannenberg, S. Dapprich, A. D. Daniels, Ö. Farkas, J. B. Foresman, J. V. Ortiz, J. Cioslowski and D. J. Fox, Gaussian, Inc., Wallingford CT, 2009.

40   M. Reiher, O. Salomon and B. Artur Hess, *Theor. Chem. Acc.*, 2001, **107**, 48–55.

41   O. Salomon, M. Reiher and B. A. Hess, *J. Chem. Phys.*, 2002, **117**, 4729–4737.

42   P. J. Hay and W. R. Wadt, *J. Chem. Phys.*, 1985, **82**, 270–283.

43   A. D. McLean and G. S. Chandler, *J. Chem. Phys.*, 1980, **72**, 5639–5648.

44   R. Krishnan, J. S. Binkley, R. Seeger and J. A. Pople, *J. Chem. Phys.*, 1980, **72**, 650–654.

45   V. Barone and M. Cossi, *J. Phys. Chem. A*, 1998, **102**, 1995–2001.

46   M. Cossi, N. Rega, G. Scalmani and V. Barone, *J. Comp. Chem.*, 2003, **24**, 669–681.

47   S. Grimme, J. Antony, S. Ehrlich and H. Krieg, *J. Chem. Phys.*, 2010, **132**, 154104.

Part III

Oxidation of Real Lignin Streams

Chapter 7

Oxidative Cleavage of Catechols Derived from Candlenut Lignin

Abstract

In the previous chapters, the selective intradiol catechol dioxygenation of pyro-catechol was developed. For the valorisation of lignin, it is also important to investigate the ability of the catalyst to convert actual lignin-derived substrates. The depolymerisation of an organosolv lignin derived from candlenut (*Aleurites moluccana*) using Cu-doped porous metal oxide (Cu-PMO) catalysts is reported to afford a lignin-oil consisting of mainly 4-propyl-substituted catechols. These catechols were subsequently used as substrate for the intradiol-selective cleavage to *cis,cis*-muconic acid, *cis,trans*-muconic acid and γ-muconolactone derivatives. The oxidation reaction was first shown to proceed well with various pure catechols. The reactivity of the actual lignin oils was found to largely depend on the composition of the depolymerisation catalyst used: lignin oil obtained with a Cu-PMO catalyst prepared from metal chlorides was more difficult to further convert than that obtained with a Cu-PMO catalyst prepared from metal nitrates. This was attributed to poisoning of the iron oxidation catalyst, highlighting the influence of the lignin depolymerisation procedure on further downstream processing.

The work described in this chapter is based on:

Robin Jastrzebski, Narani Anand, Remco Dalebout, Bert M. Weckhuysen, Katalin Barta and Pieter C. A. Bruijnincx, *"Oxidative Cleavage of Catechols Derived from Candlenut Lignin,"* to be submitted for publication

7.1 Introduction

Copper-doped porous metal oxide (Cu-PMO) catalysts are receiving increased attention as robust and non-noble metal-based catalysts for lignin depolymerisation.[1-3] Such catalysts are prepared by calcining hydrotalcite materials to yield highly dispersed copper on a basic support. Application of Cu-PMO in the mild depolymerisation of organosolv candlenut (*Aleurites moluccana*) lignin via hydrogenolysis, was shown to afford very clean product mixtures with great efficiency. Four different 4-alkyl-substituted catechols were obtained in up to 63% combined yield.[4] In addition, some of these catechols could be isolated by column chromatography in very good yields. The fact that such catecholic monomers were obtained rather than the expected methoxylated phenols is remarkable. Since such catechols are not observed in the treatment of other lignins with the same catalyst,[5] it seems likely that the candlenut lignin itself incorporates a large fraction of non-standard catecholic monolignols. Indeed, lignins incorporating catecholic monolignols derived from caffeoyl alcohol have been previously observed in the seed coats of various species.[6-8]

While the obtained catechols themselves are interesting aromatic building blocks, they are also promising starting materials for further processing, for example for the selective intradiol catechol dioxygenation method that was developed in the previous chapters. The analogous cleavage of the catechols derived from candlenut lignin could thus afford alkylated muconic acids. These compounds could find use, after hydrogenation, as co-monomers for novel polymers or as plasticisers. The muconic acid double bonds could also undergo metathesis to afford acrylic acid.[9] Additionally, the intradiol muconic acid cleavage products can be isomerized to afford γ-lactones, which are important building blocks for high-value chemicals including pharmaceuticals.[10] While synthetic systems for (stoichiometric) catechol intradiol dioxygenation have been shown to be fairly robust in substrate scope, the reactivity of the catecholic compounds obtained after Cu-PMO catalysed depolymerisation has not yet been demonstrated. Additionally, it has previously been shown that in two-stage lignin conversion processes pure compounds display much higher reactivity than crude products from lignin; often this can be attributed to residual impurities in the lignin-derived product stream.[11-13] Indeed, it can in general be said that it is of central importance to the field that appropriate methods for upstream processing are developed that take into account possible incompatibility issues associated with the crude lignin-derived product streams.

In this chapter, the two-stage depolymerisation of candlenut lignin and further upgrading of the lignin-derived catechols obtained using the catalytic Cu-PMO and iron-based systems described above is described (Figure 7.1). First, the depolymerisation of an organosolv Candlenut lignin over copper-doped porous metal oxides to catechols is reported. Furthermore, the selective intradiol oxidative cleavage of these lignin-derived
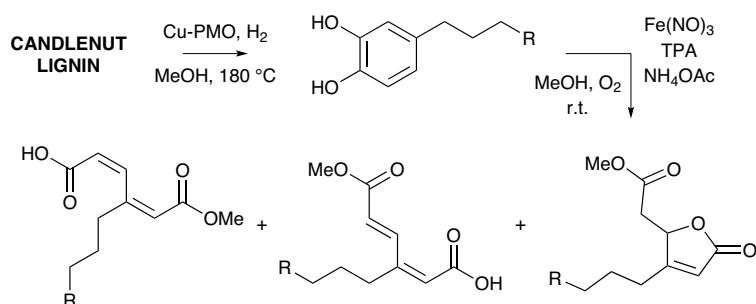
Figure 7.1: Two-step upgrading of candlenut lignin as described in this work: first the candlenut lignin is depolymerised over a Cu-PMO catalyst under H_2 atmosphere to yield a limited number of 4-propylcatechols. Subsequent intradiol dioxygenation of these catechols using an *in-situ* prepared iron(III) catalyst affords a mixture of muconic acids and γ-muconolactone.

product mixtures is described and their reactivity is compared to individual catechol substrates. In contrast with the previous chapters on pyrocatechol, where the *cis,cis*-muconic acid derivative was formed almost exclusively, in this case a mixture of *cis,cis*, *cis,trans* and γ-muconolactone isomers was observed. Notably, the outcome of the oxidation reaction using the lignin oil was found to be highly dependent on the composition of the depolymerisation catalyst in the step prior to oxidation. Much better results were obtained with a Cu-PMO prepared from metal nitrate precursors than with one derived from metal chloride precursors. This could be attributed to poisoning of the second-stage dioxygenation catalyst by residual chloride.

7.2 Results

7.2.1 Oxidative Cleavage of Pure Catechols

While the previous chapters developed a procedure for the catalytic intradiol oxygenation of pyrocatechol, catalytic oxidation of *4-substituted* catechols has so far not been reported. In stoichiometric model reactions, as was also observed in Chapter 6, a strong influence of catechol substituents has been observed on reactivity, however.[14,15] The dioxygenation of the pure substrates 4-(3-hydroxypropyl)catechol (**1a**) and 4-(*n*-propyl)catechol (**2a**), two of the anticipated main components in the lignin-oil was therefore first investigated, to facilitate the translation of the approach to real lignin-derived streams. For this purpose, the system from Chapter 5, based on iron(III) nitrate, the tris(2-pyridylmethyl)amine (TPA) ligand and ammonium acetate as added base was adapted. To enable reactions to be run on a small scale, pure oxygen in large headspace vials was employed, giving an effective oxygen concentration in the liquid comparable

to the high-pressure system at 20 bar 5 vol% O_2 of Chapter 5. In addition, 10 vol% acetonitrile was added to the methanol solvent to ensure good solubility of all components.

In a solution of catechol, the [Fe(TPA)(catecholato)]$^+$ complex is then rapidly formed from the catalyst precursors, with the catechol moiety bound in a bidentate fashion; again this particular mode of chelation gives rise to the characteristic charge transfer absorptions at visible and near IR wavelengths. The iron-catecholato complex reacts with molecular oxygen to form an intermediate muconic anhydride, which is rapidly hydrolysed or solvolysed to the corresponding *cis,cis*-muconic acid or its ester. Indeed, after adding the catalyst components to the solution of **1a**, the solution immediately turned to intense purple and UV-Vis-NIR spectroscopy showed the appearance of the characteristic charge transfer bands of iron(III) catecholate complexes with maxima at 534 nm and 856 nm; the purple colour gradually disappeared to give a greenish reaction mixture as the reaction proceeded. After acid workup, to decompose the iron catalyst, the products were identified and quantified by NMR spectroscopy.

The 1,3-dienes of the geometrical isomers of the expected muconic acid products are easily identified and quantified by their characteristic chemical shifts in ^{1}H NMR.[16] Using zTOCSY and long-range COSY experiments (Figure 7.2), three principal separate spin systems can be observed between 5 and 9 ppm, with matching peaks in the ^{1}H NMR between 3.5 and 3.7 ppm, suggesting these are muconic acid methyl esters derived from solvolysis of the acid anhydride intermediate by methanol. In addition, small amounts of the free acid (deriving from hydrolysis) can be observed. The first spin system (red in Figure 7.2), corresponds to the *cis,trans* isomer **1b**, based on the characteristic peak at 8.42 ppm. The NOESY spectrum further corroborates this assignment, as strong cross-peaks between the peak at 2.38 ppm (corresponding to the first -CH$_2$- in the propyl chain) and the peaks at 5.94 and 6.28 ppm are observed, which are only possible with this specific stereochemistry. The second spin system (green) corresponds to **1c**, which is rather the *cis,cis* isomer. Although the peak at 6.97 ppm of this spin system might suggest a *cis,trans* isomer, this assignment is discarded based on the NOESY spectrum, which shows strong cross-peaks between 5.70 ppm and 2.36 ppm (again, -CH$_2$-) that is only possible in the *cis,cis* isomer. In addition, the formation of a γ-muconolactone (purple, **1d**) was identified, which has previously also been observed in the catalytic cleavage of sterically hindered catechols such a 3,5-*tert*-butylcatechol.[17] The formation of three major products, although all derived from selective intradiol dioxygenation contrasts with what was observed in Chapters 4 & 5, where only the formation of the *cis,cis*-isomer as major product was observed, as well as with the (stoichiometric) cleavage of 3,5-*tert*-butylcatechol, for which only the acid anhydride intermediate and lactone are observed.[17]

As shown in Chapter 5, the isomerisation of *cis,cis*-muconic acid to *cis,trans*-muconic acid can proceed under mildly basic conditions through a γ-lactonic transition state.
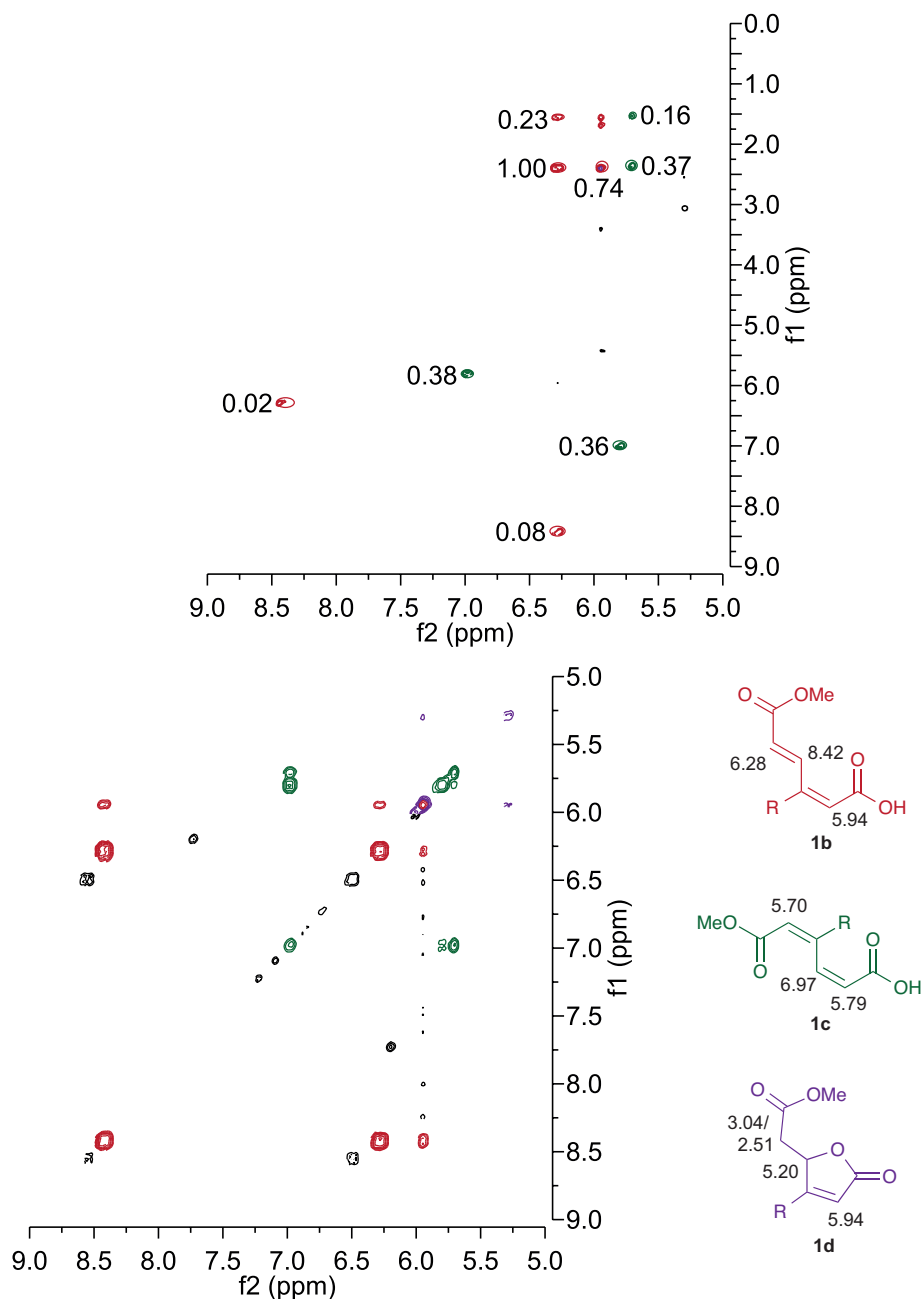
Figure 7.2: NOESY (top) and long-range COSY (bottom) ¹H NMR spectrum, with the cross-peaks corresponding to principal products marked. Integrals for the NOESY cross-peaks are given.
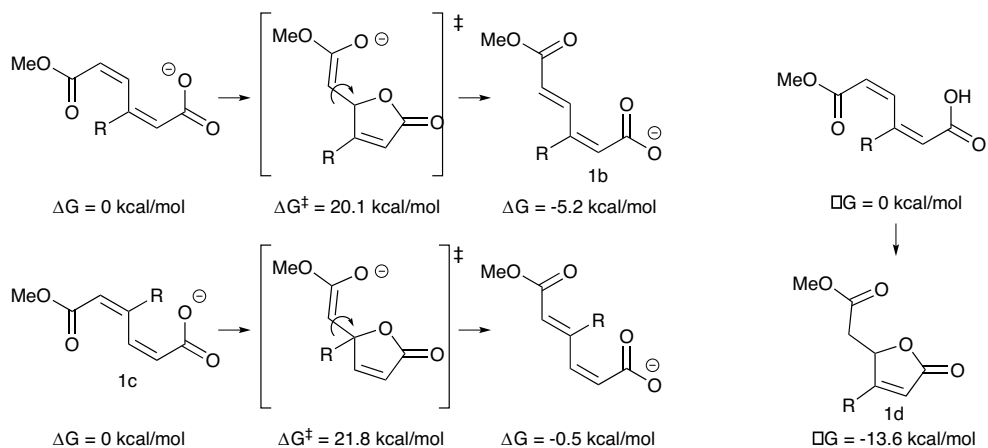
Figure 7.3: The isomerisation of *cis,cis*-muconic acids to *cis,trans*-muconic acids proceeds through a lactonic transition state: the isomerisation to **1b** is favoured by 5 kcal/mol (top left), whereas isomerisation of **1c** (bottom left) is only favoured by 0.5 kcal/mol with a higher barrier for isomerisation. Formation of γ-lactone **1d** (right) is thermodynamically favoured by -13.6 kcal/mol.
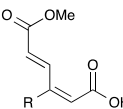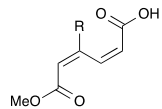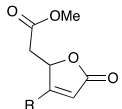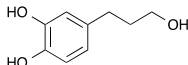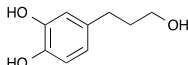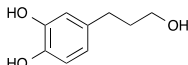
This mechanism allows only the double bond connected to the methyl ester to be isomerised and limits itself to a single bond isomerisation, which is consistent with the products observed and the absence of any *trans,trans* isomer. Qu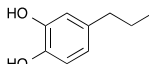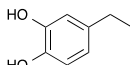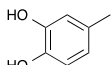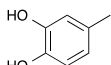alitatively, the tendency of the propyl group to drive isomerisation towards the *cis,trans* isomer **1b** can be explained by a relief of steric strain induced by the relatively close proximity of the propyl group to the carboxylic acid in the initial (preferably flat) *cis,cis* geometry. On the other hand, isomerisation of **1c** is likely to generate even more steric strain, which is consistent with that only one of the two possible *cis,trans* isomers is found. To further corroborate this, DFT calculations on the *cis,cis* and *cis,trans* isomers and the corresponding lactonic transition states were performed to determine their relative energies (ADF, BP86 functional, TVZP basis set).

Comparing the energy of (deprotonated) **1b** with its corresponding *cis,cis* isomer shows that the *cis,trans* isomer is indeed 5.2 kcal/mol lower in energy (Figure 7.3), with the barrier for isomerisation being 20.1 kcal/mol. Both values are approximately 2 kcal/mol lower than observed for the unsubstituted muconic acid, which may account for the increase in isomerisation observed. In the case of **1c** on the other hand, isomerisation to the *cis,trans* isomer is only favoured by 0.5 kcal/mol, which can presumably be attributed to the limited strain relief. The barrier to isomerisation is also higher at 21.8 kcal/mol, which helps explain why we only observe the *cis,cis* isomer in this case. The mechanism of lactone formation, which necessarily involves a proton transfer, is challenging to approach computationally, but energy minimisation of **1d** did show it to be very stable (-13.6 kcal/mol compared to the *cis,cis* isomer), whereas lactone formation

for the unsubstituted *cis,cis*-muconic acid was found only to be favoured by 6 kcal/mol. Presumably, the large thermodynamic drive towards the lactone product also considerably lowers the barrier, leading to extensive formation of **1d**.

The product yields of the intradiol dioxygenation were determined using quantitative ^{1}H NMR spectroscopy (Table 7.1).[18,19] Under standard conditions (10 μmol catalyst, 2 h reaction time), which were used to identify the products of **1a** oxidation, both **1b** and **1c** were formed in equal amounts together with a significant amount of the lactone **1d**. At full conversion, the sum of the identified compounds was limited to 44% of the initial catechol intake, even though all major peaks in the NMR spectrum can be assigned to the products **1b-d**. To check whether the formed products were lost during the acid work-up and the subsequent extraction of the organic products, we also performed UV-Vis measurements of the extracted aqueous layers, as muconates show a very strong UV absorption at 259 nm.[20] Taking into account the absorbance expected for the TPA ligand,

Table 7.1: Results of the catalytic oxidative intradiol cleavage of 4-substituted catechols.[a]

Substrate		Cat.[b] (%)	t (h)	C.[c] (%)	b[d]	c[d]	d[d]	Σ
HO-⬡-CH₂CH₂CH₂-OH	(**1a**)	0.01	2	100	16	16	13	44
HO-⬡-CH₂CH₂CH₂-OH	(**1a**)	0.01	0.5	100	21	12	17	50
HO-⬡-CH₂CH₂CH₂-OH	(**1a**)	0.002	0.5	97	22	9	12	43
HO-⬡-CH₂CH₂CH₃	(**2a**)	0.01	0.5	100	25	12	16	53
HO-⬡-CH₂CH₃	(**7a**)	0.01	0.5	100	32	13	14	59
HO-⬡-CH₃	(**8a**)	0.01	2	100	31	23	17	71
HO-⬡-CH₃	(**9a**)	0.01	0.5	100	33	12	17	62

Yield (%) column heads above b, c, d correspond to the structures: (b) methyl ester muconate, (c) muconic acid / methyl ester, (d) lactone.

[a] Conditions: 0.120 mmol substrate, 0.010 mmol Fe(NO$_3$)$_3$, 0.010 mmol TPA, 0.020 mmol NH$_4$OAc, 0.2 mL CH$_3$CN, 1.8 mL MeOH, 18 mL O$_2$ [b] Catalyst amount (mol%) [c] Conversion [d] Includes both free acid and methyl ester

the residual muconate in the aqueous layer was estimated to be only 1% of the original catechol intake. Loss of catechol could also be due to radical oxidation to form 1,2-benzoquinones, which are unstable and may condense further to larger oligomeric species. Gel permeation chromatography with tandem UV and refractive index detection on the organic extracts did not show any indication that such higher molecular weight products were formed, though. To check if consecutive reactions contributed to the loss in mass balance, reactions were also performed for only 0.5 h. Full conversion was again seen, accompanied with a somewhat higher mass balance of 50%. Even at much reduced iron catalyst loading of 0.002 mmol (1.7 mol%) at 0.5 h reaction time nearly full conversion of the substrate was observed, with a mass balance comparable to the reaction run for longer at higher catalyst loadings. In all cases **1b** remained the major product.

To assess the influence of the 4-substituent on catechol intradiol dioxygenation, we also performed the reaction using 4-propyl, 4-ethyl and 4-methylcatechol. In all instances, we found products analogous to **1b**, **1c** and **1d**, with a comparable product distribution. The catechols with shorter alkyl chains, however, afforded better mass balances. This seems to be in agreement with the previous results for pyrocatechol oxidation, where mass balances ranged from 75% to 90% at full conversion.

7.2.2 Oxidation of Lignin-Derived Catechols

The Cu-PMO catalyst used for candlenut lignin depolymerisation has been previously studied for the conversion of organosolv lignin, crude lignocellulose, and other substrates derived from renewable sources.[2,3,21-23] The catalyst was prepared by nominally replacing 20 mol% of the Mg^{2+} ions with Cu^{2+} ions in a Mg^{2+}/Al^{3+} (1:3 molar ratio) hydrotalcite structure. Two catalyst samples were prepared: one in which the catalyst was prepared from metal chlorides and one in which metal nitrates were used. The resultant hydrotalcite materials were calcined at 460 °C for 24 h to yield Cu-PMO with a largely amorphous, porous structure. The material showed a BET surface area of around 127 m^2/g when prepared from the chloride precursor and 147 m^2/g when prepared from the metal nitrates. The X-ray diffraction patterns of the copper-doped hydrotalcite (nitrate) and both fresh and spent Cu-PMO are shown in Figure 7.4. The hydrotalcite exhibited typical diffraction lines at 11.8, 23.2, 34.9, 39.4, 46.4, 60.6 and 62.0° corresponding to the (003), (006), (012), (015), (018), (110) and (113) planes, respectively, of a crystalline double-layered hydrotalcite structure.[24] After calcination, the characteristic diffraction peaks of the hydrotalcite structure disappeared and weak CuO and periclase MgO peaks appeared for the Cu-PMO catalyst. The structure of the Cu-PMO catalyst remained intact after the reaction. SEM-EDAX and SEM-mapping measurements showed a homogeneous distribution of Cu over the material (not shown).
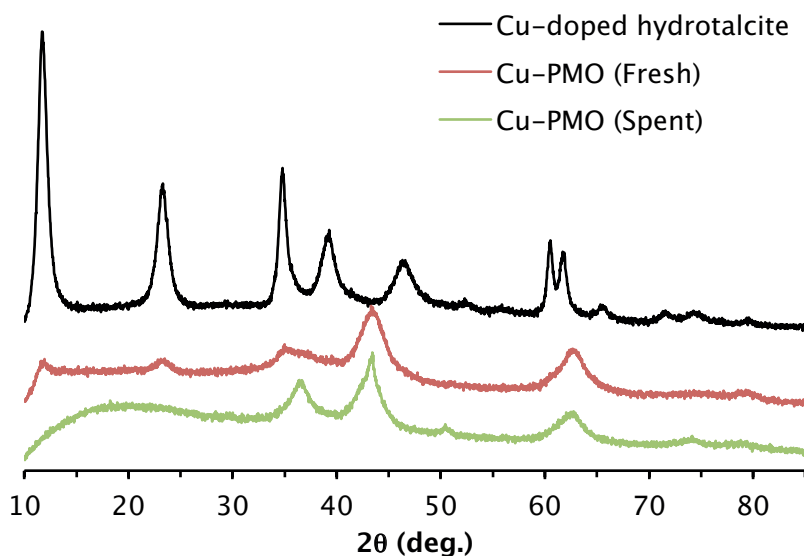
Figure 7.4: X-ray diffraction patterns of copper-doped hydrotalcite prepared from nitrate precursors and the corresponding fresh and spent Cu-PMO catalysts.

The candlenut nutshell lignin used in this study was extracted as indicated in literature.[4] Additional GPC analysis of the extracted candlenut organosolv lignin gave an M_w of 1025 g/mol with a polydispersity of 1.24, in accordance with literature.[4] The lignin was then subjected to depolymerisation by Cu-PMO in methanol under H_2 atmosphere. The resulting product mixture consisted of a methanol-soluble crude viscous lignin-oil, accounting for 70 wt% of the lignin intake, and a small amount of insoluble solids. GPC analysis of the lignin-oil (M_w = 430 g/mol, PD = 1.82) showed a significant reduction in molecular weight, as expected. The sharp peaks in the GPC trace are indicative of low-molecular weight monomeric products; a smaller tail of higher molecular weight products is observed as well. NMR data subsequently revealed the crude product mixture to contain 4-(3-hydroxypropyl)catechol (**1a**), 4-propylcatechol (**2a**), 2,3-dihydro-1H-indene-5,6-diol (**3a**), and 4-(3-methoxypropyl)catechol (**4a**) (Figure 7.5) as main products, in line with the previous report.[4] Quantitative NMR analysis revealed the lignin-oil to consist of approximately 37 wt% of these catecholic monomers. The monomer composition of lignin oils obtained with both catalysts was comparable, showing that any differences or residual impurities in the catalyst do not affect the depolymerisation step.

Having demonstrated oxidative cleavage of the pure 4-substituted catechols, the crude candlenut lignin-oil was subsequently subjected to the oxidative cleavage protocol. The oxidation reaction was initially tested on a lignin-oil obtained from a reaction with a Cu-PMO catalyst prepared from metal chloride precursors (Table 7.2, #1-2). Using a
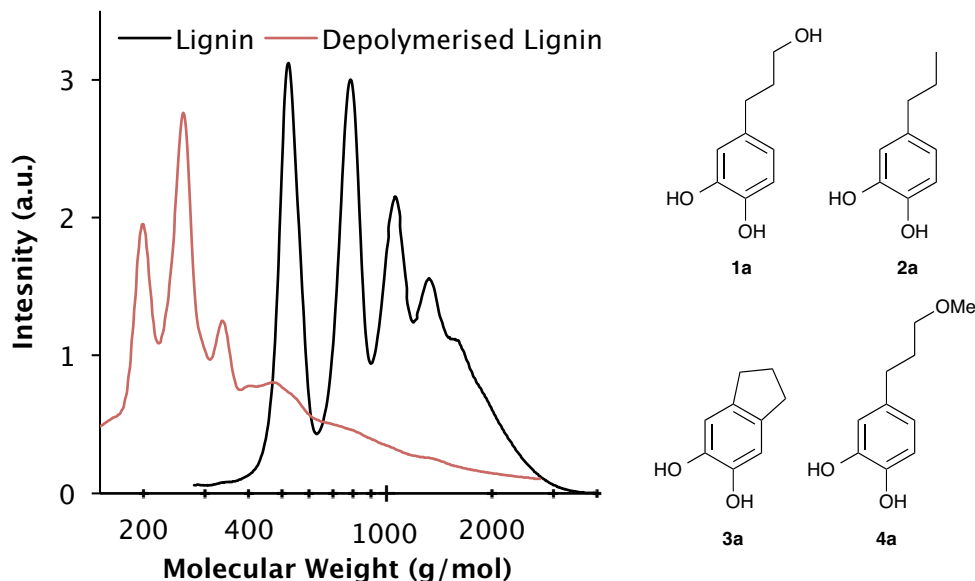
Figure 7.5: Molecular weight distribution of the candlenut lignin before and after depolymerisation determined by GPC and monomeric catechols observed as major components in lignin-oil obtained by Cu-PMO-catalysed depolymerisation of lignin extracted from candlenut nutshells.

high catalyst loading, full conversion of the catechols was observed and muconate structures of type **b**, **c** and **d** were identified. As the characteristic muconate peaks are at practically identical chemical shifts, regardless of the nature of the alkyl groups present in the original catechols (**1a**-**4a**), attempts to further distinguish these were not made; all are grouped and listed as **b-d** in Table 7.2. It can nonetheless be said that the ratio of product isomers (*cis*,*trans*/*cis*,*cis*/lactone) appears to be comparable to what was observed for **1a** and **2a**; the total amount of products observed is significantly lower, however. At lower catalyst loading, despite significant conversion, no muconate or lactone formation was observed at all. This is in stark contrast with the results presented above for the pure compounds, as these afforded the muconates with full substrate conversion under comparable conditions.

This loss of activity is tentatively attributed to residual chloride ions in the catalyst material. As was demonstrated in Chapter 4, chloride ions appear to prevent the formation of the active catecholato complex after only a few turnovers. The same experiments were therefore also conducted using a lignin-oil prepared with a Cu-PMO catalyst prepared from metal nitrate precursors. At a high catalyst loading, the catechols in this lignin oil were also fully converted and the mass balance improved significantly to 29%, with primarily more of the lactone being formed. In addition, the monomethyl ester of *cis*,*cis*-muconic acid (**5c**) was now also observed in the reaction mixture at high catalyst

Table 7.2: Results of the catalytic oxidative intradiol cleavage of candlenut-derived lignin oils.[a]

Yield (%)

Lignin Oil	Cat.[b] (%)	C.[c] (%)	5a	5c	b[d]	c[d]	d[d]	Σ
1 (Cu-PMO-Cl)	0.01	100	-	-	8	3	7	18
1 (Cu-PMO-Cl)	0.002	40	-	-	-	-	-	-
2 (Cu-PMO-NO$_3$)	0.01	100	-	3	8	7	14	32
2 (Cu-PMO-NO$_3$)	0.002	100	6	-	10	8	12	36
3 (Cu-PMO-NO$_3$)[c]	0.01	100	-	5	10	7	20	41

[a] Conditions: lignin-oil/solution corresponding to 0.065 mmol catechol, 0.010 mmol Fe(NO$_3$)$_3$, 0.010 mmol TPA, 0.020 mmol NH$_4$OAc, 0.2 mL CH$_3$CN, 1.8 mL MeOH, 18 mL O$_2$; yield based on catechol content of the lignin oil. [b] Catalyst amount (mol%) [c] Conversion [d] Includes both free acid and methyl ester

loading, which would result from the cleavage of pyrocatechol (Figure 7.6). Notably, full conversion of the starting material was now observed with concomitant formation of the muconic acid and lactone products at low catalyst concentration. This shows the high sensitivity of the system towards residual impurities in the lignin oil, but also that by careful selection of the lignin upgrading conditions this can be circumvented. This example shows that one should not only be aware of the impurities contained in the biomass, but also of the impurities introduced by prior process steps. Interestingly, at low catalyst loading we observed unreacted pyrocatechol (**5a**) in the reaction mixture rather than the *cis,cis*-muconic acid methyl ester. This pyrocatechol component was not initially identified in the lignin oil, as its signals overlap with the other catechols in the ^{1}H NMR spectrum. The fact that at lower catalyst loading some of the pyrocatechol remains, is consistent with the observation that alkylated catechols react more quickly in the catechol intradiol dioxygenation, as was observed for 4-methylcatechol in Chapter 6. While the mass balances for the lignin oil conversion are still somewhat lower than we observed for the pure compounds, the catechols can clearly still be converted, despite the residual lignin oligomers still present in the lignin oil.

As the catalytic lignin depolymerisation step and the oxidative cleavage are both run in methanol, the crude reaction mixture of the depolymerisation could also be directly applied in the dioxygenation reaction. Indeed, taking the reaction mixture of the lignin depolymerisation (after removal of the catalyst by filtration) and applying the same conditions also showed formation of the muconate products. Again, the lactone is observed as the major product with an improved overall mass balance.
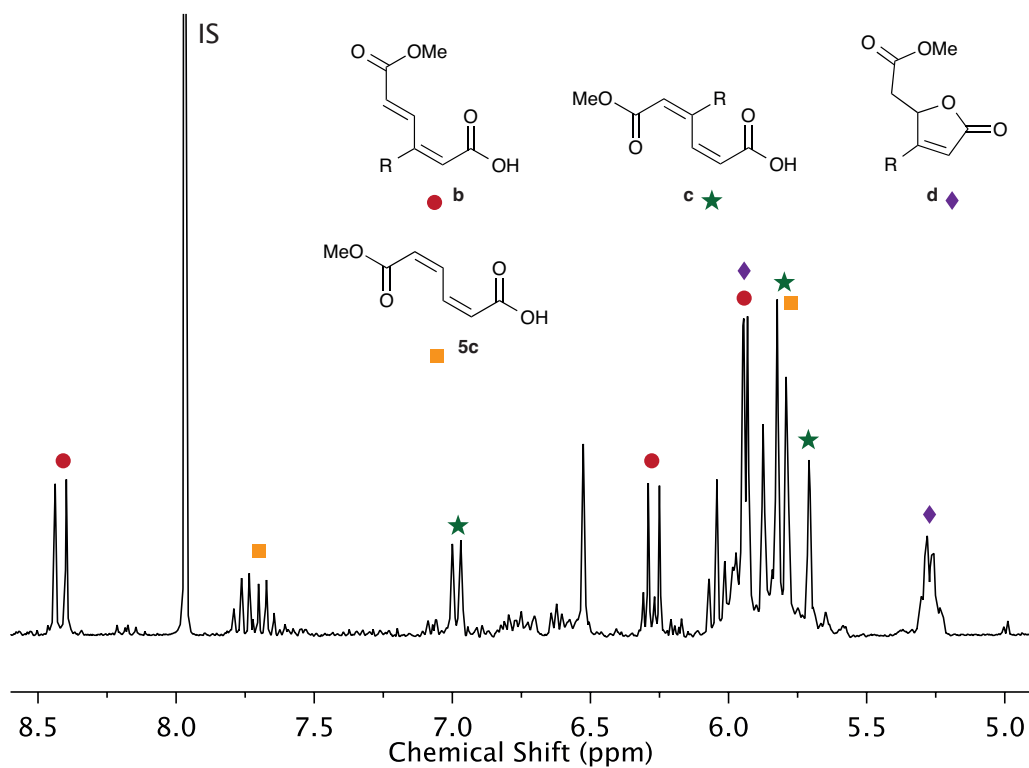
Figure 7.6: ^{1}H NMR spectrum of lignin oil 2 after intradiol catechol dioxygenation. Peaks of the major muconate species are marked identically to Figure 7.2. Pyrocatechol-derived *cis,cis*-muconic acid methyl ester was observed as well.

7.3 Conclusions

In conclusion, a two-step reaction sequence to convert lignin from candlenut shells into propyl substituted muconic acid derivatives and lactones has been developed. The ability of iron(III) complexes of TPA to perform intradiol catechol dioxygenation on 4-propyl-substituted catechols was also demonstrated, thus expanding the substrate scope for catalytic oxidative cleavage. In contrast with the results presented in Chapter 4 and 5, which afforded only the methyl ester of *cis,cis*-muconic acid as the major product, a mixture of muconic acid products was observed instead: methyl esters of *cis,cis* and *cis,trans*-muconic acids as well as the corresponding γ-muconolactones were all found. Crude mixtures (still containing residual lignin oligomers) obtained from the Cu-PMO-catalysed depolymerisation of candlenut lignin could be successfully converted to these muconic acid products as well. In this case, a strong dependence on the catalyst used in the lignin depolymerisation was observed: if the catalyst was prepared from metal chloride precursors, only low intradiol dioxygenation activity was observed. On the other hand when a depolymerisation catalyst prepared from metal nitrates was used, the

catechols in the resulting lignin oil could be cleaved with an activity comparable to the pure compounds, which was tentatively attributed to the poisoning of the iron catalyst by residual chloride transferred in the subsequent reaction steps. This highlights the importance of testing two-stage lignin conversion strategies on real lignin streams, as impurities introduced the first stage can significantly affect the second.

7.4 Acknowledgements

7.5 Experimental

Materials. Iron(III) nitrate nonahydrate (98+%) was purchased from Acros. Ammonium acetate (HPLC grade) was obtained from Fisher Scientific. Methanol (p.a. grade) and sodium hydroxide (>99%) were obtained from Merck. Magnesium nitrate hexahydrate (98%), aluminium nitrate nonahydrate (≥98%), copper(II) nitrate hemi(pentahydrate) (98%) and sodium carbonate (>99%) were purchased from Sigma-Aldrich. All other reagents were obtained from Sigma Aldrich in reagent grade and used as received. Tris(2-pyridylmethyl)amine was synthesised according to a previously published procedure[25] and crystallised from boiling hexanes. The Centre for Green Chemistry & Engineering at Yale University graciously provided the candlenut nutshells.

Physical Measurements. NMR spectra were recorded on an Agilent spectrometer operating at 400 MHz (^{1}H) or 100 MHz (^{13}C) in DMSO-d6 (unless mentioned otherwise) and referenced against the signal of the residual protio impurity of the solvent (2.50 ppm for DMSO-d6). Data was processed using MestReNova software. For analysis of the ^{1}H and ^{13}C NMR of candlenut lignin and lignin oil, approximately 50 mg was dissolved in 0.7 mL methanol-d4. ^{1}H-^{13}C HSQC spectra of candlenut lignin were acquired in DMSO-d6 (50 mg in 0.7 mL) using a standard pulse sequence HSQC programme with a spectral width of 160 ppm, 16 scans, 128 increments in the f1 dimension and 11 ppm in the f2 dimension. UV-Vis-NIR spectra were recorded on a Varian Cary 50 spectrometer using a quartz cuvette with 10.00 mm path length and corrected for absorption by the solvent. Powder X-ray diffraction patterns were recorded at room temperature using a Bruker X-ray diffractometer at 40 kV and 40 mA with CuKα radiation over a 2θ range from 10° to 90° with a step size of 0.05° and 2 s acquisition time per step. Elemental analysis (ICP-MS) was performed on Perkin Elmer Instrument (Optima 7000 DV).

GPC. GPC analyses of (depolymerised) lignin samples were performed using a HP1100 system equipped with three 300 × 7.5 mm PL gel 3 μm MIXED-E columns in series using a GBC LC 1240 RI detector. THF was used as the eluent at a flow rate of 1 mL/min (140 bar) at a column temperature of 40 °C, with a 20 μL injection volume and a 10 mg/mL sample concentration. Toluene was used as a flow marker. Average molecular weight calculations were performed using

the PSS WinGPC Unity software from Polymer Standards Service. GPC analysis of samples after oxidative cleavage were performed on an Alliance 2695 with a 2487 dual wavelength detector at 254 and 280 nm and a 2410 Refractive Index Detector, using an Agilent Oligopore column with THF as eluents and a flow rate of 1 mL/min at 30 °C.

Nitrogen Physisorption. Surface area, pore volume and pore size distribution were determined from the nitrogen adsorption/desorption isotherms at −196 °C, using a Micromeritics' ASAP2020 Instruments gas adsorption device. Before analysis, all samples were outgassed at 180 °C under vacuum for 5 h. Samples containing carbon were outgassed at 180 °C for 12 h. The isotherms were elaborated according to the BET method for surface area calculation, with the Horwarth–Kavazoe (HK) and Barrett–Joyner–Halenda (BJH) methods used for the evaluation of micropore and mesopore distributions, respectively.

Scanning Electron Microscopy (SEM). The morphology of the samples was investigated by scanning electron microscopy measurements carried out by using a *Philips XL-30-FEG Scanning Electron Microscope* at an accelerating voltage of 5-15 kV. Specimens were deposited as powders on an aluminium pin flat stubs. The qualitative and semi-quantitative analysis of elemental composition was also performed by SEM-EDX (Energy Dispersive X-ray) measurements; elemental profile maps showing the elemental distribution in the samples were also obtained under the same conditions.

Benzyl O,O'-dibenzyl caffeate. Caffeic acid (5.26 g, 29.2 mmol) was suspended in acetone and benzyl bromide (14.36 g, 84.0 mmol) and potassium carbonate (12.1 g, 87.5 mmol) was added. The suspension was refluxed for 16 h and after cooling the solids were removed by filtration. The solvent was removed in vacuo and excess benzyl bromide removed by vacuum distillation at 100 °C. The resulting thick paste was recrystallized from 50 mL boiling ethanol to afford 5.481 g (12.2 mmol, 42%) of the title compound as off-white crystals. Analysis was in agreement with previously published data.[26] ^{1}H NMR (CDCl$_3$): ∂ 7.61 (d, J = 15.9 Hz, 1H), 7.50 – 7.28 (m, 15H), 7.12 (d, J = 2.1 Hz, 1H), 7.06 (dd, J = 8.3, 2.0 Hz, 1H), 6.91 (d, J = 8.3 Hz, 1H), 6.29 (d, J = 15.9 Hz, 1H), 5.23 (s, 2H), 5.19 (s, 2H), 5.17 (s, 2H).

4-Hydroxy-3-propylcatechol. The compound was synthesized by adaption of a literature procedure.[27] Benzyl O,O'-dibenzyl caffeate (5.48 g, 12.2 mmol) was dissolved in 50 mL anhydrous THF and cooled to 0 °C under inert atmosphere. A solution of 2.0 M lithium aluminium hydride (12.5 mL, 25 mmol) in THF was added dropwise over 30 minutes. After stirring for 1 hour at 0 °C the solution was allowed to come to room temperature and stirred for one more hour. Subsequently the mixture was cooled again to 0 °C and carefully quenched with 5 mL methanol and subsequently 100 mL 1M HCl solution. The mixture was extracted three times with 100 mL diethyl ether. The combined organic layers were dried over magnesium sulphate, filtered and concentrated in vacuo to afford a mixture of crude O,O'-dibenzyl-4-hydroxy-3-propylcatechol and O,O'-dibenzyl-4-hydroxy-3-(2-propenyl)catechol. The complete oil was dissolved in a mixture of ethyl acetate (10mL) and methanol (50 mL), palladium (5 wt%) on carbon (295 mg) was added and the suspension stirred for 16 h under hydrogen atmosphere. The solids were removed by filtration and the filtrate concentrated in vacuo to afford a pale yellow viscous oil. The oil was purified by silica-gel chromatography using a 10:1 mixture of chloroform:methanol as eluent (Rf 0.30), to afford 0.88 g (5.2 mmol, 36% yield) of the title compound as a colourless oil. Analysis was in agreement with previously reported data.[28] ^{1}H NMR (DMSO-d6) ∂ 8.61 (br s, 2H), 6.60 (d, J = 7.9 Hz, 1H), 6.55 (d, J = 2.1 Hz, 1H), 6.41 (dd, J = 8.0, 2.1 Hz, 1H), 4.37 (br s, 1H), 3.37 (t, J =

6.5 Hz, 3H), 2.41 (t, J = 7.7 Hz 2H), 1.62 (q, J = 6.5 Hz, 2H); ^{13}C NMR (DMSO-d6) 144.94, 143.02, 132.91, 118.78, 115.66, 115.37, 60.17, 34.59, 30.97.

4-propylcatechol.[29] 3',4'-dihydroxypropiophenone (1.02 g, 6.15 mmol) was dissolved in 30 mL ethanol and palladium (5 wt%) on carbon (200 mg) was added. The suspension was stirred for 48 h under hydrogen atmosphere. The solids were removed by filtration and the filtrate concentrated in vacuo to afford 0.62 g (4.11 mmol, 67%) of the title compound. Analysis was in agreement with previously reported data.[30] ^{1}H NMR (DMSO-d6) δ 8.64 (s, 1H), 8.54 (s, 1H), 6.59 (d, J = 7.9 Hz, 1H), 6.53 (d, J = 2.1 Hz, 1H), 6.38 (dd, J = 7.9, 2.1 Hz, 1H), 2.33 (t, J = 7.3 Hz, 2H), 1.48 (h, J = 7.3 Hz, 2H), 0.83 (t, J = 7.3 Hz, 3H); ^{13}C NMR (DMSO-d6) δ 144.91, 143.05, 132.91, 118.85, 115.69, 115.35, 36.69, 24.31, 13.64.

Preparation of Cu-PMO Catalysts. The Cu-PMO catalyst with a nominal 0.03:0.12:0.05 ratio of Cu^{+2}, Mg^{+2} and Al^{+3} respectively was prepared according to a literature procedure.[2] In a typical procedure, an aqueous solution containing magnesium nitrate hexahydrate (15.384 g, 0.06 mol), aluminium nitrate nonahydrate (9.378 g, 0.025 mol) and copper(II) nitrate hemi(pentahydrate) (3.488 g, 0.015 mol) in 150 mL of deionized water was added drop wise to an aqueous solution of sodium carbonate (2.65 g, 0.025 mol) in 200 mL of deionized water (pre heated to 65 °C) under vigorous stirring. The pH of the solution was maintained relatively constant at ~ 10 by the addition of an aqueous solution of NaOH (1 M). The resultant slurry was continuously stirred for 3 days. The solution was removed by vacuum filtration and the residue was washed with deionized water. The resulting light blue solid cake was re-suspended in 2 M warm aqueous sodium carbonate (26.5 g, 125 mL) and stirred for 16 h. The copper-doped hydrotalcite material obtained by vacuum filtration was then thoroughly washed with deionized water until the filtrate was of neutral pH. The resulting light blue solid was dried in an oven at 120 °C for 16 h and calcined at 460 °C for 24 h in air to obtain the green Cu-PMO catalyst.

Lignin Isolation. Lignin isolation was performed at the Centre for Green Chemistry & Engineering at Yale University, using the isolation procedure also reported in literature.[4] In a typical procedure, pre-ground candlenut nutshells were refluxed in methanol for 12 h. The solid residue was removed by vacuum filtration and washed with several portions of methanol. The combined filtrate was concentrated under rotary evaporation and precipitated over ice. The resultant brown crude lignin was collected by filtration and dried under vacuum. The crude lignin was purified with dichloromethane under reflux conditions for 12 h. The purified lignin was further fractionated in ethyl acetate under reflux conditions for 12 h. The mixture was filtered and solids were washed with small portions of ethyl acetate. The ethyl acetate-soluble lignin was obtained by removing the solvent of the filtrate *in vacuo*. The material was characterized by ^{1}H, ^{13}C NMR and GPC.

Catalytic Depolymerisation of Candlenut Lignin. The catalytic depolymerisation of Candlenut lignin was carried out in a 50 mL Parr 4843 reactor equipped with magnetic stirrer and temperature controller. Typically, 0.25 g of Cu-PMO catalyst was added to the reaction mixture containing 0.5 g of Candlenut lignin dissolved in 15 mL of methanol solvent. The reactor was sealed and purged several times with nitrogen and hydrogen. The reactor was pressurized with 3.5 MPa Hydrogen at room temperature and heated to 180 °C and stirred with 700 rpm for 18 h. After completion of the reaction, the reactor was rapidly cooled down to room temperature in an ice water bath. The pressure was noted upon after room temperature was reached and the reactor was depressurized carefully. The content of the reactor was collected in centrifuge tubes by washing

the reactor with methanol several times and the solids were separated from the methanol soluble products by centrifugation. The solutions were decanted and the solids were washed with small portions of methanol and washing solutions were combined with decanted solutions. The solvent was removed by rotary evaporation under vacuum to give a dark, viscous liquid that was sampled for ^{1}H NMR, ^{13}C NMR and GPC analysis. The remaining catalyst solid residue was washed with diethyl ether and dried for further characterization.

Oxidative Cleavage of Pure Compounds & Lignin-Oils. In a typical experiment, the catechol (0.120 mmol) or lignin-oil (30 mg) was dissolved in 1.55 mL methanol and 0.2 mL acetonitrile in a glass vial (20 mL). Aliquots of stock solutions of iron (III) nitrate nonahydrate (0.010 mmol), TPA (0.010 mmol) and ammonium acetate (0.020 mmol) were added for a final volume of 1.98 mL. The vial was flushed with pure oxygen and left to stir for 2 h. Afterwards, the reaction was quenched with 5 mL 1 M HCl and extracted three times with 5 mL ethyl acetate. The combined organic layers were dried over magnesium sulphate and concentrated in vacuo. 2,4,6-triiodophenol was added to the resulting film and the material was subsequently dissolved in DMSO-d6 for NMR analysis.

Computational Methods. Density functional theory (DFT) calculations were performed with the Amsterdam Density Functional (ADF 2014.01) package[31-33], using the BP86 functional[34,35] and the triple zeta slater orbital basis set with polarisation functions (TZP) that is included with ADF.[36] Energies were corrected for solvation using the conductor-like screening model (COSMO)[37] and for dispersion interactions using Grimme's DFT-D3 dispersion correction[38] with Becke-Johnson damping.[39] All structures were subjected to geometry optimizations without any constraints followed by a full analytical frequency calculation. All reported structures were characterized by no (minima) or one (transition states) imaginary frequencies. Energies reported are Gibbs free energies at 298 K relative to the monomethyl *cis,cis*-muconate anion.

7.6 References

1   G. S. Macala, T. D. Matson, C. L. Johnson, R. S. Lewis, A. V. Iretskii and P. C. Ford, *ChemSusChem*, 2009, **2**, 215–217.

2   K. Barta, T. D. Matson, M. L. Fettig, S. L. Scott, A. V. Iretskii and P. C. Ford, *Green Chem.*, 2010, **12**, 1640–1647.

3   K. Barta and P. C. Ford, *Acc. Chem. Res.*, 2014, **47**, 1503–1512.

4   K. Barta, G. R. Warner, E. S. Beach and P. T. Anastas, *Green Chem.*, 2014, **16**, 191–196.

5   X. Huang, T. I. Korányi, M. D. Boot and E. J. M. Hensen, *ChemSusChem*, 2014, **7**, 2276–2288.

6   F. Chen, Y. Tobimatsu, D. Havkin-Frenkel, R. A. Dixon and J. Ralph, *Proc. Natl. Acad. Sci. U.S.A.*, 2012, **109**, 1772–1777.

7   F. Chen, Y. Tobimatsu, L. Jackson, J. Nakashima, J. Ralph and R. A. Dixon, *Plant J.*, 2013, **73**, 201–211.

8   Y. Tobimatsu, F. Chen, J. Nakashima, L. L. Escamilla-Treviño, L. Jackson, R. A. Dixon and J. Ralph, *Plant Cell*, 2013, **25**, 2587–2600.

9   A. Behr, S. Toepell and S. Harmuth, *RSC Adv.*, 2014, **4**, 16320–16326.

10   A. L. Flourat, A. A. M. Peru, A. R. S. Teixeira, F. Brunissen and F. Allais, *Green Chem.*, 2014, **17**, 404–412.

11   A. L. Jongerius, P. C. A. Bruijnincx and B. M. Weckhuysen, *Green Chem.*, 2013, **15**, 3049–3056.

12   W. Schutyser, S. Van den Bosch, J. Dijkmans, S. Turner, M. Meledina, G. Van Tendeloo, D. P. Debecker and B. F. Sels, *ChemSusChem*, 2015, **8**, 1805–1818.

13   A. A. Dwiatmoko, S. Lee, H. C. Ham, J.-W. Choi, D. J. Suh and J.-M. Ha, *ACS Catal.*, 2015, **5**, 433–437.

14   M. Pascaly, M. Duda, F. Schweppe, K. Zurlinden, F. K. Müller and B. Krebs, *J. Chem. Soc., Dalton Trans.*, 2001, 828–837.

15   Y. Hitomi, M. Yoshida, M. Higuchi, H. Minami, T. Tanaka and T. Funabiki, *J. Inorg. Biochem.*, 2005, **99**, 755–763.

16   J. A. Elvidge and P. D. Ralph, *J. Chem. Soc. C*, 1966, 387–389.

17   H. G. Jang, D. D. Cox and L. Que Jr., *J. Am. Chem. Soc.*, 1991, **113**, 9200–9204.

18   G. F. Pauli, B. U. Jaki and D. C. Lankin, *J. Nat. Prod.*, 2007, **70**, 589–595.

19   T. Rundlöf, M. Mathiasson, S. Bekiroglu, B. Hakkarainen, T. Bowden and T. Arvidsson, *J. Pharm. Biomed. Anal.*, 2010, **52**, 645–651.

20   J. A. Elvidge, R. P. Linstead, P. Sims and B. A. Orkin, *J. Chem. Soc.*, 1950, 2235.

21   W. Yin, R. H. Venderbosch, G. Bottari, K. K. Krawzcyk, K. Barta and H. J. Heeres, *Appl. Catal. B*, 2015, **166-167**, 56–65.

22   A. J. Kumalaputri, G. Bottari, P. M. Erne, H. J. Heeres and K. Barta, *ChemSusChem*, 2014, **7**, 2266–2275.

23   T. D. Matson, K. Barta, A. V. Iretskii and P. C. Ford, *J. Am. Chem. Soc.*, 2011, **133**, 14090–14097.

24   R. Zăvoianu, R. Ionescu, O. D. Pavel, R. Bîrjega and E. Angelescu, *Appl. Clay Sci.*, 2011, **52**, 1–10.

25   G. J. P. Britovsek, J. England and A. J. P. White, *Inorg. Chem.*, 2005, **44**, 8125–8134.

26   S. Galland, N. Mora, M. Abert-Vian, N. Rakotomanomana and O. Dangles, *J. Agric. Food Chem.*, 2007, **55**, 7573–7579.

27   G. García, I. Serrano, P. Sánchez-Alonso, M. Rodríguez-Puyol, R. Alajarín, M. Griera, J. J. Vaquero, D. Rodríguez-Puyol, J. Álvarez-Builla and M. L. Díez-Marqués, *Eur. J. Med. Chem.*, 2012, **50**, 90–101.

28   A. M. Villegas, L. E. Catalán, I. M. Venegas, J. V. García and H. C. Altamirano, *Molecules*, 2011, **16**, 4632–4641.

29   W. H. Hartung and F. S. Crossley, *J. Am. Chem. Soc.*, 1934, **56**, 158–159.

30   A. Ozanne, L. Pouységu, D. Depernet, B. François and S. Quideau, *Org. Lett.*, 2003, **5**, 2903–2906.

31   C. F. Guerra, J. G. Snijders, G. te Velde and E. J. Baerends, *Theor. Chem. Acc.*, 1998, **99**, 391–403.

32   G. te Velde, F. M. Bickelhaupt, E. J. Baerends, C. Fonseca Guerra, S. J. A. van Gisbergen, J. G. Snijders and T. Ziegler, *J. Comp. Chem.*, 2001, **22**, 931–967.

33   ADF2014, SCM, Theoretical Chemistry, Vrije Universiteit, Amsterdam, The Netherlands, http://www.scm.com

34   J. Perdew, *Phys. Rev. B*, 1986, **33**, 8822–8824.

35   A. D. Becke, *Phys. Rev. A*, 1988, **38**, 3098–3100.

36   E. Van Lenthe and E. J. Baerends, *J. Comp. Chem.*, 2003, **24**, 1142–1156.

37   C. C. Pye and T. Ziegler, *Theor. Chem. Acc.*, 1999, **101**, 396–408.

38   S. Grimme, J. Antony, S. Ehrlich and H. Krieg, *J. Chem. Phys.*, 2010, **132**, 154104.

39   S. Grimme, S. Ehrlich and L. Goerigk, *J. Comp. Chem.*, 2011, **32**, 1456–1465.

Chapter 8a

Summary & Concluding Remarks

Summary

Fossil fuels, specifically crude oil, are currently the most important feedstock in industry for both the production of bulk and fine chemicals. There are, however, several drivers for replacing these non-renewable feedstocks with alternative ones: first, the future availability of these resources is uncertain. Changes in feedstock composition, particularly the large-scale use of shale gas in the United States, means that some components, particularly aromatics, are less available and, as a result, alternative sources are required. Finally, fossil fuel resources contribute significantly to the emission of carbon dioxide and urgent reduction of emissions is required to prevent further global warming.

Lignocellulosic biomass can be an important alternative renewable feedstock for the chemical industry. Large amounts of lignocellulose are available, as it is the cell wall material that makes up the bulk of non-edible plant matter, such a stems, stalks and branches, and its use would not directly compete with food production. This type of biomass is comprised of three main components: cellulose (a polymer of glucose), hemicellulose (a polymer of mainly pentose sugars) and lignin (a polymer of aromatic monomers). Processing of the biomass has been proposed to proceed analogously to crude oil in a biorefinery, converting the biomass into a portfolio of products including fuels and chemicals, e.g. by first fractionating the feed into the constituent components, which are then individually valorised.

The lignin component is the only part of lignocellulosic biomass of significant abundance that contains aromatic fragments and is therefore an ideal candidate for the production of aromatic bulk and fine chemicals (and non-aromatic chemicals produced through aromatic intermediates). However, lignin is also the most difficult biomass component to valorise, as it does not have a single well-defined structure, but has multiple bond motifs linking the different monomers, including ones based on difficult-to-break carbon-carbon bonds. A detailed, critical review of lignin chemistry, ranging from bio-synthesis and its engineering, lignin separation, catalytic depolymerisation and subsequent valorisation is presented in *Chapter 2*.

Briefly, lignin biosynthesis occurs through the phenylpropanoid pathway, which starts with the amino acid phenylalanine and converts it into one of the three principal lignin monomers *p*-coumaryl alcohol, coniferyl alcohol or sinapyl alcohol. These monomers are then transported to the cell wall, where they undergo radical coupling into the growing lignin matrix. The phenylpropanoid pathway is now well understood and may be altered by genetic modification; this also allows incorporation of non-native monomers into the lignin structure. If these monomers are linked through easily cleavable bonds (such as esters), this can afford species with lignin that can be more readily separated and cleaved. However, at the same time, the natural functions of the lignin (inferring strength to the plant, channelling water and acting as a biological barrier) must be maintained.

Finding suitable and viable transgenic varieties of commercially relevant species, which grow well not only in greenhouse but also in field conditions, is a very time-consuming process and consequently such transgenic lignins are currently not available to the community working on (catalytic) lignin valorisation.

Separation of the lignin from the other biomass components is an essential step in any valorisation scheme. Presently the commercially most relevant separation method is the Kraft process, which is the principal method by which cellulose fibres are liberated in the paper and pulp industry. In the Kraft process the wood is cooked in the presence of an aqueous sodium hydroxide/sodium sulphide solution, breaking down ether bonds in the lignin to release smaller fragments in solution. Lignin obtained by the Kraft process is, however, significantly changed from the native structure, as cleavage of the ether linkages releases reactive fragments that subsequently condense to form new carbon-carbon bonds. These carbon-carbon bonds are clearly more difficult to break than the original ether bonds and thus pose a problem in further lignin processing. Newer separation processes based on organic solvents, which use an acid catalyst to release soluble lignin fragments, also suffer from these recondensation reactions. One emerging method to overcome this and enable reactivity to occur on the native lignin structure is to catalytically convert the lignin during the isolation procedure itself.

The field of catalytic lignin depolymerisation has been a very active one and a large variety of methods have been developed in recent years. Roughly, these can be divided into 'mild' methods that target specific linkage patterns (typically the β-O-4 aryl ether) and 'harsh' methods that operate in a regime in which both thermal and catalytic reactions may take place. For the former, the choice of an appropriate lignin feedstock is paramount: the targeted linkage must still be abundant for the depolymerisation to be successful. In harsher depolymerisation methods, the conditions are such that even recalcitrant carbon-carbon bonds may be broken as well. However, as these methods are generally far less selective, complicated product mixtures with numerous aromatic products are often obtained. Whatever the depolymerisation method, the issue of avoiding recondensation of the liberated monomers and oligomers is also of paramount importance. Successful depolymerisation strategies therefore are typically able to 'trap' reactive intermediates and products and convert them into stable monoaromatic end products.

Further processing of oxygenated aromatics (insofar as they are not valuable products in their own right) obtained from lignin depolymerisation has primarily focused on removal of oxygen by hydrodeoxygenation. This allows one, for example, to obtain the same benzene-toluene-xylene (BTX) mixtures that are currently obtained from crude oil; further conversion can therefore take place with existing chemistry and infrastructure. However, as subsequent chemistry often again involves the incorporation of oxygen, it would be more efficient if the oxygenated aromatics obtained from lignin

can be directly converted to the desired end-products. Such examples are, however, still scarce in literature.

The aim of the work in this thesis was to develop new catalytic routes for the valorisation of lignin, with a specific emphasis on the use of catalytic carbon-carbon bond cleavage reactions. Given the importance of trapping reactive intermediates in lignin depolymerisation, a process was developed that uses catalytic decarbonylation to remove aldehydes to prevent subsequent condensation, ultimately allowing high amounts of monomeric aromatics to be obtained. In addition, as the direct conversion of small oxygenated aromatics to useful products is highly desirable, a two-step process for the conversion of catechol to the nylon-6,6 monomer dimethyl adipate was developed. Key in this process is the iron-catalysed oxidative ring cleavage of the aromatic carbon-carbon bond in catechol to obtain the α,ω-dicarboxylic acid motif. Given the difference in reactivity that is often observed between model compounds or pure starting materials and real biomass-derived feeds, both the lignin depolymerisation and oxidative cleavage were investigated in the conversion of real biomass.

In *Part I (Chapter 3)* the development of a new lignin depolymerisation method is described, which uses a water-stable Lewis acid-catalysed hydrolysis step to cleave the β-O-4 aryl ether and a rhodium/diphosphine-catalysed decarbonylation step to remove the reactive aldehyde products formed upon hydrolysis, to ultimately afford 4-methylphenols (Figure 8.1). Using model compounds representing the β-O-4 linkage, scandium triflate as the water-stable Lewis acid and a rhodium complex prepared *in-situ* from [Rh(cod)Cl]$_2$ and 1,3-bis(diphenylphosphino)propane, the concept of the reaction could be validated. Investigation of the mechanism revealed the cleavage to take place by an initial Lewis acid-catalysed dehydration of the α-hydroxyl functionality to afford a styryl ether. This functionality is then hydrolysed (again catalysed by the Lewis acid) to afford an aldehyde, which is the substrate for the subsequent rhodium-catalysed decarbonylation. Key is that the steady-state concentration of the aldehyde is very low throughout the reaction; when the rhodium catalyst was not sufficiently active, aldol condensation products were found instead and the monomer yield was significantly reduced. Quite remarkable, an alternative pathway appeared to be available as well, which led to the formation of styrene-derivatives, products that have not been observed before.

Actual lignin, isolated from poplar using a mild dioxasolv procedure which leaves a large fraction of the β-O-4 aryl ether bonds intact, was subsequently subjected to the depolymerisation procedure. In line with the mechanism seen with the model compound, decarbonylated 4-methylphenols were also formed as major products, demonstrating that the chemistry translates well to actual lignin. In addition, 4-(1-propenyl)phenols were also isolated as major products, which presumably form analogously to the styrenes observed in the model compound studies. The selectivity towards the products could be
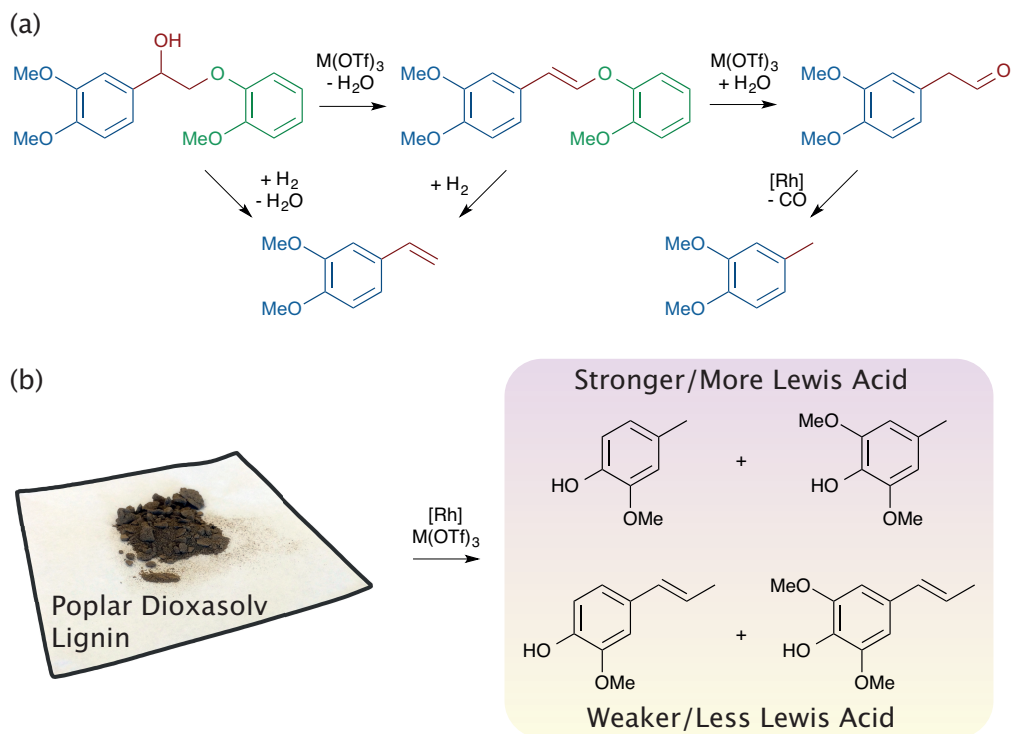
Figure 8.1: The lignin depolymerisation procedure developed in Chapter 3. (a) A model compound study revealed that cleavage occurs through an initial Lewis acid-catalysed dehydration to a styryl ether, followed by hydrolysis to an aldehyde, which is susceptible to rhodium-catalysed decarbonylation. An alternative pathway leading to styrenes exists as well. (b) The depolymerisation of poplar dioxasolv lignin affords either 4-methylphenols or 4-(1-propenyl)phenols in agreement with the above mechanism; the selectivity can be steered by varying the amount and strength of Lewis acid catalyst.

steered by the choice of Lewis acid catalyst; by using weaker Lewis acids or less Lewis acid, selectivity shifted towards the generation of the 4-(1-propenyl)phenols, while stronger Lewis acids or more Lewis acid led to the formation of more decarbonylated 4-methylphenols. Both product types are valuable; particularly the 4-(1-propenyl)phenols may be useful synthons for the production of fragrances and pharmaceuticals. Under optimised conditions 12.4 wt% of monomeric products could be obtained; although this may seem low at first, it represents more than 80% of the maximum monomer yield that can be obtained by solely by cleaving β-O-4 bonds in the lignin.

The general applicability of the depolymerisation method was demonstrated by applying it to lignins isolated from spent brewer's grain and pine sawdust as well. As mentioned before, the development of depolymerisation procedures that act directly on the wood are also interesting, as this allows access to the largest amount of the cleavable β-O-4

bonds. Depolymerisation carried out directly on poplar sawdust also afforded the same lignin-derived 4-methylphenols and 4-(1-propenyl)phenols, with yields comparable to those obtained with the isolated lignin. Undoubtedly, further investigation of the role of the carbohydrate fraction in the depolymerisation procedure will allow even higher amounts of aromatics to be obtained directly from the wood.

Part II describes the development of an iron catalyst for the oxidative ring cleavage of pyrocatechol, which is a key step in a novel route for producing the nylon-6,6 monomer dimethyl adipate. Iron(III) complexes of tris(2-pyridylmethyl)amine have previously been shown to ring-cleave the (activated) model compound 3,5-di-*tert*-butylcatechol in stoichiometric reactions; in *Chapter 4* the *catalytic* cleavage of pyrocatechol with molecular oxygen using this complex is demonstrated (Figure 8.2). The cleavage reaction is fully selective for intradiol cleavage and afforded the half-methyl ester of *cis,cis*-muconic acid as the major product, with the methyl ester deriving from the methanol solvent. Several other isomers are observed in smaller amounts; however, all of these derive from selective intradiol cleavage and are the result of subsequent isomerisation.
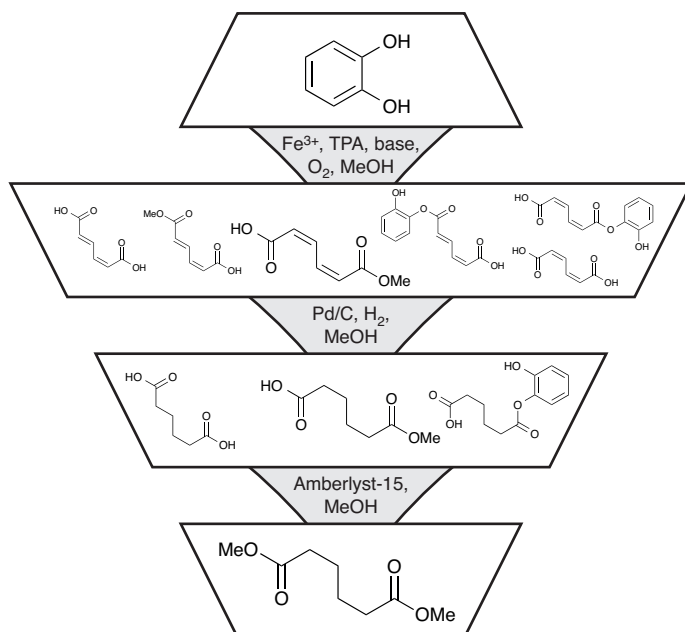

Figure 8.2: Summary of the route developed in this thesis in which catechol is converted to dimethyl adipate; key is that the first step proceeds with complete intradiol catechol dioxygenation selectivity to convert catechol to a mixture of muconic acid isomers. Subsequent hydrogenation and transesterification steps convergently convert the mixture to dimethyl adipate.

The reaction proceeds through an iron(III) catecholato complex, whose absorption bands in the visual part of the spectrum conveniently allow for for monitoring the oxidative cleavage by UV-Vis-NIR spectroscopy (and affords the solutions a distinctive purple colour). In order to form the catecholato complexes, it is necessary to deprotonate the catechol by addition of base; notably, once the catecholato species are formed, the reaction can continue for multiple cycles without the addition of any additional base, despite the fact that an acidic product is formed. Spectroscopic measurements further confirmed that the concentration of catecholato complexes indeed remained nearly constant despite the formation of the acidic products. This is attributed to the remarkably strong binding of the catecholato moiety to the iron centre, which means that even a very weak base, i.e. the product muconate anion, can deprotonate the catechol, if this allows binding to the iron centre. Consequently, the base that is needed to initiate the reaction can then also be very weak; even acetate salts such as ammonium acetate were found to be sufficient. Eventually, the catechol concentration becomes so low that catecholato complexes no longer form and resultant iron species were identified as dimeric μ-oxo, μ-carboxylato species, which are often found as deactivation product in iron-catalysed oxidation chemistry. Remarkably, upon addition of fresh catechol, the catecholato complexes would form again and the catalyst regain its activity, highlighting the reversibility of the deactivation pathway.

Chapter 5 continued the investigation of the iron-catalysed ring cleavage of catechol. By using a suitable, liquid batch autoclave system with a continuous, pressurised gas flow, a wide range of conditions could be studied. Variation of the important parameters catalyst concentration, pressure and temperature showed that the system nicely follows all the appropriate rate laws: conversion is approximately 0th order in substrate and 1st order in catalyst and oxygen. Based on the data obtained from experiments at different temperatures, the enthalpy and entropy of activation could be estimated to be 5.7 kcal/mol and 41 cal mol^{-1} K^{-1} respectively. Importantly, full selectivity towards the intradiol cleavage products was observed even under the most severe conditions; consequently, the turnover frequency could be improved to 120 h^{-1} at 25 bar pressure (5 vol% oxygen in nitrogen) and 80 °C, which is a 35-fold improvement over the activity observed under the conditions used in *Chapter 4* (air at atmospheric pressure, 50 °C).

As the ultimate goal of the oxidative ring-cleavage was to afford valuable commodity chemicals, the further conversion of the obtained mixture to dimethyl adipate, a monomer for nylon-6,6 was demonstrated as well, with initial experiments in *Chapter 4* and a more expansive study in *Chapter 5*. The fact that a mixture of compounds was obtained from the ring cleavage in this case was not an issue, as the subsequent conversion steps are convergent (Figure 8.2): the different double bond isomers are all hydrogenated to the same saturated carbon chain and (trans)esterification can convert the present free acids

and various esters into a single ester product. Indeed, all that matters is that the cleavage occurs with complete intradiol selectivity. The hydrogenation was shown to proceed well over standard commercial palladium on charcoal catalysts. A commercial Raney®-nickel catalyst, avoiding the use of scarce noble metals, was also able to hydrogenate the double bonds, although in that case some half-hydrogenated products remained. Esterification with methanol also proceeded well over the commercially available solid acid catalyst Amberlyst-15. Both subsequent reaction steps can thus be carried out with readily available catalysts, which due to their heterogeneous nature can also be easily separated from the products. As both subsequent reactions can also be carried out in the same methanol solvent, this means that workup between the reactions is limited to simple removal of the palladium catalyst by filtration. As dimethyl adipate is somewhat volatile, the final purification could take place by vacuum distillation, which allowed the isolation of highly pure dimethyl adipate in 62% yield from catechol over all reaction steps.

In order to better understand the chemistry behind the catalytic dioxygenation step and gain further insight in how the activity of the catalyst may be further improved, a mechanistic study was carried out. This entailed a combined experimental and computational approach and is described in *Chapter 6*. As it had been previously suggested that the Lewis acidity of the iron centre in the catecholato complex was related to the activity, a novel analogue of TPA, tris(4-chloro-2-pyridylmethyl)amine (Cl_3-TPA) was synthesised. The additional chloride substituents are electron-withdrawing and the ligand should thus afford a structurally analogous, but more Lewis acidic iron complex. Experimental rate constants for the cleavage were determined for iron(III) complexes of both ligands, with a variety of substituted catechols. As was previously observed, the more electron-rich catechols reacted faster. This substituent effect could also be fit to the Hammett equation, which indicated that that the rate-determining step should involve an electrophilic attack of oxygen on the catecholate. In addition, complexes with the electron-deficient Cl_3-TPA ligand indeed also reacted faster.

The major mechanistic controversy in the intradiol catechol dioxygenation reaction centres around the mode of initial oxygen attack, with some authors suggesting that oxygen attacks the catecholato moiety first, while others have proposed the oxygen to coordinate to iron first, which only then leads to attack of oxygen on the catecholato ring. Several mechanisms of oxygen attack were therefore investigated computationally; remarkably, the only pathway that afforded a reasonable barrier for activation was where oxygen coordinated to iron, with a simultaneous partial dissociation of the catecholato moiety to provide the binding site for oxygen (Figure 8.3). Subsequent attack of oxygen onto the catecholate ring forms a bridging peroxide, which splits heterolytically and the resulting oxygen radical rapidly inserts itself into the ring, leading to the muconic acid anhydride product. The attack of oxygen on the catecholate ring was calculated to be
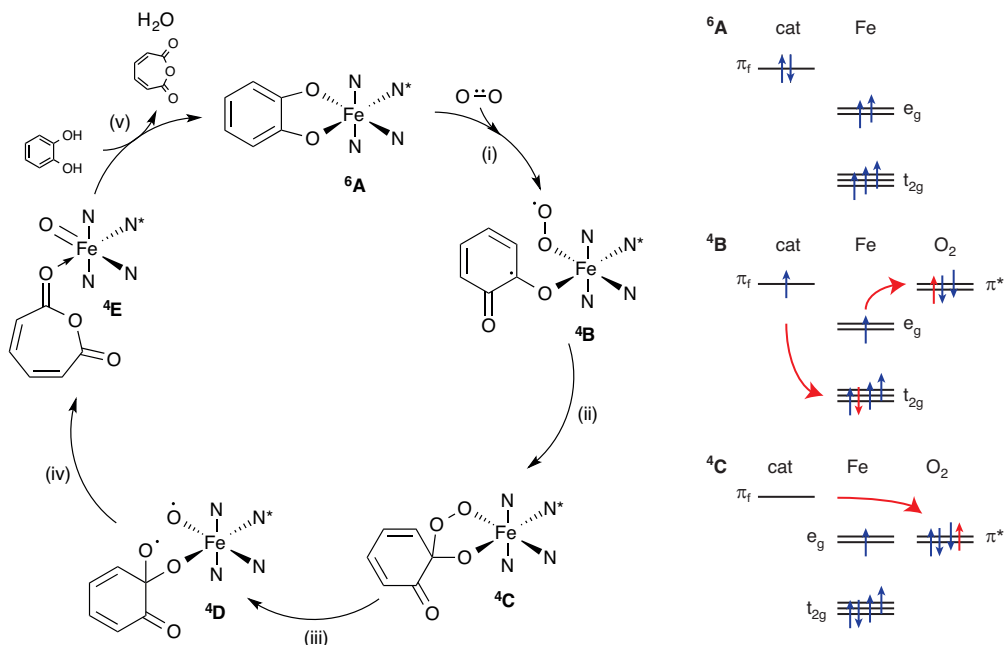
Figure 8.3: (left) Catalytic cycle, showing the mechanism of catechol intradiol dioxygenation. (right) Approximate electron configurations in the three initial states of the cycle, showing the 'buffer' function of iron. Upon coordination of oxygen, it is reduced by a single electron from iron, which is simultaneously reduced by another single electron with opposite spin from the catecholate. The frontier orbitals of oxygen and the semiquinonate then have two partially occupied orbitals with opposite spins, which facilitate subsequent carbon-oxygen bond formation.

the rate-determining step. Crucially, the computational results were accurately able to reproduce the effects on the rate observed with different catechols and the difference between the two studied TPA ligands, giving significant credence to the mechanism.

Analysing the molecular orbitals involved in the formation of the superoxide and bridging peroxide iron afforded more insight into how this remarkable reaction takes place. In the ground state of the iron-catecholato complex, the iron is in a high-spin state (i.e. the iron d orbitals are each occupied by a single electron, with all spins in the same orientation (up)). As the oxygen atom binds to the iron centre, the spins of the two-unpaired electrons are oriented anti-parallel (down) to those in the iron centre; at the same time the oxygen is reduced to a superoxide by the catecholato moiety, which is reduced to a semiquinonato species. As the oxygen π orbitals already contain two down electrons, only an up electron can be donated. If this would occur directly from the catecholato (which does not have any unpaired electrons), both superoxide and semi-quinonato would be left with a single down electron: a subsequent reaction between the two to form the carbon-oxygen bond would be strongly spin-forbidden. Instead, the iron centre acts as a redox-neutral buffer by changing from a high to intermediate spin

state, accepting one down-electron from the quinonate and donating one up-electron to oxygen. Consequently, oxygen and the semiquinonate now have unpaired anti-parallel electrons, which together can readily form the new carbon-oxygen bond. The influence of the ligand on the activity can then be clearly understood by the ability of the iron centre to stabilise this intermediate spin state. The symmetry of the TPA family of ligands is such that the pyridine π-orbitals all show overlap with the same, single d orbital of iron, which is therefore stabilised by π-backbonding. Double occupation of this single stabilised d-orbital then makes the intermediate spin state more favourable. Thus, for the development of novel catalytic systems for catechol intradiol dioxygenation, it is of crucial importance that the ligand is able to sufficiently stabilise this intermediate spin state.

In *Part III (Chapter 7)*, the developed catalytic catechol cleavage method is applied to catechols that have been directly obtained from lignin. A lignin depolymerisation procedure that affords pyrocatechol in good yields does not yet exist, thus the chemistry described in chapters 4 and 5 could not be directly translated. The hydrogenolytic depolymerisation of lignin derived from candlenut shells using copper on porous metal oxide catalysts had, however, been reported to afford a variety of propyl-substituted catechols in good yield and the oxidative cleavage of these compounds was therefore investigated. The two major catechols in the lignin depolymerisation mixture were synthesised and as pure compounds shown to undergo oxidative cleavage with our iron (TPA) catalyst as well. The propyl substituents did somewhat complicate the product mixtures, as the initial *cis,cis*-muconic acid products undergo isomerisation much more rapidly, forming not only *cis,trans*-products but also γ-muconolactones. In addition, mass balances for these compounds were significantly lower than those obtained with pyrocatechol; the selectivity towards intradiol cleavage products remained intact, however.

Application of the catalytic system towards actual lignin oil obtained from the depolymerisation of candlenut lignin, showed a remarkable connection between the depolymerisation catalyst used and the activity of the mixture in the subsequent oxidative cleavage. For those catecholic lignin oils obtained with a copper catalyst synthesised from metal nitrate precursors, the oxidation proceeded smoothly and the same oxidation products were observed as with the pure compounds. However, for those lignin oils obtained with a catalyst prepared from chloride precursors, the reaction proceeded slower, or with lower amounts of oxidation catalyst, not at all. This was suggested to be due to poisoning of the iron catalyst by residual chloride left in the depolymerised lignin mixture and highlights the importance of investigating the interdependencies in two-stage lignin conversion schemes.

Concluding Remarks

The work described in this thesis contributes to the development of the chemistry that is required for the application of lignin as a renewable feedstock for the production of chemicals. The subject was not limited to only depolymerising the lignin: an important goal was also to develop new chemistry to convert products obtained from a lignin depolymerisation step into those chemicals that are presently important products of the chemical industry. A particular emphasis was placed on the use of carbon-carbon bond cleavage reactions. The successful development of the two catalytic system described in this thesis highlights that this is very complimentary to carbon-oxygen bond cleavage reactions more typically employed in biomass upgrading. Specifically, the use of the decarbonylation catalyst in the tandem reaction with a Lewis acid not only facilitates the successful outcome of the reaction, but also affords a structural motif in the products that is otherwise hard to access. Likewise, the oxidative cleavage of catechol ring affords the six-carbon dicarboxylic acid motif that is again difficult to acquire through other means from biomass, but is very valuable, as for example demonstrated by the further conversion to dimethyl adipate.

Selective carbon-carbon bond cleavage reactions are, nevertheless, fundamentally challenging. To afford both high activity and selectivity, some highly specific chemistry may be required. This is clearly highlighted in the mechanism of the catechol intradiol dioxygenation, where eventual carbon-carbon bond cleavage is only made possible by the distinct redox-properties of the 1,2-arenediol functionality. At the same time, the (spin) properties of oxygen and the ability of the iron complex to have multiple accessible spin states opens up only a single, specific pathway, which leads to the very high selectivity that is obtained. In the broader context of biological oxidation chemistry, this is also very relevant, as this mechanism avoids the high-valent (and highly reactive) iron-oxo species normally associated with such reactivity. Although very specific, the concepts might nevertheless prove useful to develop other mild oxidation catalysts based on iron.

The tandem Lewis acid/rhodium lignin depolymerisation procedure highlights the important principle of trapping reactive intermediates to prevent repolymerisation of lignin fragments. Although this necessity has been pointed out previously by some key contributions in the field, the approach described in this thesis takes this one step further by using the trapping procedure itself to also steer the outcome of the depolymerisation to more desirable products. In this sense, the availability of not just one, but two accessible trapping pathways was a very interesting serendipitous discovery, especially because the product distribution can then be selected by choice of the appropriate (amount of) Lewis acid catalyst. This paves the way to steerable lignin depolymerisation procedures, which can afford products with different residual aliphatic carbon chains as desired. At the same time, this formation of 4-(1-propenyl)phenols is quite remarkable,

as this amounts to a formal reductive carbon-oxygen bond cleavage, while leaving the carbon-carbon double bond intact. The next question is then how this cleavage occurs precisely, which needs further investigation. Not only should this lead to better control of lignin depolymerisation, but if the reaction can be made more general it should also be synthetically useful.

The chemistry of lignin has for a long time been hindered by a lack of appreciation of the extent with which the lignin is altered during its isolation procedure; particularly, the significant loss of the often targeted β-O-4 aryl ether fragment meant that conceptually sound depolymerisation methods often failed to produce significant amounts of monomer, as they made use of too recalcitrant, condensed lignins containing little of the targeted linkage. Combined with the realisation that condensation of reactive fragments during the isolation step is responsible for this recalcitrance, the application of lignin depolymerisation (with appropriate trapping strategy) directly on the wood has allowed some dramatic improvements in the yield of small aromatics. Although only briefly covered in Chapter 3, the results obtained there also show that simply substituting lignin for wood is at the same time no guarantee for improved yields. The specific causes will need to be investigated further, but the interplay between sugar and lignin components may play an important role in this. Additionally, as the cellulose and hemi-cellulose components are then also important products it needs to be clearly investigated what happens to these components and if those products are also still amenable to further processing. Despite the additional complications, the advantages of performing depolymerisation *and* trapping on the native lignin structures are significant. Lignin depolymerisation directly on the wood is therefore likely to gain more importance in the future.

At the same time, it is clear that, when faced with the realities of lignin chemistry, there is still a gap between the products obtained in depolymerisation and those products desired by the chemical industry. This is of course in part because these chemicals (especially those produced in large amounts) have been developed because of the ease with which they can be obtained from crude oil. One can therefore approach the problem starting from potential products, which was certainly part of the motivation for Part II. Adipic acid esters fit the bill perfectly as potential bulk chemicals from lignin as they are attractively priced, produced in large volumes and the route from crude oil is sufficiently laborious that routes starting from biomass can actually be more efficient. However, one then almost inevitably runs into the problem that the starting material (here, catechol) is not *quite* the product that can be obtained from lignin (so far). The most recalcitrant functionality that needs to be removed is of course the alkyl chain, which requires some sort of carbon-carbon bond cleave (either as a separate step, or during lignin depolymerisation).

The decarbonylation described in Chapter 3 already shows that selective partial removal of the carbon chain is now possible. A question that remains is whether the

decarbonylation approach can be extended to afford products where the complete alkyl chain is removed. Aside from three decarbonylation steps, this also requires three formal oxidations/dehydrogenations. Several recent publications, for example deal with the selective oxidation of the β-O-4 aryl ether fragment, which has revealed the aryl alkyl ether to become considerably more labile. If, in this way, the hydrolysis of the ether can proceed, *without requiring the α-hydroxyl to be eliminated*, and a tandem oxidation or dehydrogenation can convert all the remaining hydroxyls into carbonyls, complete decarbonylation might be possible. However, this will clearly require some considerable research effort.

Although not further explored in this thesis, one could wonder if the removal of the final methyl group is necessary or if one should simply continue with what nature provides. The same oxidation chemistry of Part II can still be carried out on 4-methylcatechol (although some complications were found in the third part of this thesis) leading to dimethyl 3-methyladipate. As the single major usage of adipates is the synthesis of Nylon-6,6, the question is then if a 'bio-nylon' with this alternative monomer exhibits macroscopic properties that are acceptable to use as a substitute. This is a question for polymer chemists to answer; however, the barrier to successful introduction will of course always be higher for an alternative product than for a bio-based product that is chemically indistinguishable from its petrochemical counterpart. On the other hand, a 'bio-nylon' derived from a different chemical precursor might also exhibit superior properties for some applications. As a very relevant example, the bio-based 'PEF' polymer has superior barrier properties over the currently used PET in soda bottles, making it ideally suited as a replacement for this purpose. This can be a good justification for the adoption of a new bio-based product, despite the additional investments required.

Challenging the existing petrochemical chemistry with new bio-based routes is no mean feat; after all, the 'old' chemistry has had decades to develop and be optimised. At the same time, the reasons for moving to a bio-based chemical industry are, despite low oil prices, stronger than ever. Valorisation of lignin remains a challenging topic, but at the same time, comparing the field to where it was even just four years ago, it is clear that considerable progress has already been made. Advances in lignin depolymerisation, especially the advent of reactive pulping processes, now allows large amounts of a limited number of aromatic products to be obtained from the lignin. At the same time, how this affects the possibilities of processing the carbohydrate stream within existing biorefinery concepts will need to be addressed. Equally important, the final connections between the products of lignin depolymerisation and the eventual end products will need to be established. If these challenges can be met in the coming years, it will undoubtedly not be long before actual lignin-to-chemicals processes become reality.

Chapter 8b

Nederlandse Samenvatting

Samenvatting

Fossiele brandstoffen spelen nog steeds een centrale rol in de wereldwijde energievoorziening. Aardolie is daarnaast ook de belangrijkste grondstof voor de productie van fijn- en bulkchemicaliën. Het grootschalige gebruik van deze fossiele grondstoffen brengt echter aantal grote problemen met zich mee: ten eerste is de hoeveelheid aardolie eindig. Daarnaast vinden er nu al veranderingen plaats in de samenstelling van de mix van fossiele grondstoffen. In de Verenigde Staten wordt bijvoorbeeld op grote schaal schaliegas gewonnen en gebruikt als grondstof voor de productie van brandstof en chemicaliën. In tegenstelling tot aardolie levert de verwerking van schaliegas slechts weinig aromatische verbindingen op. Deze moeten dus uit andere bron verkregen worden. Ten slotte is het verband tussen klimaatverandering en de uitstoot van kooldioxide door het gebruik van fossiele brandstoffen onomstootbaar aangetoond. Er is daarom steeds meer aandacht voor het vervangen van fossiele brandstoffen door duurzame grondstoffen.

Lignocellulose is een interessant duurzaam alternatief als grondstof voor de chemische industrie. Lignocellulose is het celwandmateriaal in de niet-eetbare delen van planten, zoals de takken, stengels en boomstammen. Er is een grote hoeveelheid van beschikbaar en een belangrijk bijkomend voordeel is dat er geen directie concurrentie is met de voedselvoorziening. Chemisch gezien is lignocellulose opgebouwd uit drie componenten: cellulose (een polymeer van glucose), hemicellulose (een polymeer van voornamelijk pentosesuikers) en lignine (een polymeer bestaande uit aromatische componenten). Een manier om waardevolle producten te verkrijgen uit lignocellulose is, vergelijkbaar met de petrochemie, door middel van bioraffinage. In een geïntegreerde set van processen wordt de lignocellulose dan omgezet in een breed scala aan producten, waaronder brandstoffen en chemicaliën. Vergelijkbaar met een olieraffinaderij kan dit plaatsvinden door de lignocellulose eerst te scheiden in de drie basiscomponenten en deze vervolgens onafhankelijk van elkaar verder te verwerken.

Lignine is de enige biomassacomponent die op grote schaal beschikbaar is en die bestaat uit aromatische bestanddelen. Het zou daarom een ideale grondstof zijn voor de productie van aromatische fijn- en bulkchemicaliën, alsmede de niet-aromatische verbindingen die op dit moment met een aromatische verbinding als tussenstap worden geproduceerd. Lignine is echter de lastigste component van lignocellulose om verder te verwerken, omdat lignine (in tegenstelling tot cellulose) geen goed-gedefinieerde structuur heeft. In plaats daarvan zijn er meerdere soorten bindingen tussen de monomeren en bestaan sommige van deze ook nog eens uit zeer sterke koolstof-koolstofbindingen. In *Hoofdstuk 2* wordt een uitgebreide beschrijving van lignine gegeven; aan bod komen de biosynthese, mogelijkheden van het aanpassen van de lignine door middel van gentechnologie, het scheiden van lignine van de rest van de lignocellulose, het katalytische omzetten van lignine en het uiteindelijk omzetten van dit biopolymeer in waardevolle chemicaliën.

De synthese van lignine in de plant verloopt via het zogeheten 'phenylpropanoïde'-pad. Het aminozuur phenylalanine wordt via een complexe serie biochemische transformaties omgezet in de drie monomeren van lignine: *p*-coumarylalcohol, coniferylalcohol en sinapylalcohol. Deze monomeren worden vervolgens naar de celwand getransporteerd, waar ze door middel van radicaalreacties in de groeiende lignine-matrix worden opgenomen. Onderzoek naar het phenylpropanoïde-pad heeft ertoe geleid dat het nu mogelijk is om dit proces met gentechnologie aan te passen. Dit maakt het mogelijk om ook monomeren in de lignine op te nemen die daar van nature niet in voorkomen. Door gebruik te maken van monomeren die ingebouwd worden met behulp van bindingen die makkelijker te breken zijn (zoals esters) dan de normale bindingen in lignine, kunnen plantsoorten gecreëerd worden met een lignine die makkelijker te scheiden en verder te verwerken is. Lignine zorgt echter ook voor de mechanische sterkte van de plant en is daarnaast belangrijk in het intercellulaire watertransport en als barrière tegen infecties. Bij het aanpassen van de samenstelling en de structuur van lignine moet dus wel opgepast worden dat het materiaal zijn natuurlijke functie niet meer kan vervullen. Daarnaast is het vinden van de juiste genetisch gemodificeerde varianten van commercieel relevante plantensoorten een tijdrovende aangelegenheid. Als gevolg hiervan zijn dergelijke genetisch gemodificeerde lignines op dit moment nog niet beschikbaar voor diegenen die werken aan de verdere verwerking, zoals processen voor het omzetten in chemicaliën.

De manier van scheiden van de lignine van de andere componenten van lignocellulose is een belangrijke eerste stap en heeft gevolgen voor de verdere verwerking. Om hoogwaardige cellulosevezels te verkrijgen wordt op dit moment in de papier en pulp industrie op grote schaal het 'kraft' proces toegepast. In dit proces wordt het hout sterk verwarmd in een waterige oplossing van natriumhydroxide en natriumsulfide. Onder deze omstandigheden breken de etherbindingen in de lignine en kunnen de zo gevormde kleinere fragmenten oplossen. Belangrijk hierbij is dat de lignine die op deze manier wordt verkregen, een beduidend andere structuur heeft dan de lignine in de plant. De kleine fragmenten die vrijkomen door het breken van de etherbindingen zijn namelijk zo erg reactief dat ze vervolgens met elkaar reageren en nieuwe koolstof-koolstofbindingen vormen. Deze koolstof-koolstofbindingen zijn nog moeilijker om te breken dan de oorspronkelijke etherbindingen, wat uiteraard problemen oplevert wanneer men probeert deze lignine verder te verwerken. Nieuwere scheidingsmethoden van lignocellulose op basis van katalyse met zuur in organische oplosmiddelen, zogenaamde organosolvprocessen, hebben ook last van dit soort condensatiereacties. Een recent ontwikkelde strategie om hiermee om te gaan, is om het scheidingsproces direct te koppelen aan verdere (katalytische) omzetting. Door bijvoorbeeld een extra katalysator aan het scheidingsproces toe te voegen kunnen de reactieve fragmenten worden omgezet in stabiele eindproducten en worden condensatiereacties vermeden.

Het katalytisch depolymeriseren van lignine is een veld waarin de laatste jaren veel vooruitgang is geboekt. Er zijn een groot aantal methodes ontwikkeld, die ruwweg in twee soorten onderverdeeld kunnen worden. 'Milde' methodes richten zich op specifieke bindingen in de ligninestructuur, voornamelijk de veel voorkomende β-O-4 alkyl-arylethers. Voor het succesvol toepassen van een dergelijke milde methode is het wel van belang dat de lignine op een dusdanige manier is geïsoleerd dat er nog een substantiële hoeveelheid van dit fragment aanwezig is. 'Heftige' methodes gebruiken daarentegen reactieomstandigheden waaronder zowel katalytische als thermische reacties plaats kunnen vinden. Daardoor is het mogelijk om zelfs de zeer sterke koolstof-koolstofbindingen te breken. Daar tegenover staat dat dit ten koste gaat van de selectiviteit. Hoewel de totale opbrengst vaak hoger is, wordt wel een complex mengsel van een groot aantal verschillende aromatische verbindingen verkregen. Ongeacht de toegepaste methode blijft het vermijden van het opnieuw condenseren van reactieve kleinere fragmenten tijdens elk depolymerisatieproces van belang. Succesvol zijn dan ook die depolymerisatiemethoden die in staat zijn om dit soort reactieve fragmenten snel om te zetten in stabiele producten.

Het verder verwerken van monomere, zuurstofhoudende aromaten gevormd in de depolymerisatiestap is vaak nodig, al zijn sommige van deze producten zelf al waardevol. De meeste van deze vervolgstappen zijn gebaseerd op hydrodeoxygenatiereacties: het verwijderen van zuurstofatomen door middel van waterstof. Het hydrodeoxygeneren van een mengsel van verbindingen verkregen uit lignine kan bijvoorbeeld een mengsel van benzeen, tolueen en xyleen (BTX) opleveren. Omdat BTX op dit moment een belangrijk product uit aardolie is, kan verdere verwerking plaatsvinden met de bestaande chemie en petrochemische infrastructuur. Dit zou echter wel tot een behoorlijke omweg leiden: verdere verwerking bestaat vervolgens namelijk vaak juist weer uit het toevoegen van zuurstofatomen. Het zou dus efficiënter zijn als de monomere producten van ligninedepolymerisatie direct tot de gewenste eindproducten zouden kunnen worden omgezet. Hiervan bestaan echter nog maar weinig voorbeelden.

Het doel van het werk beschreven in dit proefschrift was om nieuwe katalytische routes te ontwikkelen om waardevolle producten te verkrijgen uit lignine. Daarbij werd in het bijzonder gekeken naar het katalytisch breken van koolstof-koolstofbindingen. Zoals eerder genoemd speelt het afvangen van reactieve fragmenten een belangrijke rol in succesvolle ligninedepolymerisatie. Daartoe werd een nieuw proces ontwikkeld, waarin door middel van katalytische decarbonylatie reactieve aldehydeintermediairen tot stabiele producten worden omgezet. Hercondensatiereacties konden zo worden vermeden en werd een grote hoeveelheid aromatische producten uit lignine verkregen. Het is daarnaast van belang om zuurstofrijke aromatische verbindingen direct om te kunnen zetten in de uiteindelijk gewenste producten. Daartoe werd een twee-staps proces ontwikkeld om catechol om te zetten in dimethyladipaat, een monomeer van nylon-6,6. De belangrijkste stap in dit proces is het selectief openen van de aromatische ring van catechol,

wat werd bereikt met behulp van een ijzerkatalysator. Vaak worden er ook verschillen in reactiviteit tussen pure of modelverbindingen en daadwerkelijke biomassastromen waargenomen. Zowel de depolymerisatie als de oxidatieve ringopeningsreactie werden daarom ook op lignines danwel op uit biomassa verkregen lignineoliën uitgevoerd.

In *Deel I (Hoofdstuk 3)* wordt de ontwikkeling van een nieuw proces voor de depolymerisatie van lignine beschreven. Er wordt gebruik gemaakt van een Lewiszuur dat stabiel is in water, om de β-O-4 aryl ether te hydrolyseren. De reactieve aldehydes die gevormd worden tijdens de hydrolyse worden meteen met een rhodium/difosfine complex gedecarbonyleerd, zodat uiteindelijk 4-methylphenolen als producten worden gevormd (zie Figuur 8.1). Het concept werd eerst gevalideerd en geoptimaliseerd door gebruik te maken van modelverbindingen voor de β-O-4 akyl aryl ether. Als Lewiszuur werd scandium triflaat gekozen, als decarbonyleringskatalysator een complex dat *in-situ* werd gemaakt uit $[Rh(cod)Cl]_2$ en 1,3-bis(difenylfosfino)propaan. Met de modelverbindingen kon het mechanisme van de reactie worden onderzocht. Hieruit bleek dat de eerste stap een Lewiszuur-gekatalyseerde dehydratie van de α-hydroxylgroep is, waardoor een styrylether wordt gevormd. De hydrolyse van deze styrylether wordt wederom door het Lewiszuur gekatalyseerd; dit leidt tot de vorming van een aldehyde, dat door de rhodiumkatalysator wordt gedecarbonyleerd. Belangrijk voor het succesvol verloop is dat tijdens de reactie de concentratie van het aldehyde erg laag blijft. Als de activiteit van de decarbonyleringskatalysator niet hoog genoeg is, vindt in plaats van de gewenste decarbonylering een competitieve aldol condensatie plaats. De totale monomeeropbrengst van de reactie neemt dan ook aanzienlijk af. Verassend genoeg bleek er nog een tweede reactiepad mogelijk te zijn, waarbij styreenderivaten werden gevormd. Deze producten zijn niet eerder gezien in de omzetting van modelverbindingen voor de β-O-4 akyl aryl ether.

Met lignine zelf bleek de ontwikkelde depolymerisatieprocedure ook goed te verlopen. Omdat het van belang is dat de lignine nog een groot aandeel β-O-4 ethers bevat, werd deze geïsoleerd uit zaagsel van populier door middel van een milde dioxasolvmethode. Zoals op basis van de resultaten met de modelverbindingen werd verwacht, werden inderdaad de gedecarbonyleerde 4-methylfenolen gevormd. Ook werden tijdens de reactie 4-(1-propenyl)fenolen gevormd, waarschijnlijk op dezelfde manier als de styrenen bij de modelverbindingen. Door de eigenschappen en de hoeveelheid van het Lewiszuur aan te passen, kon de selectiviteit van de reactie worden beïnvloed. Bij het gebruik van minder of een zwak Lewiszuur, werden meer 4-(1-propenyl)fenolen gevormd. Daarentegen leidde het gebruik van meer of een sterker Lewiszuur juist tot meer 4-methylfenolen. Beide producttypen zijn waardevol;. met name de 4-(1-propenyl)fenolen kunnen nuttige uitgangsmaterialen zijn voor de productie van fijnchemicaliën zoals geurstoffen en medicijnen. Na het optimaliseren van de reactie kon uiteindelijk 12.4 gewichtsprocent aan monomere aromaten uit lignine worden verkregen. Hoewel dit wellicht op het
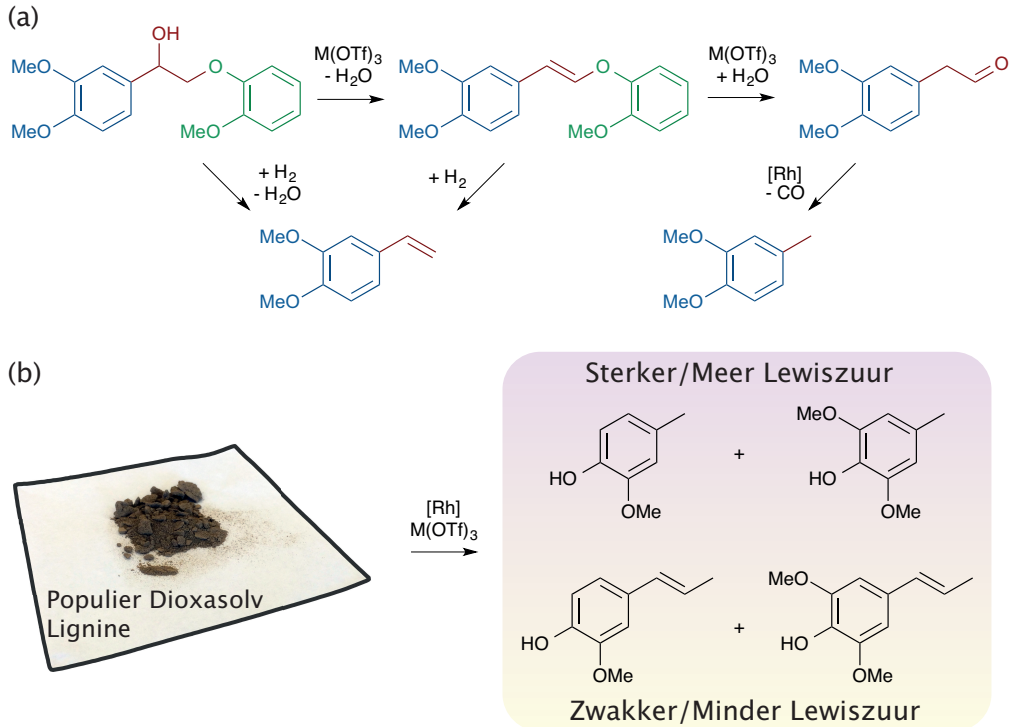
Figuur 8.1: Het depolymerisatieproces voor lignine dat is ontwikkeld in Hoofdstuk 3. (a) Uit onderzoek naar modelverbindingen blijkt dat het breken van de binding begint met een Lewiszuur-gekatalyseerde dehydratatie. De gevormde styrylether wordt vervolgens gehydrolyseerd tot een aldehyde, dat door de rhodiumkatalysator wordt gedecarbonyleerd. Daarnaast bestaat er een alternatief reactiepad dat leidt tot de vorming van styreenderivaten. (b) In de depolymerisatie van lignine worden, in overeenstemming met bovenstaand mechanisme, 4-methylfenolen of 4-(1-propenyl)fenolen gevormd. De selectiviteit kan worden beïnvloed door variatie van de sterkte en hoeveelheid van het Lewiszuur.

eerste gezicht weinig lijkt, is dat al meer dan 80% van de maximale opbrengst gezien het aantal β-O-4 bindingen in deze lignine.

Lignines uit andere plantsoorten konden met deze methode ook gedepolymeriseerd worden, waarmee ook de brede toepasbaarheid ervan werd gedemonstreerd. Zoals eerder besproken kan het daarnaast interessant zijn om de ligninedepolymerisatie direct op de lignocellulose uit te voeren. Ook wanneer de nieuwe methode direct werd toegepast op zaagsel van populier, werden dezelfde 4-methylfenolen en 4-(1-propenyl)fenolen gevormd. De opbrengst was in dit geval vergelijkbaar met de opbrengst die werd verkregen uit geïsoleerde lignine uit populier. Verder onderzoek naar de rol die de koolhydraatfractie speelt in het depolymerisatieproces, zal het ongetwijfeld mogelijk maken

om het proces verder te verbeteren en grotere hoeveelheden aromaten direct uit hout te verkrijgen.

In *Deel II* van het proefschrift wordt de ontwikkeling van een ijzerkatalysator voor de oxidatieve ring-opening van catechol beschreven als methode voor het verder verwerken van monomere, uit lignine verkregen, aromaten. Dit is de cruciale stap in een nieuwe route naar het nylon-6,6 monomeer dimethyladipaat. Het was al langer bekend dat een ijzer(III) complex van tris(2-pyridylmethyl)amine dit stoichiometrisch kan doen met de geactiveerde modelverbinding 3,5-di-*tert*-butylcatechol. Met dit als uitgangspunt is vervolgens in *Hoofdstuk 4* aangetoond dat dit katalytisch mogelijk is op het echte substraat catechol (zie Figuur 8.2). De reactie blijkt zeer selectief te verlopen en breekt alleen de koolstof-koolstofbinding tussen de twee hydroxylgroepen (intradiol). Het belangrijkste product is de half-methyl ester van *cis*,*cis*-muconzuur; de methyl ester wordt gevormd omdat methanol als oplosmiddel wordt gebruikt. Een aantal andere isomeren werd daarnaast in kleinere hoeveelheden gedetecteerd. Deze zijn echter allemaal afkomstig van de intradioloxidatie en worden door secundaire isomerisatiereacties gevormd.

De oxidatiereactie verloopt via een ijzer(III)-catecholato complex. Deze complexen vertonen sterke absorpties in het zichtbare en nabije infraroodspectrum, wat het mogelijk maakt om de reacties eenvoudig spectroscopisch te volgen. Daarnaast geeft het de reactiemengsels een zeer karakteristieke paarse kleur. Om de catecholato-complexen te vormen is het nodig om de catechol te deprotoneren met een base. Het is derhalve opmerkelijk dat als het eerste catecholatocomplex eenmaal gevormd is, de reactie meerdere cycli kan doorlopen zonder dat nieuwe base nodig is, ondanks het feit dat er een zuur als product gevormd wordt. Ook spectroscopisch blijkt de concentratie catecholatocomplexen in oplossing tijdens de reactie vrijwel gelijk te blijven. Waarschijnlijk is de zeer sterke binding tussen ijzer en de catecholatogroep hiervoor verantwoordelijk. Derhalve kan zelfs met een zeer zwakke base, zoals de muconaat-anionen, het catechol gedeprotoneerd worden, mits het catecholaat dan aan ijzer bindt. Om de reactie op gang te krijgen is dan ook zeker geen sterke base nodig; zelfs ammoniumacetaat bleek als base te voldoen. Bij hoge conversie wordt de concentratie catechol wel te laag om nieuwe catecholato complexen te vormen. Het ijzer reageert in dat geval weg tot dimere μ-oxo, μ-carboxylatoverbindingen. In de ijzer-gekatalyseerde oxidatiechemie wordt dit veelal beschouwd als een irreversibel deactiveringsproces. In dit geval bleek echter dat na toevoeging van nieuwe catechol, de catecholato complexen opnieuw gevormd werden en de oxidatiereactie gewoon verder kon gaan. Het deactivatieproces blijkt derhalve onder deze condities reversibel te zijn.

In *Hoofdstuk 5* werd de ijzer-gekatalyseerde ring-opening van catechol verder onderzocht. Het bereik van condities dat kon worden onderzocht werd flink uitgebreid door gebruik te maken van een vloeistoffase *batch*autoclaaf met een continue (hogedruk) gastoevoer. De belangrijke parameters katalysatorconcentratie, (zuurstof)druk en
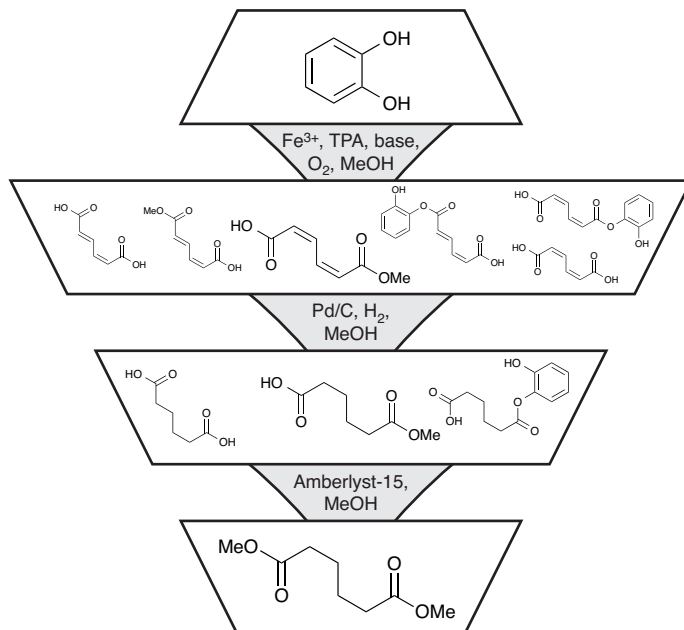
Figuur 8.2: Samenvatting van de in dit proefschrift ontwikkelde route waarin catechol wordt omgezet in dimethyladipaat. Het is van belang dat de eerste stap met volledige intradiolselectiviteit verloopt om het catechol in een mengsel van muconzuurisomeren om te zetten. De daaropvolgende hydrogenerings- en veresteringsstappen zetten het verkregen mengsel vervolgens convergent om in dimethyladipaat.

temperatuur bleken zich netjes te gedragen volgens de vergelijkingen voor reactiekinetiek: de reactie is 0de orde in catechol en 1ste orde in zowel katalysator en zuurstof. Aan de hand van de data die werd verkregen bij verschillende temperaturen kon ook de activeringsenthalpie en -entropie worden bepaald: deze waren respectievelijk 5.7 kcal/mol en 41 cal mol^{-1} K^{-1}. Zelfs onder de meest heftige condities bleef de katalysator selectief de intradiol ringopeningsproducten vormen. Bij 25 bar druk (5 vol% zuurstof in stikstof) en 80 °C maakte dit het mogelijk om in vergelijking met de resultaten in *Hoofdstuk 4*, de activiteit 35 keer te verhogen.

Omdat het uiteindelijke doel van de oxiditieve ringopening was om waardevolle chemicaliën te verkrijgen, werd ook aangetoond dat het verkregen reactiemengsel verder kan worden omgezet in dimethyladipaat. Dit is een monomeer dat gebruikt wordt in de productie van nylon-6,6 en derhalve een product van industrieel belang. Het feit dat in de ring-opening een mengsel van producten wordt verkregen, is in dit geval geen probleem, omdat de volgende processtappen *convergent* zijn (zie Figuur 8.2). Alle stereo-isomeren worden naar hetzelfde product gehydrogeneerd. Een tweede (trans)esterificatiestap zet

vervolgens de verschillende esters om naar één enkel eindproduct. Voor de hydroge-nering kan simpelweg een commercieel verkrijgbare palladium-op-koolkatalysator worden gebruikt. Het gebruik van een Raney® nikkelkatalysator, waarbij het gebruik van edelmetalen wordt vermeden, bleek ook mogelijk. In dit geval bleven echter wel wat half-gehydrogeneerde producten over. Ook de veresteringsreactie verloopt prima met een commerciële katalysator, in dit geval Amberlyst-15. Doordat voor de vervolgstappen gebruik gemaakt wordt van heterogene katalysatoren, kunnen deze makkelijk van de producten gescheiden worden. Daarnaast kunnen beide reacties in hetzelfde oplosmid-del uitgevoerd worden; de enige bewerkingsstap die tussendoor nodig is, is het filtre-ren van de palladium-op-koolkatalysator. De dimethyladipaat kon tenslotte zeer zuiver worden verkregen door een vacuümdestillatie uit te voeren. Uiteindelijk kan daardoor in drie stappen dimethyladipaat in 62% opbrengst uit catechol worden gemaakt.

Om de bijzondere chemie van de ringopening van catechol beter te begrijpen, werd ook een mechanistische studie uitgevoerd. Deze studie, die wordt beschreven in *Hoofdstuk 6*, omvatte zowel een experimentele als een computationele component. Eerdere studies aan het mechanisme suggereerden dat er een verband bestaat tussen de Lewiszuurheid van het ijzerion in de katalysator en de uiteindelijke reactiviteit. Daarom werd een nieuw, electronenzuigender variant van TPA, tris(4-chloro-2-pyridylmethyl)amine (Cl$_3$-TPA), gesynthetiseerd. Vervolgens werden de reactiesnelheidsconstanten bepaald voor com-binaties van beide liganden met verschillende gesubstitueerde catecholen. Zoals eerder was gezien, bleken de electronrijke catecholen sneller te reageren. Dit substituenteffect kon verder gekwantificeerd worden via de Hammett-vergelijking. Hieruit bleek dat de snelheidsbepalende stap in de reactie een electrofiele aanval van zuurstof op het catecho-laat moet zijn. Daarnaast bleek dat de complexen met het nieuwe Cl$_3$-TPA ligand inder-daad sneller reageerden.

De belangrijkste controverse in het intradiol mechanisme is de manier waarop zuurstof het ijzer-catecholato complex in eerste instantie bindt. Er zijn zowel voorstanders van een 'substraat-activatie' mechanisme, waarin zuurstof direct met de catecholato groep reageert, als van een 'ijzer-activatie' mechanisme, waarin zuurstof eerst aan het ijzer moet binden. Meerdere mechanistische mogelijkheden werden daarom door middel van computationele chemie verkend. Het enige pad dat een redelijke activeringsener-gie voor de reactie opleverde was een route waarin zuurstof inderdaad eerst aan het ijzer bindt. Tegelijkertijd dissocieert een van de catecholato-armen van het ijzer, om plek te maken voor het binden van zuurstof (zie Figuur 8.3). Zuurstof valt vervolgens aan op één van de twee O-gesubstitueerde koolstoffen van het catecholaat, waardoor een peroxide-brug ontstaat. Dit peroxide kan vervolgens een homolytische splitsing ondergaan. Het zuurstofradicaal dat daarbij aan de catecholzijde overblijft voegt zich-zelf daarbij vervolgens zeer snel in de ring, waarmee een cyclisch muconzuuranhydride wordt gevormd. Dit intermediair kan vervolgens zeer eenvoudig door water of een ander
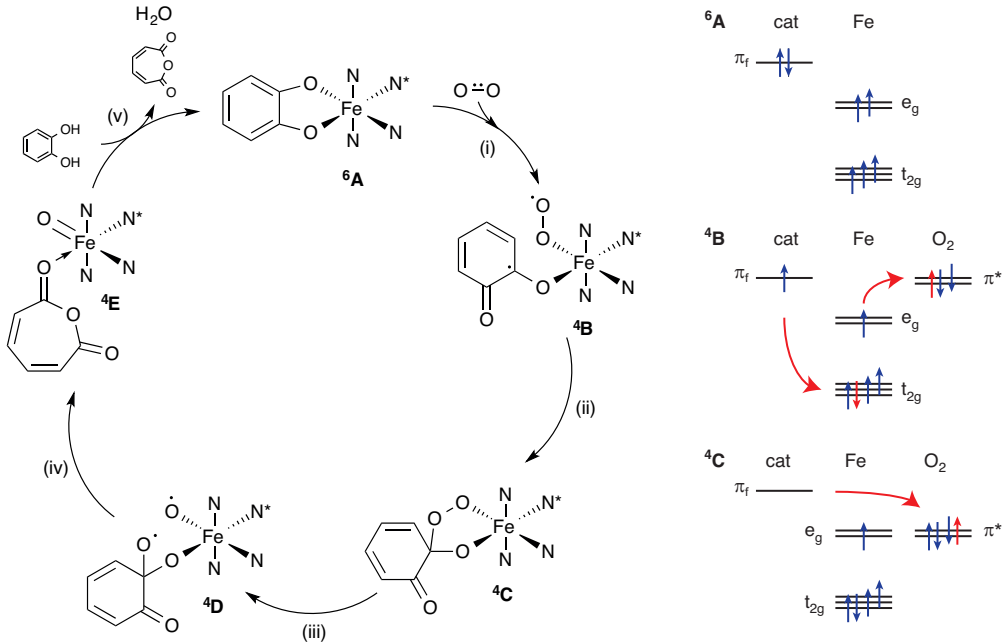
Figuur 8.3: (links) Katalytische cyclus van de intradiol ringopeningsreactie van catechol. (rechts) Schematische weergave van de electronenconfiguratie in de drie eerste stadia van de cyclus. Dit geeft de 'bufferfunctie' van ijzer weer. Als ijzer zuurstof bindt, wordt het direct met één electron gereduceerd door ijzer (tot een superoxide); tegelijkertijd wordt het ijzer zelf ook met één electron, met omgekeerde spin, gereduceerd door het catecholaat. De hoogst-energetische orbitalen van zowel zuurstof als het catecholaat hebben nu beiden één electron met tegengestelde spins; dit faciliteert vervolgens de vorming van de koolstof-zuurstofbinding.

protisch oplosmiddel worden gesolvolyseerd, waardoor de *cis,cis*-muconaatproducten ontstaan. Uit de berekeningen bleek dat de aanval van zuurstof op het catecholaat de snelheidsbepalende stap is. Verder bleken de berekening en het experimenteel geobserveerde effect van ligand en substraat op de activiteit goed overeen te komen. Dit is een goede indicatie dat dit mechanisme inderdaad overeenkomt met de werkelijkheid.

Een analyse van de moleculaire orbitalen die betrokken zijn bij de vorming van het superoxide en vervolgens de peroxidebrug maakt duidelijk hoe deze bijzondere reactie plaatsvindt. In de grondtoestand van het ijzer-catecholato complex is het in een zogenaamd 'hoge' spintoestand: dat wil zeggen dat de 3d orbitalen van ijzer elk gevuld zijn met één electron; elk electron heeft dezelfde spintoestand (volgens de conventie 'op'). De twee ongepaarde electronen in het zuurstof hebben dan een tegenovergestelde spin ('neer'). Tijdens het binden van zuurstof aan ijzer, wordt zuurstof gereduceerd tot een superoxide; dit gebeurt door het catecholaat, wat daardoor tot een semiquinonaat wordt geoxideerd. Omdat de zuurstof al twee 'neer' electronen heeft, kan dit alleen

plaatsvinden met een 'omhoog' electron. Als deze reductie van zuurstof echter direct vanuit het catecholaat zou plaatsvinden, houden zowel het catecholaat als het zuurstof beiden een 'neer' electron over. Vorming van de peroxidebrug via een reactie tussen catecholaat en zuurstof zou dan vervolgens spin-verboden zijn en niet plaats kunnen vinden. In plaats daarvan neemt het ijzer een 'neer' electron op van het catecholaat, terwijl het een 'op' electron doneert aan het zuurstof. De spintoestand van ijzer wordt hierdoor verlaagd naar de tussentoestand. Door deze bufferfunctie van ijzer hebben catecholaat en zuurstof nu ongepaarde electronen met een tegenovergestelde spin, waardoor zij vervolgens gemakkelijk een nieuwe koolstof-zuurstofbinding kunnen vormen. Met dit inzicht wordt het ook duidelijk dat bij de stabilisatie van de tussenspintoestand het ligand een belangrijke rol speelt. De symmetrie van het TPA ligand is dusdanig dat π-orbitalen van de pyridine met dezelfde d-orbitaal van ijzer overlappen, dat dus door π-backbonding wordt gestabiliseerd. De dubbele bezetting van dit d-orbitaal zorgt ervoor dat de tussenspintoestand wordt gestabiliseerd. Om nog betere katalysatoren te ontwikkeling voor de ijzer-gekatalyseerde dioxygenatie, is het dus van belang dat het ligand de tussenspintoestand kan stabiliseren.

In *Deel III (Hoofdstuk 7)* is de ontwikkelde ringopening van catechol toegepast op catecholen die direct uit lignine zijn verkregen. Er bestaan echter nog geen depolymerisatiemethoden voor lignine die direct pyrocatechol opleveren. Door lignine hydrogenolytisch te depolymeriseren met een katalysator van koper op een poreus metaaloxide, kan echter een mengsel van propyl-gesubstitueerde catecholen in hoge opbrengst worden verkregen. De oxidatieve ringopening van dit catecholenmengsel werd daarom ook onderzocht. De twee belangrijkste bestanddelen van het catecholmengsel werden eerst gesynthetiseerd en apart als zuivere verbinding getest. Met de ijzer-TPA katalysator ondergingen deze catecholen ook de oxidatieve ring-opening. Door de propylstaart werd het productmengsel echter wel gecompliceerder: de isomerisatie van het *cis,cis*-muconzuur verloopt veel sneller, waardoor daarnaast ook *cis,trans*-muconzuren en γ-muconolactonen gevormd werden. Hoewel de massabalans voor deze verbindingen wel lager was, bleef de selectiviteit naar de intradiolproducten wel volledig behouden.

Bij het toepassen van de ijzerkatalysator op een echte lignine-olie bleek er een opmerkelijk verband te zijn tussen de activiteit in de oxidatie en de katalysator die was gebruikt voor de depolymerisatiestap. Gebruik van een koperkatalysator die uit metaalnitraten was gesynthetiseerd, leverde een lignineolie op dat net zoals de pure verbindingen kon worden geoxideerd. Bij gebruik van een koperkatalysator die uit metaalchlorides was gesynthetiseerd, verliep de oxidatie echter veel langzamer, of met minder ijzerkatalysator, helemaal niet. Waarschijnlijk speelt het chloride dat achterblijft in de gedepolymeriseerde lignine een belangrijke rol in de deactivering van de ijzerkatalysator. Dit toont aan dat inzicht in de onderlinge afhankelijkheden tussen verschillende stappen in multistapslignineconversie ook erg belangrijk is en dat dit goed onderzocht moet worden.

Slotbeschouwing

De resultaten die worden beschreven in dit proefschrift dragen bij aan de ontwikkeling van de chemie die nodig is om lignine als duurzame grondstof in de chemische industrie toe te passen. Hierbij werd niet alleen de depolymerisatie van lignine zelf onderzocht, maar werd ook aandacht besteed aan de vervolgstappen die nodig zijn om producten van ligninedepolymerisatie om te zetten in waardevolle chemische producten. De nadruk lag daarbij op het gebruik van methodes om katalytisch koolstof-koolstofbindingen te breken. De twee nieuwe katalytische methodes die gedurende dit onderzoek zijn ontwikkeld, tonen ook aan dat deze methodes complementair zijn aan het breken van koolstof-zuurstof bindingen. Door bijvoorbeeld een decarbonyleringskatalysator in tandem met een Lewiszuur te gebruiken kon lignine succesvol worden gedepolymeriseerd. Dit leverde producten op met een structuur die anders moeilijk is te verkrijgen. Ook een α,ω-dicarbonzuur met zes koolstofatomen, zoals verkregen kon worden uit de ijzer-gekatalyseerde oxidatie, is op andere wijze lastig uit biomassa te maken. Dat dit waardevolle producten zijn bleek duidelijk uit de verdere omzetting naar dimethyladipaat.

Dit neemt niet weg dat het breken van koolstof-koolstof bindingen een fundamenteel lastige opgave is. Om dit zowel met hoge activiteit als selectiviteit te doen, is het vaak nodig om zeer specifieke chemie toe te passen. Dit blijkt dan ook uit het mechanisme van de oxidatieve ring-opening van catechol: het breken van de koolstof-koolstofbinding is alleen mogelijk met de specifieke redox-eigenschappen van het 1,2-benzeendiolsubstituent. Daarnaast is er, door de spineigenschappen van zuurstof en de eigenschap van ijzer om meerdere spintoestanden aan te kunnen nemen, slechts één specifiek reactiepad mogelijk, wat tot een zeer hoge selectiviteit leidt. Dit is ook relevant binnen de bredere context van biologische oxidatiereacties. De vorming van de hoog-valente (en zeer reactieve) ijzer-oxo complexen, die normaal geassocieerd worden met dit soort oxidatiereacties, wordt via dit reactiepad namelijk vermeden. Hoewel dit een zeer specifiek mechanisme is, kunnen de algemene concepten wellicht van waarde zijn om nieuwe, milde oxidatiekatalysatoren op basis van ijzer te ontwikkelen.

De gecombineerde Lewiszuur en rhodium-gekatalyseerde depolymerisatie laat zien dat het snel weg laten reageren van reactieve intermediairen een belangrijk concept is om hercondensatie van ligninefragmenten te voorkomen. Hoewel de noodzaak hiervan al eerder is aangetoond, gaat de depolymerisatieprocedure in deze thesis een stap verder, door de decarbonyleringsreactie te gebruiken om ook nuttigere producten te verkrijgen. Het feit dat er vervolgens niet één maar twee reactiepaden mogelijk zijn was daarbij een zeer gelukkige ontdekking. Door de juiste keuze van de hoeveelheid en het type Lewiszuur kan de selectiviteit naar de gewenste producten worden aangepast. Dit maakt het vervolgens dan ook mogelijk om lignine selectief te depolymeriseren tot producten met de gewenste lengte van de koolstofketen. Tegelijkertijd is de vorming van de

4-(propenyl)fenolen opmerkelijk, omdat in deze reactie formeel een reductie van een koolstof-zuurstofbinding plaatsvindt. Hoe deze reactie precies plaatsvindt is een vraag die verder onderzocht dient te worden. Enerzijds kan daarmee de ligninedepolymerisatie nog beter gestuurd worden; anderzijds is de reactie dan wellicht ook breder toepasbaar in de organische synthese.

Dat lignine tijdens de isolatieprocedure al aanzienlijke structurele veranderingen ondergaat en daarbij al een groot deel van de β-O-4 bindingen verliest, werd gedurende lange tijd niet voldoende op waarde geschat. Dit leidde er echter toe dat conceptueel solide strategieën voor ligninedepolymerisatie toch geen significante hoeveelheid monomere producten opleverden, omdat gebruik werd gemaakt van een recalcitrante lignine, die slechts weinig van de te breken bindingen bevatte. Het inzicht dat het condenseren van reactieve ligninefragementen (tijdens de isolatiestap) hiervoor verantwoordelijk is, heeft recentelijk geleid tot onderzoek naar het gebruik van depolymerisatiemethoden direct op het hout. Hiermee werd in sommige gevallen een spectaculaire toename van de opbrengst van kleine monomere aromaten waargenomen. Tegelijkertijd tonen de resultaten in Hoofdstuk 3 aan dat het simpelweg vervangen van lignine door hout ook geen garantie voor hogere opbrengsten is. Wat de exacte reden hiervoor is, dient verder onderzocht te worden, maar ongetwijfeld speelt de interactie tussen de suikerfracties en de lignine hierin een belangrijke rol. In dergelijke processen zijn de cellulose en hemicellulose fracties daarnaast ook belangrijke producten. Wat er precies met deze fracties gebeurd en wat de consequenties voor de mogelijkheden van verdere verwerkingsstappen hierop zijn, dient daarnaast ook verder uitgezocht te worden. De voordelen van het doen van de reacties direct op de lignine zoals die in de plant voorkomt zijn, ondanks de extra complicaties, echter aanzienlijk. Waarschijnlijk zal een dergelijke aanpak in de toekomst dan ook belangrijker worden.

Tegelijkertijd is ook duidelijk geworden uit dit proefschrift dat er nog steeds een lacune is tussen de producten die uit ligninedepolymerisatie worden verkregen en de uiteindelijk gewenste producten voor de chemische industrie. Een niet onbelangrijke reden hiervoor is natuurlijk dat juist de huidig belangrijke (bulk)chemicaliën zijn geselecteerd op het gemak waarmee ze uit aardolie kunnen worden verkregen. Een mogelijke aanpak is om nieuwe routes te bedenken, die leiden tot een identiek eindproduct, wat een deel van de onderbouwing van het onderzoek Deel II was. Esters van adipinezuren zijn dan ook ideale kandidaten voor uit lignine verkregen chemicaliën: ze hebben een aantrekkelijke prijs, worden op grote schaal geproduceerd en de huidige route uit aardolie is ook dusdanig gecompliceerd dat een alternatieve route op basis van biomassa efficiënter kan zijn. Uiteindelijk loopt men dan toch tegen het probleem aan dat het startmateriaal voor dit proces (in dit geval catechol), qua structuur nog net niet het product is dat uit lignine kan worden verkregen. De meest recalcitrante functionaliteit in kleine monomere aromaten verkregen uit lignine die nog verwijderd moet worden is dan de propylstaart,

door middel het breken van een koolstof-koolstofbinding. Dit zou zowel tijdens of na de depolymerisatie plaats kunnen vinden.

Met de decarbonylatiestrategie die in Hoofdstuk 3 wordt beschreven, is in ieder geval aangetoond dat het selectief gedeeltelijk verwijderen van de koolstofstaart nu mogelijk is. Een openstaande vraag is of met deze aanpak ook de gehele koolstofstaart verwijderd kan worden. Afgezien van de decarbonyleringsstap zijn hiervoor ook drie oxidatie- of dehydrogenatiestappen nodig. Een aantal recente publicaties heeft bijvoorbeeld de selectieve oxidatie van de α-hydroxyl in het β-O-4 fragment beschreven; een bijkomend voordeel hiervan is dat de etherbinding daardoor veel makkelijker te breken is. Als het op deze manier mogelijk is om de ether te hydrolyseren, *zonder daarbij de α-hydroxyl te elimineren*, en met een tandemreactie de overige alcoholen te oxideren of dehydrogeneren, is complete decarbonylatie wellicht mogelijk. Om te laten zien of een dergelijke strategie mogelijk is, is echter wel veel meer onderzoek nodig.

Hoewel op dit onderwerp in dit proefschrift verder niet is ingegaan, kan men zich afvragen of het verwijderen van de laatste methylgroep wel echt nodig is. Uit Deel III blijkt dat de oxidatiechemie, met enige complicaties, ook succesvol op 4-methylcatechol kan worden uitgevoerd. Als de strategie uit Deel II dan wordt doorgezet zou dit uiteindelijk tot dimethyl 3-methyladipaat leiden. Veruit de belangrijkste toepassing van de adipaten ligt in de synthese van nylon-6,6. De vraag is dan of een 'bio-nylon' met dit alternatieve monomeer ook de juiste macroscopische eigenschappen heeft om petrochemische nylon-6,6 te vervangen. Polymeerchemici zullen deze vraag moeten beantwoorden. Het zal echter altijd moeilijker zijn om een compleet nieuw product te introduceren, dan één die chemisch niet te onderscheiden is van het bestaande petrochemische product. Een bijzonder relevant voorbeeld is het gebruik van het op biomassa gebaseerde polymeer 'PEF' als vervanger voor de welbekende PET flessen. Juist omdat de barrièreigenschappen van PEF beter zijn dan PET is PEF in deze toepassing een uitstekende vervanger. Dit kan dan een goede reden zijn om dergelijke nieuwe op biomassa gebaseerde producten te gebruiken, ondanks de extra investeringen die hiervoor nodig zijn.

Het vervangen van de bestaande petrochemische processen met nieuwe, op biomassa gebaseerde routes is geen gemakkelijke opgave. Deze 'oude' chemie heeft zich tenslotte al decennia lang kunnen ontwikkelen en optimaliseren. Ondanks de huidige lage olieprijzen zijn de redenen om over te stappen op een bio-gebaseerde chemische industrie echter relevanter dan ooit. Dit doen op basis van lignine blijft een lastige opgave, maar tegelijkertijd is er in de afgelopen vier jaar ook erg veel vooruitgang geboekt in het veld. De ontwikkelingen in ligninedepolymerisatie, in het bijzonder het combineren van depolymeriseren en verder omzetten tijdens de isolatie, hebben ertoe geleid dat het nu mogelijk is om een hoge opbrengst van een beperkt aantal producten uit lignine te verkrijgen. Wat voor een gevolgen dit heeft voor de mogelijkheden om de koolhydraatfractie in de bioraffinaderij verder te werken, zal wel verder onderzocht moeten worden.

Daarnaast is het van belang om producten van ligninedepolymerisatie aan te laten sluiten op de uiteindelijke gewenste eindproducten. Als deze uitdagingen in de komende jaren kunnen worden opgelost, zal het ongetwijfeld niet lang meer duren voordat processen die lignine in chemicaliën omzetten, daadwerkelijk worden toegepast.

List of Publications

This thesis is based on the following publications:

Chapter 2:
Roberto Rinaldi, Robin Jastrzebski, Matthew T. Clough, John Ralph, Marco Kennema, Pieter C. A. Bruijnincx and Bert M. Weckhuysen, *"Paving the Way for Lignin Valorisation: Recent Advances in Bioengineering, Biorefining and Catalysis,"* Angew. Chem. Int. Ed., accepted for publication

Chapter 3:
Robin Jastrzebski, Sandra Constant, Christopher S. Lancefield, Nicholas J. Westwood, Bert M. Weckhuysen and Pieter C. A. Bruijnincx, *"Tandem Catalytic Depolymerization of Lignin by Water-Tolerant Lewis Acids and Rhodium Complexes,"* submitted for publication

Chapter 4:
Robin Jastrzebski, Bert M. Weckhuysen and Pieter C. A. Bruijnincx, *"Catalytic Oxidative Cleavage of Catechol by a Non-Heme Iron(III) Complex as a Green Route to Dimethyl Adipate,"* Chem. Commun., 2013, **49**, 6912–6914

Chapter 5:
Robin Jastrzebski, Emily J. van den Berg, Bert M. Weckhuysen and Pieter C. A. Bruijnincx, *"Sustainable Production of Dimethyl Adipate by Non-Heme Iron(III) Catalysed Oxidative Cleavage of Catechol,"* Catal. Sci. Technol., 2015, **5**, 2003–2009

Chapter 6:
Robin Jastrzebski, Matthew G. Quesne, Bert M. Weckhuysen, Sam P. de Visser and Pieter C. A. Bruijnincx, *"Experimental and Computational Evidence for the Mechanism of Intradiol Catechol Dioxygenation by Non-Heme Iron(III) Complexes,"* Chem. Eur. J., 2014, **20**, 15686–15691

Chapter 7:
Robin Jastrzebski, Narani Anand, Remco Dalebout, Bert M. Weckhuysen, Katalin Barta and Pieter C. A. Bruijnincx, *"Oxidative Cleavage of Catechols Dervived from Candlenut Lignin,"* to be submitted for publication

Other publications by the author:

Pieter C.A. Bruijnincx, Robin Jastrzebski, Peter J.C. Hausoul, Robertus J.M. Klein Gebbink and Bert M. Weckhuysen, *"Pd-Catalyzed Telomerization of 1,3-Dienes with Multifunctional Renewable Substrates: Versatile Routes for the Valorization of Biomass-Derived Platform Molecules,"* Top. Organomet. Chem., 2012, **39**, 45-101

Anna L. Jongerius, Robin Jastrzebski, Pieter C.A. Bruijnincx and Bert M. Weckhuysen, *"CoMo sulfide-catalyzed hydrodeoxygenation of lignin model compounds: An extended reaction network for the conversion of monomeric and dimeric substrates,"* J.Catal., 2012, **285**, 315-323

Dankwoord

Het schrijven van een proefschrift is een opgave die lang niet altijd zonder slag of stoot gaat. Gelukkig zijn er een groot aantal mensen die mij op verschillende manieren hebben bijgestaan en geholpen; zonder hen zou dit proefschrift er niet in deze vorm zijn.

Ten eerste wil ik natuurlijk *Bert (Weckhuysen)*, mijn promotor, bedanken voor het vertrouwen dat je de afgelopen vier jaar in mij (en Pieter) hebt gesteld. Niet alleen omdat je mij een promotieplaats in deze groep hebt aangeboden, maar ook omdat je me de vrijheid hebt gegund om het onderzoek naar eigen inzicht uit te voeren.

Verreweg de belangrijkste bijdrage aan dit proefschrift is geleverd door *Pieter*, mijn co-promotor en directe begeleider. Als jij in je kantoor zat (dit werd gedurende de vier jaar wel steeds minder), was je altijd bereid om me met raad en daad bij te staan en me de goede kant op te sturen; dit heb ik altijd bijzonder gewaardeerd. Je hebt mijn iets wildere ideeën wat getemperd en gezorgd dat deze wel uitvoerbaar werden. Het was daarnaast erg lastig om omzin in geschreven vorm langs jou te krijgen; je kritische blik heeft alle manuscripten die we de afgelopen jaren geproduceerd hebben ontzettend verbeterd.

Tijdens mijn promotie-onderzoek heb ik het voorrecht gehad om een aantal externe samenwerkingen aan te gaan, waarbij ik de mogelijkheid heb gehad om kennis op te doen die binnen onze eigen vakgroep niet beschikbaar was. *Sam*, met mijn bezoek aan jouw vakgroep in Manchester werd de (tot dan toe voor mij duistere) wereld van DFT berekeningen eindelijk helder en ik ben erg blij dat het werk dat we samen hebben gedaan een van de mooiste hoofdstukken van dit proefschrift heeft opgeleverd. *Matt*, my fellow office-mate in Manchester, thank you for patiently explaining all this DFT stuff to me, as well as joining for the many pints and games of pool that took place after work.

Katalin, I still recall your enthusiasm when we first sat down at N3C to discuss our collaboration and I don't think that enthusiasm has faded since. Although the plans we had initially were perhaps a bit too optimistic, I think we managed to get some nice results in the end. Of course, many thanks also go to *Anand*, who did so much work on the candlenut lignin. *Chris*, I'm in your debt for providing the additional lignin samples that took the work in Chapter 3 even further and I'd like to thank *Nick* for being very supportive and constructive throughout that project. A lot of work went into the review that is the basis for Chapter 2, so I would like to thank *John*, *Matthew*, *Marco* and especially *Roberto* for all the valuable discussion and contributions. Finally, I was often seen skulking about 'upstairs' at the *Organic Chemistry & Catalysis* group; I would especially like to thank *Marc-Etienne* for working together on a crazy project involving iron-boranes (that unfortunately didn't make it into the thesis) and for the talks we

had over coffee on the balcony. *Bert (Klein Gebbink)*, ook jou wil ik bedanken voor alle apparatuur (met name de NMR) en middelen van organische chemie die ik gedurende mijn hele promotie-onderzoek heb mogen gebruiken. Bij *Henk* en *Jort* kon ik daarnaast altijd terecht om wat chemicaliën te lenen (en in het geval van Henk ook om sterke verhalen aan te horen). Daarnaast heb ik *Mies* lastig mogen vallen voor het vriesdrogen van de lignines.

Zonder de toewijding van de technici in onze vakgroep, zou het onderzoek al snel in het honderd lopen. *Ad^M*, of er nou een leidinkje gelegd moest worden of een vacuümpomp gereviseerd, jij zorgde altijd voor een degelijke (dus zonder duck tape!) oplossing. *Ad^E*, heel erg bedankt voor alle hulp met de autoclaven, met name het weer in gebruik nemen van het monster van Bart, en natuurlijk dat je altijd een oog op de veiligheid van het lab hield. *Pascal*, jouw hulp met het repareren van zo'n beetje alle chromatografie-apparatuur in het lab was van onschatbare waarde. Ook *Fouad, Herrick*, *Jan-Willem*, *Oscar, Marjan* en *Rien* mogen niet in dit lijstje ontbreken. Ook de ondersteuning van het secretariaat is natuurlijk onmisbaar; *Dymph*, *Monique* en *Iris*, jullie flexibiliteit om als het nodig is snel iets te regelen is geweldig.

Tijdens mijn onderzoek heb ik daarnaast het voorrecht gehad een aantal studenten te begeleiden. *Zaynab*, aangezien jij mijn eerste student was, was jouw project een leerproces voor ons beiden. *Emily,* het masterproject dat ik voor jou bedacht was uiteindelijk helemaal niet zo simpel als het in eerste instantie leek; en dan liet ik je ook nog eens twee maanden in de steek omdat ik in Engeland was. Gelukkig bleek je mij eigenlijk helemaal niet zo nodig te hebben en het werk dat jij gedaan hebt heeft uiteindelijk een hele mooie plek in dit proefschrift en het bijbehorende artikel gekregen. *Sebastian*, I really admire the attitude you demonstrated during your Erasmus project; no matter the challenge, you just went into the lab and tried and tried again. Although your work ultimately is not part of thesis, this is certainly not for your lack of efforts and I wish you all the best in the future. *Remco*, volgens mij kwam jij altijd vrolijk naar het lab toe, en jouw positiviteit werkt dan ook aanstekelijk. Jouw inzet heeft daarnaast in korte tijd een belangrijke bijdrage geleverd aan Hoofdstuk 7.

Mijn collega's in het biomassalab zorgen ervoor dat het onderzoek ook vier jaar lang leuk bleef. *Annelie,* als jouw oud-student bleef je, ook toen je collega was, altijd een beetje mijn mentor. Daarnaast hebben we ook ontzettend veel lol gehad, bijvoorbeeld op vrijdagmiddag met *hele slechte* muziek. *Ilona* was daar mede verantwoordelijk voor, maar o wee als de lab-sheriff je erop betrapte dat je je rommel niet opruimt. Onvergetelijk was het tripje naar Europacat in Lyon, ook met Ilona en samen met *Peter*. *Sandra*, not long after you joined our group we became partners in lignin crime; thank you for all your help with the NMR on the brown stuff, as well as feeding me the delicious results of the weekend baking sprees. Other biomass warriors, *Joe*, *Fiona, Wenhao*, *Dilek*, *Antonio*, *Fang*, *Ana*, *Kiichi*, and of course the *dark side Rob, Tomas* and *Daniël* also contributed to

the excellent atmosphere, as well as adoptees like *Zafer* and people who came wandering in for no good reason like *Clare. Frank*, drie jaar lang hebben we tegenover elkaar gezeten en ik hoop dat je mijn hoofd inmiddels al mist. *Arjan*, als inmiddels de fossielen van de groep hebben we zo'n beetje alles wel meegemaakt; daarnaast bedankt voor al het advies tijdens het kopen van auto's. Voor een beetje mentale ondersteuning van *Emma* (of een klaagsessie over ijzer) hoefde ik alleen maar even naar boven te lopen.

I will not even attempt to list everyone, but all the wonderful people that have been part of the Inorganic Chemistry & Catalysis clan have contributed to the unforgettable experience and memories of the last four years. Whether it was gossiping during coffee breaks, crazy conversation topics over lunch, borrels on our wonderful balcony, celebrating fresh doctors, Long Island Ice Tea, more borrels, sushi-eating contests or all the other stuff we did, it is all of you who made this great.

Om in een geestelijk gezonde toestand te blijven is het ook noodzakelijk om af en toe te ontspannen en dat dan bij voorkeur met een (verre) reis. Ik wil alle reisgenoten bedanken, maar in het bijzonder *Frits, Lidy, Chris, Anja, Marloes, Manon, Bart, Vera, Kim, Kim* en *Michel* voor jullie gezelschap in verre continenten.

Chris, Daan, Paul, Emma en Sabine; onze bestuursetentjes werden steeds schaarser de afgelopen jaren (en ik maak het nu niet makkelijker door in het buitenland te gaan wonen, sorry!). Dat nam niet weg dat als we wel weer met z'n zessen samen waren het altijd weer een feestje was!

Nicole, dankzij jouw kookkunsten stond er altijd weer iets lekkers op tafel als ik weer eens langskwam. Daarnaast hield je Remi gelukkig een beetje bezig en in bedwang als ik niet genoeg aandacht voor haar had. *Johann,* het is af en toe wel erg handig als je vader toevallig ook chemicus is in hetzelfde gebouw! Bedankt voor alle adviezen, zowel van chemische als niet-chemische aard. *Halina,* het is erg fijn dat ik altijd langs kon komen en dat jullie altijd voor me klaar staan en voor me zorgen als Remi dat niet kan.

Ten slotte, *Remi*. Jij gelooft onvoorwaardelijk in mij en bent er altijd om mij te steunen. Met jou stort ik me vol overgave op het volgende avontuur in ons leven; zoals je me hebt beloofd wordt het nooit saai met jou.

Curriculum Vitae

Robin Jastrzebski was born on the 27th of April, 1987 in the fair city of Utrecht, the Netherlands. After graduating from Het Nieuwe Lyceum in Bilthoven, he started his undergraduate studies in chemistry at Utrecht University in 2005. He obtained his Bachelor of Science degree in 2009 with the thesis titled "*PAMAM Dendrimer Supported Pincer Ligands for Catalysis,*" supervised by Niels Pijnenburg and prof. dr. Bert Klein Gebbink. Continuing his graduate studies at Utrecht University, he graduated *cum laude* in 2011 with the thesis titled "*Fundamental studies on the hydrodeoxygenation of lignin model compounds,*" supervised by Annelie Jongerius, dr. Pieter Bruijnincx and prof. dr. ir. Bert Weckhuysen. As part of his masters degree, he also spent six months at the polymer division of the Institute of Chemical and Engineering Sciences in Singapore. Robin returned to working in the field of lignin valorisation, starting his PhD studies in 2011, again under the supervision of dr. Pieter Bruijnincx and prof. dr. ir. Bert Weckhuysen. As part of these studies he also spent two months in the group of dr. Sam de Visser at the University of Manchester. The results of the PhD project are described in this thesis.

Presently, Robin is working as an Automation Chemist at Chemspeed Technologies in Augst, canton Basel-Landschaft, Switzerland.